Poznan University of Technology
Faculty of Chemical Technology
Institute of Chemical Technology and Engineering

Ph.D. thesis

NATURALLY FORMED CHITIN-BASED SCAFFOLDS: CHARACTERIZATION, FUNCTIONALIZATION, AND PRACTICAL UTILITY

Tomasz Machałowski, M.Sc., Eng.

Supervisor: Professor Teofil Jesionowski

Co-supervisor: Professor Hermann Ehrlich

Poznan, 2022

Acknowledgments

I would like to extend my sincere thanks to my supervisors, **Professor Teofil Jesionowski** and **Professor Hermann Ehrlich**, for the chance to develop on many levels, support and consideration. My doctorate was a fascinating adventure that I went through thanks to you.

Special thanks for **Marcin Wysokowski PhD**, for being a guiding lights, for patience, for being friend as well as formal and informal expeditions. Marcin I am very grateful to you.

It is impossible not to mention other, **Agnieszka Rusak PhD** (Wroclaw Medical University), **Joanna Idaszek PhD** (Warsaw University of Technology), **Iaroslav Petrenko PhD** (TU Bergakademie Freiberg), **MD Aneta Popiel** (Wroclaw Medical University), **Dr. Jakub Zdarta** (Poznan University of Technology), **Prof. Filip Ciesielczyk** (Poznan University of Technology), **Colleagues** from scientific group, for all helpful scientific discussions we have shared.

Lastly, I bow to my family, Patrycja, Henio, thank you for being with me in good and bad moments, Parents, lovely Sisters, Friends who supported me and never doubt me. I am lucky to have you close by.

Table of content

Chapter 1. Introduction

If our planet's history was compared to one-year, human existence would only be the last 15 minutes. With these assumptions, industrial progress would occur in less than 20 seconds. Despite such a small part, the industrialization observed in the last two centuries is on a larger scale than since the beginning of mankind. The rapid pace of industrialization has a positive effect on many aspects, such as the development of technology, the extension of life expectancy, or the control of the spread of many harmful pathogens. Nevertheless, several negative effects of "*rapid development*" are also observed. Need to list here, e.g. pollution and contamination of the natural environment, diseases of civilization, or climate warming. Although many of the side impacts of industrialization cannot be stopped anymore, it is worth looking for new solutions to limit or minimize their negative influence. The key to sustainable development may be nature, which is an inexhaustible source of inspiration. By learning about the mechanisms that it has developed over millions of years of evolution, we can create more efficient and less harmful ways of materials synthesis while being in harmony with the world around us. Without any doubt, it is worthwhile to investigate the subject of natural materials. Their biocompatibility, high porosity, renewability, and ecological safety affect them to become a real competition with synthetic ones. Natural biopolymers as proteins or polysaccharides, obtained from microorganisms to higher animals are similar to human macromolecules and could successfully mimic the extracellular matrix. Therefore, the risk of toxicity, chronic inflammatory response, and immunological reactions frequently observed with the products of degradation of synthetic polymers are not observed here as often. Chitin is one of the most interesting candidates among them. As a natural component of the exoskeletons of the many invertebrates, chitin is widely distributed in diverse taxonomic groups. The magnitude of its biosynthesis

means that chitin can be found in more than 70% of all living organisms in the world. However, the difficulties in their processing make its application potential very limited. Chitin is non-soluble in conventional solvents what hinders its industrial application. Nevertheless, its enormous abundance and limited usability prompt to look for new possibilities of functionalization of naturally prefabricated chitinous scaffolds.

In this thesis, for the first time, it is stated that chitin, a structural aminopolysaccharide, originating from marine sponges and spider molting cuticles, can be used as renewable "*ready to use*" scaffold for several applications. Its unique structural arrangement and biocompatibility were mostly used in tissue engineering. High porosity and preferred pores size enabled well cells attachment and nutrient diffusion. In contrast to commercial chitin, such sources allow overcoming technical limitations of chitin processing. Scaffolds obtained by these strategies represent unique 3-dimensional morphology, directly after isolation without additional processing. It makes them especially attractive and opens several ways for further functionalization. Thus, chitinous matrices were covered by calcium carbonate phase and a collagenous matrix. Moreover, for the first-time chitin–based composite material which contain silver and silver bromide was developed as an antibacterial filter. Immobilization of laccase onto chitinous scaffold enabled for the improvement of removal efficiency of tetracycline from aqueous solutions. Preliminary, investigations of spider chitin showed its potential in biomedical engineering and environmental protection applications. A detailed discussion of obtained results, concerning physicochemical, morphological as well as practical applications of prepared materials, is the main part of this thesis. Finally, the results are summarized and presented in the form of main conclusions.

Chapter 2. Literature review

Contents

2.1. Biomimetics as a basic tool for design of bioinspired materials

During millions of years of evolution, nature has developed survival strategies that allow living organisms to produce many amazing structures to protect them and adapt to their habitat [1]. The treasury of solutions, which is the natural environment, not only allows us to understand the interdependencies between the morphology and the function of a given biological material but also becomes an inspiration for the development and creation of new functional materials generation. Due to the research and observation of structures of natural origin, these solutions can be transferred to the world of medicine and engineering including architecture (**Figure 1**). Depending on the fulfilled functions, these natural structures differ from each other, adapting optimally to the performed tasks, and are changing rely on environmental conditions. Natural materials are often specific biocomposites made up of both, organic and inorganic phases [2]. Commonly, as organic matter, three main biopolymers, like chitin, collagen, and cellulose may be distinguished. They act like fibrillar structures with the hierarchical

organization from nano- up to macrolevels. Natural matrices perform several functions but mainly constitute a template and scaffold for biomineralization and minerals (inorganic phases) formation. The minerals that occur most frequently are carbonates, phosphates, and silicates. Therefore, the great examples of such biocomposites are, for example, human bones and teeth, snail shells, or crustacean's exoskeletons [3–6]. Due to the mutual interaction between individual components (phases), the resulting structures are characterized by much better mechanical or functional properties than single phases [7]. Their understanding may allow us to solve dozens of complex technical problems today.

The field of science called biomimetics uses nature as the ultimate model, standard, and advisor [8]. Genesis originates from the two Greek words '*bios*' (life) and '*mimesis*' (to mimic) and was used for the first time by the German-American neurophysiologist Otto Schmitt in the half of the 1950s [9]. The concept assumes specifically to create technology, materials, or art "*that uses or mimics nature to improve human life*" [8]. During the past years, several other synonyms of biomimetics were proposed, including *"biomimicry"*, *"bioinspiration"*, *"bionics"*, *"biologically inspired design"* or *"intellectual structure"* [10]. In practice, the concept of biomimetics has not been a trend in recent years, because traces of such human activities were already observed thousands of years ago. One of the first pieces of evidence was discovered on today's China territory when natives tried to make artificial silk (3000 years ago) [10] or Mayans Indians which utilized nacre as a dental implant (2000 years ago) [11]. Excellent examples of biomimetics are Leonardo da Vinci (1472–1519) prototypes. The "*flying machine*" designed by him was inspired by the observation of flying birds. Later, the same inspiration took note of the Wright brothers (1867–1948) to construct successfully first powered airplane (1903). Today, many of the new generation technologies and materials are based on

biomimetics, e.g. self-cleaning paints based on lotus leaf [12] or naturally highly hydrophobic spiders for crude oil spill removal [13]. Recently, a very interesting branch of biomimetics has become "*extreme biomimetics*", which focuses on mineralization and metallization of various biomolecules, such as chitin or spongin, under extreme (from the biological point of view) temperature and pressure conditions [14]. In contrast to "*classical biomimetics*", where ambient conditions are used primarily, herein the chemical and thermal stability of the biopolymers used are especially important. Such parameters mimic the environment of aquatic niches such as hydrothermal ducts or hot springs, to create new generations of functional materials [15–19]. However, materials synthesized with an agreement with both biomimetics philosophy found application in various branches of technology today, such as wastewater treatment [20–23], enzyme immobilization [24,25], electrochemistry [26], catalysis [27,28] or biomedicine and tissue engineering [29–33]. In this context, biomimetics is a multidisciplinary field of modern science (see **Figure 1**).
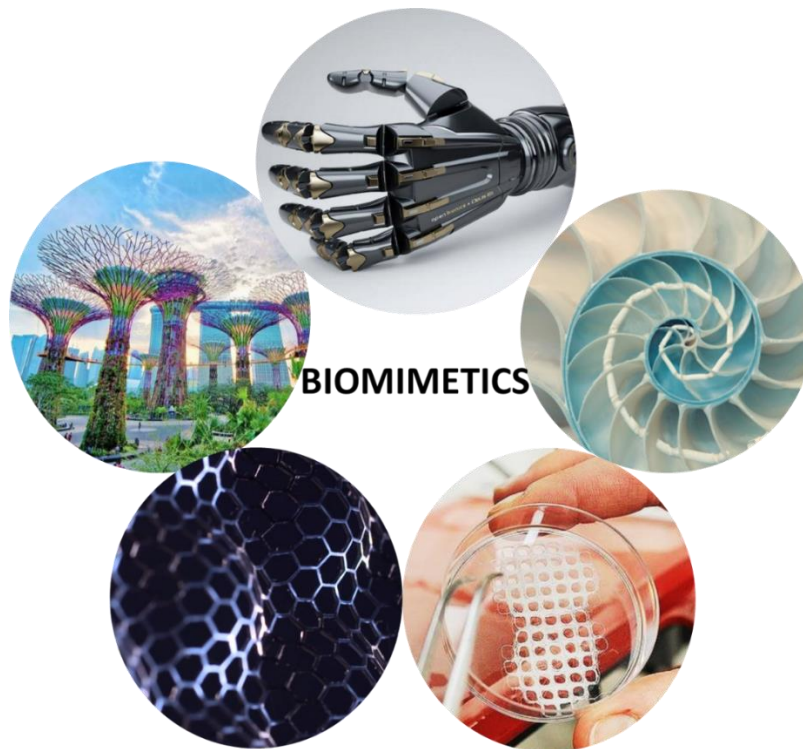
Figure 1. Examples of multiple areas of application of biomimetics, including medicine, engineering, art, tissue engineering or architecture.

2.1.1. 3D scaffolds as a support for diverse cell cultures

Despite the rapid development of medical research, large tissues damaged by diseases, serious trauma, or life-threatening accidents cannot be regenerated by the organism itself. Mostly, it is related to a high level of the tissue defect area or an irreparable range of damages. Today, the commonly accepted method of fixation for such cases is organ and tissue transplantation. However, limitation due to an insufficient number of donors and ethical concerns prompts the search for new solutions and possibilities. Recently, tissue engineering (TE) has proven to be a very promising and revolutionary field of regenerative medicine [34]. TE is a multidisciplinary field of study which combines principles of several science areas, like chemistry, biology, medicine, and engineering. As can be seen in currently published articles [35–37], promising results concerning the variety of tissues and organs regeneration, including joints, bones, skin, cardiovascular and nervous system were described. The basic concept of TE assumes three main strategies (**Figure 2**), including (I productive) acquisition of appropriate cell lines, such as pluripotent stem cells (iPSC) or normal adult cell lines, (II conductive) creation of scaffolds that act as supports for cells culture, and (III inductive) development of cells signaling molecules [34]. The great examples of the signaling biomolecules could be adhesive peptides, extracellular matrix proteins, growth factors, cytokines, genes, or hormones [34]. On the other hand, very important aspects include physical and mechanical properties of scaffold, as e.g. wettability of the surface, mechanical resistance properties, surface roughness or nano- and micropattern. As described by Bacakova and co-authors, the advantageous geometrical conformation, physical and chemical properties of the surface of artificial materials have a direct influence on cells behavior during the TE regeneration [38]. Signaling molecules are often incorporated into the scaffold or added to the culture medium during *in vitro* cell culture.

However, from an engineering point of view, scaffolds creation is the greatest challenge, since it is responsible for the microenvironment for cells attachment, spreading, and differentiation. Furthermore, the scaffold acts as the reservoir of signaling molecules that ensure the specific tissue regeneration behavior [3,39]. As recognized, cells possess the ability to sense and respond to mechanical signals from their surroundings. In a living organism, cells are elements of tissue whose stiffness may be as low as ~0.1 kPa for neuronal tissue, but as much as ~1 MPa for soft cartilage or bone [40,41]. As observed Newman et al., low-stretch type I collagen-based scaffolds with low stiffness (< 1 kPa) can promote adipose cell proliferation [42]. In other work by Leipzig and Shoichet, [43] it was proven that photo-crosslinked methacrylamide–chitosan (MAC) hydrogels with stiffness less than 1 kPa favored neuronal and astrocyte differentiation, respectively. Another study, carried out in 2015 by a group of scientists from Ireland, [44] showed that collagen–hyaluronic acid (CHyA) scaffolds with a compressive modulus of 0.5 kPa and pore size in the range 94–300 μm can stimulate the proliferation of mesenchymal stem cells, chondrogenic gene expression, and cartilage-like matrix deposition. Other example of mechanosensitivity of the cells was presented by a Japanese group of researchers [45], herein chondrocytes. The authors synthesized and characterized the properties of gelatinous scaffolds with controlled pore structure and compressive moduli ranging from 0.5 to 6 kPa. While soft scaffolds (about 1 kPa) underwent cellular contraction, stiff scaffolds resisted contraction and enabled significantly higher cell proliferation. The opposite situation was observed with respect to the bioprinted 3D porous scaffold composed of alginate–gelatin scaffold and human mesenchymal stem cells (hMSCs) [46]. The authors observed that after a long-term *in vitro* experiment (42 days), significantly more mineralized tissue was formed in soft scaffolds (0.66 ± 0.08 kPa) than in stiff scaffolds (5.4 ± 1.2 kPa). In addition, investigations indicated a higher DNA content, enhanced ALP activity, and stimulated

osteogenic differentiation of human mesenchymal stem cells (hMSCs) for soft scaffold [46]. Thus, mechanosensitivity, understood as the ability to transform a physical stimulus into a biochemical signal plays a key role in the process of cells spreading, cells differentiation, and migration. Recently, scientists try to mimic the natural environment of cells similar to the tissues of the human body [47]. Previously, researchers used flat 2D cell cultures grown on a plate to study cell culture *in vitro*. Mostly because such models are simple, cost-effective, and easy to proceed with. However, these methods possess very serious disadvantages which exclude them in modern TE applications. First of all, 2D culture creates an unfavorable oxygen gradient, which in practice means deprivation of access to oxygen for inner cell layers and is prompted for cells necrosis. A similar behavior is observed for nutrient diffusion. Finally, a flat 2D environment is inconsistent with the naturally observed cells spreading on the three-dimensional extracellular matrix. Therefore, 3D porous scaffolds for cell cultures have become more popular in recent decades because they are more physiologically relevant, allow free movement of oxygen and nutrients, and better represent *in vivo* tissue [48,49]. Moreover, it is worth to highlight that scaffold is crucial for the cultivation of so-called adherent cells. They need to have an appropriate surface for differentiation and proliferation. In addition to TE, the three-dimensional scaffolds found application in modeling disease mechanisms and discovering drug therapeutics. Cell cultures made in this way can be used to screen for small molecules of drugs or genetically manipulated to understand disease pathways. Compared to flat 2D cultures, three-dimensional cultures predict more accurately the efficacy or toxicity of drug treatment onto cells culture [50].

Currently, tissue engineering assumes two scenarios such as cellular (*in vitro*) and acellular (*in vivo*) strategies. In the cellular approach, cells are seeded on a 3D scaffold containing cell signaling stimulators (like growth factors or sustainable surface properties of the scaffold) followed by *in vitro*

culturing of the cells. Then, the engineered scaffold is implanted at the defect site *in vivo* as a support for the generation of new tissue. In the second scenario, the 3D scaffold is implanted directly into the damaged area *in vivo* without seeding any cells. The new tissue is regenerated by infiltration of innate cells [34]. From a clinical point of view, the selection of the source of the cells is a very important stage of injury success. In the ideal case, cells are dived directly from the patient's body or from his family members.
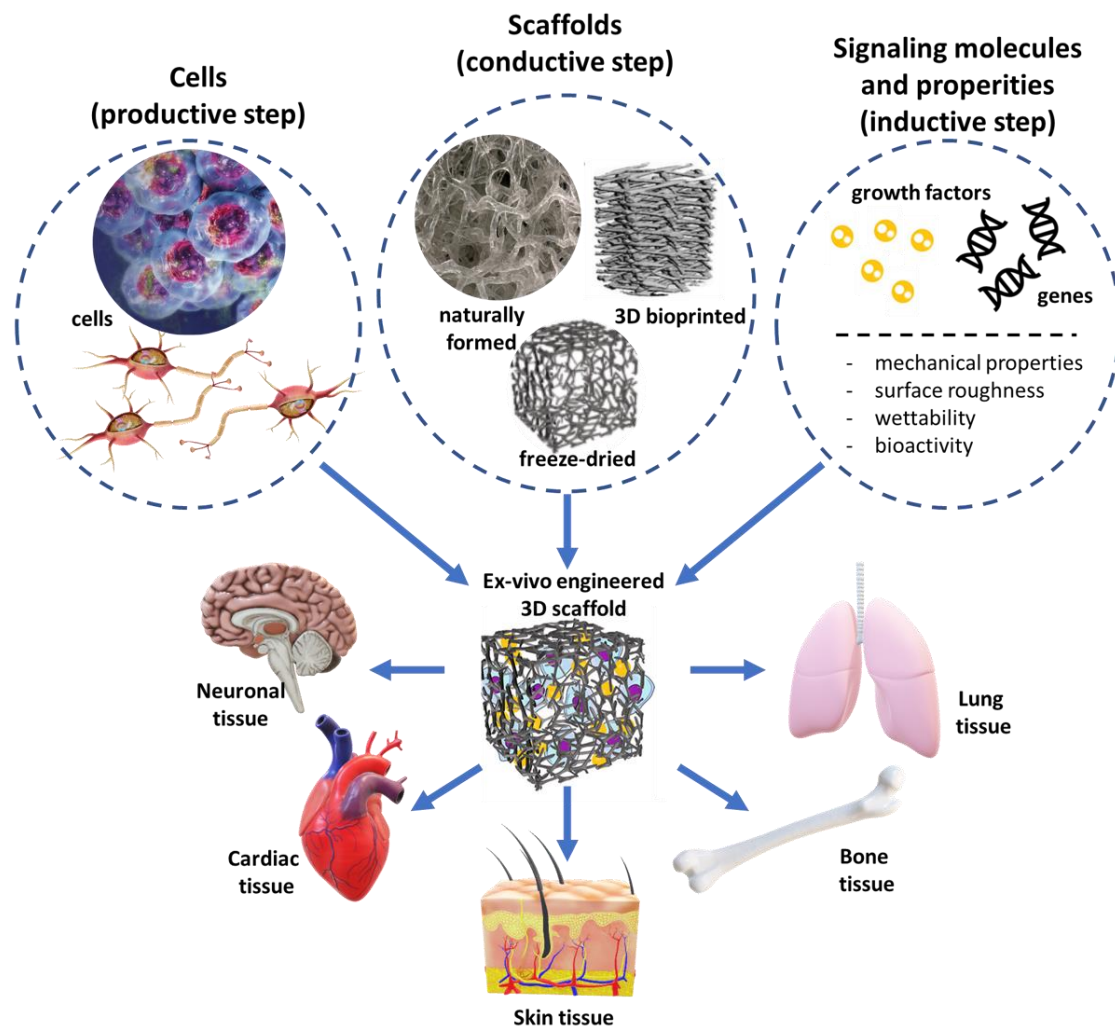
Figure 2. Basic schematic concept of tissue engineering and major barriers, based on [39,50–52].

However, obtaining a pure cell line by passaging is very long and difficult due to its multistage. Thus, unique properties of stem cells are mostly used here. However, on the laboratory scale, for the development of new scaffold

biomaterials, commercially available cell lines are used, omitting the step of obtaining them from the recipient.

The ideal scaffold model possesses several requirements and specific properties. On the one hand, it should be biocompatible, immunologically inert, and support the normal functioning of cells and tissues [35]. The most important is biocompatibility because the scaffold cannot exhibit a cytotoxic effect, which consequently leads to cell ultrastructural changes and necrosis. As stated by Litowczenko and co-authors, when biomaterials induce inflammatory response, organisms start to produce a foreign body reaction, which consequently leads to rejection of the implant [35]. On the other hand, scaffolds should have a defined morphology, pore size, mechanical resistance and processability [52]. All the requirements depend mainly on the cell type and the tissue to be regenerated. In this context, it is not surprising that for scaffold manufacturing several different materials are used. Among them, materials consisting of natural and synthetic polymers (e.g. proteins, polysaccharides, glycosaminoglycans, poly(glycolic acid) − PLG, poly(lactic acid) − PLA, poly-ε-caprolactone − PCL, inorganic compounds, such as metals (e.g. titanium, nickel, iron, and its alloys, etc.) ceramics (e.g. zirconia, calcium phosphates, cements (CPCs), etc.), or their composite combinations [3,53,54]. Scaffolds are manufactured in several shapes (depending on the intended *in vitro* cell culture or *in vivo* model). Among others, scaffolds in the form of hydrogels, sponges, fibers, membranes, particles (nano and micro-sized), tubes, or spheres can be distinguished [30,42,44,55–58]. A detailed description of the properties requirements of each scaffold is presented in **Table 1**.

Table 1. Detailed description of the ideal scaffold requirements, based on [52].

Desirable properties	Description
Biocompatibility	Both scaffold and its degradation products should not produce a cytotoxic and immune response.
Biodegradability	In some cases, scaffold should have degradation rates compatible with the new tissue formation.
Pore morphology	Scaffolds should exhibit high porosity to control the adequate diffusion of nutrients and oxygen to all cells, metabolite dispersal, and local pH stability.
Pore size	Pores size is a crucial feature due to cell infiltration and tissue vascularization. The scaffolds must satisfy the condition of providing an empty volume of pores.
Mechanical resistance	The mechanical properties of the scaffold respond directly to the morphology, behavior, and differentiation of the cells (mechano-signaling).
Bioactivity	Scaffolds can act like supports or reservoirs for bioactive and signaling molecules which accelerate tissue regeneration.
Processability	From an economical point of view, a scaffold should be easily processed in a variety of shapes, sizes, and possess low fabrication costs. Moreover, it must be reproducible, scalable, storable, and resistant to sterilization.

Modern strategies of scaffolding production for TE application assume two main paths. First, the creation of the matrices with artificially pre-designed 3D architecture. To this group, scaffolds created by 3D bioprinting [37,59–61], macro-porous hydrogels synthesis [62–64], electrospinning [65–68], freeze-

drying, phase separation, gas forming and others [52] can be included. As Loh and Choong observed, some of them, like gas-forming and freeze drying, do not allow for precise control of the internal scaffold architecture [51]. Recently, as the most accurate and repeatable method, rapid prototyping techniques combined with the use of computer-aided design (CAD) modeling are considered. However, an undeniable disadvantage of these methods is the cost of specialized equipment and the requirements to use harsh solvents. The more detailed description of the technologies for scaffold fabrication is presented in **Table 2**. The second strategy assumes the use of decellularized renewable sources with naturally formed micro-architecture in their original shape [69]. Great examples could be an autogenic or an allogenic extracellular matrix (ECM) [69,70], multicellular organisms skeletons with proper architecture [71–73] or plant-based structure [74]. Decellularization of tissues is commonly carried out by one of the methods in a chemical, physical, or biological (enzymatic) manner [70,75]. In the article by Smith and co-workers [76], authors observed improved osteoinductive capacity in case of aged donors after a comparative analysis of human decellularized bone scaffolds with samples obtained from young donors. This fact has important implications for clinical usability because the osteogenic capacity of a bone scaffold is crucial when ensuring a positive host response, new bone formation, osseointegration, and clinical success. Some decellularized mammalian ECMs are commercially available, e.g. AlloMax®, Strattice®, ReadiGRAFT®, Lyoplant®, Meso BioMatrix®, TissueMend®, OrACELL® or ArthroFLEX® [69]. However, such materials remain controversial due to ethical concerns in some cultural fields, donor-related functionality variations, and high production cost [77]. Thus, the aforementioned drawbacks have prompted a search for new and alternative sources of 3D natural scaffolds, e.g. from invertebrate animals or plants. Mutsenko [78] reported that the isolated chitinous skeleton from the *Ianthella basta* marine demosponge could be successfully used as a scaffold for the

cultivation of human mesenchymal stromal cells (hMSCs). Due to their high biocompatibility, evolutionarily porous design, and simple isolation method, chitin−based scaffolds from marine sponges accelerate interdisciplinary research and interest from the biomedical scientific community.

Contessi Negrini and co-authors [74] developed a method of production of 3D natural scaffolds for regeneration of adipose, bone, and tendon tissue from decellularized plants. The complex analyses and *in vitro* tests proved that the decellularized plant tissues (carrot, apple, and celery) may support human cell adhesion, proliferation, and restore functional human tissues. Thus, depending on the tissue engineering strategy, various biomaterials and processing technologies should be considered to optimize the properties of the scaffolds. For example, surface morphology, mechanical resistance, and physicochemical properties deserve special attention. The diversity of materials and advanced synthesis techniques nowadays allow us to choose an appropriate technology for potential application. However, a fundamental understanding of the nanoscale details of the environment will be crucial for designing biomaterials that mimic the natural ECM. Many features of local parameters have profoundly influenced cell adhesion, proliferation, differentiation, and viability. The successful outcome of the exploitation of biomaterials in biomedical applications will require multidisciplinary cooperation between scientists from different research areas and is still a challenging task.

2.1.2. Bioscaffolds in tissue engineering applications

Among the numerous materials used to fabricate scaffolds, polymers are the most popular because of their vast diversity of properties and bioactivity [79]. The basic division of these group assumes the presence of two, natural and synthetic polymers.

Table 2. Examples of studies on selected strategies for design and fabrication of 3D scaffolds for TE application.

Technology	Material	Biological assessment	Outcomes	Ref.
Freeze-drying	Carbon Nanotube/chitosan(CS)/hydroxyapatite(HA) composite	Human osteosarcoma cell line, MG-63	The negatively charged functional groups on the scaffolds attract calcium cations and provide self-assembly of bone-like HA	[80]
	Hydroxyapatite (HA)/gelatin (GEL) composite	Osteoblast-like cells (SaOS-2)	Excellent cell attachment, migration, and penetration into the porous structure	[81]
	α-chitin hydrogel/nano-hydroxyapatite (nHA) composite	Human osteosarcoma cell line, MG-63	Cytocompatible scaffold promoting cell attachment and spreading	[82]
	Silk fibroin/β-tricalcium phosphate (TCP) composite	Human adipose stem cells (hASCs)	High interconnectivity of micropores, significant proliferation and differentiation	[83]
	Collagen(Col)/denatured collagen (DCol)	Rabbit chondrocytes	Better redifferentiation of chondrocytes by Col scaffolds than DCol scaffolds	[84]
	Silk fibroin (SF)	n.d.	Pore sizes ranging 4 - 77 μm. Elastic modulus ranging 100 - 900 kPa	[85]
	Poly(ε-caprolactone) (PCL)	Osteosarcoma-derived cell line (SAOS-2)	Less orthogonal elements, indicate better mimicking ECM	[86]

Table 2. cont.

3D bioprinting	Poly(ε-caprolactone) (PCL)/calcium phosphate (CaP) composite	Human bone marrow mesenchymal stem cells (hMSCS)	Adherence of hMSCS initially higher in coated than pristine PCL, osteogenic differentiation almost 3 times higher in mineralized scaffolds	[61]
	Gelatin methacrylamide (GelMA)/methacrylated hyaluronic acid/HAp composite	Human adipose derived stromal cells (hASCs)	Excellent printability, intense matrix formation	[87]
	α-tricalcium phosphate (TCP)/collagen composite	Mouse osteoblast precursor cells (MC3T3-E1)	Physical and bioactivities properties of scaffold demonstrating significantly higher cellular activities than control	[88]
	Fibrin/wollastonite(CaSiO$_3$) composite	Rabbit bone marrow mesenchymal stem cells (BMSCs)	BMSCs adhered and showing well spreading on the scaffold but without apparent proliferation *in vitro* after 28 days	[89]
	Hyaluronic acid/hydroxyethyl-methacrylate-derivatized dextran (dex-HEMA)	Chondrocytes	Excellent viability was observed for encapsulated chondrocytes	[90]
	(GelMA)/ chondroitin sulfate aminoethyl methacrylate (CS-AEMA)/ hyaluronic acid methacrylate (HAMA)	Bone marrow-derived human mesenchymal stem cells (BM-MSCs)	Enhanced viability and chondrogenic differentiation of BM-MSCs	[91]

Table 2. cont.

	Matrigel™/alginate	Mice for *in vivo* analysis of vessel formation	New generation of the smart scaffold with vascularization potential	[92]
	Gelatin/fibrinogen/HA composite	Myogenic progenitor C2C12	Multicellular construct aimed at mimicking the myotendinous	[93]
Electrospinning	PCL/collagen composite	Human endometrial stem cells (hEnSCs)	Higher wettability, attachment, proliferation rates of hEnSCs on PCL / collagen scaffolds than single phase PLC	[94]
	PCL/Silk fibroin (SF) composite	Human BJ fibroblast cells	Presence of silk fibroin enhanced scaffold wettability and cells proliferation	[95]
	Polylactic acid (PLLA)	Mouse fibroblasts (NIH3T3)	Additional ultrasonication increased scaffold thickness and improved cell infiltration	[96]
	Poly (L-lactic acid)-*co-poly*(ε-caprolactone)/ collagen	Nerve stem cell (C17.2)	The nanofibrous scaffold mimics nerve EXM and has great potential as a substrate for nerve regeneration	[97]
Phase separation	Cartilage-derived ECM/PLGA/β-TCP/collagen composite	Rabbit bone marrow mesenchymal stem cells (BMSCs) and rabbit *in vivo*	The compact layer significantly enhanced the biomechanical properties of the scaffold *in vitro* and the regeneration of osteochondral tissue *in vivo*	[98]

n.d. – no data

Recently, biopolymers were widely used for tissue engineering and regeneration of soft and hard tissue due to their extraordinary properties. As described, their good biocompatibility, high porosity, renewability, and ecological safety predispose them to become real competition with synthetic ones. Natural polymers obtained from microorganisms, plants, and animals are similar to human macromolecules [35]. Thus, the risk of toxicity, chronic inflammatory response, and immunological reactions frequently observed with the products of degradation of synthetic polymers are not observed here [3]. Due to their thermoplastic properties, synthetic polymers were recognized as cheaper and more processable than natural ones. Moreover, their excellent mechanical resistance and controllable degradation made them even more attractive. Furthermore, the conductive and piezoelectric properties of some synthetic polymers make them promising in future electrically sensitive tissue engineering applications, such as nerve or heart muscle regeneration [35]. However, the most serious limitation is the lack of cell-binding sites due to their hydrophobicity. Nevertheless, synthetic polymers are attractive as composite components or matrices for functionalization by bioactive signaling molecules. Therefore, naturally derived biopolymers were attracting the interest of scientists all over the world [46,49,99,100]. Nowadays, they are one of the most extensively studied group of materials, and the literature is rich in research papers dating back to the turn of the 18th and 19th centuries [101,102]. Based on the Scopus database search analysis, up to September 2022, more than 40,000 records were detected containing the phrase "*biopolymers*" and the trend is growing especially in the last ten years (**Figure 3**). The classification of natural biomaterials involves several groups, such as protein-based biopolymers (e.g. collagen, gelatin, silk), polysaccharide-based biopolymers (e.g. cellulose, chitin, chitosan, alginate, gellan gum and derivatives), and decellularized tissue-derived biomaterials (decellularized cartilage, blood vessels, skin and other) [3,99].
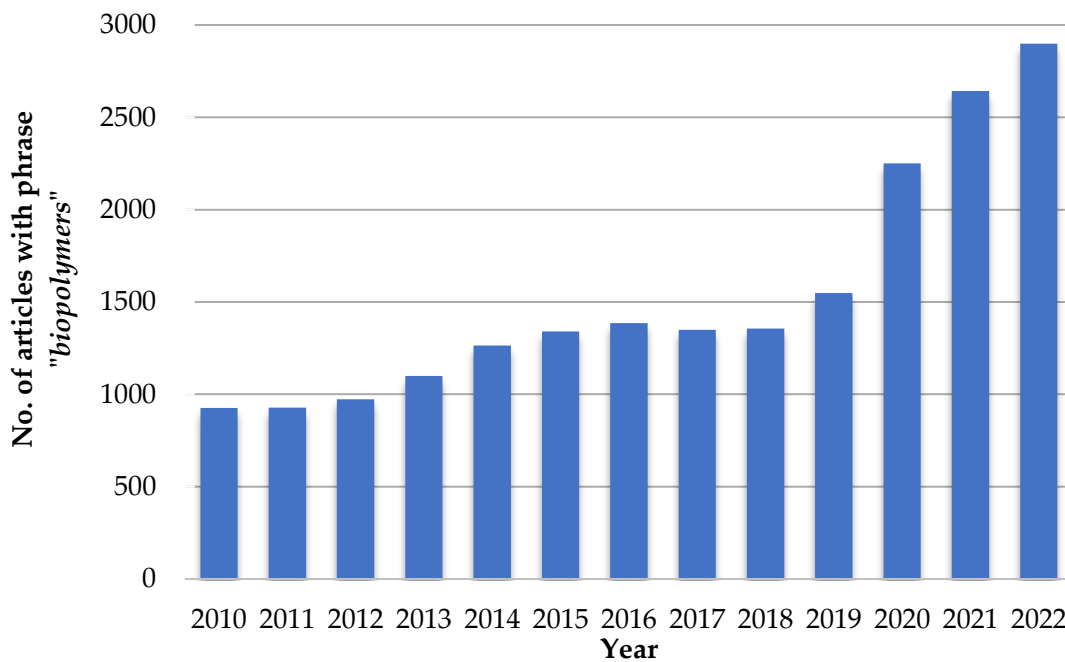
Figure 3. Search results for the phrase "biopolymers" in years 2010 - 2022, according to the SCOPUS database, on date 09/2022.

The most detailed overview of popular biopolymers for scaffold fabrication with their main advantages and limitations is briefly described in **Table 3**. Bioscaffolds can be fabricated in two different ways. First assumes use of proteins or polysaccharides from living organisms, dissolution, and fabrication of assumed shape as described in Section 2.1.1. The second very promising method of 3D bioscaffold fabrication is decellularization. These processes could be carried out by one of the several methods, but commonly three of them are used: chemical (using solvents), biological (using microorganisms), or enzymatic (using enzymes) [75]. As described by Wu and co-authors, decellularized matrices are morphologically appropriate and ensure a biochemical microenvironment for cell proliferation and differentiation [103]. Furthermore, as compared to allogeneic and xenogeneic transplantations, decellularized scaffolds indicate a lower risk of immunogenic response risk [74]. However, due to ethical concerns and limited sources, scientists are looking for alternative matrices, for example, made of naturally prefabricated structural polysaccharides such as chitin [29,30,104–108].

Table 3. The most commonly used biopolymers for the biomedical engineering field; their main advantages and limitations, and current potential application.

Type of biopolymer	Example	Advantages	Limitations	Application	Ref.
Polysaccharides	Chitin	Non-toxic, bioactive, biodegradable, thermostable, low immunogenicity	Insoluble in conventional solvents, difficult to process	Cardiac, skin, neuronal tissue regeneration, wound healing	[29,30,33,100,107,109,110]
	Chitosan	Biocompatible, hemostatic active, biodegradable, antibacterial	Low-mechanical resistance, may cause allergic reactions	Cardiac, skin, liver, and muscle tissue engineering, wound healing	[80,111,112]
	Alginate	Non-toxic, biocompatible, biodegradable, non-immunogenic, and hydrophilic	Limited strength, toughness, difficulty in controlled gelation	Bone, skin and neuronal regeneration	[35,46,113]
	Hyaluronic acid	Easy to biodegradation and esterification, processable, biocompatible	Rarely may cause allergic reactions	Cartilage regeneration, lip filler in plastic surgery	[90,114,115]
	Cellulose	The most abundant polysaccharide worldwide, low-cost, easy to modification	Not degradable by humans	Skin repair wound dressings, drug carrier	[115–118]

Table 3. cont.

Proteins	Spongin	Promote bone mineralization, ability to hydrate to a high degree, interconnected pores	Significant adhesion of bacteria, requirements of harsh solvent for purification	Bone tissue regeneration	[14,119,120]
	Collagen	Biodegradable, ECM mimicking, poorly immunogenic, bioactive	Poor mechanical properties	Skin, vascular, cartilage, bone regeneration	[35,42,120–122]
	Gelatin	Low immunogenic, inexpensive, water-soluble, bioactive	Poor mechanical properties	Cartilage, adipose neuronal regeneration	[35,45,110]
	Conchiolin	Exhibit similar properties to collagen, biodegradable, non-toxic	Difficult to isolate	Wound healing, cartilage, and hard tissue engineering	[110,123]
	Elastin	Bioactive, good biophysical and biomechanical properties	Water-insoluble, difficult to manipulate *in vitro*, risk of contamination, risk of inflammation	Skin, tendon, liver regeneration	[35,42]
	Fibrin	Biodegradable, ECM mimicking, low immunogenic, biocompatibile	Poor mechanical properties, expensive, risk of contamination	Retina, cartilage, vascular, neural regeneration	[35,89]
	Silk Fibroin	Low immunogenic, high tensile strength, excellent mechanical properties, low-cost	Weak, brittle as scaffolds	Hepatic, neuronal regeneration	[57,95,124]

2.1.3. Bioinspired materials and their importance in environmental protection

The environmental pollution of water and air is a very serious and complex problem that consists of many factors [125]. Mostly it is related to non-compliance with standards by many countries or companies, which results in contamination of the natural environment, rivers and lakes. Another problem is strictly related to an increase in human population, which results in increased industrialization and unplanned urbanization [126]. As a consequence, the quality of water resources is deteriorating due to the accumulation of dangerous compounds. In general, pollutants can be classified as organic, like: dyes [20,127–130], pharmaceuticals [131–133], endocrine-disrupting chemicals (EDCs) [134–138], pesticides [139], inorganic: hazardous metals, sulphates, nitrates [140,141], radioactive compounds [142] and bacterial contaminations [143,144]. It should be stated that some of them are persistent and might have a negative effect on human beings and environment (ecologic catastrophe) [145]. An appropriate example of ecologic catastrophe can be largest oil spill in history which happened in Mexico Gulf in 2010 [146]. This tragic accident caused 4.9 million barrels of crude oil escaped into the waters [147]. This incident has long damaging impact to marine life, coastal wetlands, water transport, fisheries industry, tourism, and others [146].

Nowadays, several wastewater treatment methods are required to control and eliminate the risk of pollution. Herein, it is worth to highlight: biological treatments [148], enzymatic conversion [25], membrane processes [149], photocatalysis [150,151], reverse osmosis [152], ion exchange [153], electrodialysis or adsorption [154]. However, several of them are very complex and expensive, such as reverse osmosis, electrodialysis, electrolysis, and ion exchange. Furthermore, the drawbacks associated with these processes include high energy consumption, high cost of regeneration, generation of toxic sludge, and high reagent requirements [154]. The most common technologies used

by researchers and companies for the removal of dangerous pollutants from wastewater are described in **Table 4**.

Table 4. Examples of commonly used methods to remove water pollutants, based on [154].

Technology	Advantages	Disadvantages
Chemical precipitation	Simple process Economically feasible	Sludge creation High maintenance cost Sludge utilization requirements
Coagulation-flocculation	Bacterial inactivation capability Simple, low-cost	Reagents consumption Sludge utilization requirements
Enzymatic bioconversion	Highly efficient Possible reusability of biosystems	High cost of enzymes Enzyme immobilization requirements
Adsorption	Wide spectrum of pollutants removal Highly efficient Fast kinetics Easy operating Low-cost	Performance depends on the type of adsorbent and pollutants
Membrane filtration	Low waste emission Low chemical's consumption	Limited membrane "life" High operating costs

Considering the methods presented above, adsorption seems to be especially interesting. This method makes it possible to use even waste materials in the native and modified form as sorbents. The use of natural materials for environmental protection, e.g. as green adsorbents or enzyme supports, is prompt because of their renewability, low cost, and well-developed chemical structure [155,156], see **Figure 4**. Moreover, adsorption could be combined with other methods to improve removal efficiency e.g. such as enzymatic conversion [25]. In the next part of this chapter, several of a natural materials will be described as potential adsorbents.

Figure 4. Examples of organic and inorganic biosorbents of water pollutants, based on [157–160].

Lignin and its derivatives. Lignin is an example of a natural waste material that is produced in large quantities in wood processing. This biopolymer is part of the wood cell together with cellulose and hemicellulose. The percentage of lignin in lignocellulosic raw materials remains at an average

level of 15–30% [161]. The quantity and composition of lignin are strictly related to the origin of the plant species (i.e. conifer wood, deciduous wood, grass) [162]. However, in all cases, lignin is composed of three main components, coniferyl, sinapyl and *p*-coumaryl aromatic alcohols. The fundamental role of this biopolymer is to provide mechanical resistance to plants and protection of water loss [163]. The annual production of lignin as a by-product of the paper industry varies by about 50 million tons. However, a significant part of it is still used in energy production processes [164]. Recently, lignin was recognized as an effective hazardous metal sorbent due the presence of several functional groups [165]. As described by Dizhbite and co-authors [166], modification of lignin *via* hydrolysis induced by quaternary ammonium salts can result in a notable enhancement of sorption efficiency of organic contaminants. Moreover, the authors indicate that the amination of lignin with epoxy amines enhance its sorption activity toward hazardous metals. As described above, aminolignins possess a high sorption capacity for compounds such as bile acids and cholesterol. Thus, satisfying sorption properties of lignin and its derivatives predisposed them for use in the environmental protection field [166]. It is worth highlighting that lignin can also be used as a component to produce novel hybrid materials. Advanced functional silica–lignin or chitin–lignin material were used as sorbents for the removal of nickel(II) and cadmium(II) ions from aqueous solution [167,168].

Cellulose and its derivatives. Cellulose is the most widely distributed and important organic compound produced worldwide [116]. These polysaccharides can be found as a fibrous, stiff, water insoluble material which is typically present in cellular walls of plants, particularly in case of cells found in stalks or trunks, as well as in microorganisms and in algae [169]. However, the main source is wood, where cellulose constitutes between 38 to 50% of its cells [162]. Cellulose mainly consists of β-D-glucopyranose units linked by

β-1,4-glycosidic bonds, established by a simple polymerization of glucose residues [116]. Because of the presence of several hydroxyl groups that hold the cellulose chains together, these biopolymers exhibit a high degree of crystallinity, low solubility, and poor degradation *in vivo*. It is one of the most serious limitations of cellulose, for example in biomedical applications. However, on the other hand, the presence of functional group opens a wide range of modification possibilities. Chemical modification of the cellulose-based sorbents improves their adsorption capacity by increasing active binding sites and incorporation of functional groups that favor higher uptake of pollutants [126]. As an example, methylcellulose, hydroxypropylcellulose, and carboxymethylcellulose could be mentioned [116]. As showed by Wei et al., carboxymethylcellulose (CMC) can be used as a binding site for hazardous metal cations, like Cd(II), As(III), Pb(II), and others [170,171]. Further, chemical methods of cellulose modification include esterification, halogenation, etherification, oxidation, grafting [171]. The abundance of cellulose and its derivatives makes them one of the cheapest sustainable adsorbents today [126,172,173]. Recently, Garba and co-authors indicated the importance of microcrystalline cellulose (MCC) as a good candidate for textile dyes adsorption, encourage their renewability, nontoxicity, low density, well-developed surface area, strength, fibrous nature, high mechanical strength, water insolubility, and biodegradability [172]. Another solution could be to use cellulose as a composite component. Nguyen and others [174], synthesized cellulose–methyltrimethoxysilane (MTMS) material for cleaning crude oil spills. The aerogel achieved high sorption capacities of 18.4 g/g, 18.5 g/g, and 20.5 g/g for different types of crude oil at 25 °C, respectively.

Collagens and spongin. Collagens represent a superfamily of long-lived extracellular matrix (ECM) structural proteins of key evolutionary significance and could be found in both, invertebrate and vertebrate taxa [120]. Commercial

sources of these high molecular weight proteins are of bovine and porcine origin, but recently marine organisms, such as fish, became a very intriguing source [122]. Collagens existing in several types, depending on their specific organization in the tissue (**Table 5**).

In general, collagens **consist of** polypeptide chains composed of repeating triplet units Gly-X-Y of glycine and two other amino acids. However, proline, hydroxyproline, or their isomorphs are the most widespread [122]. Due to the fibrous microarchitecture, collagens were successfully applied as dyes adsorbents.

Table 5. Representation of the most widely distributed collagen types with their sources, based on [122].

Type of the collagen	Source
Type I	Bone, dermis, tendon, ligaments, cornea
Type II	Cartilage, vitreous body, nucleus pulposus
Type III	Cartilage, vitreous body, nucleus pulposus
Type IV	Basement membranes
Type V	Often co-distributes with type I collagen, especially in the cornea.

For instance, Marandi and others [175], synthesized collagen-based hydrogel nanocomposites as sorbents for the removal of Methylene Green (MG) and Crystal Violet (CV) from aqueous solutions. The authors determined several process parameters, such as the initial concentration of the dye solution, pH, or contact time, to achieve maximum removal effectiveness. The experimental data showed that more than 90% removal efficiency was achieved within the initial ten minutes. Another study, prepared by Gu and co-authors [176], showed that Fe(III)-dopped collagen fibers (FLCF) were successfully applied in the adsorption of anionic dyes (such as Acid Yellow 11, Reactive Blue 19, or Direct

Yellow 11). As observed, lower pH leads to a higher adsorption efficiency because the adsorbent is more positively charged. The possibility of creating collagen-based composites was described by an Iranian group of scientists, which synthesized collagen-g-poly(acrylic acid-co-N vinylpyrrolidone) combined with $Fe_3O_4@SiO_2$ material. The adsorption affinity of this magnetic nanocomposite hydrogels was studied and the removal efficiency of about 93% for Methylene Blue, 96% for Brilliant Green, and 89% for Rhodamine B, at a concentration of 50 mg/L and at pH 7, was achieved [177].

In recent years, poriferan-derived collagen-related protein, called spongin, was extensively developed as functional material [19,20,127,178]. In contrast to collagen or keratin, the chemistry and molecular biology of spongin remain unknown. One of the probable hypotheses assumes that the horny matter of sponge is closely analogous to silk-related proteins. However, as stated, spongin contains additional halogens in the structure [120]. As described by Croockewit, the chemical formula of the horny matter is as follows: $20(C_{39}H_{62}N_{12}O_{17}) + I_2S_3P_{10}$ [179]. Nevertheless, in addition to various hypotheses, spongin remains the last enigmatic proteinaceous biopolymer worldwide [120]. Spongin creates structural skeletons of diverse bath sponges, like *Hippospongia communis*. These materials were used since ancient times to paint, bathe, and clean, as a filler component for a battle helmet, as medical equipment or as a container for drinking water [180]. Recently, spongin has found several advanced applications in environmental protection. Their complex hierarchical network composed of protein-based fibers and well-developed internal surface area (between 25 and 34 m^2/g) make this material especially interesting as a sorbent [181]. As an example, Norman and co-authors investigated spongin as an adsorbent of anthocyanin dye (adsorption capacity q_m = 1413.9 mg/g) [127], Rhodamine B degradation (q_m = 83.36 mg/g) [22] or C.I. Natural Red 4 (q_m = 18.55 mg/g) [128]. In another study, Szatkowski and co-authors [182] used

the chemically and thermally stable spongin, for the development of the next generation of biologically inspired functional composite. Obtained 3D spongin-TiO$_2$ material showed high efficiency of C.I. Basic Blue 9 dye removal through both adsorption and photocatalysis (removal efficiency of 85.4%).

Keratin and keratin-based composites. Keratin is an important structural protein widely distributed in nature as the integument of vertebrate organisms. Keratin-based materials were determined as fiber-reinforced composites and belong to a group of insoluble proteins known as intermediate filaments (8–10 nm). As determined, keratins are not soluble in conventional protein solvents and are not degradable with trypsin or pepsin [183]. Depending on the origin, they represent different functions, proteins content, and morphologies. However, keratins can be divided into two classes such as epithelial and trichocyte keratins, commonly known as soft and hard keratins, respectively [184]. They are found in a variety of biological fibrous materials, including sheep's wool, human hair, bird's feathers, and the nails and horns of mammals. Due to their abundance and well-developed chemical structure, keratin-based materials found dozens of applications for pollutants removal [185–187]. The mechanism assumes a combination of both physisorption and chemisorption [184]. Physisorption implies the trapping of contaminants in a porous network or on the surface of keratin materials by weak interactions. Chemisorption is based on the functional groups' interactions, including peptide bonds and side chains of amino acid residues. They act like active chemical sites for the removal of pollutants, such as metal ions and organic-based contaminants. For example, Zhu and co-workers prepared a keratin-based adsorbent with excellent adsorption performance for Reactive Black 5 (RB5) removal [187]. As described, the adsorption capacity was really high (550 mg/g) and removal efficiency was equal 95.3%. Moreover, the material had outstanding regeneration and recycling ability as a result of its

polymeric mechanical reinforcement. Another interesting solution was the enhancement of adsorption capacity by creating keratin-based composites with active oxides, for example TiO$_2$ [188] or GO [189]. In the study by Khosa and Ullah [185], *in-situ* modification of the keratin biopolymer was performed using selective dopants such as poly(ethylene glycol) (PEG) diglycidyl ether, poly(*N*-isopropyl acrylamide) (PNIPAM), allyl alcohol (AA), and TrisilanolCyclohexyl POSS. It was proposed that AA and POSS modified keratin exhibited high removal efficiency toward As(III), up to 11.5×10^{-2} and 11.0×10^{-2} mg/g, respectively.

Carbonized materials. Recently, the use of adsorption as a technique for wastewater decontamination is economically feasible because of the availability of biomass as adsorbents, their high adsorption capacities, and almost zero cost. However, additional activation of biomaterials by carbonization was recognized as a highly efficient method for improving the sorption properties. Such an activation enhances surface area of the adsorbent and allows for the interaction of pollutants with groups bound to the edges of graphite-like layers (such as carboxyl, carbonyl, phenol, quinone) [154]. In the work by Benzekri and co-authors [190], waste material such as olive stone was transformed to an efficient granular activated carbon (AC) to remove Methylene Blue (MB) dye from aqueous solutions. The activation process was performed in two steps: (i) impregnation of raw material with 50% phosphoric acid at 170 °C for 2.5 h and (ii) physical activation of a sorbent at 750 °C using a carbonization oven. The material obtained had specific surface area estimated at 1029.2 m^2/g. The Langmuir model was found to correctly describe the sorption of MB which resulted in adsorption capacity of 107 mg/g. As estimated by Suhas and others, cellulose can be a promising precursor for the production of carbonized sorbents with appreciable surface area (~1300 m^2/g) and total pore volume (~0.6 cm^3/g) [191]. The utilization of cellulose-based materials for the

production of ACs, like coconut shells, bamboo, rice husks, corn stalks, cotton fibers, vegetable leaves, wood, and others, is economically feasible and enables their activation. A study of Kadirvelu [192] showed the high application potential of activated carbon obtained from coconut coir pith as an adsorbent of Cd(II) from an aqueous solution. The adsorption capacity of 93.4 mg/g was calculated from the Langmuir isotherm. Other studies by the same author [193] assumed to use *parthenium* plant waste as activated carbon precursor to eliminate Ni(II) from aqueous system. As a result, the adsorption capacity of 54.35 mg/g was achieved. The review article by Zhang et al. describes and compares the adsorption behavior of different types of carbonaceous adsorbents (granular, fiber, and nanotube-based). Authors indicate correlations between the structural parameters of adsorbents and their adsorption capacities towards organic dyes. As observed, that adsorption capacity could be projected by the surface areas of these materials, much more than their structural type [194].

Calcium carbonate. Inorganic solid-phase adsorbents have received a great attention in recent years. Calcium carbonate show several properties of an ideal adsorbent. It is inexpensive, widespread in nature, harmless to humans, and environmentally-friendly [195]. Calcium carbonate is commonly distributed in four polymorphic forms: calcite, aragonite, vaterite, and amorphous. However, the most stable crystalline form is calcite. Calcite belongs to the hexagonal crystalline system and could be found, for example, as the main component of mollusks shells [100,196,197]. These polymorphs are also heat and corrosion-resistant and are usually used in the metallurgy, cement, paper, and glass industries. As determined, the chemical composition of carbonates, morphological characteristics, particle size, and polymorphism, strictly determine their sorption capacities [195]. However, large-scale production of porous superstructure formation of $CaCO_3$ remains a challenge.

Yamanaka and co-authors [198], developed mesoporous calcium carbonate and applied it as a formaldehyde vapor adsorbent. As described, the material obtained possessed a high surface area (207.3 m^2/g) and was able to adsorb 8.2 mg/g of formaldehyde. Authors observed, that in formaldehyde vapor adsorption, vaterite was more efficient in comparison to calcite. A recently published study by Lin and others [195], showed the practical potential of oyster shells as precursors to prepare vaterite-based hazardous metals adsorbents. The experimental results showed that prepared vaterite microspheres exhibited various removal efficiencies for, Pb^{2+} (99.9%), Cr^{3+} (99.5%), Fe^{3+} (99.3%), and Cu^{2+} (57.1%). The authors described the removal mechanism as an ion-exchange reaction between Ca and the hazardous metal ions, resulting in recrystallization. Qin and co-authors synthesized chitin−$CaCO_3$ aerogel material for Congo Red (CR) adsorption [199]. Thanks to the nanostructure of $CaCO_3$ and the active groups of chitin, the authors obtained a maximum adsorption capacity that was approximately 266.4 mg/g.

2.2. Chitin − general overview

Chitin ($C_8H_{13}O_5N)_n$ is an ancient biopolymer recognized as the second most abundant organic compound worldwide with an annual production established at 10^{12}–10^{14} tons [200,201]. From a chemical point of view, this fibrous material is a structural amino polysaccharide composed of *N*-acetylglucosamine units linked by β-(1,4) glycosidic bonds [202]. However, because alkali treatment is required during its isolation, commercially available chitin is a copolymer of *N*-acetylglucosamine and glucosamine units [203]. These structures are very similar to the cellulose, and only one difference can be observed − the presence of *N*-acetylamino group at C-2 position instead of a hydroxyl group (in cellulose), see **Figure 5**. Chitin possesses a natural tendency to form microfibrils (also known as rods or crystallites) of ~3 nm in diameter, that are stabilized by intermolecular hydrogen bonds formed

between the amine and carbonyl groups. Its peritrophic matrix microfibrils can reach 0.5 μm in length and are frequently grouped in bundles containing parallel groups of ten or more single ones [204]. Naturally, chitin plays a crucial role as an integral part of the exoskeletons of invertebrates and the crystal−directing templates during biomineralization [205]. Thus, in nature, chitin does not occur in pure form, but as nanoorganized chitin proteins, chitin pigments, or chitin−minerals composite biomaterials [73].
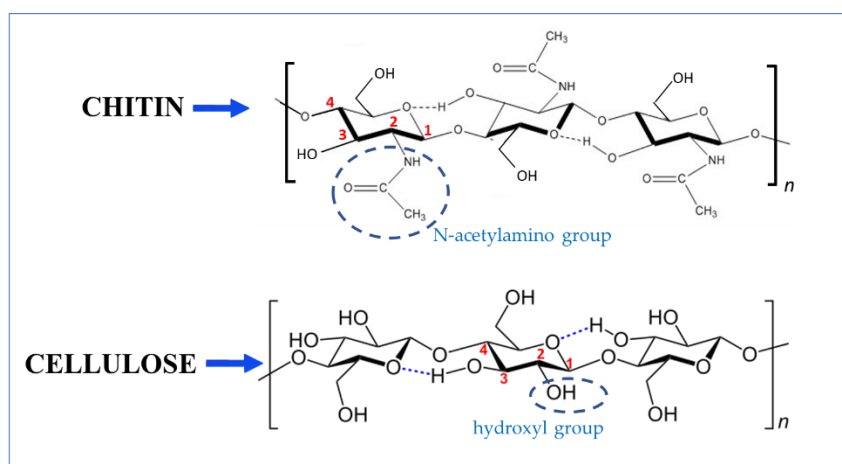
Figure 5. Differences between the chemical structure of chitin and cellulose.

Chitin can be well preserved throughout geological time. Their ancient origin was proved in fossil filaments of fungi established as 810 to 715 million years (Myr) old dolomitic shale [206] or 505 Myr old marine sponge fossil *Vauxia gracilenta* [207] from Burgess shale. The first mentions about chitin date to the ancient centuries. For the first time, the Greek word *visώm* (kithon), meaning "*sheath/tunic*" was used by Aristotle (384–322 BC) in his main work on animal biology "*Historia animalium*" [208]. However, the historical discovery of chitin is usually attributed both to the French chemist Henri Braconnot in 1811, who discovered the presence of an alkali-resistant substance in fungi structure and to Auguste Odier in 1823, who isolated hornlike material after KOH treatment of elytra beetle cuticle [209]. The first named the insoluble residue as *fongine/fungine* [210,211]. However, the name *chitine* was proposed by Odier

[212]. He observed that after alkali treatment the retained transparent substance represented ~25% of the initial weight of the elytra. Odier mentioned that chitin contains carbon and nitrogen but in very low value as compared to other animal substances such as hairs and horns. However, the first known scientific experiments were probably carried out by the English chemist Charles Hatchett, who reported the presence of "*a material particularly resistant to usual chemical*" during the remineralization of molluscan shells in 1799 [101]. The year 1859 is a particularly important date for the development of chitin, when the French physiologist Charles Rouget described the deacetylation of chitin through its boiling in concentrated potassium hydroxide, during which chitosan was obtained [209]. The following years brought mainly research on the occurrence of chitin in other species and attempts to determine its chemical structure [209]. However, in the turn of XIX and XX centaury Fränkel and Kelly [213] isolated *N*-acetyl-D-glucosamine as the main structural unit of chitin by its gentle hydrolysis at room temperature using 70% sulfuric acid. The twentieth century was mainly marked by the development of advanced research methods such as X-ray diffraction, which allowed for more in-depth understanding of the elemental cell crystallography of this biopolymer. Moreover, transmission electron microscopy (TEM) and scanning electron microscopy (SEM) were useful for understanding its ultrastructure and nanoscale, microscale, and macroscale organization. Other breakthroughs occurred in the 1970s, when chitin and its derivatives were intensively researched because of their beneficial properties and attempts were made to find the first application in paper, textile, photographic and other industries. The general overview of the most important points in the history of chitin is presented in **Figure 6**. Surprisingly, the 21st century brings new discoveries of chitin, for example, among Porifera (sponges), by the Ehrlich research group in 2007 [214]. For more details, see its almost 220-year history description in a review article prepared by French scientist Georgio Crini [209] or book chapter *Chitin: Structure, Chemistry and*

Biology prepared by Bernard Moussian [208]. Today, despite long-term research, chitin and its derivatives seem to be particularly important in tissue engineering, medicine, environmental protection and as a component of functional materials [215].

2.2.1. Chitin sources in nature and methods of its isolation

As a natural component of the exoskeletons of the many invertebrates and an integral part of the other organisms, chitin is widely distributed in several taxonomic groups [71] (see examples in **Figure 7**). The enormity of its biosynthesis makes us aware of the fact that chitin can be found in more than 70% of all living organisms in the world [202]. Thus, it could be identified in simple organisms such as fungi (for example, from the mycelia of *Aspergillus niger, Mucor rouxii, Agaricus bisporus*) [216–218], green algae [219], protists [220,221], diatoms [222–225], marine and freshwater sponges [226–230], and more complex (from evolutionary point of view) organisms as insects [106,204,231–235], arachnids [13,71,236], crustaceans [4,200,237–239], and molluscs [197,240]. Interestingly, chitin has also been identified among vertebrates in some amphibians and fishes [241].

The seafood processing industries assemble a large number of wastes, which were recognized as the main commercial sources of chitin. Mineralized shells of various crustaceans such as crabs, lobsters, and shrimp shells are the most common examples [242,243]. Chitin is found in them as a particular constituent tightly bound complexes, organized network with proteins and other compounds such as pigments, lipids, and minerals (mostly carbonates). Some parts of the polypeptides are suggested to be covalently linked to a small number of C-2 amino groups of the chitin [243]. The exoskeleton structure is constructed of layers of mineralized chitin
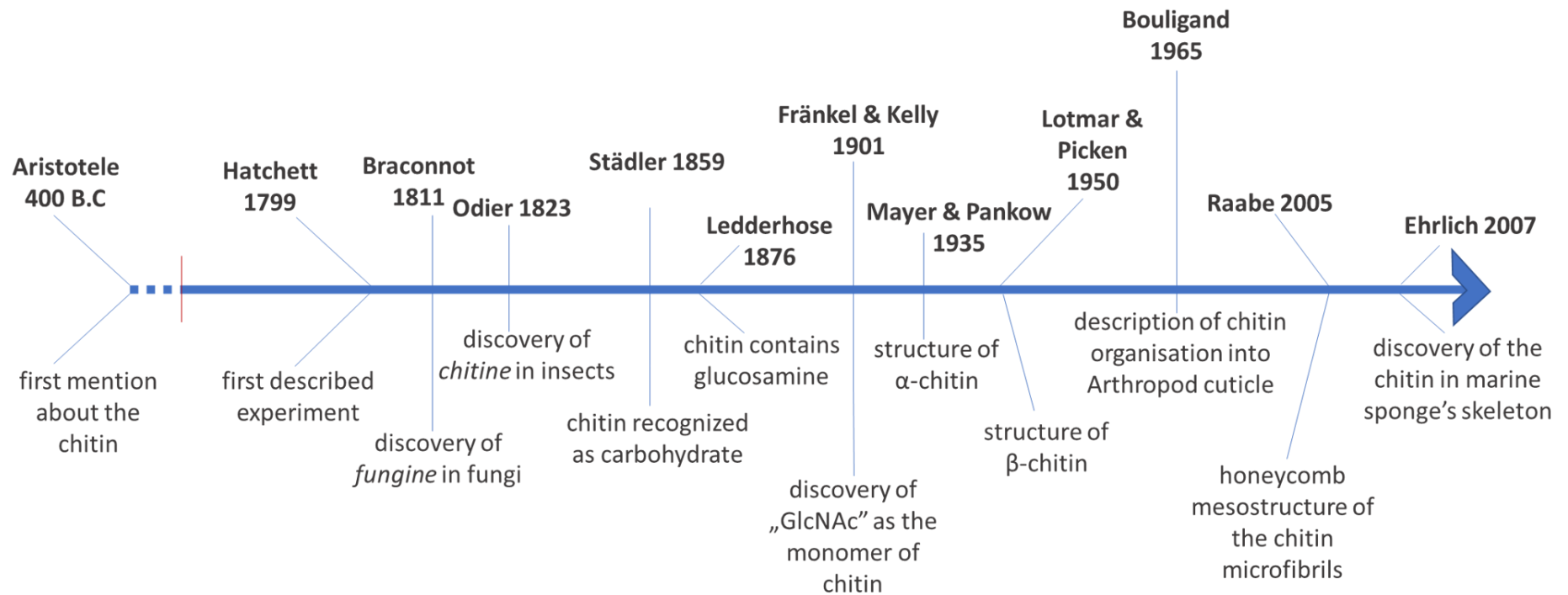
Figure 6. *Graph of the most important achievements in chitin history.*

in a Bouligand pattern. As described by Duan and others [4], chitinous matrix create *"successive layers arranged at the same angle to each other, resulting in a helicoidal stacking sequence and in-plane isotropy"*. Due to the specific interactions between chitin and other organic-inorganic components of exoskeletons, these biopolymers significantly impact their mechanical properties, especially the rigidity and stiffness [75].
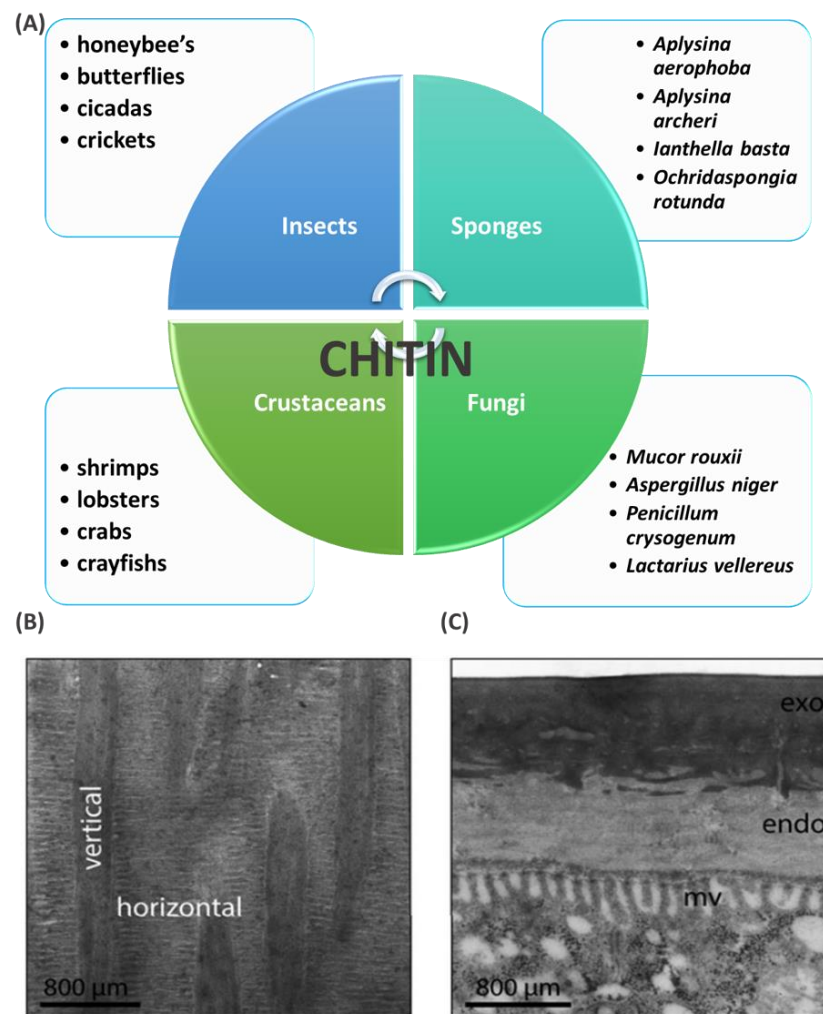
Figure 7. (A) Examples of natural chitin resources. (B) Higher organization of chitin in the cuticle of the beetle elytra (Tribolium castaneum). See vertical and horizontal chitin–protein matrices. (C) The procuticle of the larval cuticle of T. castaneum is divided into two subregions with highly cross-linked (exocuticle, exo) and weakly cross-linked (endocuticle, endo) chitin adjacent to the microvilli (mv) that are involved in cuticle secretion, adopted from [208].

As established, crustacean shells are made up of chitin (15-40%), proteins (20-40%), and calcium carbonate (20–50%) as the main components. Its amount and form are closely related to its origin [243], see **Table 6**. Pigments and other salts are only minor components. Furthermore, chitin was proposed to be characterized as one of the fundamental and oldest biomineralization templates with respect to both biocalcification and biosilicification [205,244]. However, chitin was recognized not only as a structural component of extracellular matrices (ECM), but can also be involved in organ shape arrangement during organisms development [208]. Merzendorfer and Zimoch described very interesting functions of chitin in insects [204]. The authors observed that chitin acts like an integral part of their peritrophic matrices, which form a permeability barrier between the food bolus and the midgut epithelium. In addition, it may protect the brush border from mechanical disorders and attacks from toxins and pathogens.

Table 6. Chitin and calcium carbonate content in selected sources, based on [243,245–247].

Source	Chitin (%)	$CaCO_3$ (%)
Crab cuticle	15-30	40-50
Shrimp cuticle	30-40	20-30
Squid pen	20-40	50-60
Calm/oyster	3-6	85-90
Marine sponges	5-70	1-5
Spider cuticle	6-9	negligible
Spider molt	15-20	negligible
Insect cuticle	5-25	negligible
Fungi cell wall	10-25	negligible

However, the effective extraction of pure chitin, from the various sources listed above, is strongly dependent on their origin and is usually limited to removal of mineral and organic phases. Consequently, industrial methods of chitin isolation are based on chemical treatment that hydrolyze proteins – (I) deproteinization, (II) depigmentation (only in some cases) and (II) demineralization of inorganic matter [75]. The isolation procedures can be carried out using chemical (alkali-acidic) and enzymatic treatment.

Chemical treatment was the first approach used for chitin isolation [101]. In case of deproteinization, a wide range of chemicals have previously been tested as reagents, including NaOH, KOH, Na_2CO_3, $Ca(OH)_2$, Na_3PO_4 and Na_2S [242]. The authors developed several methods, where reaction conditions differ considerably in each study. However, sodium hydroxide (NaOH) is preferred reagent for the removal of cells and proteins. As described by Younes and Rinaudo [242], NaOH concentration can range from 0.1 to 4.0 M. Furthermore, the process can be carried out in various treatment duration from a few minutes up to a few days, at a temperature of up to 160 °C. However, long-term NaOH treatment always results in partial deacetylation of chitin and hydrolysis of materials, lowering its molecular weight [200]. Furthermore, it is important that sodium hydroxide concentration does not exceed 4 M. The use of a higher NaOH concentration can result in a transformation of metastable β- and γ-chitin into α-polymorph which may cause an uncontrolled deacetylation (chitosan formation). Pigments, lipids, and proteins are removed mostly at the same time. However, in some cases, additional hydrogen peroxide treatment is required [245]. The demineralization step allows to remove minerals, primary calcium carbonate, from raw material. Industrially, this process is carried out using acidic treatment with hydrochloric acid (HCl), nitric acid (HNO_3), sulfuric acid (H_2SO_4), acetic acid (CH_3COOH) solutions [202], however, other agents as chelators (ethylenediamine tetraacetic acid − EDTA) can be also used [123].

From a practical point of view, to completely dissolve inorganic salts, the amount of acid should be applied in excess relative to the stoichiometric amount of the mineral phase. In addition, it is worth noting that the diffusion of acid deeply into the chitinous matrix depends on the particle size. For highly mineralized crustacean shells, larger volumes or more concentrated acid solutions have traditionally been used because of their heterogeneity. In some cases, demineralization is carried out at higher temperature [75]. As described, time is of the essence here, because prolonged demineralization (even up to several days) can lead to biopolymer degradation [248]. An alternative to the chemical method is that deproteinization and demineralization maybe carried out using microorganisms and appropriate enzymatic treatment [249]. It was established that biological treatment allows for significant preservation of the natural structure of chitin. However, it is much more time-consuming and requires appropriate bioreactors and testing apparatus. New data on chitin isolation methods, including the use of ionic liquids and eutectic solvents, have recently been published by several authors [250,251]. Additionally, electrochemical method for the isolation of chitin isolation was also investigated [252]. However, the method that is fast, simple, nondestructive to chitin, and allows a much better reduction of solvents application is the microwave-assisted chemical treatment [219]. Exposure to microwave energy is excited by rotational vibrations of water molecules. The energy of the vibrating molecules dissipates because of the strong attenuation of the vibrations and is transformation to heat. As a result, proteins, pigments, and minerals are removed much faster. The study of Klinger and co-authors [75], showed very interesting solution for isolation of chitin from marine sponge *Aplysina archeri,* using microwaves at a frequency of about 2450 MHz. The results obtained showed that short-term exposure to microwaves did not adversely affect the chemical structure of chitin and that the resulting material had both, a high degree of acetylation and a high degree of crystallinity. Furthermore, it allowed for reduction of time of chitin isolation from almost

7 days to 30 min (see Chapter 5). A schematic overview of the comparison of biological and chemical methods of chitin isolation is present in **Figure 8**.
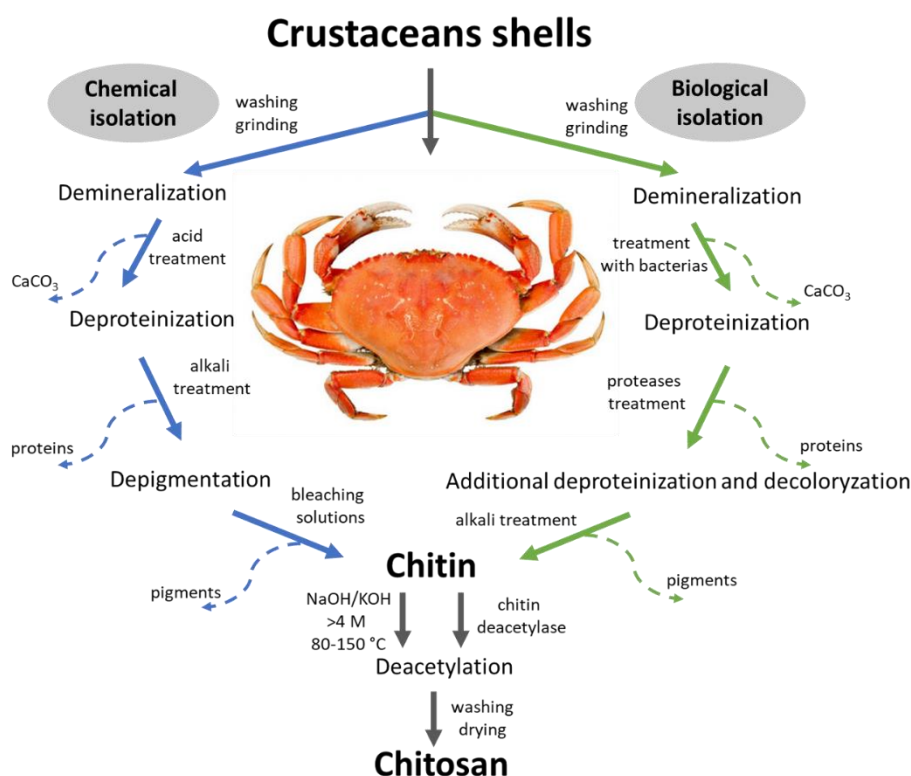
Figure 8. Comparison of the chemical and biological processes of chitin isolation and chitosan formation from crustaceans.

2.2.2. Structural properties of chitin and its application potential

Depending on its origin, chitin occurs as two main polymorphs, namely the α, and β forms [253]. However, in the literature also the third form, known as γ was described [202]. α-isomorph was recognized as the most distributed in nature; it occurs in the walls of fungal and yeast cells, sponges, spiders and insect cuticles, and in the shells of mineralized crustaceans' shells [208,214]. Due to its high thermodynamical stability α-chitin is systematically formed after recrystallization of other forms [242]. Its single chains are arranged in an antiparallel way (see **Figure 9**) [4]. Such chain arrangement favors the formation of stabilizing hydrogen bonds, which strictly influence the difficulties in its dissolution due to the problematic infiltration of the solvent [4]. There are two

distinct hydrogen bond types that can be identified in such systems − intramolecular C(6)OH···O=C(7) within the sheet of chitin fibres (intrasheet), and intermolecular C(6)OH···HOC(6) between sheets (intersheet) (see **Figure 9**) [15,208]. As a result, the splitting of the I amide bands in the FTIR spectra of α-chitin (1652 cm^{-1} and 1620 cm^{-1}) can be observed because of differences in its hydrogen bonding environment [73,254]. Until today, the commonly accepted crystalline structure of α-chitin was proposed by Minke and Blackwell in their fundamental work from 1978 [255]. The authors proposed an orthorhombic unit cell containing two disaccharide motifs in an antiparallel arrangement with the planes of the pyranose rings perpendicular to *a* axis. Scientists estimated the dimensions of the unit cells (*a* = 4.76 Å, *b* = 10.28 Å and *c* = 18.85 Å) and indicated the presence of the space group P2$_1$2$_1$2$_1$ [85]. It was observed that α-chitin polymorph was developed in biosources, where high mechanical properties are required (from the origin point of view). The great examples of α-chitin sources are Mantis shrimp dactyl club, lobsters of *Homarus americanus* exoskeleton, or holdfast of endemic freshwater sponge *Lubomirska baicalensis* [15,256].

The second most abundant chitin polymorph is β form, which could be found, e.g. in the cuttlebone of *Sepia officinalis* or tubes synthesized by pogonophoran and vestimetiferan worms [242]. In a monocrystalline spine form, β-chitin was also isolated from *Thalassiosira fluviatilis* diatoms [257]. The first report on the β-chitin structure was identified in the bristles of the polychaete *Aphrodite aculeate* by Lotmar and Picken, by using X-ray diffraction [258]. However, in 1961 Dweltz determined the P2$_1$ space group and identified that the unit cell in β-chitin is monoclinic [259]. Their lattice parameters were established as *a* = 4.819, *b* = 9.239 Å, *c* = 10.384 Å, *β* = 97.16° [260]. From a structural point of view, the β-chitin has chains arranged in a parallel manner (**Figure 9**) [204]. Thus, intersheet hydrogen bonds along the *b* axis are not

observed, which makes it more vulnerable for intracrystalline swelling of polar guest molecules (like water, alcohols and amines) [15,242]. However, their molecules may infiltrate the crystalline lattice without destroying the sheet organization and the crystallinity index of the material. This phenomena suggests that in nature, β-chitin usually occurs in a hydrated state, which was confirmed by Kobayashi [15]. The crystallinity index of β-chitin fibrils was estimated at around 70%. Furthermore, the greater distance between the side biopolymer chains makes this form more reactive and flexible as compared to α-chitin [200]. Moreover, the less tight molecular packing and the ease of infiltration of β-form make it easier to isolate, even in milder conditions [243].

γ-Chitin was recognized as a combination of α and β forms orientation, where two parallel biopolymer chains are alternately arranged with one anti parallel chain (**Figure 9**) [200]. For the first time, these polymorph was described in 1963 in *Loligo*, a squid genus by Rudall [233]. Based on XRD analysis, the author recorded two interesting maximum peaks 2θ ≈ 9.6° and 2θ ≈ 19.8°, which indicated that γ-chitin, has similar XRD pattern to α-chitin. A recent study described the presence of γ-form in cocoon threads of beetle larvae *Ptinus tectus*, dragonfly, silkworm larvae (*Antheraea pernyi)*, sawfly larvae (*Phymatocera aterrima*) and others [202]. However, all chitin polymorphs can be isolated into one organism. These phenomena indicate that differences in chitin forms are related to their functions, rather than taxonomic origin [233,261]. Nevertheless, to conclude, all chitin polymorphs are insoluble in common solvents. This fact is problematic in view of the development of processing and general application of chitin.

From a physical point of view, chitin is a highly thermostable biopolymer. By analyzing differential scanning calorimetry (DSC) curves, it could be observed that the thermal stability of chitin is strictly related to the number of hydrogen bonds. Thus, the decomposition of the crystalline structure should be

carried out at least at 330 °C for α-chitin, 230 °C for β-chitin and 310 °C for γ-chitin [208]. However, as described by Wysokowski et al., the thermal stability of chitin also depends on biomaterial source [15]. This properties and natural affinity of the chitinous templates to the inorganic phase, allow for multiple application of chitin in extreme biomimetics and hydrothermal synthesis. These solutions may become an inspiration for novel biomaterials for catalysis, biosensing, environmental protection and other application [262–264].
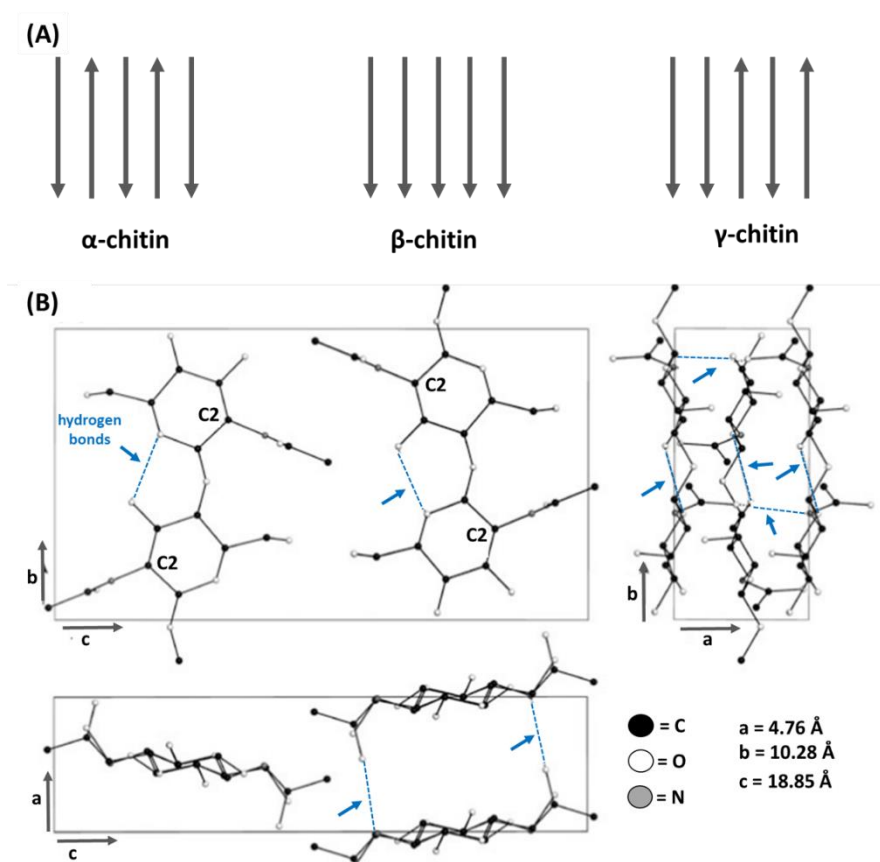
Figure 9. (A) Three different possible organization of chitin fibres. (B) Schematic view of the three main projections of the α-chitin unit cell. Hydrogen bonds are represented by blue dotted lines and blue arrows. The model is detailed in the CIF file (from The Cambridge Crystallographic Data Centre (CCDC), Deposition Number: 1264751), based on [208].

Generally, chitin was established as a noncytotoxic material that could be degraded by human lysozyme, but its immunogenic properties are still a controversial topic. Several studies showed that animals cells exposed to chitin produced pro-inflammatory/allergic immune response [265–267]. On the other

hand, reports that indicate their inert or immunosuppressant effects also exist [268,269]. Therefore, based on a careful review, it could be concluded that the 'allergic' response is not the domain of the material, but its purity, size and origin. The study described by Alvarez showed the effect of the size, shape, source, and purification method of chitin on immune recognition [270]. Chitin was isolated by chemical and biological treatment from shellfish, yeast cell walls of *Candida albicans*, and fungi *Aspergillus fumigatus* and *Mucor circinelloides*. The immune response of the chitin, that raises from different sources, was tested by the response of human peripheral blood mononuclear cells. Consistent with previous literature examples, small chitin particles, of an average size of 0.2 μm, were not immunogenic. However, larger chitin particles induced a pro-inflammatory response in some cases, but particles of 70–100 μm were unable to induce cytokines. Furthermore, some types of fungal chitin were able to induce cytokine response, for example, chitin from M. *circinelloides* strongly induced the pro-inflammatory cytokines IL-6 and IL-1β, in contrast to yeast from *C. albicans.* The results of this work suggest that not only the purity and size of the chitin particles but also their shape can influence the immune recognition. Thus, dozen examples of its application as a scaffold component for TE and wound treatment can be found [71,107,271,272]. However, to date, most studies are based on commercial shellfish or fungal chitin, which naturally occurs in the form of powder, flakes, or granules. There is a dearth of natural 'prefabricated' three-dimensional chitinous scaffolds because such structures are difficult to produce via purely synthetic routes. Fabrication of 3D porous scaffolds from such semi processed chitin requires various costly preparative steps, such as its dissolution in often harsh solvents (e.g. LiCl/dimethylacetamide solution, $Na_2CO_3/Ca(OH)_2$/urea system, ionic liquids or deep eutectic solvents (DESs) [199,273], micro-molding, electrospinning, supercritical drying, or emulsification [119,274]. However, recent development allowed one to obtain such constructs by natural resources. Excellent examples are chitinous skeletons of marine

sponges or spider cuticles used as scaffolds for tissue engineering [29–31,71,275]. As compared with other chitin sources, these ones possess negligible content of mineral phase and have 3D architecture.

2.2.3. Chitin and chitosan as adsorbents

An annual production of chitin was estimated in range between 10^{12}–10^{14} tons [200]. However, despite the high availability, crystallinity and insolubility of chitin devalue its commercial applications [200]. When the degree of N-acetylation (DA) is <50%, its derivative called chitosan appears (see **Figure 10**) [253]. Chitosan is soluble in acid aqueous solutions (pH < 6.0) thus, is easier to process [253]. As observed by Yadav et al., [200], the degree of deacetylation (DD) is a crucial parameter that affects the properties of chitin and its derivatives. DD influences both, chemical and physical (tensile strength, solubility, surface area, adsorption capacity, viscosity, porosity, and flexibility) as well biological (biodegradability, bioavailability, and biocompatibility) parameters.
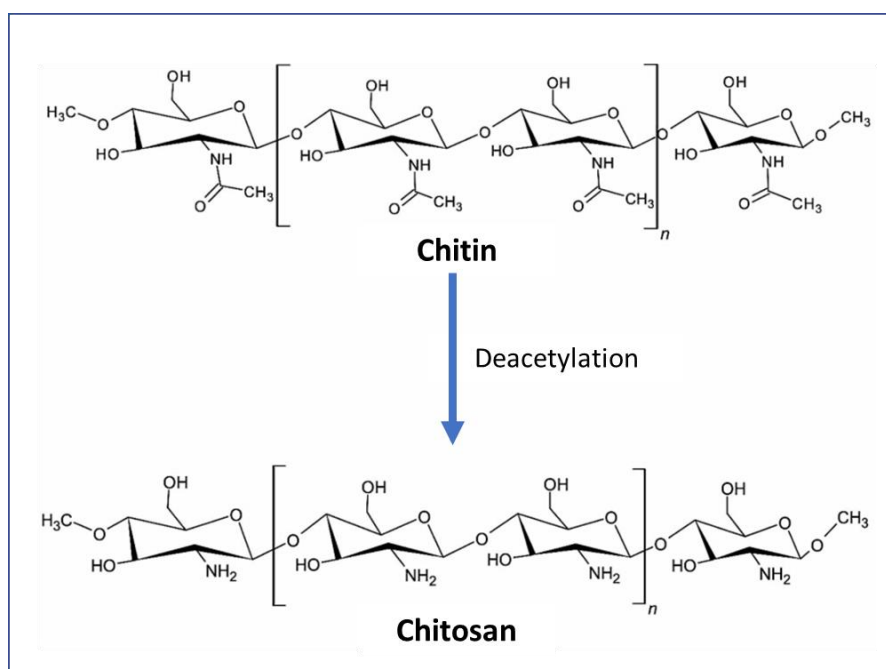
***Figure 10**. Chemical structures of 'ideal' chitin and chitosan chains, based on [200].*

In recent years, chitin and its derivatives were recognized as valuable materials for application in pollutant remediation. For example, Schleuter and co-authors [142], used 3D chitinous matrices of poriferan origin for effective uranium adsorption. The sorption capacity obtained was recognized as 288 mg/g. Moreover, based on solid-state NMR, infrared, and Raman spectroscopies, it was determined that uranyl species are bound to chitin by weak interactions. The authors indicated that the unique microarchitecture of this poriferan chitin allowed the sorption capacities to be higher than those of commercial chitinous sources. Other studies, described by Setti and others [276], showed crude oil sorption by chitin and chitosan in the form of 2-5 mm flakes. The authors compared the obtained results with synthetic polymers and keratin. The observed sorption capacity was determined as follows: chitin (260 mg/g), chitosan (2300 mg/g), keratin (2100 mg/g), PET (1440 mg/g), PTFE (600 mg/g). However, the crude oil sorption capacity of chitinous materials is strictly related to the sorbent morphology. For instance, Barros [277] determined crude oil sorption by chitin powder (170 mg/g) and chitosan powder (281 mg/g). In another study, the chitin−protein−based spider molting cuticle was recognized as an excellent crude oil biosorbent, due to its high oil sorption capacity, low susceptibility to water pickup, cost-effectiveness, and reusability [13]. These natural waste materials had a very low surface free energy of 4.47 ± 0.08 mN/m and show superhydrophobicity through a water contact angle close to 131.63° ± 0.54°. In consequence, the crude oil removal efficiency from seawater, distilled water, and freshwater was equal to 12.6 g/g, 15.8 g/g, and 16.6 g/g, respectively. Moreover, the material was examined in four sorption-desorption cycles and still retained a high sorption capacity. The authors explained the sorption mechanisms of the centimeter-sized molting cuticle as the physical trapping of crude oil drops by pores and micro hairs (see Chapter 10). Chitin and chitosan were also recognized as effective dye sorbents, due to their large number of functional amino and hydroxyl groups [278]. For instance, studies

performed by Filipowska [278] showed adsorption and desorption of four reactive dyes, i.e. Reactive Yellow 84 (RY 84), Reactive Red 11 (RR 11), Reactive Black 5 (RB 5) and Reactive Black 8 (RB 8), onto chitin (1) and chitosan (2) in the form of flakes. As determined, the sorption capacity of chitin ranged from 180 mg/g to 350 mg/g, where sorbent 2 showed results ranging 387 mg/g to 690 mg/g, depending on the type of dye and pH [278,279].

2.2.4. Representatives of Porifera and Aranea as a source of 3D chitin scaffolds

Sponges (Porifera) are among the oldest multicellular organisms on our planet, as confirmed by numerous geological discoveries [207,280,281]. They lead a sedentary life attached to the substrate, where they filter out microscopic sized microorganisms and other food particles [227]. The four classes within the phylum Porifera; Hexactinellida, Demospongiae, Calcarea and Hexactinellida can be distinguished and consist of more than 500 species [214]. Sponges owe their evolutionary success to rigid but flexible skeletons. For their creation sponges use two main structural biopolymers (spongin or chitin), and biominerals (mainly calcium carbonates and silica) [282]. To provide mechanical support to cell tissue, both biopolymers are made of fibers that can be inosculated to form a network of organized sets or form variously dendritic structures [227]. Similarly, as in other organisms of invertebrates, chitin also appears to be the crucial factor for skeleton stability in this case. Research on poriferan chitin was initiated by Professor Ehrlich and his research group in 2007, when its presence in *Verongida rigida* demosponge skeleton was confirmed for the first time [230]. The authors proved their structural similarity to α-chitin; however, its 3D fibrous structure organization was unprecedented before (see **Figure 11**). Recently, chitin was identified in the skeletons of 21 species of marine sponges and 3 freshwater sponges species (see [226] and **Figure 12**). Among marine demosponges, the most numerous groups are in Verongiida order. They are able to synthesize biologically active compounds (i.e. bromotyrosines) and

3D chitinous skeletons [283]. Moreover, their representatives can grow up to 1.5 meter in length as in the case of Caribbean stovepipe sponge *A. archeri* (Higgin, 1875) [247]. It should be stated that marine sponges represent an excellent renewable source of chitin due to their high ability to regeneration and cultivation under marine farming conditions. In 2011, Rohde and Schupp [284], determined that *Ianthella basta, a* marine verongiid sponge, is capable to regenerate the damaged fragments of its chitin–containing skeleton. The authors reported that these organisms may rapidly grow at a rate of 20 cm/year. Thus, it is quite possible to breed them under water farming conditions as a natural manufacture of renewable chitinous skeletons.
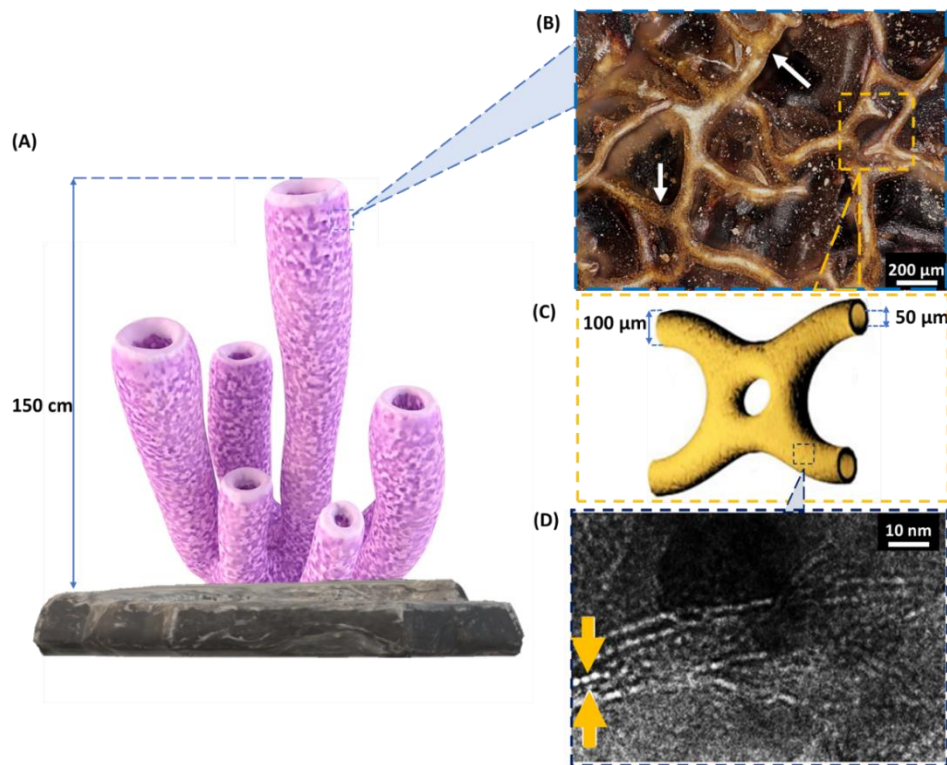
Figure 11. Schematic view on marine sponge chitinous skeleton organization from macro-, micro-, and nanolevel. (A) Model of a marine sponge of Verongiida order with up to 1.5 meter long as an example of a renewable natural source for the isolation of unique tubular chitinous macro-scaffolds. (B) High-magnification microscopic image of an air-dried marine sponge; see chitinous skeleton fibers (white arrows). (C) The model of microfiber arrangement with diameter around 100 μm and tubular hollow 50 μm. (D) HRTEM image: A bundle of chitin nanofibrils (orange arrows) from Verongiida sponge (Verongula gigantea) with a diameter of 2 nm, based on [72].

Distribution of chitin in sponges (Porifera)

Hexactenellida

marine species

- *Euplectella aspergillum*
- *Farrea occta*
- *Ressella fibulata*
- *Sericolophus hawaiicus*

Calcarea

marine species

- *Sycon ciliatum*

Homoscleromorpha

marine species

no data

Demospongiae

marine species

- *Aiolochoria crassa*
- *Aplysina aerophoba*
- *Aplysina archeri*
- *Aplysina cauliformis*
- *Aplysina clatrata*
- *Aplysina fistularis*
- *Aplysina fulva*
- *Aplysina gerardogreeni*
- *Aplysina revillagigedi*
- *Ernstilla lacunosa*
- *Ianthella basta*
- *Mycale euplectellioides*
- *Psedoceraina arabica*
- *Psedoceratina purpurea*
- *Suberea clavata*
- *Verongula gigantea*

freshwater species

- *Lubomirskia baicalensis*
- *Spongilla lacustris*
- *Ochridaspongia rotunda*

Figure 12. Recent overview of 24 sponge species that produce chitin as a component of their skeleton, based on [72,226].

From a taxonomic point of view, spiders (Araneae) are a huge group of invertebrates that include about 4000 genera [285,286]. According to the online taxonomic catalog [287] till today, 50,384 species of spiders were described worldwide (data from September 2022). The Araneae (spiders) settle almost all habitats except Antarctica. The oldest fossils of spiders are dated at carboniferous times (~320 million years), two times earlier than the oldest mammals [288]. Especially attractive among the Araneae are Theraphosidae spiders, which can reach lengths of more than 25 cm. It is also worth noting that the Theraphosidae family (the so-called ''bird-eater spiders'' or ''tarantulas'') is very popular through breeder and hobbyist [71]. The spider exoskeleton is a natural biocomposites of chitin/proteins. As observed by Professor Barth in 1973 [289], the overall organization of the chitinous microfibrils from the spider exoskeleton

resembles a Bouligand model. Single microfibers run parallel to the cuticle surface, in which all fibers within a layer have the same orientation, the assembly being closely correlated with cuticle depth. Thus, three various layers of chitin/protein can be observed: the endo, meso (intermediate), and external exocuticle. However, to grow up, spiders (like other arthropods) must create a new, larger exoskeleton (10–15%) and shed the old one during the molting process (ecdysis) (**Figure 13**). Such "cuticle change" occurs several times per year (depending on the age and species of the spider). Nyffeler and Birkhofer determined [290], that the mass of the entire group of spiders can reach up to 25 million metric tons. This huge value was calculated as the average biomass of spiders per square meter in various terrestrial biotopes around the world. Another report assumed that all spider species lose about $8 \pm 0.16\%$ of their own weight during a ecdysis [291]. Thus, it could be highlighted that spiders are capable of producing 2-6 million tons of cuticles due to ecdysis worldwide year by year [71]. Kaya and co-authors [246] determined that spiders cuticles chitin exist in α-isomorph with a high degree of acetylation (about 97%). From a morphological point of view, two kinds of surface pores may be distinguished, larger 190-240 nm and smaller between 11 and 32 nm.

Figure 13. *Harpactira pulchripes Theraphosidae spider during molting (ecdysis). Cuticles (molts) from diverse species of Theraphosidae as bulk biological waste source for the isolation of chitin.*

Interestingly, the possibility to utilize the molts of Araneae as a renewable source of chitin has attracted limited attention despite the fact that they are a diverse and widespread group of invertebrate organisms. The nonhomogeneous morphology of the molt (porous structure, microhair setae, and unique tubular chitin from the legs part) makes them very promising for several further applications.

Chapter 3. Aim of work and research hypothesis

The research hypothesis of the doctoral thesis assumes that the use of alternative sources of chitin such as marine demosponges' skeletons or spider's molts cuticles, will allow to obtain functional three-dimensional scaffolds with a unique shape and properties predisposing them for preparation of biomaterials for tissue engineering and environmental protection applications. Additional surface functionalization of selected structural matrices should enhance their antibacterial properties and improve the bio-integration with human cells.

The overall goal of the doctoral dissertation is to use the chitin in forms of naturally prefabricated scaffolds as matrices for the development of selected organic-inorganic composites and determine application possibilities for this biological material before and after functionalization process. Due to the wide range of research, the activities were divided into the following stages:

- **Marine demosponges' skeletons case:**

1. Development of a fast and non-invasive method of chitin isolation using the microwave-assisted technique.

2. Examination of the structural and physicochemical properties of renewable, three-dimensional chitinous scaffolds using such techniques as SEM, FTIR, Raman, TGA, DMA or AFM.

3. Determination of the application potential of isolated chitinous scaffolds in pure form, as a framework for the cultivation of selected cells line of keratinocytes (HaCaT), as well as fibroblasts (Balb/3T3, NHDF).

4. Preparation of chitin–calcium carbonate composite material using the *ex-vivo* biomineralization method. Characteristics of the obtained biocomposites in terms of physicochemical properties and application possibilities as a scaffold for the growth and proliferation of human fetal osteoblasts (hFOB 1.19).

5. Preparation of the chitin–nanosilver/silver bromide (chitin–Ag/AgBr) composite material with the use of simple chemical reduction of $AgNO_3$ and determination of its usability as an antibacterial filter for water purification.

6. Immobilization of laccase on selected chitin scaffolds and use of such biocatalytic systems to remove pharmaceutical from aqueous solutions.

- **Spiders molt cuticles case:**

1. Development of a fast and non-invasive method of chitin isolation using the microwave-assisted technique.

2. Examination of the structural and physicochemical properties of renewable, three-dimensional chitinous scaffolds using such techniques as SEM, FTIR, Raman, NMR, XRD and BET.

3. Preliminary investigation of scaffold biocompatibility by human cardiomyocytes (iPSC-CM) cultivation.

4. Determination of crude oil sorption properties of native spider molt cuticles.

Chapter 4. Materials and methods

Contents

4.7.6. Powder X–ray Diffraction (XRD)

4.7.7. Scanning Electron Microscopy (SEM) and Energy-Dispersive X-ray Spectroscopy (EDS)

4.7.8. Transmission Electron Microscopy (TEM)

4.7.9. Thermal Analysis (TGA/DTG)

4.7.10. Micro Computer Tomography (μ-CT)

4.7.11. Mechanical Testing – Dynamic Mechanical Analysis (DMA)

4.7.12. Fluorescence, Light and Digital Microscopy

4.7.13. Atomic Force Microscopy (AFM)

4.7.14. Contact Angle determination

4.7.15. Confocal Microscopy

4.7.16. Alizarin Red S Staining

4.7.17. Calcofluor White Staining

4.7.18. Low−temperature N_2 sorption

4.1. Chitin isolation and preparation methods

4.1.1. α–Chitin isolation from selected marine demosponges

Marine demosponge's specimens were collected at depths of 15–20 m by scuba divers around the Caribbean islands of Saint Vincent and at the scientific sponge aquaculture in the Adriatic Sea (Kotor Bay, Montenegro). Then, air-dried specimens were delivered by Internationales Institut für Biomineralogie GmbH (INTIB) (Freiberg, Germany) to the Laboratory of Biomineralogy & Extreme Biomimetics Group, TU Bergakademie Freiberg (Germany).

In brief, chitinous scaffold was obtained by three basic steps treatment (**Figure 14**). Isolation processes started by immersion of fragments of collected sponge into the deionized water for 4 h to remove corresponding water-soluble compounds and impurities (i). Then, the isolated sponge skeleton was treated by 2.5 M NaOH for 2 days at 40 °C, to remove proteins and residual pigments (ii).

Next, partially deproteinized skeleton was neutralized with ultrapure water several times and immersed for 5 h into 20% acetic acid (room temperature) to remove calcium and magnesium carbonates (iii). The following was replicated until pure, colorless chitin was obtain. Finally (after 7 days), transparent chitinous scaffolds were purified with deionized water and then kept in 70% ethanol at 4 °C for further actions.

Corresponding procedure was performed for 3 representatives of the Verongiida order marine sponges' species: *Aplysina aerophoba*, *A. archeri* and *A. fistularis*. Schematic view on chitin scaffold isolation is presented in **Figure 14**.
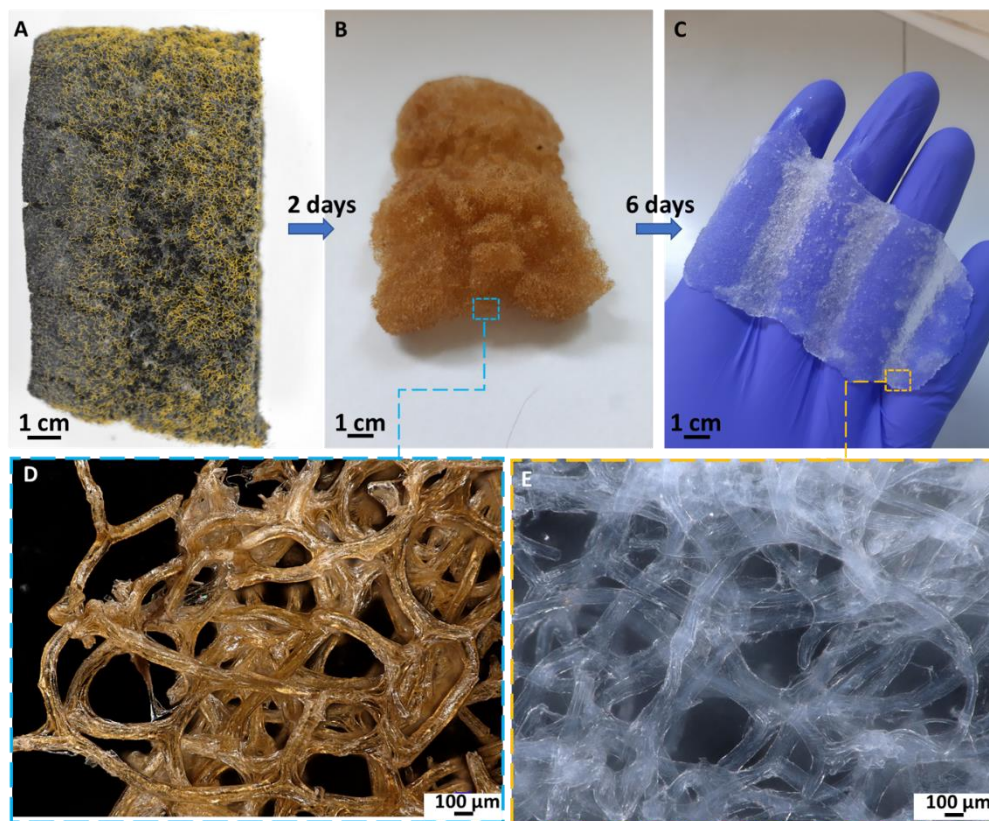
Figure 14. Schematic illustration of chitinous scaffold isolation from marine sponge A. fistularis. (A) Selected fragment of air-dried sponge. (B,E) The same fragment of the skeleton after 2 days of acid-base treatment. (C,F) Fully transparent and soft chitinous scaffold after isolation. (D) Extract of pigments, which contain mostly brominated derivatives (e.g. bromotyrosines) isolated at pH 14.

In case of *A. archeri* marine sponge express method for the production of naturally prefabricated 3D chitin was developed [75]. New method assumed

utilization of microwaves irradiation (MWI) for chitin isolation without destruction of the unique tubular fibrous structure and deacetylation of the isolated skeleton. Briefly, in first step (i) the water-soluble salts were removed by pretreatment of sponge specimens in distilled water using MWI (750 W and 2450 MHz) for 3 min. Next, in second step (ii), the skeleton was treated with 1% NaOH solution under microwaves for 2 min. The 3D scaffold was then carefully purified with distilled water to neutral pH and to remove residual brownish pigments. In third step (iii), the 3D chitinous skeleton was treated with 20% acetic acid under microwaves irradiation for 1 min and afterwards it was rinsed with distilled water until the pH value reached 6.5. In the last step (iv), sample was depigmented by 30% H_2O_2 treatment at pH~10 under MWI for 1 min. Steps ii–iv were repeated several times until pure, transparent chitinous scaffold was obtained.

4.1.2. α–Chitin isolation from spider's molting cuticle

Theraphosidae spider *Caribena versicolor* and *Avicularia sp. "Peru purple"* molting cuticles were delivered by SPIDERWORLD.EU spiders breeding facility (Cracow, Poland). Permits were no required for the described research, which complied with all relevant regulations. The isolation process was carried out under microwave irradiation (750 W and 2450 MHz) as follow (see **Figure 15**). First waxes from the cuticle surface were removed using chloroform:ethanol (2:1) mixture under microwave irradiation for 1 min. Then, cuticle was transferred to 2.5 M NaOH solution for 3 min to remove proteins bounded with chitinous matrix and pigments. As an effect of microwaves interactions with water molecules, temperature of the solution increased to 95 °C. At the last stage, soft and almost transparent chitinous skeleton was immersed in 30% H_2O_2 (pH~10 rinsed by NaOH) for 2 min. Finally, after purification by distilled water, scaffold was kept in a refrigerator for storage (4 °C) [245].
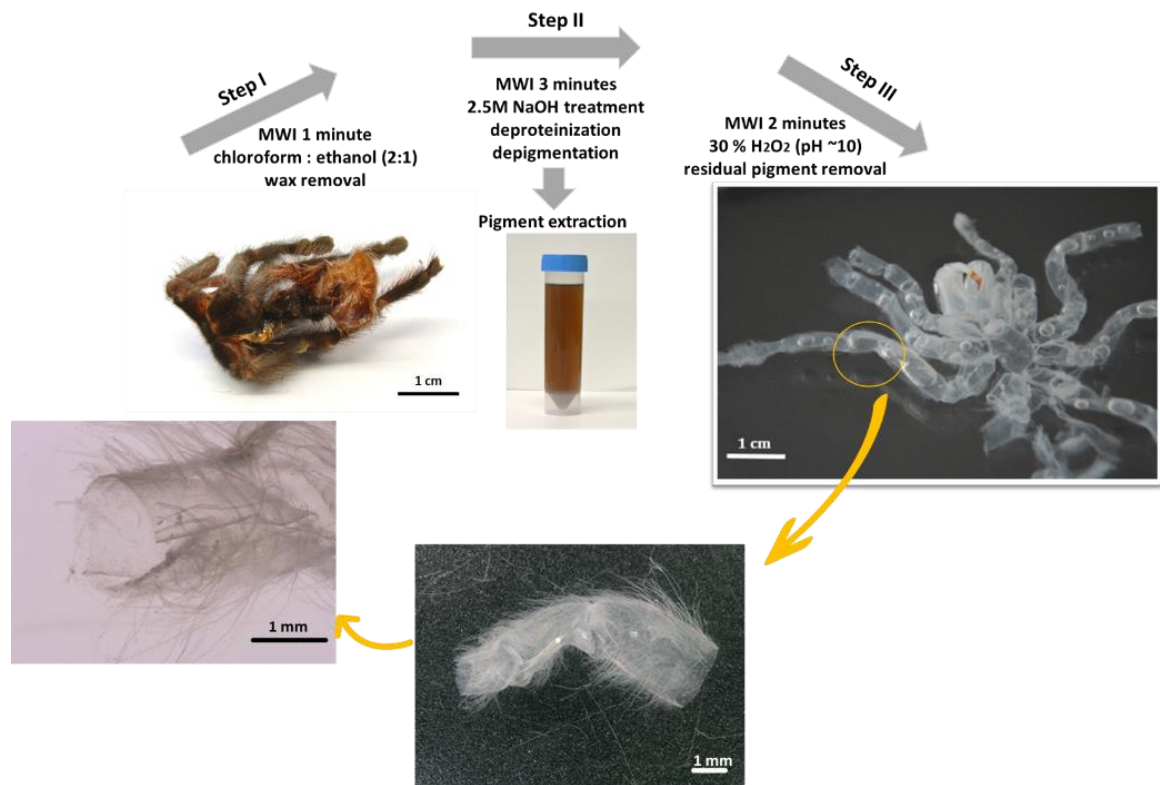
Figure 15. *Step-by-step procedure of chitinous scaffold isolation from C. versicolor spider molt using microwave-assisted method (MWI)* [245].

4.2. *Ex-vivo* functionalization of naturally pre–designed chitinous scaffold by biomineralization

Ex-vivo biomineralization of chitinous scaffold was carried out by mimic *Cornu aspersum* snail shell regeneration using its hemolymph (**Figure 16**). In this case, process was divided into two steps. Prior to the synthesis, snail shell surface was carefully cleaned with 70% ethanol. Next, a small fragment of the shell (3x3 mm) was removed and the snail was transferred in a moist, sterile box for 1 h to trigger a natural cascade and to regenerate the damaged area (hemocytes activation) [292,293]. After that, about 1 mL of hemolymph was isolated from a damaged area by vessel puncture using a sterile syringe and needle. In next step, pure chitinous skeleton scaffold from *A. fistularis* marine demosponge (about 10x10 mm) was immediately immersed in the isolated biological medium for 1 h. The composition was then placed on a sterile glass slide at 25 °C until completely dried. Both steps were repeated twice. The natural biocomposites

composed of chitin and calcium carbonate were washed with distilled water several times and stored at 4 °C.
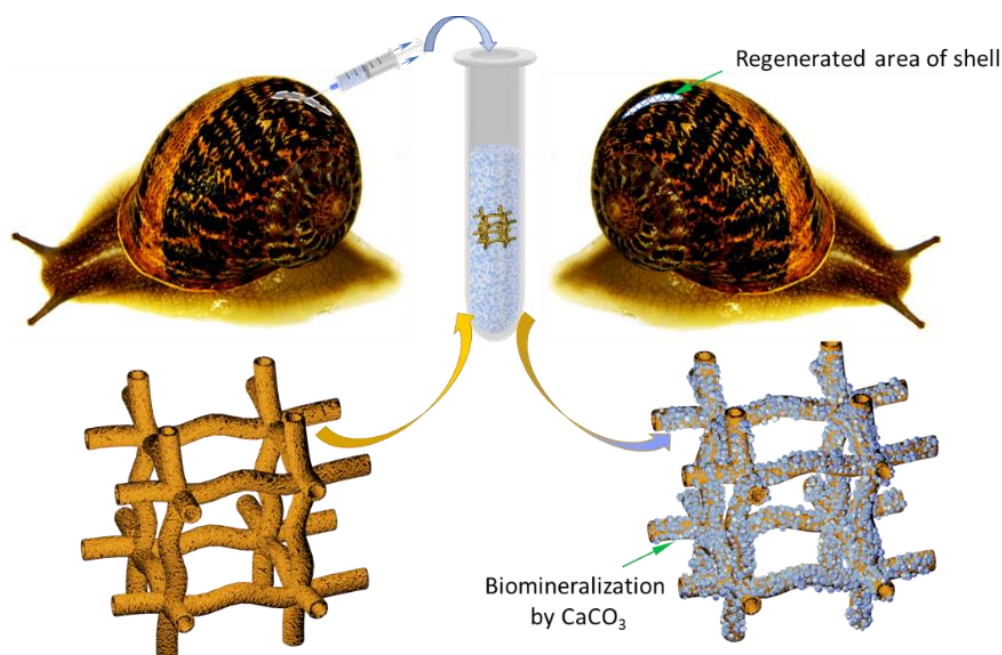
Figure 16. Schematic view of principals of non-lethal hemolymph extraction of C. aspersum snail and their applicability in ex vivo biomineralization, using 3D chitinous scaffolds from marine sponges.

4.3. Laccase immobilization onto 3D chitinous scaffold of sponge origin

Chitinous scaffold isolated from *A. archeri* marine demosponge was used here [25]. Briefly, small piece of scaffold (about 5 mg) was placed in a 5 mL vessel which contained 2 mL of laccase solution (concentration 5 mg/mL), dissolved previously in 50 mM acetate buffer at pH 5. The mixture was subjected to gentle stirring at 150 rpm for 1 h at 25 °C, using an IKA Werke GmbH incubator (Staufen im Breisgau, Germany). Upon enzyme immobilization by adsorption, the samples were removed from the reactor, washed with acetate buffer to remove unbounded enzyme, and used in tests involving the removal of tetracycline from aqueous solutions (see **Table 7**).

Table 7. Process details of enzymes immobilization onto chitinous scaffold.

Immobilized enzyme	Laccase
EC number	EC 1.10.3.2
Producer	Sigma Aldrich (MO, USA)
Support	chitin from *A. archeri*
Support amount	5 mg
Incubation time and temperature	1 h/25 °C
Enzyme solution concentration	5 mg/mL
Buffer	50 mM acetate buffer (pH 5)

The amount of immobilized enzyme and the immobilization yield were determined as follows. Supernatant of laccase solution after immobilization and acetate buffer solutions used for biosystem washing, were analyzed by spectroscopic analysis using the Bradford method [294]. Bradford reagent was mixed with investigated solutions (1:1 v/v) and after that the absorbance at 595 nm was measured. The enzyme concentration was calculated based on reference curve. In order to estimate the immobilization efficiency, following formula was used:

$$\text{Immobilization yield (\%)} = \frac{C_R + C_W}{C_I} \cdot 100\% \qquad (1)$$

where:

C_R – concentration of enzyme in solution after immobilization,

C_W – concentration of enzyme in solution after washing,

C_I – initial concentration of the enzyme.

The activity and thermochemical stability of a free and immobilized enzyme were calculated based on the spectroscopic measurements, using a

model oxidation reaction of 2,2'-azino-bis(3-ethylbenzothiazoline-6-sulfonic acid) (ABTS). Process was carried out using 10 mg of free enzyme or appropriate amount of biocatalytic system after immobilization, containing 10 mg of laccase, that was added to 5 mL of a solution containing 10 mM of ABTS in phosphate buffer (pH 5). Process was conducted for 120 min at 25 °C. After that, absorbance at 420 nm was measured. The activity of free and immobilized laccase was calculated as the amount of enzyme required to convert 1 mM of ABTS per 1 min, under process conditions defined above. The activity retention (%) was calculated as the ratio between the percentage activity of immobilized laccase to the percentage catalytic activity of the free enzyme. The storage stability was defined using the same reaction, but the process was conducted over 30 days at 4 °C. The inactivation constant (k_D) and the half-life ($t_{1/2}$) were calculated based on the linear regression slope.

To determine the Michaelis–Menten constant (K_M) and the maximum reaction rate (V_{max}) of free and immobilized laccase, the ABTS oxidation reaction (process conditions described above) was carried out in the ABTS concentration range from 0.01 to 10 mM. Defined kinetic parameters were evaluated using the Hanes-Woolf plot.

4.4. Development of chitin–Ag/AgBr ternary composites

For these experiments partially purified 3D matrix from *A. aerophoba* marine demosponge was used [23]. In this case, isolation procedure was shortened to 2 days to obtain completely decellularized skeleton matrix. Originally, various brominated derivatives (mainly bromotyrosines) are naturally located as intercalated layers of chitinous skeleton [283]. They act like a biochemical barrier against harmful pathogens (e.g. viruses, bacteria) and predators [295]. To obtain the nano (AgNPs) and macro silver (AgMPs) particles coating of the surface of chitinous skeleton, the chemical reduction of $AgNO_3$ was performed. For this purpose, a 10x30 mm part of the skeleton was placed in

30 mL of 1 M AgNO$_3$ solution for 1 h at 25 °C to conduct surface adsorption. The mixture was then combined with 15 mL of 0.8 M NaOH, which resulted in the formation of a brownish precipitate (Ag$_2$O↓). Afterwards, drop-wise addition of a concentrated ammonia solution was carried out to achieve a complete dissolution of the precipitate. Subsequently, the reaction catalyst, which consisted of ethanol (1 mL) as well as a mixture of 0.08 M glucose and 0.04 M citric acid (25 mL), was added. The reaction was manifested by the appearance of metallic silver on the wall of the vessel. Moreover, the highly alkaline environment of this reaction favored the washing out of the Br-rich compounds from the skeleton and the precipitation of silver bromide directly to the surface of the scaffold. Finally, obtained materials were washed with distilled water in an ultrasound bath (Elmasonic GmbH, Germany) for 10 min at 60 kHz (300 W) to remove non-attached particles. All reagents were purchased from Sigma-Aldrich (MO, USA).

4.5. Evaluation of the biomedical properties of the obtained materials

4.5.1. Cytotoxicity study

The pure chitinous scaffold isolated from the demosponge *A. fistularis* was analyzed according to the direct method of cytotoxicity evaluation ISO 10993-5: 2009 "*Biological evaluation of medical devices—Part 5: In vitro cytotoxicity studies*" [296,297]. Firstly, materials were sterilized using Steril-Clave 18B (Cominox, Italy) in PBS applying high-temperature program (121 °C). Then, the highly sensitive Murine fibroblasts line Balb/3T3 cells were cultured in a 6-well plate (1.0×10^5 cells per well, 5% CO$_2$, 37 °C, 95% humidity) with DMEM medium (Lonza, Switzerland), 10% fetal bovine serum, FBS (EeroCell, UK) and 1% L-glutamine with penicillin and streptomycin solution (Sigma-Aldrich, MO, USA). After one day, sterilized materials (5x5 mm) were immersed in the cell culture for 24 h. The qualitive observations were performed by fluorescence/light microscope coupled with inverted contrast-phase model BX51 (Olympus, Japan).

Control culture was evaluated in the same conditions but without contact with the chitin. Any morphological changes of cells surrounding the scaffold were observed directly in the culture. Moreover, cytotoxicity was determined by attached cells ultrastructure observations using TEM analysis (see section 4.7.8). Studies were performed at the Wroclaw Medical University, Poland.

4.5.2. Cell culture and staining

4.5.2.1. Bone cells – human fetal osteoblast cell line hFOB 1.19

A human fetal osteoblast cell line hFOB 1.19 (ATCC® CRL-11372™) was purchased from (ATCC®, VA, USA). Cells culture was carried out in DMEM/F12 medium w/o phenol red (Gibco, UK) mixed with 10% heat-inactivated fetal bovine serum, FBS (EeroCell, UK) and 0.3 mg/ml of geneticin selective antibiotic G418 (Gibco, UK). The biological evaluations of the cell's behavior under chitinous scaffold were performed at 34 °C and 5% CO_2 (culture conditions) within 7 days.

Sample preparation: pure chitinous and biomineralized scaffolds (5x5x4 mm) (see section 4.2) were stored in 70% ethanol overnight. Before the immersion into cell culture, the chitinous scaffolds were washed four times with autoclaved deionized water and twice with sterile phosphate buffered saline. After that, materials were transferred in a complete cell culture medium for overnight incubation. Next, the scaffolds were placed in empty wells of a non-treated cell culture 48-well plate (Eppendorf, Germany) and 2×10^5 cells were seeded directly onto their surface adding 10 μL of cell suspension. The inoculated samples were maintained for 2 h at 34 °C. After that, 0.5 mL of warm cell culture medium was added. Observations and evaluations were carried out at two time points, after 24 h and 7 days.

To evaluate biomedical applicability of prepared pure chitinous and biomineralized scaffolds, the spreading and morphology of hFOB, after 24 h and

7 days of culture, were determined using confocal microscopy. In this context, the samples were washed with PBS, fixed with 4% paraformaldehyde at room temperature, permeabilized with 0.2% Triton X-100 (Sigma-Aldrich, MO, USA) at room temperature for 15 min, and stained for F-actin exoskeleton visualization with Alexa Fluor 488 Phalloidin Conjugate (1:40, A12379, Invitrogen, USA) overnight at 4 °C. Cell nuclei were stained with Draq5 (1:1000, Thermo Fisher Scientific, UK) at room temperature for 30 min. The samples were immersed in PBS and observed using confocal microscope at excitation wavelengths of 488 nm and 633 nm.

Described studies were performed at the Warsaw University of Technology, Poland.

4.5.2.2. Skin cells –Balb/3T3, NHDF and HaCaT

The mouse normal fibroblasts cell line Balb/3T3 was purchased from (ATCC®, VA, USA), the normal human dermal fibroblasts line (NHDF) was purchased from (Lonza, Switzerland), the human epidermal keratinocyte line (HaCaT) was purchased from (DKFZ, Germany). The Balb/3T3 and HaCaT lines were growth with DMEM medium (Lonza, Switzerland) with 10% fetal bovine serum (FBS) and 1% L-glutamine with penicillin and streptomycin solution (Sigma-Aldrich®, MO, USA). NHDF was cultured in FGMTM Fibroblast Growth Medium BulletKitTM (Lonza, Switzerland). Cell culture was kept in following conditions, 5% CO_2 at 37 °C and 95% humidity under a controlled gentle rocking platform BioRocker™ XL 3D (Thomas Scientific, NJ, USA), which allowed verification of the real cell's adhesion onto the scaffold surface. The fresh culture medium was changed after each 2 days. Observations and evaluations were carried out at two time points, after 24 h and 7 days.

Sterilized pure chitinous scaffolds isolated from the demosponge *A. fistularis* were prepared as follow: 10x10x4 mm pieces were cut, and then cell amount of

1.0×10^5 (24 h cell culture) and 5.0×10^4 (7-day cell culture) in 3 mL of complete medium were seeded onto scaffold in 6-well plate.

To visualize cells adhesion and spreading, Crystal Violet staining was performed. In this context, scaffolds moved on cell culture were washed twice with cold PBS and then incubated for 10 min in cold methanol (−20 °C) (Chempur, Poland). Afterwards, cells were incubated for 10 min in a 0.5% solution of Crystal Violet in 25% methanol [58]. Subsequently, stain was removed by washing several times in water, and the cell adhesion to the scaffold surfaces was visualized using an CKX53 (Olympus, Japan) inverted contrast-phase microscope.

Described studies were performed at the Wroclaw Medical University, Poland.

4.5.2.3. Cardiomyocytes line iPSC–CMs

Human Induced Pluripotent Stem Cell-Derived Cardiomyocytes line iPSC-CM were cultured in E8 medium (Gibco, UK). Differentiation was performed in a differentiation medium containing RPMI1640 with HEPES and Glutamax (Gibco, UK) combined with 250 mg albumin (Sigma-Aldrich, MO, USA), 100 mg ascorbic acid (Sigma-Aldrich, MO, USA) and the modulators CHIR99021 (4 μM, day 0) and IWP2 (5 μM, day 2), both purchased from Merck (Germany). From day 6, the medium was changed to B27 medium (Gibco, UK) (RPMI1640 with HEPES, Glutamax, supplemented with 2% B27) and the first beating iPSC-CMs were obtained at day 8. After 10–14 days, Collagenase B (Worthington Bio- chemical, 1 mg/mL in RPMI1640) was used for 1 h at 37 °C to detach and separate the iPSC-CM layers from other cell types. The iPSC-CMs were subsequently digested using Trypsin/EDTA (Thermo Fisher Scientific, UK) for 8 min at 37 °C, resuspended in digestion B27 medium supplemented with 15% FBS, and 2 μM of Thiazovivin (Merck, Germany) and centrifuged for 5 min at 200 rpm. The iPSC-CMs were resuspended in the digestion medium, and

0.5–1.0×10^6 cells in 1.5 mL of medium were seeded on uncoated or Geltrex-coated (Thermo Fisher Scientific, UK) chitinous scaffolds from *C.versicolor* spider molt. The coating was performed for 1 h at 37 °C before seeding. Cells were cultured at 37 °C, 5% CO_2, 95 % humidity. After 24 h, the medium was changed to standard B27 medium. Cells were documented using light microscopy model Axiovert100 (Leica, Germany). The number of replicates per experiment was n=2 per condition.

To detect sarcomeres as a structural hallmark of cardiomyocytes, phase-contrast microscopy was used. In this case, α-actinin immunostaining was performed as follow. After 30 days, the chitin scaffolds were fixed with 4% paraformaldehyde (Carl Roth, Germany) for 20 min at room temperature, followed by blocking with 1% bovine serum albumin (Merck, Germany) in PBS for 16 h at 4 °C. Incubation with α-actinin primary antibody (Sigma Aldrich A7811-100UL; 1:500 in PBS, with 0.1% Triton, 1% BSA) was performed for 16 h at 4 °C. Afterwards, incubation with secondary antibody donkey anti-mouse Alexa Fluor 488 (Invitrogen A21202, 1:1000 in 1% BSA in PBS) for 1 h at room temperature, was performed. Finally, Hoechst33342 staining (in-vitro gen H3570, 20.25 µM) was performed for 10 min at 25 °C. Cells were visualized using a Imaging system BZ-X710 (Keyence, Japan).

Described studies were performed at the Dresden University of Technology, Germany.

4.5.3. *Colorimetric cells proliferation (MTS)*

To determine cell viability onto pure and $CaCO_3$ biomineralized chitinous scaffold quantitative MTS analysis was performed. Briefly, samples were immersed in DMEM/F12 medium w/o FBS and moved to wells of a 24-well plate. Then, about 120 µL of MTS (CellTiter 96® AQueous One Solution Cell Proliferation Assay, Promega) was injected to each well and the plate was

incubated at the same conditions as hFOB culture. After 1 h, 150 μL of 10% SDS was added to each well to stop the reaction, and the plate was shaken on a rotary shaker at room temperature for 1 h. Next, 100 μL aliquots were transferred into new wells of a 96-well plate and the absorbance was measured at 490 nm. Five replications were tested at each time point (after 24 h and 7 days) for both materials, pure chitinous scaffold from *A. fistularis* before and after $CaCO_3$ biomineralization. The results were evaluated statistically by means of post hoc one-way ANOVA (KyPlot 2.0 beta 15 software). Study was performed at the Warsaw University of Technology, Poland.

4.6. Environmental protection utilities of prepared materials

4.6.1. Removal of tetracycline from aqueous solution using chitin−laccase biosystem

Tetracycline was removed from aqueous solutions by chitin−laccase biocatalytic system applying various antibiotic concentration, and process conditions such as pH and temperature. Prior to enzymatic removal of tetracycline, the efficiency of its adsorption was evaluated using pure chitinous scaffold and the scaffold with immobilized, inactivated enzyme (thermal inactivation was carried out at 80 °C for 4 h). To determine the efficiency of tetracycline removal by simultaneous adsorption and catalytic conversion chitin−immobilized laccase biosystem was used (without thermal inactivation). In following experiment, effect of tetracycline concentration on the rate of its removal was determined using its solutions at concentrations of 0.1, 0.5, 1.0, and 3.0 mg/L, prepared in an acetate buffer at pH 5 at 25 °C. In order to evaluate the impact of pH, 1 mg/L tetracycline solutions were studied, and the process was conducted at 25 °C with pH values ranging from 3 to 9. Consistently, the impact of temperature on the efficiency of tetracycline removal was evaluated using 1 mg/L tetracycline solution at pH 5, with temperature ranging from 5 °C to 65 °C (10 °C per step). After the removal experiments the obtained biosystems were removed and the reaction mixture was analyzed by UV-VIS spectroscopy.

4.6.2. Antibacterial activity of chitin–Ag/AgBr composite

The chitin–Ag/AgBr composite material was tested for antibacterial activity using three various experiment: (i) determination of zones of inhibition in agar diffusion method, (ii) test tube assay and (iii) efficiency of filtration test.

In case of first experiment (i), 0.01 g of the obtained material was prepared and grounded using a mortar. As a reference, chitinous scaffold before silver coating and commercially available antibacterial wound dressing material Suprasorb® A+Ag, were used. Two strain of bacteria were used, *Escherichia coli* (ATCC® 25922, Gram-negative) and *Bacillus subtilis* (B9, Gram-positive). In both experiments concentration of microorganisms equaled 1.5 on the McFarland scale and was applied with agar Mueller–Hinton medium. After that, plates were incubated at 37 °C for 24 h. The diameter of inhibitory zone, surrounded the materials pieces, was measured. Tests were performed three times (for each material) and a mean value was given.

In case of second experiment (ii), analogous weight of materials was moved on sterile test tubes and immersed in 1.5 mL of *E. coli* suspension (0.8 on the McFarland scale, approx. 10^6 CFU/µL) at 37 °C for 1, 3, 6, 12 and 24 h. Afterwards, 100 µL of suspension was seeded on Columbia LabAgar plates (Biomaxia, Poland) + 5% sheep blood and incubated at 37 °C for 24 h, to determine the number of survival bacterial colonies. Tests were performed three times (for each material) and a mean value was given.

The last experiment (iii) was carried out to determine possible usability of synthesized materials as an antibacterial filter. In this case 500 mg of chitin–Ag/AgBr composite was placed in a sterile 50 cm³ falcon tube (as filter bed) and connected with the pump MK-650 (Aquael, Poland). Then, filtration set was immersed in 1000 mL container filled with 0.9% sodium chloride suspension of *E. coli* bacteria (0.8 on the McFarland scale, approx. 10^6 CFU/µL) and filtered at a flow rate of 330 mL/min. The number of survival bacteria colonies were

determined after 1, 3, 6, 12 and 24 h in analogous way to the (ii) described above. Schematic view of described process is presented in **Figure 17**. As a reference, chitinous skeleton before metallization was used. Number of repetitions n=3. Described studies were performed the TU Bergakademie Freiberg, Germany and University of Life Science in Lublin, Poland.
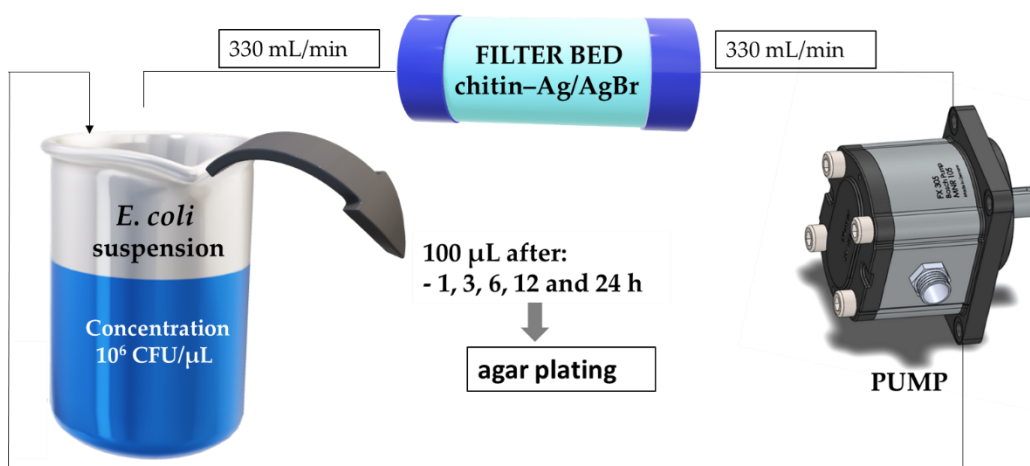
Figure 17. *Schematic view of filtration process using chitin–Ag/AgBr as a filter bed.*

4.6.3. Study of crude oil sorption

Determination of crude oil sorption capacity was performed by immersing a known weight of *A. sp. "Per purple"* spider molted cuticle (~100 mg) in a mixture of water (60 mL) with crude oil (2 g). Sorbents were placed on the oil layer and exposed for self-sorption at time intervals from 30 s to 32 min. The amount of crude oil adsorbed by the sorbent (s) was calculated according to the Equation (2) [298]:

$$s = \frac{w_a - w_b}{w_b} \qquad (2)$$

where:

w_a and w_b correspond to the weight of cuticle after sorption and before sorption, respectively.

Desorption efficiency of crude oil from the sorbent was carried out by immersion of cuticle with adsorbed oil in a chloroform:ethanol (v/v 1:1) mixture, under microwave irradiation (MWI) for 1 min (750 W and 2450 MHz). The desorption (d) was calculated based on Equation (3):

$$d = \frac{w_{b1} - w_{a1}}{w_{b1}} \cdot 100\% \qquad (3)$$

where:

w_{b1} and w_{a1} are the weight of cuticle before desorption and after desorption, respectively.

The crude oil spill removal test was carried out by Standard Test Method for Sorbent Performance of Adsorbents (ASTM F726-99) [299]. In these experiment three types of water were used: tap water, deionized water and simulated sea water. The beaker was filled with 60 mL of water, then 2 g of crude oil was dropped to create a thin layer under the top. Experiment was performed under the analytical balance. Then, ~100 mg of the cuticle, was placed onto the crude oil layer. After 2 min of direct contact, the sorbent was removed out. Finally, the difference in weight before and after adsorption, was measured. The final value was calculated as a mean of 20 repetitions.

The percentage removal of oil was calculated using following Equation (4) [300]:

$$\%Removal = [(\frac{Mr}{Ma}) \cdot 100\%] \qquad (4)$$

where:

M_r (oil removed) = (mass of crude oil and water) – (mass of crude oil and water after removal)

M_a (crude oil added) = (mass of crude oil and water) – (mass of water).

4.7. Characterization techniques and methods

4.7.1. Attenuated Total Reflectance Fourier-Transform Infrared Spectroscopy (ATR–FTIR)

The infrared spectra were recorded using VERTEX 70 spectrometer (Bruker, Karlsruhe, Germany) equipped with an Attenuated Total Reflectance (ATR) lance. The wide wavenumber range of 4000–400 cm^{-1}, was recorded with the resolution of 0.5 cm^{-1}. In contrary to standard FTIR method, where KBr pellet is required, herein solid state of material was characterized directly. ATR–FTIR was used to characterize the chitinous scaffolds from *A. archeri* and *A. fistularis* (before and after functionalization) marine sponge and *C. versicolor* spider.

Calculation of corresponding degrees of acetylation (DA) and deacetylation (DD) of chitin was conducted based on the following formulas [301]:

$$DA\% = \frac{A_{1654} + A_{3432}}{1.33} \cdot 100\% \tag{5}$$

$$DD\% = 100\% - DA\% \tag{6}$$

where:

A_x – absorbance, x – wavenumber

4.7.2. Raman Spectroscopy

Raman spectroscopy was carried out using a spectrometer RamanRxn1™ (Kaiser Optical Systems Inc., MI, USA) combined with a DM2500 P (Leica Microsystems GmbH, Germany) light microscope. A diode laser secreting at a wavelength of 785 nm was utilized for excitation of the Raman scattering. Transmisson of the laser beam to the microscope was carried out using a 100 μm optical fiber, whereas focus on the samples was achieved by using a 20×/0.45 microscope objective which allowed to achieve a focal spot of approx. 50 μm. The spectroscopic indications were collected in reflection configuration and sent to the f/1.8 holographic imaging spectrograph by a 62.5 μm core optical fiber.

The wavenumber range of 150–3250 cm^{-1} was recorded with resolution of 4 cm^{-1}. Accumulations of 2 s were applied. From 4 to 40 accumulations were added to increase the s/n ratio depending on the signal quality. Raman spectroscopy was used to characterize the chitinous scaffolds from *A. archeri* and *A. fistularis* (before and after functionalization) marine sponge and *C. versicolor* spider. Measurements were performed at the TU Bergakademie Freiberg, Germany.

4.7.3. UV-Vis Spectroscopy

The spectra were recorded using a V-750 spectrometer (JASCO, Esaton, Germany) in the wavelength range of 200 nm to 800 nm. Measurements were performed using a quartz cuvette with path length of 1 cm (quartz suprasil, Hellma Analytics) and operated at a resolution of 5 nm. This technique was used to prepare a standard curve for studies on the removal of tetracycline contaminants from aqueous solutions, and to examine the quantity of immobilized enzyme, its immobilization yield, activity of free and immobilized laccase, and efficiency of removal of tetracycline. Detailed measurements were performed at 595 nm, 420 nm, and 355 nm, for the Bradford method, ABTS, and tetracycline removal experiments, respectively.

4.7.4. Electrospray Ionization Mass Spectrometry (ESI-MS)

Regarding to ESI-MS analysis an Agilent Technologies 6230 TOF LC/MS spectrometer (Applied Biosystems, CA, USA) was applied. The isolated chitin from *A. archeri* marine sponge was hydrolyzed using 6 M HCl for 24 h at 90 °C. After that, solution was gravity filtered using a 0.4-micron paper filter to remove solid residues (if present). In the next step, the solutions were freeze-dried to remove excess of hydrochloric acid and then obtained solid residues were dissolved in water for ESI-MS measurements. As the standard, d-glucosamine, purchased from Sigma-Aldrich (MO, USA), was used. As the nebulizing and desolvation gas nitrogen was chosen. Measurements were performed at the TU Bergakademie Freiberg, Germany.

4.7.5. ^{13}C Solid State NMR Spectroscopy

In order to obtain the ^{13}C cross polarization (CP) spectra, an Avance HD 400 MHz WB spectrometer (Bruker, Karlsruhe, Germany), equipped with 4 mm triple resonance CP MAS probe (1H, 400.30 MHz; ^{13}C, 100.67 MHz), was used. The following conditions were applied: spinning rate of 10 kHz, contact time of 1 ms, ramp at 70%, decoupling during acquisition time tppm15 and recycle delay of 5 s, with 1024 scans per single measurement. Tetramethylsilane (TMS) was used as a standard for chemical shifts. This technique was used to determine purity of chitinous scaffolds from *C. versicolor* spider. Measurements were performed at the TU Bergakademie Freiberg, Germany.

4.7.6. Powder X–ray Diffraction (XRD)

X-ray diffraction measurements were performed using Seifert-FPM URD6 diffractometer (Seifert-Freiberger Präzisionsmechanik, Germany). A diffractometer was equipped with a sealed X-ray tube and Cu anode operated at 40 kV and 30 mA. The fluorescence radiation and other undesirable radiation signals were reduced by a graphite monochromator positioned in the diffracted beam. All measurements were performed in Bragg–Brentano geometry. The diffraction signals were identified by a scintillation counter. The samples were fixed onto zero-background Si[510]-cut zero-background holder. The occurring of recorded phases was verified by comparison of the measured XRD patterns and with XRD patterns calculated for the respective phase mixture. Peak positions were chosen from ICDD-PDF database (PDF 4+) and pattern refinements from the Bruker Topas 5 software (Bruker AXS). XRD analysis was used to characterize chitinous scaffolds before and after functionalization with silver and calcium carbonate particles. Finally, the crystalline index (CrI; %) was calculated using formula below [302]:

$$\text{CrI}_{110} = \frac{I_{110} + I_{am}}{I_{am}} \cdot 100\% \qquad (7)$$

where:

I_{110} — the maximum signal intensity at $2\theta \cong 19.2°$,

I_{am} — the intensity of amorphous diffraction at $2\theta \cong 16°$,

Measurements were performed at the TU Bergakademie Freiberg, Germany.

4.7.7. Scanning Electron Microscopy (SEM) and Energy-Dispersive X-ray Spectroscopy (EDS)

The scanning electron microscopy of obtained samples was performed using Mira 3 microscope (Tescan, Czech Republic) equipped with EDS Ultim Max 65 (Oxford Instruments, UK). An accelerating voltage of 12 kV was used. A thin carbon or gold layer with a thickness ~20 nm was covered on each lyophilized chitinous scaffold sample using a PV205P (Balzers, Switzerland) coater. The distributions of elements concentration were obtained in the form of EDS pattern maps or in graphs form. SEM method was used to determine morphology of raw materials, chitinous scaffolds from *A. fistularis* marine sponge and *C. versicolor* spider. Moreover, it allowed to determine structure of chitinous scaffold covered with silver and calcium carbonate. Measurements were performed at Faculty of Materials Engineering and Technical Physics, Poznan University of Technology.

4.7.8. Transmission Electron Microscopy (TEM)

TEM method was used to determine ultrastructure and morphology of selected cells seeded onto chitinous scaffolds. At the beginning, chitin scaffolds with the imposed cells were fixated using a 3.6% glutaraldehyde solution in 0.2 M cacodylate buffer (4 °C, overnight). Then, the attached cells were exposed to secondary fixation in 1% osmium tetroxide diluted in 0.1 M cacodylate buffer (25 °C, 1 h), combined with washing of the samples in 0.1 M cacodylate buffer

(3 × 5 min). Next, the materials were passed through a series of graded ethyl alcohol solutions (30%, 50%, 70%, 10 min each, 25 °C) for dehydration. The next day, the dehydration process was continuously carried out by using 80% ethanol, then 90% ethanol and finally a 1:1 mixture of 90% ethanol and 90% acetone. Ultimately, the systems consisting of scaffolds and the attached cells were subjected to rinsing with increasing concentrations of acetone (90%, 95% and finally 100%). At the final step of sample preparation samples were immersed in epoxy resin and polymerized (60 °C, 7 days). Afterwards, epoxy blocks were cut on a Power Tome XL ultramicrotome (RMC, AZ, USA) with a Histo diamond knife (Diatome, Switzerland) into thin 600 nm thickness slides. Once the sections were dried using a heating plate, they were subjected to staining using Toluidine Blue (Alchem, Poland) and anhydrous sodium carbonate − Na_2CO_3 (Alchem, Poland), and closed with a Euparal mounting agent (Roth, Germany). Finally ultrathin sections (thickness ranging between 60 and 70 nm) with the use of an Ultra 45° diamond knife (Diatome, Switzerland), were prepared. The TEM images were performed using JEM-1011 transmission electron microscope (JEOL, Japan) operating at 80 kV. Analysis was performed at the Wroclaw Medical University, Poland.

4.7.9. Thermal Analysis (TGA/DTG)

The thermogravimetric analysis (TGA) was performed using a Jupiter STA 449 F3 analyzer (Netzsch, Germany), in order to determine thermal stability of *A. fistularis* chitinous scaffold and inorganic phase content after $CaCO_3$ functionalization. Approximately 10 mg of each sample was placed into analyzer using an Al_2O_3 crucible. The analysis was performed at the heating rate of 10 °C/min in a nitrogen atmosphere. Measurements were performed at temperature range from 30 to 1000 °C. Moreover, derivative thermogravimetry (DTG) curves were plotted to enhance visualization of the thermal decomposition process.

4.7.10. Micro Computer Tomography (μ-CT)

The μCT was performed in both, dry and wet conditions of chitinous scaffolds isolated from *A. fistularis*. In case of dry conditions, sample was freeze dried prior to scanning. In wet conditions, sample was dehydrated and immersed into sunflower oil to increase X-ray image contrast. Analysis was performed using a MICRO XCT-400 microfocussed X-ray tomographic system (Xradia–Zeiss, CA, USA). The following parameters were used: 40 kV voltage, 10 W power, no filter material, 0.16° rotation step in an angle interval of 184°. Three-dimensional (3D) reconstruction of the scanned materials was created with Avizo Fire (Thermo Fischer Scientific, OR, USA). Measurements were performed at the Warsaw University of Technology, Poland.

4.7.11. Mechanical Testing – Dynamic Mechanical Analysis (DMA)

The mechanical properties tests were carried out using a Q800 Dynamic Mechanical Analysis (DMA) instrument (TA Instruments, CA, USA) combined with compression clamp that enable testing in submersion. During the analysis, chitinous scaffolds before and after $CaCO_3$ functionalization were submerged in demineralized water. Samples were cut into 9x9 mm square with height ca. 1 mm. In order to determine the viscoelastic properties, cyclic sinusoidal loading of the specimen was conducted using a displacement amplitude of 15 μm with frequency ranging from 1 to 10 Hz. Based on the obtained data, the storage (E′) and loss (E″) moduli were calculated along with the tangent of the phase lag angle δ between stress and strain. All the investigated samples, preloaded to 0.005 N, were tested at room temperature after immersion in PBS. Measurements were performed at the Warsaw University of Technology, Poland.

4.7.12. Fluorescence, Light and Digital Microscopy

Microscopic observations were performed using BZ-9000 (Keyence, Japan) microscope, in light as well in fluorescence microscopy. Chitinous scaffolds were visualized also using an advanced digital microscope set consisting of a VHX-

7000 (Keyence, Japan) microscope with zoom lenses VH-Z20R (magnification up to 200×) and VH-Z100UR (magnification up to 1000×). Visualizations were carried out in respect to chitinous scaffolds from *A. archeri* and *A. fistularis* (before and after functionalization) marine sponge and from *C. versicolor* spider. Observations were carried out at the TU Bergakademie Freiberg, Germany and at Poznan University of Technology, Poland.

4.7.13. Atomic Force Microscopy (AFM)

Atomic Force Microscopy was used to characterize chitinous scaffolds from *A. fistularis*, before and after $CaCO_3$ coating. Analysis was performed in two modes, (i) surface visualization/roughness assessment and (ii) force spectroscopy. Surface visualization of the prepared chitinous scaffolds was performed using an MFP 3D BIO atomic force microscope (Oxford Instruments, UK) equipped with an ARC2 controller. Materials were tested in both, dry and wet conditions. Prior to the analysis of the dried materials, samples were freeze dried. The silicon scanning probe AC200TS (Olympus, Japan) and TR400PB (Olympus, Japan) scanning probe was used for dry state examination and wet conditions, respectively. Surface features such as roughness, skewness and kurtosis were calculated based on the recorded AFM topographical maps, using Gwyddion (ver. 2.56) freeware.

The local nanoscale mechanical properties of the surface were examined using an MFP 3D BIO (Oxford Instruments, UK). The stiffness of the scanning materials for the force spectroscopy was developed based on the thermal tune function, which was verified against an absolute calibration method. The Johnson–Kendall–Roberts (JKR) model was chosen for fitting of the obtained results. Measurements were performed at the Warsaw University of Technology, Poland.

4.7.14. Contact angle determination

The Wilhelmy method was used to determine contact angle of pure and biomineralized with $CaCO_3$ chitinous scaffold from *A. fistularis* marine sponge. The following method was chosen because of high porosity of the scaffold and difficulties in drop creation on the surface.

Another analysis of wettability determination concerned contact angles measurements for the spider molted cuticle surface based on the drop's parameters. Two liquids were applied: polar (water – Θw) and non–polar (diiodomethane – Θd). Contact angles were measured using Young–Laplace fitting, surface free energy was calculated by the Owens, Wendt, Rabel and Kaelble (OWRK) method.

The calculated values are mean of 10 measurements. Analysis was performed using a DSA100 Drop Shape Analyzer (KRÜSS, Germany). Observations were carried out at the Warsaw University of Technology, Poland and at Poznan University of Technology, Poland.

4.7.15. Confocal microscopy

The prepared samples of pure and biomineralized with $CaCO_3$ chitinous scaffold from *A. fistularis* marine sponge with hFOB 1.19 cells adhered onto its surface were immersed in phosphate-buffered saline (abbreviated PBS) Sigma Aldrich (MO, USA) and observed using a TCS SP8 confocal microscope (Leica, Germany) at excitation wavelengths of 488 nm and 633 nm. Observations were carried out at the Warsaw University of Technology, Poland.

4.7.16. Alizarin Red S staining

Alizarin Red S dye purchased from Sigma Aldrich (MO, USA) was used for visualization of calcium-containing deposits onto chitinous scaffold (orange–red color) using digital microscopy. In case of staining technique, samples were immersed in 40 mM solution of Alizarin Red S (pH 8.3) for 30 min, at 25 °C. After

that, samples were washed with distilled water several times, to eliminate the unattached dye and transferred directly to the microscope.

4.7.17. Calcofluor White staining

The isolated chitinous scaffolds were stained with 0.1% Calcofluor White (CFW) (Sigma-Aldrich, MO, USA) and compared with an unstained chitinous scaffolds. Materials were immersed in following solution for 6 h without light access at 25 °C. After that, chitin was washed with distilled water several times to eliminate the unattached dye and dried at room temperature. This fluorochrome secretes a bright blue light under UV radiation for polysaccharides containing β-glycosidic bonds (such as chitin).

4.7.18. Low − temperature N_2 sorption

The BET (Brunauer–Emmett–Teller) specific surface area (SSABET) of natural molted spider cuticule and spider chitin was measured using low − temperature N_2 sorption, applying the Quantachrome Autosorb Automated Gas Sorption System (Quantochrome Inc., FL, USA) characterized by measurement uncertainty at the level of 10%. Overall, 22 adsorption points were obtained after 163 h of degassing at 120 °C, with 10 to 12 points in the BET domain. Measurements were performed at Geoscience and Environment Toulouse, France.

Chapter 5. Structural and physicochemical properties of the chitinous scaffolds of poriferan origin

Contents

Recently, biological materials isolated from renewable sources such as plants, microorganisms, or animals remain to be very interesting candidates for scaffolds. Their strong similarity to the extracellular matrix (ECM), minimize chronic inflammation response, commonly recorded during synthetic polymers application [29]. Chitin is widely distributed structural polysaccharide in the nature. Its extraordinary features as well-developed chemical structure, biocompatibility, biodegradability, and renewability makes it interesting candidate for several modern applications. Nevertheless, chitin limitations, resulting from its structural properties, such as difficult solubility, significantly limit its application. Commercial chitin, that is traditionally isolated from fungal biomass (*Aspergillus niger, Mucor rouxii, Agaricus bisporus*) or crustaceans shells (crabs, lobsters, shrimps, crayfish, king crabs), allows to obtain granules, sheets or powder—not as 2D or 3D scaffolds, what additionally exacerbates these problems.

The solution may be to look for alternatives to the synthetically produced scaffolds and to obtain them in the required quantity directly from the source [303]. Therefore, the purpose of this study was the determination of structural and physicochemical properties of naturally prefabricated 3D chitin. In these thesis skeletons of three verongiid demosponges were used (*A. archeri, A. fistularis* and *A. aerophoba*). The detailed characterization of the chitin obtained from these sources is required for improvement of its applicability.

5.1. Structural and mechanical properties of chitin

The microCT analysis of a fragment of pure chitinous skeleton from *A. fistularis* marine sponge showed that the overall shape and morphology of the isolated skeleton closely resemble native material. Such results were possible to obtain because, chitinous scaffold from marine demosponge was analyzed by computer tomography in the water immersion, for the first time. The high resolution (2 µm) allowed to visualize the typical macro-porous character of the sponge structure (see **Figure 18 B**). The average thickness of single fibers was estimated as 98 ± 35 µm. The polydisperse nature of the interconnected pores sizes were demonstrated in **Figure 18 C**. Variations of the colors are related with differences of the pore's dimensions (see scale bar). Detailed characterization of chitinous skeleton parameters is presented in the **Table 8**. It is worth to notice, that obtained data for bulk porosity and pore size are within the ranges observed for human spongy bone [304]. This makes this material particularly interesting from the tissue engineering point of view.

Table 8. Quantitative data on porosity and pore size distributions of isolated chitin obtained from µCT analysis. Cortical and spongy bone parameters data adopted from [304].

Material	Porosity (%)	Pores size (µm)
Cortical bone	8-28	5-200
Spongy bone	30-90	15-900
Isolated chitin	79	255-341
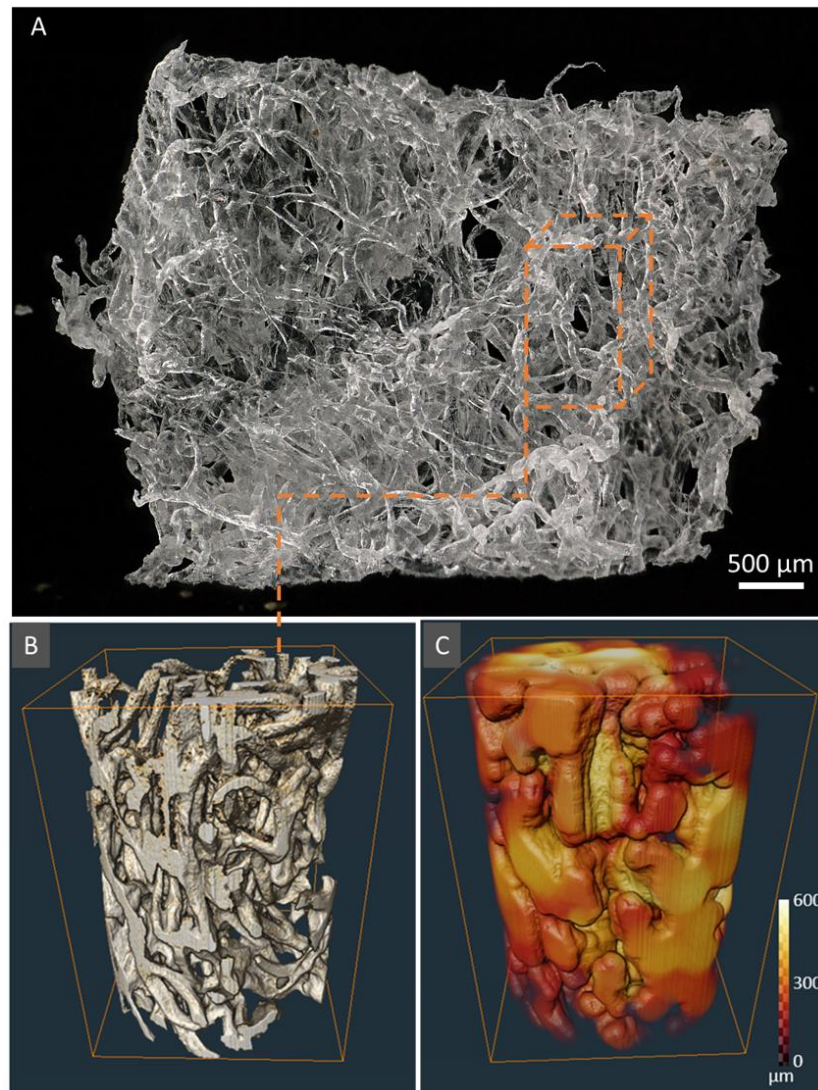
Figure 18. *(A) The digital microscopy image of a fragment of A. fistulartis marine sponge chitinous scaffold. (B) 3D reconstruction obtained from μCT under oil immersion conditions. (C) Distribution of the porous space between the chitin fibers showed their interconnected arrangement.*

SEM images indicated that pure chitinous scaffolds, isolated from sponges of *Aplysinidae* family, possess 3D arrangement of fibers connection with characteristic hollow spaces inside each of them (**Figure 19**). The individual fibers reach between 70–100 micrometers in diameter. Noteworthy is fact, that as compared with other "*chitin sources*", only sponges create a tube-like, interconnected macro-pores, and structurally organized 3D chitinous skeleton in this dimension. Therefore, successfully-conducted isolation allowed to obtain a "*ready to use*" matrices/scaffolds [29].
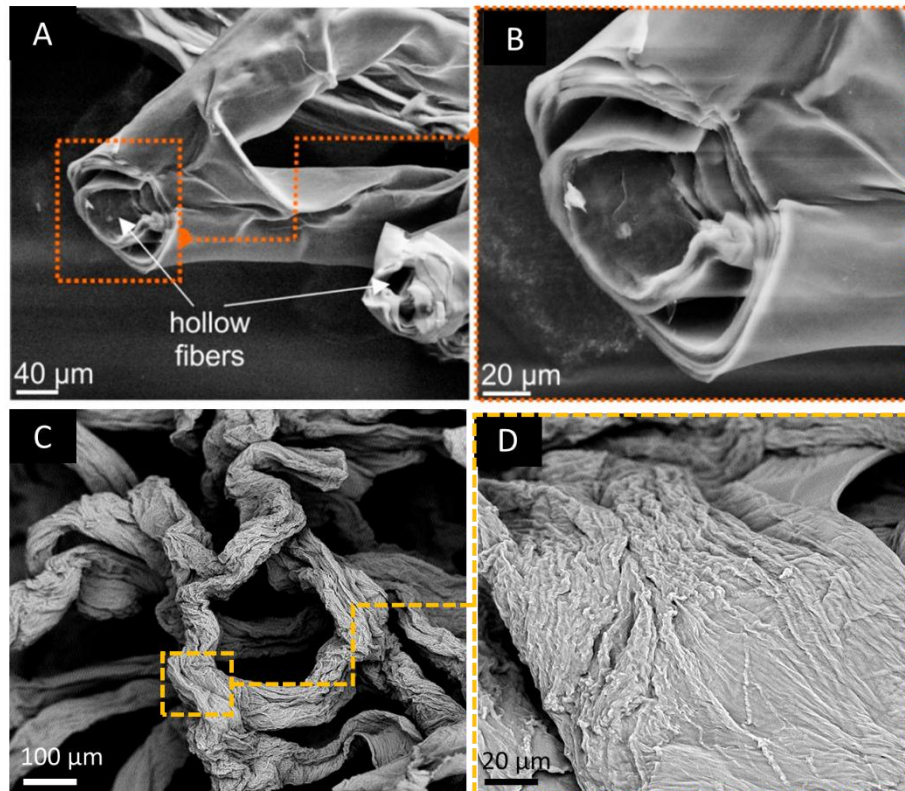
Figure 19. (A, B) SEM imagery of the demineralized and deproteinized skeleton fibers obtained from marine sponge after microwave-assisted treatment and freeze-drying, based on [75]. (C, D) SEM imagery of the demineralized and deproteinized chitinous fibers obtained from Aplysinidae family marine demosponge after standard 7-days chemical isolation and drying at room temperature.

However, it should be stated that surface structure observed on the SEM images is related with both, isolation and drying methods. As showed in **Figure 19 A** and **B**, microwave assisted method of chitin isolation and freeze-drying, allowed to obtain smooth surface. Both, short-term alkali treatment and lyophilization, enabled to preserve natural smoothness of the surface and its natural form [75]. It is worth highlighting that these chitinous scaffolds of poriferan origin are extremely sensitive to conventionally drying at ambient temperatures, which results in collapsing of fibers, increase in surface roughness and degradation of 3D morphology (see **Figure 19 C, D**). After that, 3D scaffold became flatter and even after hydration its morphology and swelling capacities are changed.

Several times Calcofluor White (CFW) staining was used for identifying the isolated biological material as chitin [305,306]. The stain is used as a fluorescent dye for staining of β-(1→3)- and β-(1→4)-linked polysaccharides, where emits a blue light. The microfibers of the skeleton scaffold isolated from *A. archeri* with the microwave-assisted treatment show characteristic intensive fluorescence after CFW staining (**Figure 20**).
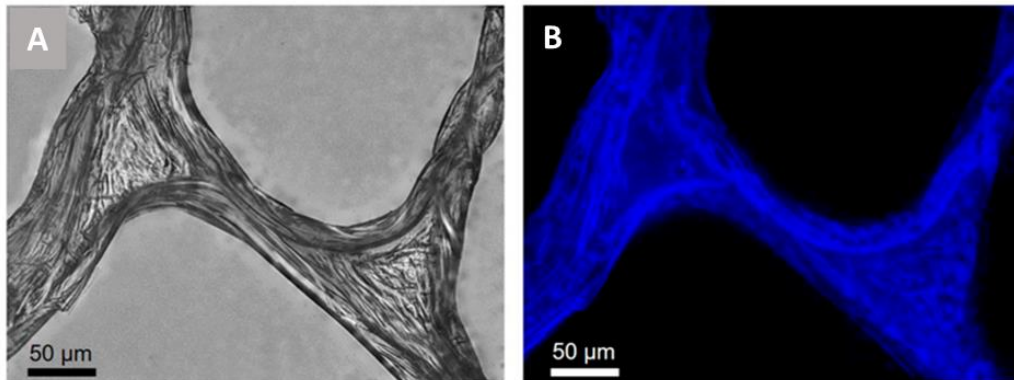
Figure 20. (A) Light microscopy and (B) fluorescence microscopy images of chitinous fibers from A. archeri marine demosponge after Calcofluor White (CFW) staining. Intensive blue fluorescence remains measurable even under a light exposure time 1/3700 s, based on [75].

The mechanical resistance of isolated chitinous scaffold is crucial parameter which needs to be determined. However, it is worth to notice that Verongiida order marine demosponge skeleton is naturally bounded with proteins. In these state this biocomposite is much more flexible and elastic than after proteins removal (see **Figure 21**). This is a natural feature of marine demosponge skeletons, which correspond to their evolutionary adaptation to sedentary life-strategy and nutrition through the filtering of seawater.
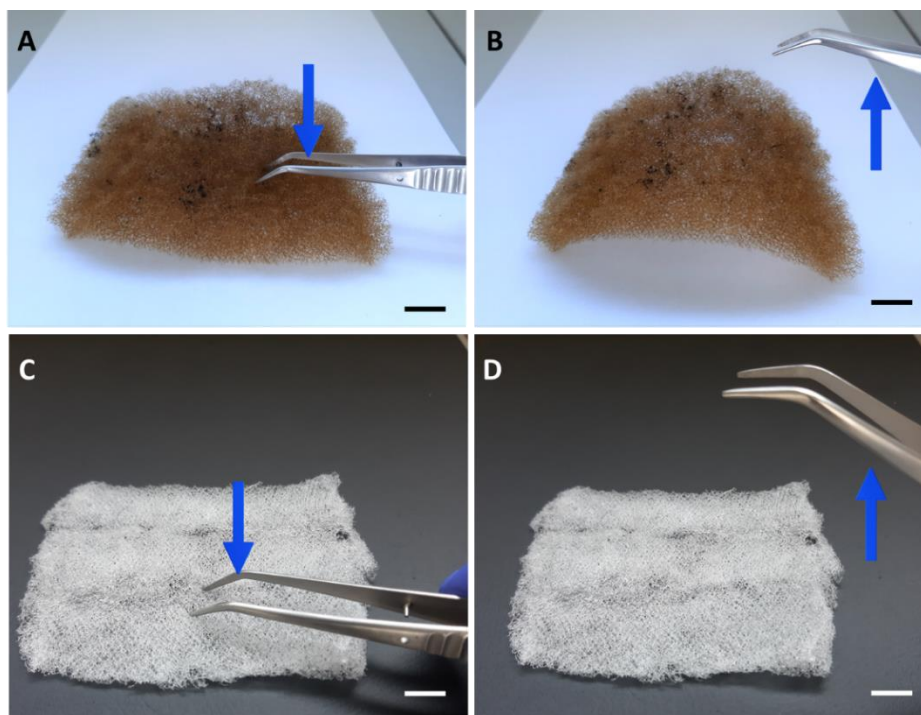
Figure 21. (A, B) Imaginary comparison of mechanical behavior of the isolated chitin/protein pigmented biocomposite skeleton and (C, D) pure chitinous skeleton from A. fistularis marine demosponge. Scale bar 1 cm.

The macro-scale mechanical compression test was used to calculate Young's modulus (**Figure 22**). The α-chitinous skeleton isolated from *A. fistularis* marine sponge was characterized in respect to mechanical properties in water immersion state for the first time. Several authors analyzed native soft tissues and organs, and as observed their Young's modulus range from 0.1 kPa to 1 MPa (varying on the function and type of tissue) [40,41]. Prádný and co-authors [64], determined, that collagenous matrix isolated from biological tissues obtained Young's modulus as follow: <1 kPa for nerve tissue, ~10 kPa for muscle tissue, and ~100 kPa for hard tissue. As could be seen in **Figure 22,** the stress–strain curves exhibit a non-linear trend without exact yielding points. In the first stage of the test, low stiffness may be observed. Then stiffness rapidly growth in the second stage, similar to natural extracellular matrices (ECMs) [307]. The overall macro-scale compressive modulus was calculated as ~0.5 kPa. However, it should be stated that these results are only illustrative. The high porosity of the scaffold is problematic here, because stress is exerted only on few fibers within

the sample cross-sectional area. Moreover, measurements could be disturbed by water flow out of the structure. Modulus is a result of proportionality between stress and strain, when stress is expressed as force per area. Thus, the calculated modulus of the structure is much lower than the modulus of the fiber in bulk. Therefore, for better understanding of the modulus of the single fiber, nano-scale mechanical properties were determined using Atomic Force Microscopy (see comparative analysis Chapter 7, section 7.3).
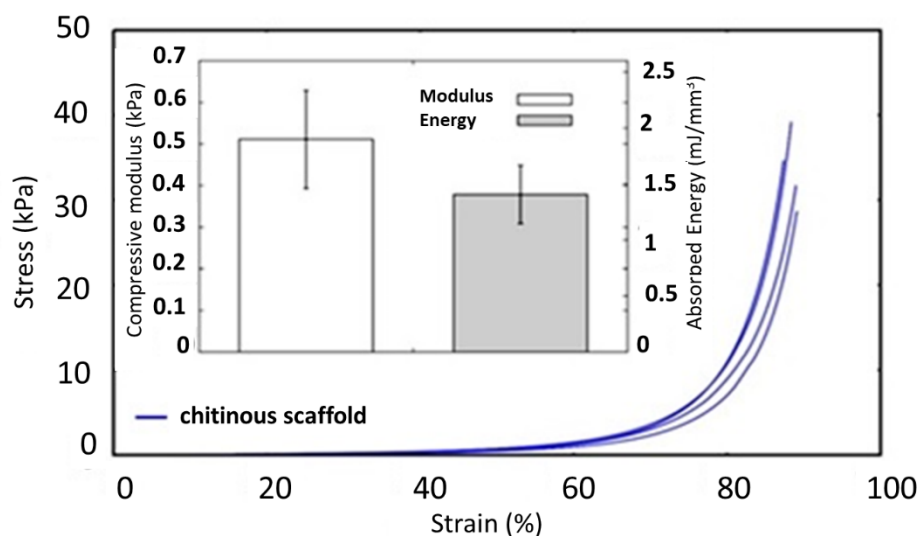
Figure 22. *The macro-scale compression stress–strain response for pure chitin–based scaffolds obtained from A. fistularis demosponge skeleton, adopted from Machałowski et al.* [29].

5.2. Physicochemical characterization of poriferan chitin

The influence of standard chemical treatment onto physicochemical parameters of poriferan chitin was determined previously [227,306,308]. In these studies, ESI-MS and TGA analysis were applied to designate purity of chitinous scaffold obtained by microwave assisted isolation method. Further analysis, as Raman and FTIR spectroscopies, were used to exclude possible transformation of chitin from *A. archeri* into chitosan, under the applied conditions.

Electrospray ionization mass spectrometry (ESI-MS) is a sensitive method used previously for chitin identification in uncharacterized biological samples [207,309,310]. In this case acetic hydrolysis of chitin by harsh solutions led to the

formation of D-glucosamine (dGlcN), as its indicator is easy visible at ESI-MS spectroscopy. The spectrum obtained after the *A. archeri* scaffold hydrolysis, showed in **Figure 23 A**, possess five main ion signals at m/z 130.16, 162.08, 180.09, 202.07 and 381.15. Four of them (m/z 162.08, 180.09, 202.07, and 381.15) are very close to the spectrum of the standard dGlcN (**Figure 23 B**). The obtained signals can be attributed to dGlcN species (m/z 180.09), species obtained after elimination of a single water molecule [M − H_2O + H^+] (m/z 162.08), species corresponding to a combination of a sodium ion with a dGlcN monomer [M + Na^+] (m/z 202.07) as well as a noncovalent dimer [2M + Na^+] (m/z 381.15). Finally, proton bound GlcN covalent dimer with m/z = 359.17, was detected. Taking into consideration the data presented above, it could be concluded that microwave assisted method allowed to obtain the highly pure chitinous scaffold from the *A. archeri* marine sponge.
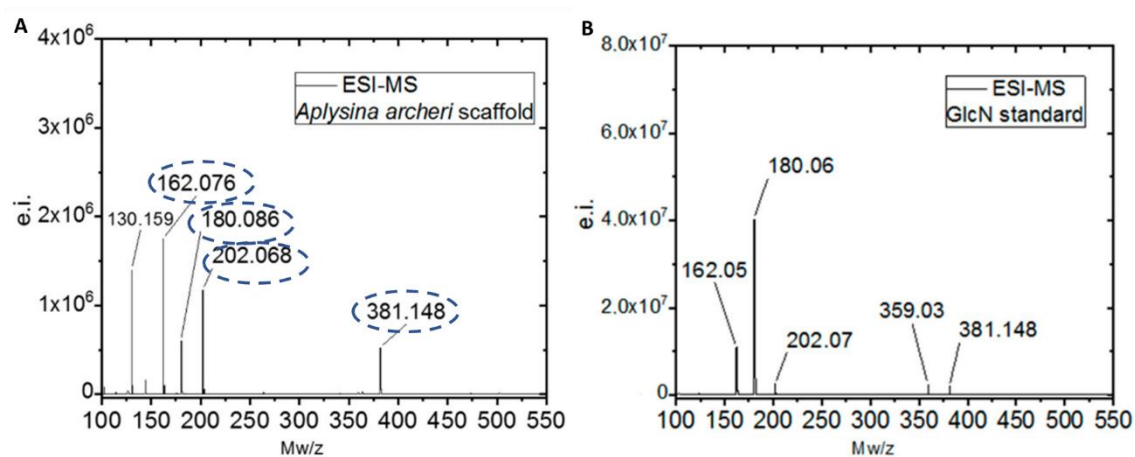
Figure 23. Electrospray-ionization mass spectroscopy (ESI-MS) spectra of (a) A. archeri skeleton chitinous scaffold; (b) pure dGlcN for comparison as reference, based on [75].

In the TGA/DTG graph showed in **Figure 24**, two significant decomposition regions are visible. The first lies at temperature of about 100 °C and corresponds to the loss of physically and chemically bound water molecules [311]. The quantity of water was estimated as 5%. The second significant mass loss was recorded in the temperature range of 200–400 °C. This region is standardly observed thought the thermal and oxidative decomposition of the

chitin [202]. The highest rate of decomposition, visible as the maximum peak of the DTG curve (grey line), was established as 8.5%/min. at 340 °C. Obtained data correspond to previously characterized pure chitinous scaffold from marine sponge [15,312]. Mass decrease visible on the graph in regions characteristic for chitin, may indirectly indicate the absence of any impurities in the isolated material.
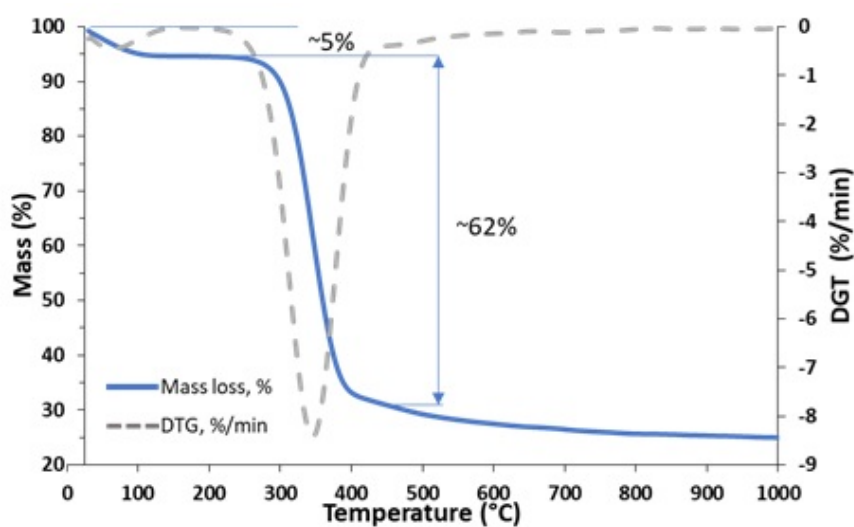
Figure 24. TGA/DTG curves of pure chitinous scaffold isolated from A. archeri marine sponge.

Both, ATR−FTIR and Raman spectroscopies are highly sensitive, qualitative and non-destructive methods for materials characterization. Herein, these analyses were used to exclude the possibility of deacetylation during the isolation of chitin with the microwave approach.

In case of the scaffold isolated from *A. archeri*, there is a splited amide I band visible at 1651 cm^{-1} and 1628 cm^{-1}, in the ATR−FTIR spectrum, which can be attributed to the stretching vibrations of the C=O bonds. Such a band behavior is a typical trait of α-chitin polymorph, that was recorded also here (see in **Figure 25**). It can be attributed to the stretching vibrations of intermolecular (C=O$\cdots$HN) and intramolecular (C=O$\cdots$HO(C6); C=O$\cdots$HN) hydrogen bonds, which occur in α-chitin [253,313]. These bands do not occur in case of chitosan, since it is a deacylated derivative of chitin. The spectra obtained for isolated

scaffold, α-chitin standard and chitosan standard also differ in terms of the amide II band. The amide II band (N–H stretching vibrations), in case of the obtained material as well as α-chitin, is visible at 1551 cm^{-1} and 1556 cm^{-1}, whereas for chitosan it occurs at 1587 cm^{-1} (**Figure 25**). Other typical feature is the amide III band position (C–N stretching and N–H bending vibrations). In the spectra of *A. archeri* scaffold and α-chitin, this band is present at 1308 cm^{-1} and 1306 cm^{-1}, respectively, whereas for chitosan the amide III band is moved to a higher value (1318 cm^{-1}).
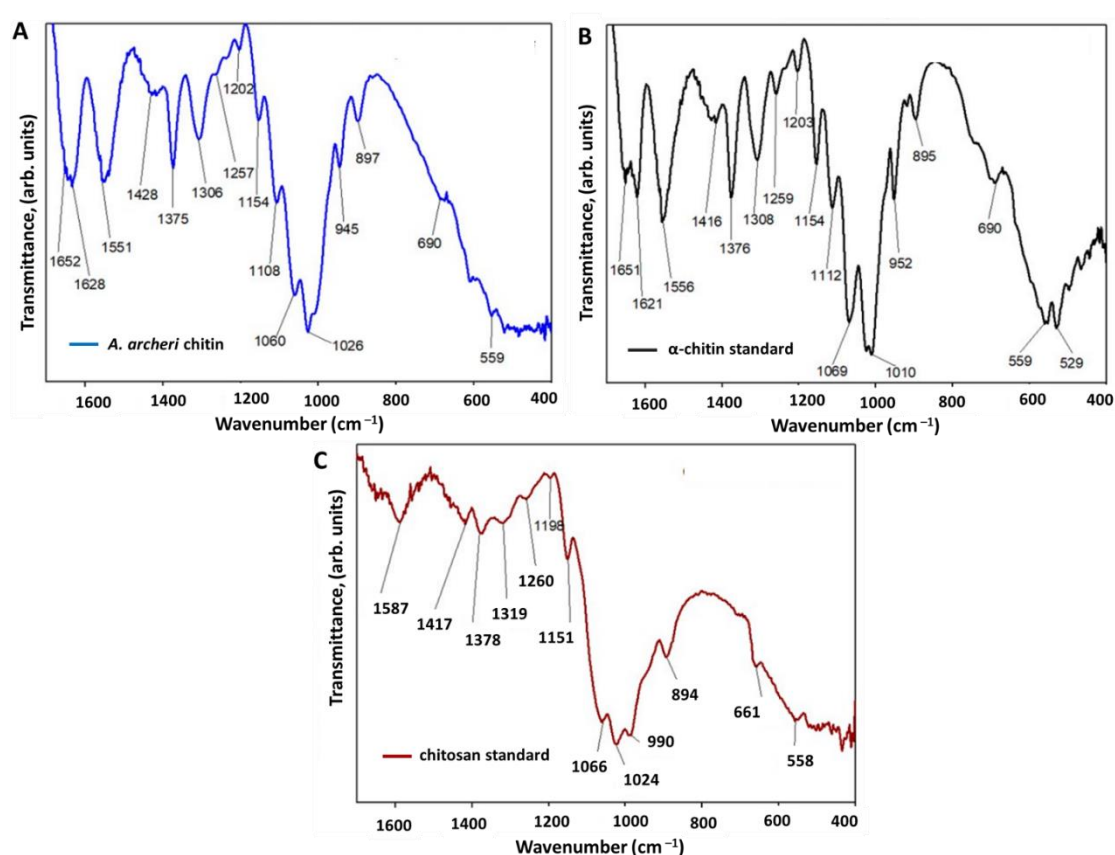
Figure 25. ATR–FTIR spectra of (A) chitin isolated from A. archeri marine demosponge using the microwave-assisted approach, (B) α-chitin standard, (C) chitosan standard, based on [75].

Moreover, its intensity is significantly much lower than for α-chitin spectra. Next differences between obtained chitin and that of chitosan were observed for bands at 952 cm^{-1} and 945 cm^{-1}, established to wagging vibrations of CH$_x$. These peaks are observed only in the isolated scaffold and the α-chitin standard, respectively (**Figure 25**). Detailed and carefully analysis of the bands without any doubt

indicates that the isolated scaffolds correspond of the α-chitin standard. Thus, it proved that microwave-assisted isolation, despite the short-term high temperature (up to 95 °C) and alkaline pH (up to pH = 14) treatment, does not lead to the deacetylation of chitin. Moreover, acetylation degree was calculated as about 85%. As compared to the long-term standard chitin isolation where acetylation degree is about 70-80% [29], this makes such a method safer for chitin chemical structure.
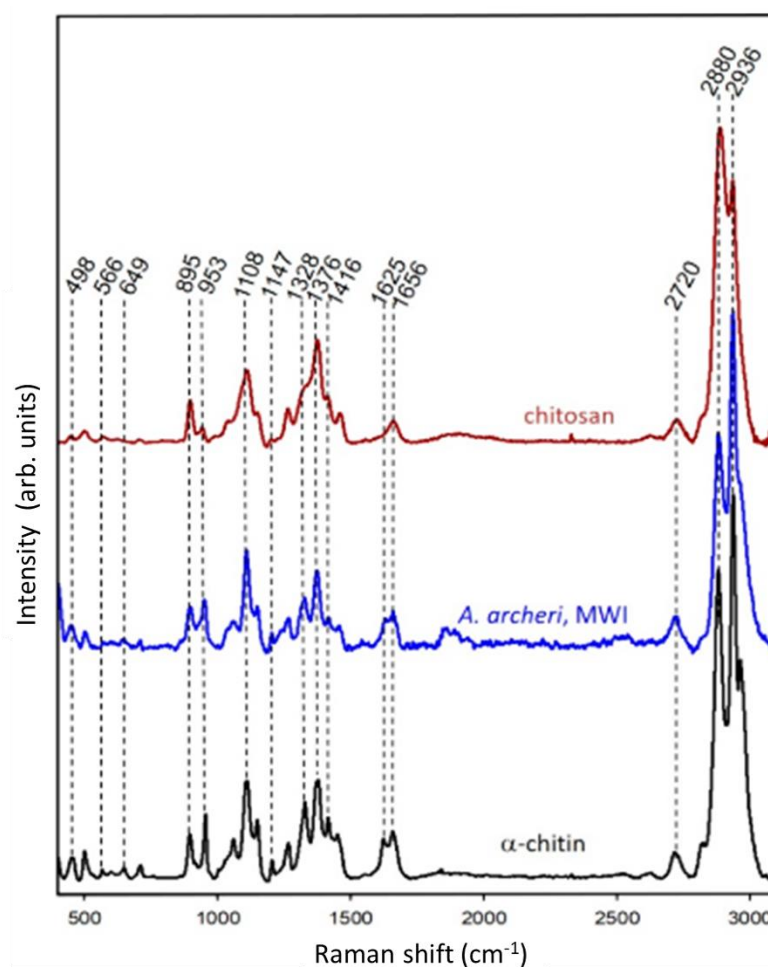
Figure 26. Raman spectra of α-chitin standard, chitin isolated from A. archeri marine demosponge using the microwave-assisted approach, and chitosan, adopted from [75].

The results of Raman analysis correspond to those of ATR−FTIR and confirm the effectiveness of proposed MWI assisted method. The Raman spectra of the isolated scaffolds exhibit high similarity with the spectrum of α-chitin standard,

and not with that of chitosan (**Figure 26**). The main differences are clearly visible in the characteristic regions of amide I, amide II, and amide III.

5.3. Conclusions

Chitinous skeletons of diverse marine sponges, which belong to *Aplysinidae* family (order Verongiida), may provide an alternative to synthetically produced 3D scaffolds with similar shape and dimensions. With the ability to easy underwater grow of marine demosponges, these materials become a renewable source of chitin with unique properties. Their three-dimensional morphology, porosity (~80%) and well-developed chemical structure is worth noting here. Results of ATR–FTIR and Raman spectroscopies confirm that isolated material is composed with pure α-chitin. Its high thermal stability may be useful feature for further functionalization e.g. to improve material roughness or mechanical properties by high temperature processes. For the first time, the macro-scale mechanical properties of porifera chitin were determined through compression test in immersion (~0.5 kPa). Its natural affinity for both, proteins and inorganic materials, opens a wide range of possibilities for application in tissue engineering and environmental protection. The presented data confirmed that chitin from marine sponges obtained under study, is resistant for short-term microwave irradiation in high alkaline environment. The benefits of using this method are incredibly significant. First of all, it reduces the isolation time from about 7 days to less than 1 h. It is connected not only with unprecedented tempo of isolation but also with significant reduction of used reagents with lower concentration. Therefore, this method is in line with the principles of "*Green Chemistry*". Structural analysis has showed that the biomaterial obtained by this method retains its natural shape and arrangement. Moreover, physicochemical studies confirmed the absence of negative effects of microwaves on the chemical structure of chitin.

Chapter 6. Evaluation of the biomedical utility of pure chitinous scaffold from selected marine demosponges

Contents

Recently observed trend in biomedicine assumes a bent towards natural materials, making their hard-to-counterfeit qualities visible. Naturally prefabricated matrices structures of marine origin that serve as models of "*marine biomimetics*", are perfectly in line with this phenomenon [314]. This tendency is well characterized in the book by Australian scientist Choi and Ben-Nissan entitled *Marine-Derived Biomaterials for Tissue Engineering Applications.* The state of Professor Pierfrancesco Morganti described them in such a way "*the use of natural polymers in substitution to the petrol-derived ones seems the best way to produce skin-friendly healthy tissues and, slowing down the increased plastics production and waste, to try to save the Earth's environment equilibrium and biodiversity*" [315].

Chitin offers extraordinary properties for various biomedical applications as drug delivery, wound dressing, TE scaffold component. Fundamental work of Barzic and Albu [316], describing in details cohesive interaction of crustaceans chitin with blood components, e.g. erythrocytes, fibrinogen, blood fluid, albumin (beneficial for preventing side-effects) and microbes (like *Streptococcus oralis, Escherichia coli, Shigella dysenteriae, Staphylococcus epidermidis Actinomyces naeslundii*), proves their bacteriostatic properties. Moreover, authors observed positive *Ws* value (adhesion) for collagen, which may positively influence cells culture. However, beside biocompatibility of the material also other parameters must meet the requirements for fabrication of an effective scaffold. The great example include advantageous 3D geometrical conformation, porosity, surface

roughness and wettability, appropriate nano- and micromechanical properties, proteins adsorption and other [38]. Recently, scaffold fabrication were developed in two paths: the first (i) assumes their synthetic production [59,61,317,318], where second (ii) focus on renewable naturally pre-designed scaffolds in their original shape [72,76,119].

Three-dimensional α-chitin scaffolds of marine demosponges origin have been recognized as an excellent support for the attachment and proliferation of the cells. However, only three types of cells have been developed up today to be seeded: chondrocytes [319], human mesenchymal stem cells [32,32] and cardiomyocyte cells [33,104]. In this study, poriferan chitinous scaffold isolated from *A. fistularis* was used as a support for the cultivation of major groups of skin cells. It is worth to highlight, that keratinocytes (HaCaT) and fibroblasts (NHDF, Balb3T3) play crucial role in wound healing and skin regeneration.

6.1. Cytotoxicity of poriferan chitin

In this study qualitive tests on cytotoxicity were carried out. Observations of cells culture were conducted under and near the α-chitin scaffolds. Cytotoxicity studies of chitin scaffolds isolated from *A. fistularis* marine demosponge did not indicate any changes in Balb/3T3 fibroblast cells morphology after 24 h incubation. Such results suggest that obtained materials exhibit lack of cytotoxicity [296]. Furthermore, the control cell culture without contact with chitin was observed. Comparative observations showed that chitin did not exhibit any symptoms of cytotoxicity (see **Figure 27**).
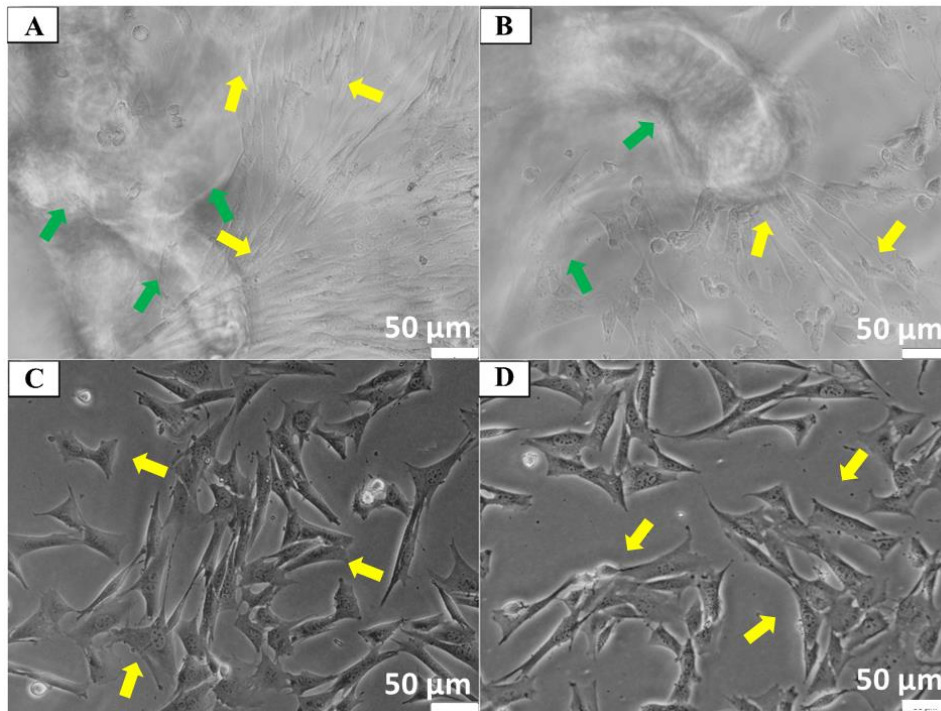
Figure 27. Estimation of cytotoxicity of chitin scaffolds isolated from A. fistularis demosponge after 24 h contact with Balb/3T3 fibroblasts cell culture. (A) Cells under the scaffold, (B) near the scaffold, (C) at a distance from the scaffold, (D) control culture. Balb/3T3 fibroblasts cell culture were indicated by yellow arrows. Chitinous scaffold fibers were marked by green arrows.

Further and detailed characterization of potential cytotoxic effect concerned the ultrastructure of human keratinocytes and fibroblasts seeded onto poriferan α-chitin scaffolds. In these case cells attached to the scaffold were immersed in epoxy resin block, sliced into 600 nm thickness slides, and observed by TEM. Keratinocytes (HaCaT) were oval-shaped or spindle-shaped, with an extended euchromatic nucleus. The nuclei had between one to three distinct and compact nucleoli and had an irregular nuclear envelope. The cytoplasm contains several lipid droplets, vacuoles, polyribosomes, scattered sacs of rough endoplasmic reticulum (RER), and intermediate filaments. Extended or oval mitochondria comprised lamellar cristae (**Figure 28 A**, **B**). Additionally, HaCaT created multi layers of cells interconnected with each other by well-developed desmosomes (**Figure 28 C**, **D**). This indicates the beginning of skin tissue formation, as desmosomes are protuberances responsible for communicating

between cells. Thus, without any doubt chitin did not negatively affect the attached cells morphology.
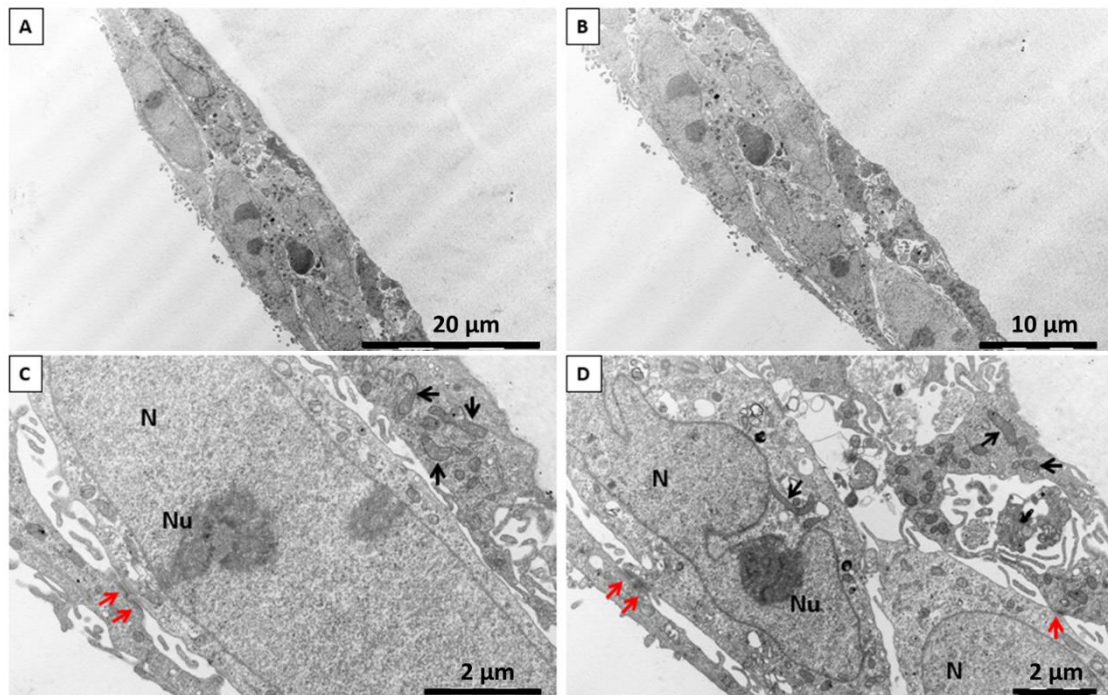
Figure 28*. Representative transition electron microscopy images of HaCaT cell morphology adhered on the chitin. Nucleus without any signs of death with the well-preserved ultrastructure of organelles is visible. Legend: N—nucleus, Nu—reticular nucleolus, black arrows— mitochondria, red arrows—desmosomes, adopted from Machałowski et al.* [29].

The ultrastructure of the human fibroblasts (NHDF) showed well-developed organelles, like Golgi apparatus, abundant vesicles, and multivesicular bodies. Additionally, the cell membrane of the fibroblasts formed little and stubby microvilli. As compared to the HaCaT (keratinocytes), the NHDF cytoplasm included more vacuoles and sacs of rough endoplasmic reticulum. Oval or elongated mitochondria present lamellar cristae. The oval euchromatic nuclei were characterized by indentations in the nuclear envelope and exhibited prominent reticular nucleoli (**Figure 29**). The ultrastructure of both skin cells types was excellently maintained and did not show signals of degeneration, which additionally support results showed above. Herein, it was showed that chitinous scaffold isolated from *A. fistularis* is nontoxic and biocompatible to both, human keratinocytes and fibroblasts cells. Noteworthy is

fact that any signals of the cell death were observed. The cells were analyzed in details with respect to shrinkage, rupture or blebbing of the plasma membrane, swelling of cytoplasm, degradation of organelle, or condensation and fragmentation of chromatin [320,321]. Moreover, any ultrastructural and morphological changes in mitochondrial cristae (remodeling or rupture) were not observed. Thus apoptosis or necrosis of the cells can be excluded [322].
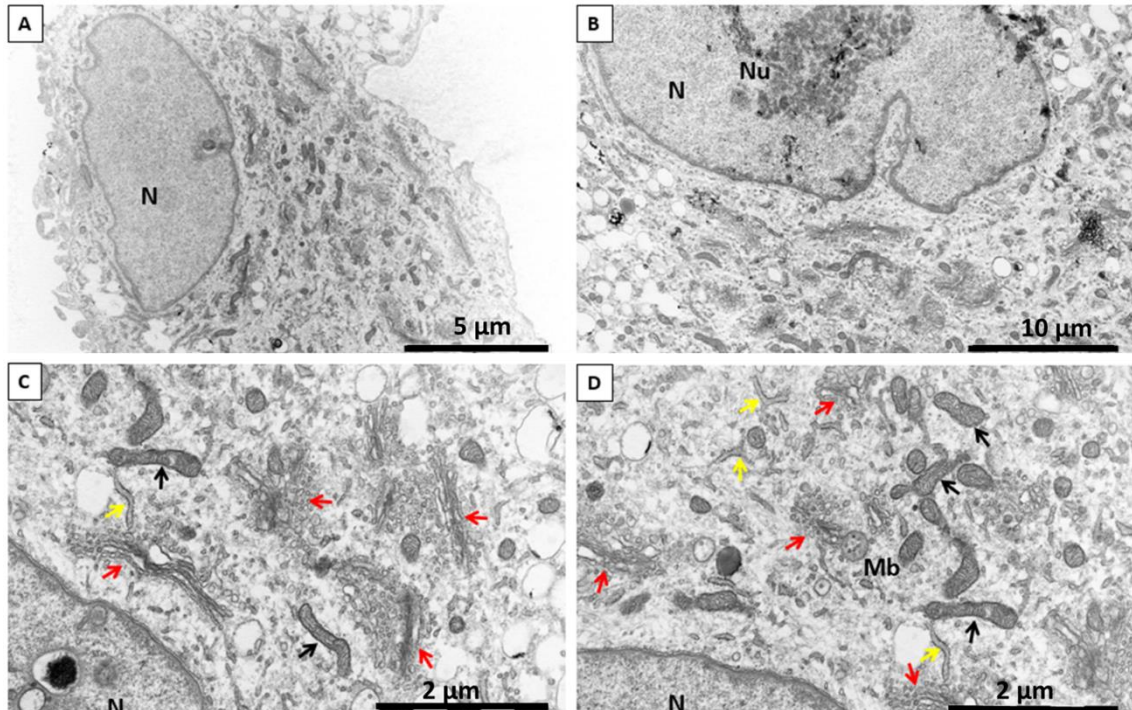
Figure 29. Representative transition electron microscopy images of NHDF cell morphology adhered on the chitin. Nucleus without any signs of death with the well-preserved ultrastructure of organelles is visible. Legend: N – nucleus, Nu – reticular nucleolus, Mb – multivesicular body, yellow arrows – rough endoplasmic reticulum, black arrows – mitochondria, red arrows – Golgi apparatus, adopted from Machałowski et al. [29].

The results presented here showed that obtained biomaterial forms a favorable environment for the cells culture. Thus, future applications of chitinous scaffolds in TE, wound repair or as dressing material should be further develop because keratinocytes are the major cell type in the skin. Because of high porosity of prepared materials and difficulties in creation exactly the same scaffold series, quantitative analyses were not carried out. Thus, cytotoxic studies were limited only to very detailed qualitive tests.

6.2. Determination of skin cells attachment and proliferation

Cells attachment is one of the most important feature of successful scaffold applicability. TEM images presented below (**Figure 30**), show human keratinocytes HaCaT cells tightly attached to the α-chitin scaffolds isolated from *A. fistularis* demosponge surface 24 h after seeding. Visualization was performed after enhancing the contrast of the cell membranes by Toluidine Blue staining and counterstaining with the hazardous metal salts, respectively.
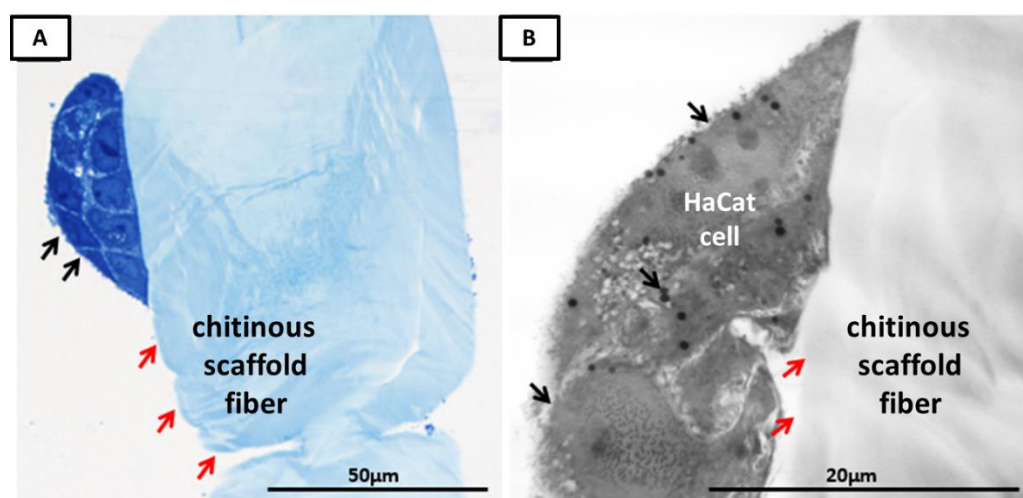
Figure 30. Groups of HaCaT cells (black arrows) after (A) Toluidine Blue staining, and (B) counterstaining with the hazardous metal salts. Cells are tightly attached to the chitin scaffolds surface (red arrows). A—semithin section; B—ultrathin section.

The real cells attachment to the surface of examined material is showed in **Figure 31**. By Crystal Violet staining it can be easy observe, that single cells of Balb/3T3, NHDF and HaCaT (blue dots), are attached to the surface of the chitin scaffold surface after 24 h of the seeding. The limited number of adhered cells may be related with gentle rocking culture or too invasive washing procedure. Other explanation could be the limited number of seeded cells/scaffold size ratio or high porosity of the scaffold. However, after 7 days of incubation, bigger groups of cells were observed onto chitin surface. Thus, it can be noticed that all cell's types proliferate on the investigated material (**Figure 31 D-F**). Because of small cell's number, they spread in first 24 h was limited and only after 7 days of incubation was observed (see yellow arrows in **Figure 31 D**). The

round/cluster form morphology adopted by cells and limited spreading may be also related with the very soft mechanical performance of the poriferan chitinous scaffold or low protein adsorption [323]. In this regard, the adhering cells may generate forces which exceed the interactions between the chitin matrix and the adsorbed proteins.
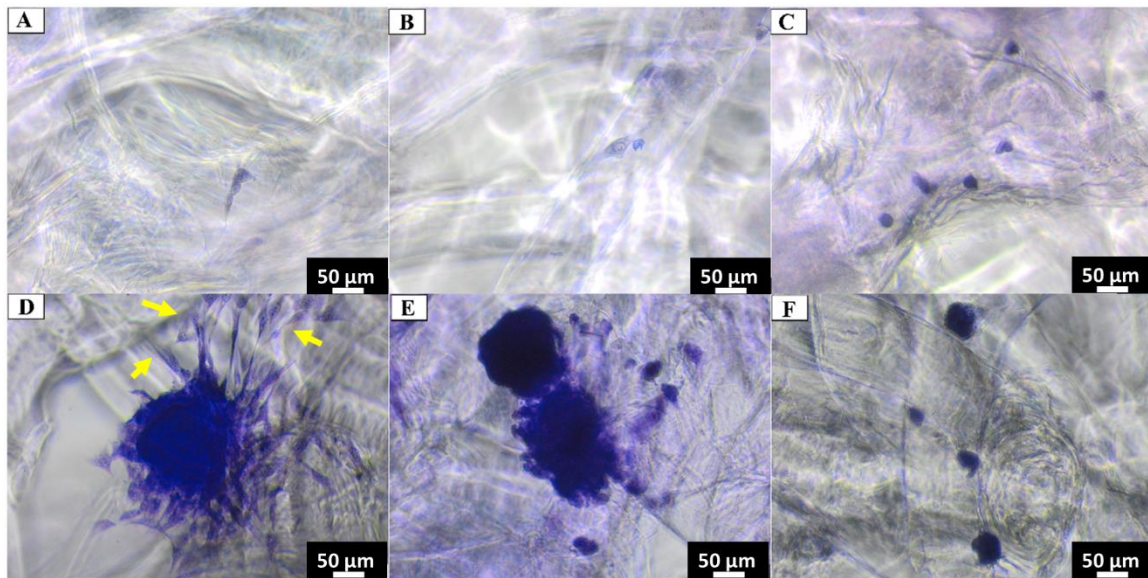
Figure 31. Cell cultures on A. fistularis chitin scaffold surface stained by Crystal Violet after incubation for (A–C) 24 h and (D–F) for 7 days. Legend: (A, D)—Balb/3T3; (B, E)—NHDF; (C, F)—HaCaT.

To investigate the biocompatibility of the 3D chitin scaffold under study, Neutral Red live-cell staining was carried out. The following stain is used as a vital dye to stain living cells. Only live cells may incorporate Neutral Red into their lysosomes (cells red color). Thus, when cells start to die, their ability to incorporate stain diminishes. Results of these study showed the live single cells of Balb/3T3, NHDF, and HaCaT adhered to the chitin surface after 24 h of incubation. However, after 7 days of the culture, groups of cells are visible on the scaffold surface under inverse contrast-phase and fluorescence microscopy, what confirms their viability (**Figure 32**).
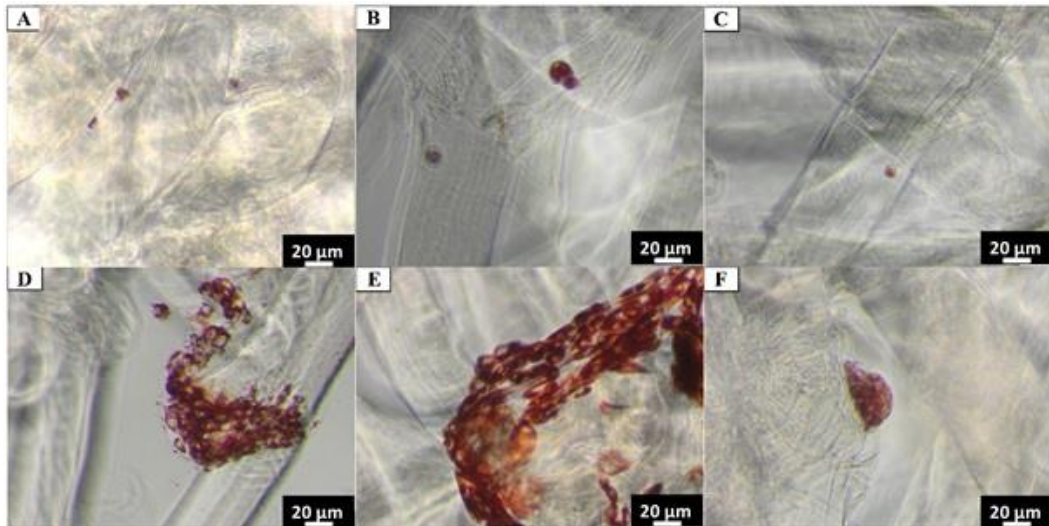
Figure 32. Adhered and viable cells on A. fistularis chitin scaffold surface stained by Neutral Red assay) after incubation for (A–C) 24 h and (D–F) for 7 days. Legend: (A, D) – Balb/3T3; (B, E) – NHDF; (C, F) – HaCaT.

To additional characterize of the Balb/3T3, NHDF, and HaCaT cells attachment to the chitin scaffold, Scanning Electron Microscopy (SEM) observations were carried out. Dehydrated and dried cells were visualized after 24 h of incubation. Similar like in the data presented above, only single cells attached to the surface are visible (yellow arrows). The observations of cells cultured for 7 days showed bigger, more extended, and flatter groups of cells on the chitinous scaffold surface. This result may suggest that the cells adhere more firmly on the material (**Figure 33**). Previously, very similar fibroblasts cells behavior was observed on a poly(e-caprolactone)/chitosan composite scaffold [324]. A significant rise in the number of cells is visible after 7 days as compared to the 24 h cell cultures. However, in future research long term (30 days) cultivation is needed to better understand the relationship between fibroblasts and keratinocytes cells and the poriferan chitin scaffold.
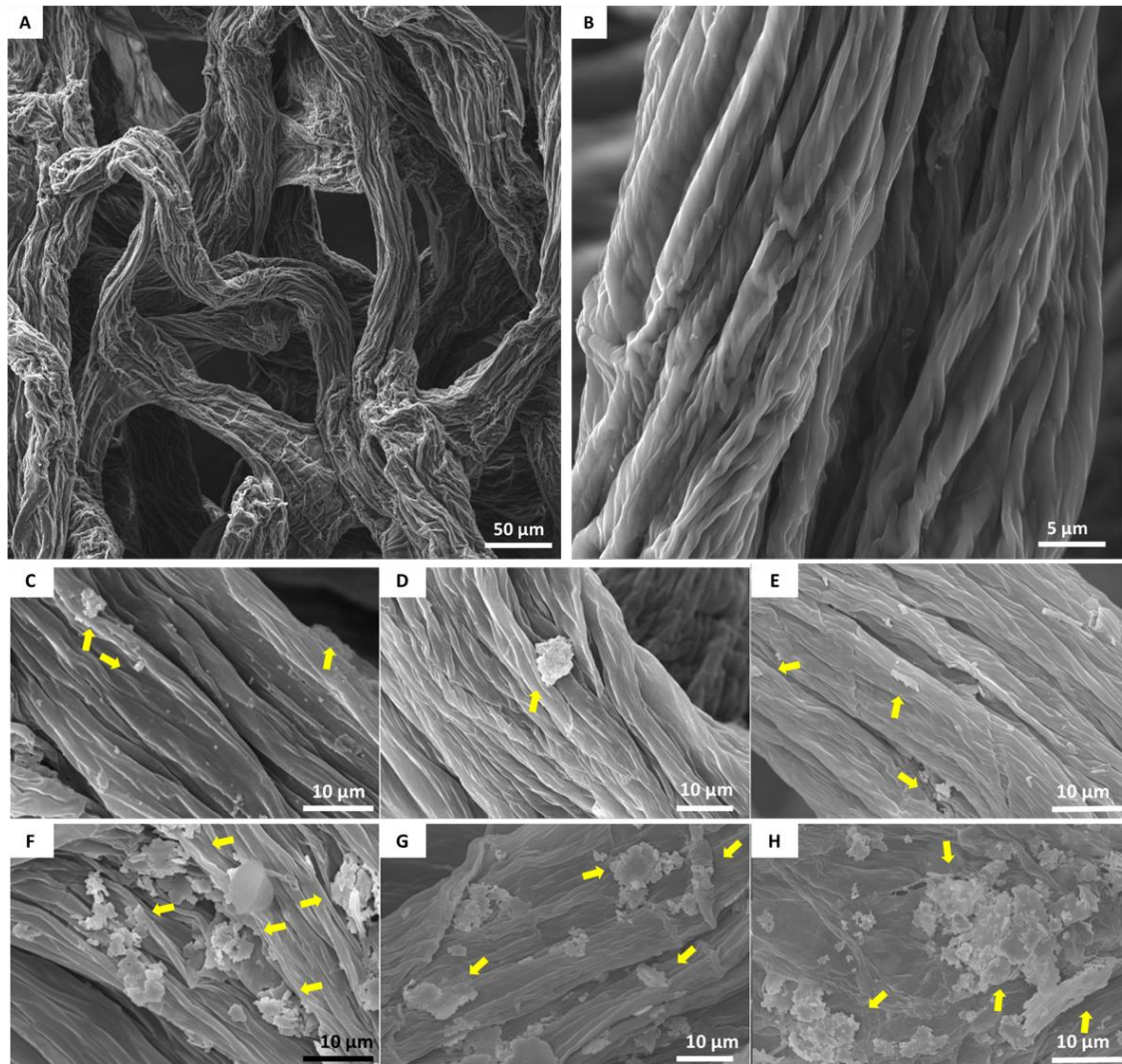
Figure 33. SEM images show cell adhesion on a chitin scaffold surface. (A, B) Pure chitinous scaffold isolated from A. fistularis. Cells after 24 h and 7 days of culture. Legend: (C, F)— Balb/3T3; (D, G)—NHDF; (E, H)—HaCaT. Yellow arrows – cells.

6.3. Conclusions

In this study naturally prefabricated chitinous skeletons from *A. fistularis* marine demosponge were used as scaffolds for skin cells cultivation. Very promising results of qualitative cytotoxicity analysis showed that prepared material did not negatively affect cells morphology and ultrastructure. Analyses were performed in both macro- and micro scale. Attached cells were carefully screened for detection of potential death signals or organelle degradation. However, their ultrastructure did not demonstrate any apoptosis or necrosis signs. The cells cytoplasm contains several lipid droplets, vacuoles,

polyribosomes, endoplasmic reticulum (RER), and well-developed nucleus. Then, specific staining and SEM analyses allowed for better observations of the cell's attachment and proliferation onto chitinous scaffold. Both keratinocytes and fibroblasts created bigger group of cells culture and started spreading after 7 days. Nevertheless, as future research long-term culture (up to 30 days) should be carried out. Moreover, due to high scaffold porosity determined here by μCT, higher initial concentration of the cells should be used in the future research. Therefore, in the future, it would be advisable to work on developing a more efficient method of cells deposition on the scaffold and more effective control over their culture. Nevertheless, the results discussed in this section confirm the research hypothesis, that chitin isolated from marine sponges in natural form is a promising material for biomedical applications. This statement can be confirmed by the lack of cytotoxicity, desmosomes formation by human keratinocytes and both fibroblasts and keratinocytes cells attachment to the chitinous scaffold surface.

Chapter 7. Naturally pre-designed chitinous scaffold biomineralized *ex-vivo,* characterization and application

Contents

Recently, significant increase in the number of publications concerning application of natural biopolymers in biomedicine is observed [35]. It is not wondering due to their attractive properties, as renewability, biodegradability, and cost-efficiency [3,36]. Chitin is one of the biological materials that offers such properties. From chemical point of view, chitin is a copolymer of *N*-acetyl-D-glucosamine and D-glucosamine units linked by β-1,4 glycosidic bonds [202] and is the most abundant polysaccharide in the animal world [73]. Only ocean-living animals may produce up to 10^{12}–10^{14} tons of chitin each year [200]. However, chitin has also some disadvantages. Firstly, this biopolymer is non-soluble in conventional solvents what definitely hinders its industrial application. From the other hand, chitin in pure form has week mechanical properties. Nevertheless, its enormous abundance and limited usability prompts to look for new possibilities of functionalization of naturally prefabricated chitinous scaffolds.

Herein, special attention was paid to biofunctionalization as an effective and powerful approach which is in line with the principles of "*Green Chemistry*" [325]. Biofunctionalization is a special type of modification aimed for enriching the surface of a selected materials (scaffold) with specific properties, e.g.

electrical charge of functional groups, wettability, surface roughness, topography, or mechanical properties. In relation to tissue engineering such properties enhancement is essential for the modulation of cells attachment, proliferation and differentiation [38]. Natural methods, living organisms or their enzymes, body fluids and others are used for this purpose. The presence of corresponding calcium-rich mineral phases on the surface of matrices is particularly important in the case of bone TE [326]. For the first time, *in vivo* deposition of calcium carbonate on the implants surface was performed in 2015, using living eastern oysters, *Crassostrea virginica* [327]. Authors observed cellular activity during shell layer formation onto different metal alloy surfaces (Ti$_6$Al$_4$V titanium, 7075-T6 aluminium, and 316 L stainless steel) and in details characterized formation of calcium carbonate onto implants surface.

In this study, for the first time, 3D chitin skeleton isolated from the verongiid demosponge *A. fistularis* was used as a scaffold for biomineralization *ex-vivo*. The novel method assumes the use of hemolymph of cultivated commercially for meat and mucus snail *C. aspersum* as biomineralization agent. The special attention was paid for detailed physicochemical characterization of created mineral phase. Moreover, the differences between pure and biomineralized scaffold were determined with respect to possible human osteoblasts (hFOB 1.19) culture.

7.1. Biological observations of biomineralization assay

The phylum Mollusca has actually around 200,000 living species [328], which represents a large, morphologically diverse group of invertebrate organisms. From economic point of view, snails play crucial role in different area of industry with respect to production of escargot meat and slime for cosmetic and pharmaceutical applications. Interestingly, Poland is one of the biggest exporter of snail meat in European Union [329]. The snail body is hidden in inorganic shell which constitute biocomposite of calcium carbonate and proteins.

Mineralized shell is a basic structure that protects their soft tissues against predators, dehydration and harmful environmental conditions [330]. Thus, over the million's years of evolution, mollusks develop highly effective and fast method of shell fixation to survive. Based on recent review [100], it could be stated that shell regeneration is very complex process which combine cellular and physical phenomena's. Cellular, because snail deliver to the regenerated area specialized cells (granulocytes) which create clot, deposit the calcium binding proteins, Ca^{2+} and HCO_3^- ions and disintegrate their cellular components [7,292,330–333]. Physical, because slow precipitation of snail's hemolymph initiate calcium carbonate minerals formation onto organic template [6,334,335]. The hemolymph of the mollusks is analogous of human blood but adopted to several additional functions. In terrestrial (land) snails, it is mostly composed of water, hemocyanins (oxygen carrier containing Cu^{2+} ion), free inorganic ions, metabolites, enzymes, hormones as well as and a number of cells (e.g. hyalinocytes and granulocytes) [100,336,337] known as hemocytes. Granulocytes constitute about 95% of circulating hemocytes and are specialized in phagocytosis, encapsulation, nodulation and shell regeneration [100]. Furthermore, these cells type contain numerous of calcium-rich vesicles and crystals serving as calcium pool [338].

During realization of this PhD thesis several attempts were made to initiate the biomineralization process out of the living organism using its natural medium – hemolymph. It should be stated that hemolymph isolation (see **Figure 34**) was made without any negative impact to *C. aspersum* snails. During whole experiments signals of premature deaths have not been observed. Isolation procedure was based on non-lethal method described by polish scientists "*New intravital method for hemolymph collection from Cornu aspersum snails and the establishment of standards for selected biochemical parameters of their hemolymph*" [293]. The puncture was made from main vessel using sterile syringe

and needle (**Figure 34 B**). After that, snails were kept in moisture container and supplemented by high calcium-diet. After few hours remineralization of damaged shell start to be visible (small crystals appear) − see article [339]. About 15 h after isolation injured shell was completely remineralized (**Figure 34 D**).
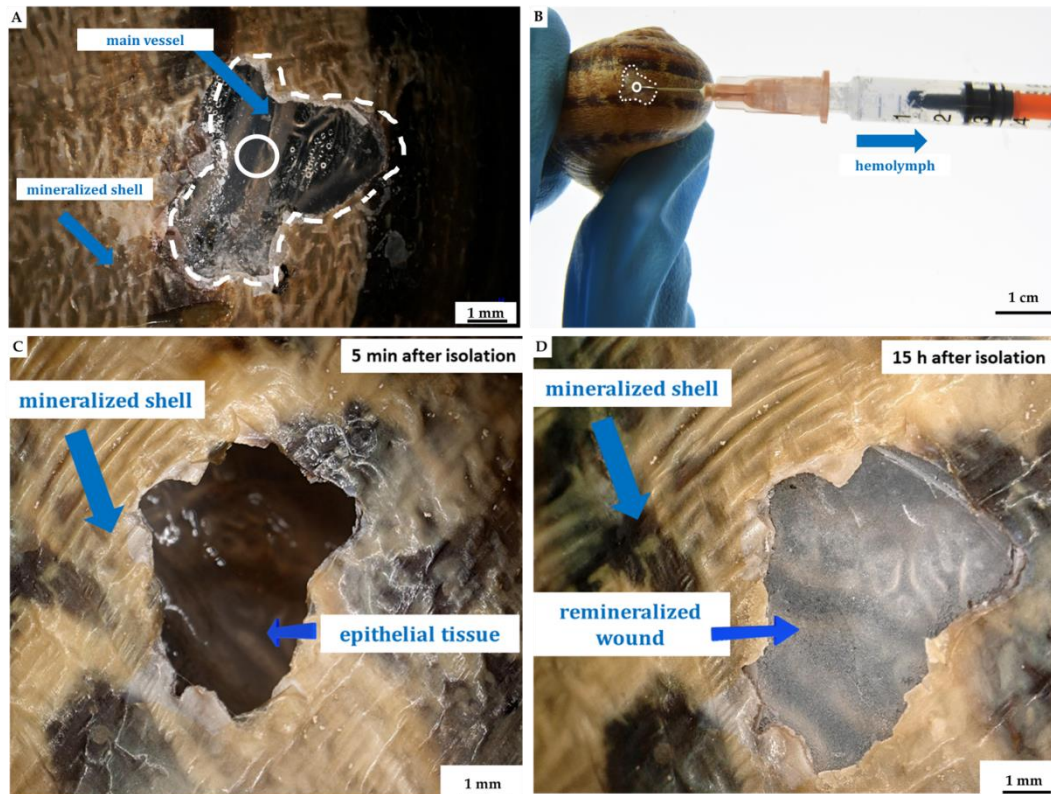
Figure 34. (A,B) The representation of non-lethal extraction of the hemolymph from cultivated C. aspersum snail, using syringe. (C) The area of mechanically caused shell damage after hemolymph isolation. (D) Quickly remineralized shell about 15 h after isolation.

The selected fragment of chitinous scaffolds was immersed in the snail hemolymph for 60 min. In this time, several very interesting observations were made (**Figure 35**). As it can be observed in **Figure 35 A**, granulocytes were detected in the medium and their self-organization was observed. Cells created bigger groups, up to 60 individuals (**Figure 35 B**). Moreover, their pseudopodia could be well visible on the image. Previously, similar phenomena of granulocytes behavior was observed during cells-organic matrix interaction as a step of shell regeneration [332]. As it is visible in **Figure 35 C**, **D**, cells created

layer onto chitinous scaffold and some of them disintegrated their nuclear content.
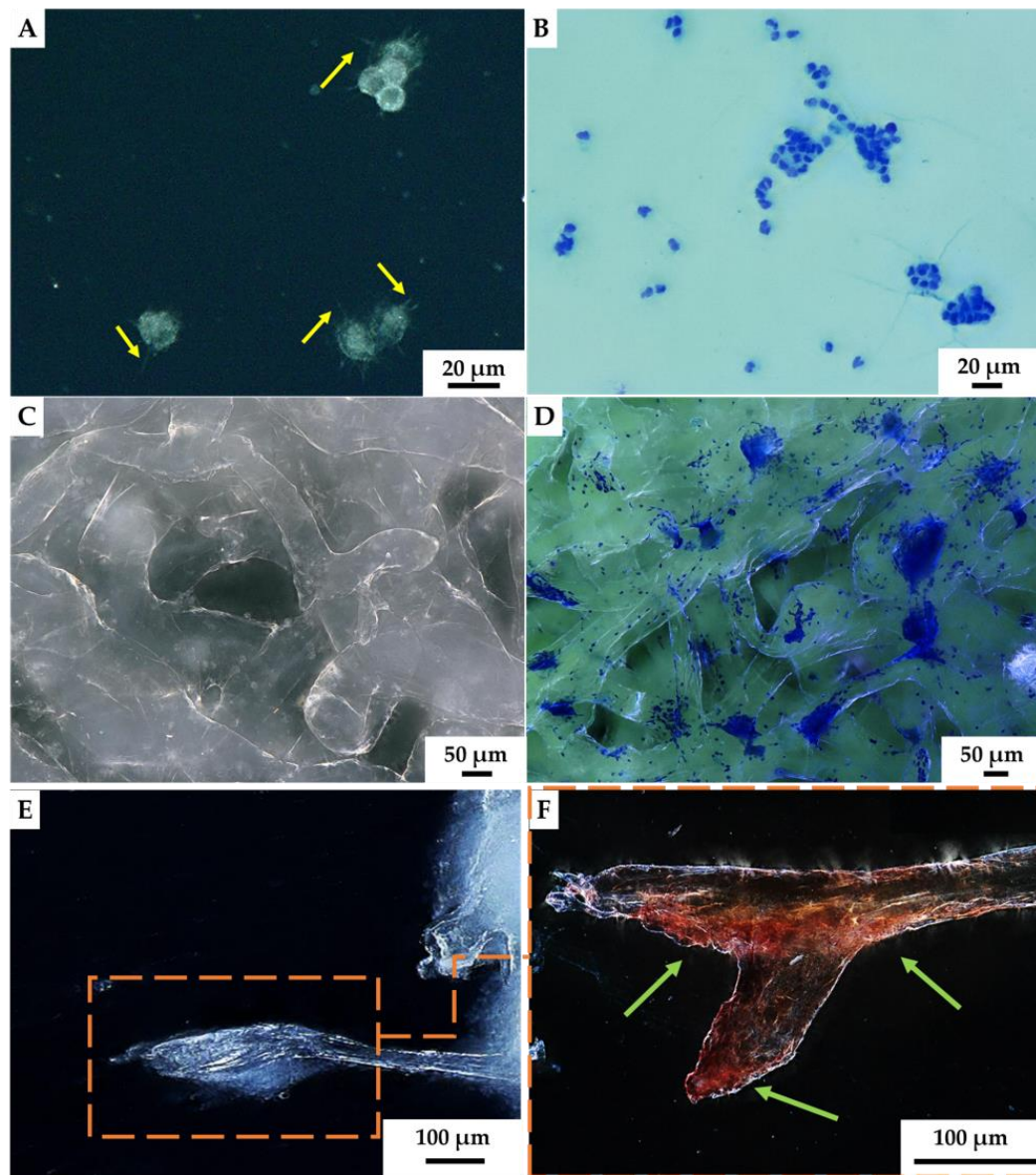
Figure 35. (A) Digital microscopy images of hemocytes present in the isolated medium (hemolymph); characteristic aggregates and pseudopodia (yellow arrows) formation are their natural response for fixation damaged shell. (B) Granulocytes from isolated hemolymph-stained with Eosin and Methylene Blue. (C) The formation of hemocytes-based groups (clots) on the surface of α-chitin scaffold, after 24 h immersion in the hemolymph, prior and (D) after staining with Eosin and Methylene Blue. (E) The cluster of hemocytes surrounded chitin before and (F) after Alizarin Red S staining.

It is in agreement with observations of Chen, "*wound healing in mollusks differs from that in vertebrates for two reasons. First, no extracellular fibers are formed in mollusks. Second, the hemocyte aggregation in mollusks is reversible and some of the*

aggregated cells later disperse, reentering the circulatory system after wound repair" [340]. Without any doubt granulocytes delivered calcium-rich compound by own disintegration to the chitin surface. Alizarin Red S (**Figure 35 E**, **F**) was used to stain their nuclear content. Probably these components take part in next biomineralization steps as calcite or aragonite nucleation centers [100].

7.2. Structural properties of biomimetically biomineralized chitinous scaffold

The digital microscopy images presented in **Figure 36** showed differences between surface of chitinous scaffold isolated from *A. fistularis* demosponge before and after biomineralization using snail hemolymph. After drying and thorough rinsing, inorganic crystals remain to be strongly attached to the scaffold surface (**Figure 36 C, D**). Their morphology seems to be similar to cubic or dumbbell-like biogenic calcite crystals (yellow arrows) [341].
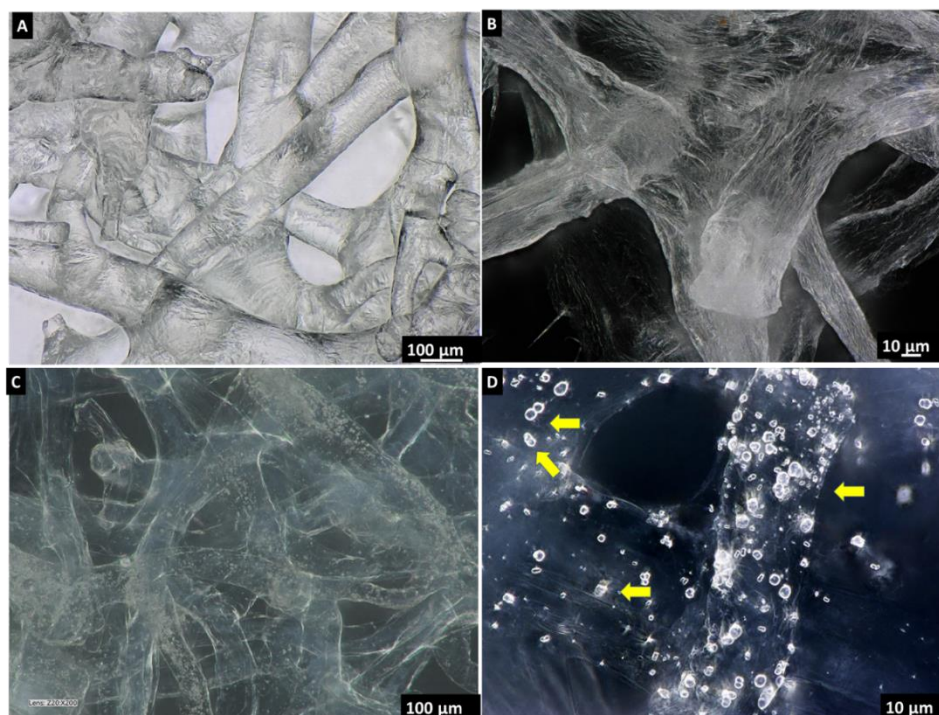
Figure 36. *(A,B) The α-chitin scaffold before and (C, D) after ex vivo biomineralization with C. aspersum hemolymph in different magnification. After drying characteristic cubic morphology crystals similar to the calcite may be observed on the scaffold surface.*

Further analysis of the materials structure by Keyence VHX-7000 digital microscope allowed to observe differences in their porosity (see **Table 9**).

Scaffolds after biomineralization were less porous but only 1% difference was observed. In case of average diameter of minimal pores, 189.74 μm for pure chitin scaffold and 170.69 μm for biomineralized one, were recorded. However, because the biological materials possess natural non-homogeneity, the differences may be related also with the sample's origin.

Table 9. Results of porosity and pore size measurements based on digital microscopy 3D analysis made on a VHX-7000 (Keyence, Osaka, Japan) for both, pure and *ex vivo* biomineralized scaffolds.

Material	Porosity (%)	Average pores diameter (μm)
Pure chitinous scaffold	79	189.74
Biomineralized chitinous scaffold	78	170.69

The formation of calcium-based inorganic phase on the surface of chitin, after its immersion into hemolymph of *C. aspersum* snail and drying, was confirmed by Alizarin Red S staining (**Figure 37**).
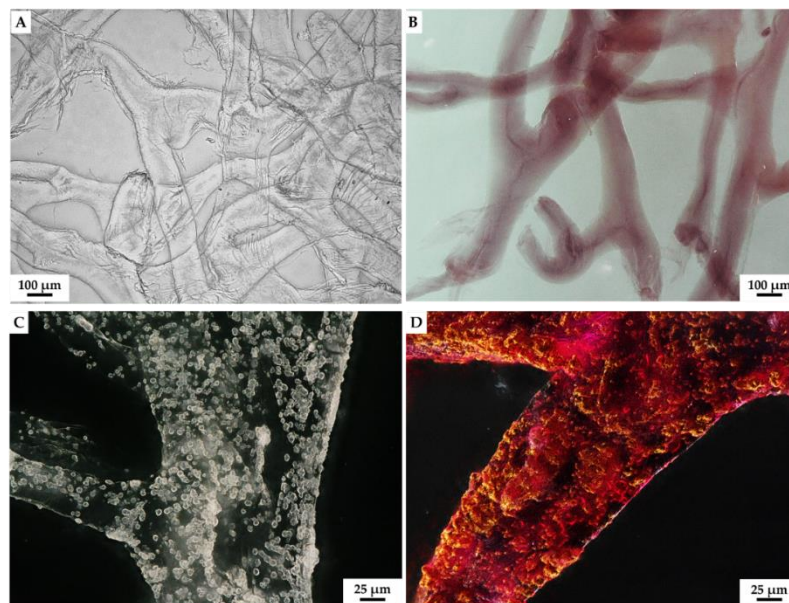
Figure 37. *(A) Poriferan chitin−based scaffold before Alizarin Red S staining and (B) after staining. (C) Biomineralized scaffold before staining and (D) after staining. Characteristic orange-red color corresponds to calcium containing minerals.*

This fact naturally raises an intriguing question regarding the nature of these calcium-based granular deposits. In the nature, first layer of remineralized shell of *C. aspersum* is found to be in aragonite form [339].
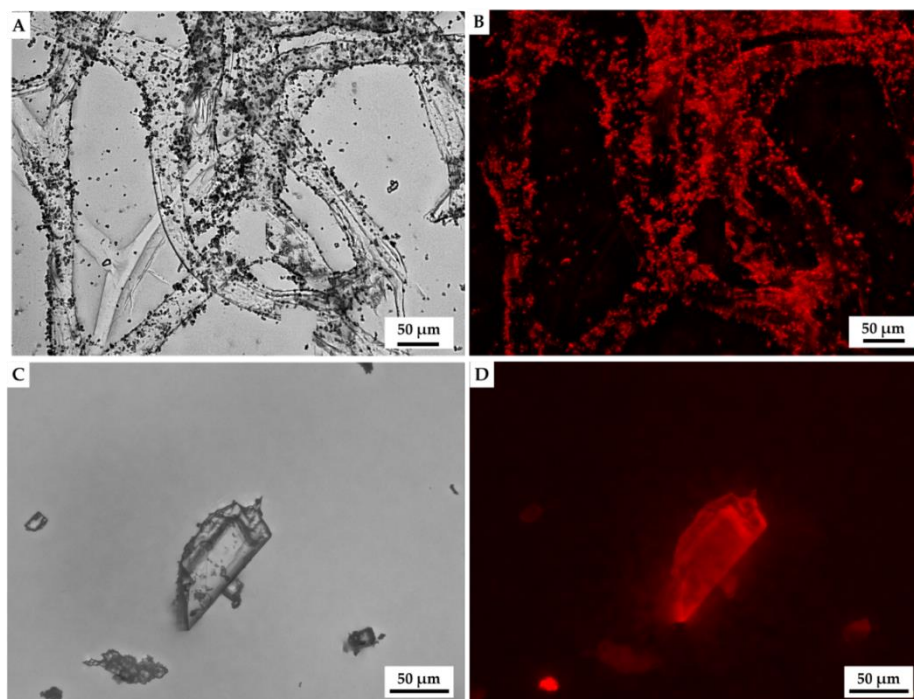
Figure 38. Fluorescence microscopy images of ex-vivo biomineralized scaffold (A) before and (B) after fluorescence in red-light. (C) Standard calcite crystal exposed to red light (D) possess remarkably similar autofluorescence in the red light to biomineralized scaffold.

The first results, which confirm calcite presence, are show in **Figure 38**. The inorganic deposits, formed *ex-vivo* by proposed biofunctionalization method, were observed using fluorescence microscopy. Obtained results clearly showed a high similarity of red auto-fluorescence between bio-calcite standard [342] and micro-size deposits formed *ex-vivo* using *C. aspersum* hemolymph. However, for detailed characterization concerning calcite formation, the traditional analytical techniques such as X-ray diffraction analysis (XRD) (**Figure 39**) and spectroscopic analyses (see below), were used.

The XRD pattern of the biomineralized sample is represented in **Figure 39**. The diffractogram showed amorphous calcium carbonate – ACC content as big hump at $2\theta \approx 20°$. Noteworthy is fact, that ACC was identified as a precursor of

other CaCO₃ polymorph phases in the biomineralization and bionucleation [343]. Superimposed, a set of diffraction peaks being characteristic for calcium carbonate in the form of calcite (ICDD #04-012-0489), were detected. The pattern also showed two unknown diffraction peaks ($2\theta \approx 27°$, $2\theta \approx 33°$). Their detailed characterization did not provide evidence for the presence of a second CaCO₃ variations (aragonite, vaterite, or the structures with crystal water). According to the database search, these two diffraction peaks can derive from a crystallised organic component (probably calcium-binding proteins from hemocytes). Rietveld refinement analysis of diffractogram indicated the differences between the recorded lattice parameters and the database standards. The refined lattice parameters were established as follow: $a = (4.973 \pm 0.001)$ Å (database: $a = 4.987$ Å) and $c = (16.987 \pm 0.001)$ Å (database: $c = 17.058$ Å). These results corresponding to a shrunk lattice. Moreover, what is interesting, calcite is not naturally occurring as a first layer of remineralized shell, thus chitinous matrix probably affect CaCO₃ polymorph nature.
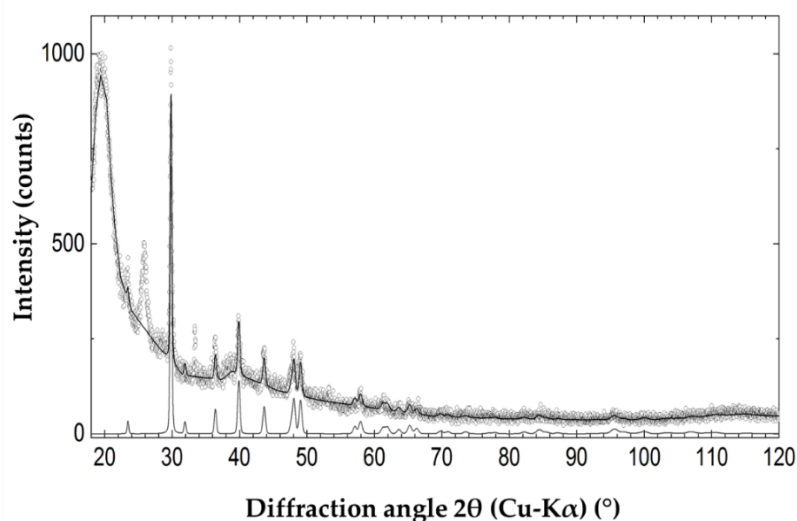
Figure 39. X-ray diffraction pattern of the calcite standard and biomineralized chitin scaffold. Biomineralized scaffold (open dots); the refinement (the solid line), calcite-CaCO₃ standard (bottom of diffractograms). Two unassigned peaks remain in the data ($2\theta \approx 27°$, $2\theta \approx 33°$). The $2\theta \approx 20°$ correspond with high content of amorphous phase in the obtained specimens.

The digital microscopy observations (**Figures 36** and **37**) were improved by SEM+EDS mapping analysis (**Figure 40**). Well-visible crystallites/granules of

calcium carbonate are present on the chitin scaffold. The crystals took, characteristic for calcite, dumbbell like and fused dumbbells shape. Rahman and Shinjo [344] suggest that glycoproteins are responsible for such initial shape of $CaCO_3$. Moreover, as showed in **Figure 40 E**, intriguing nano-connections between inorganic phases are observed.
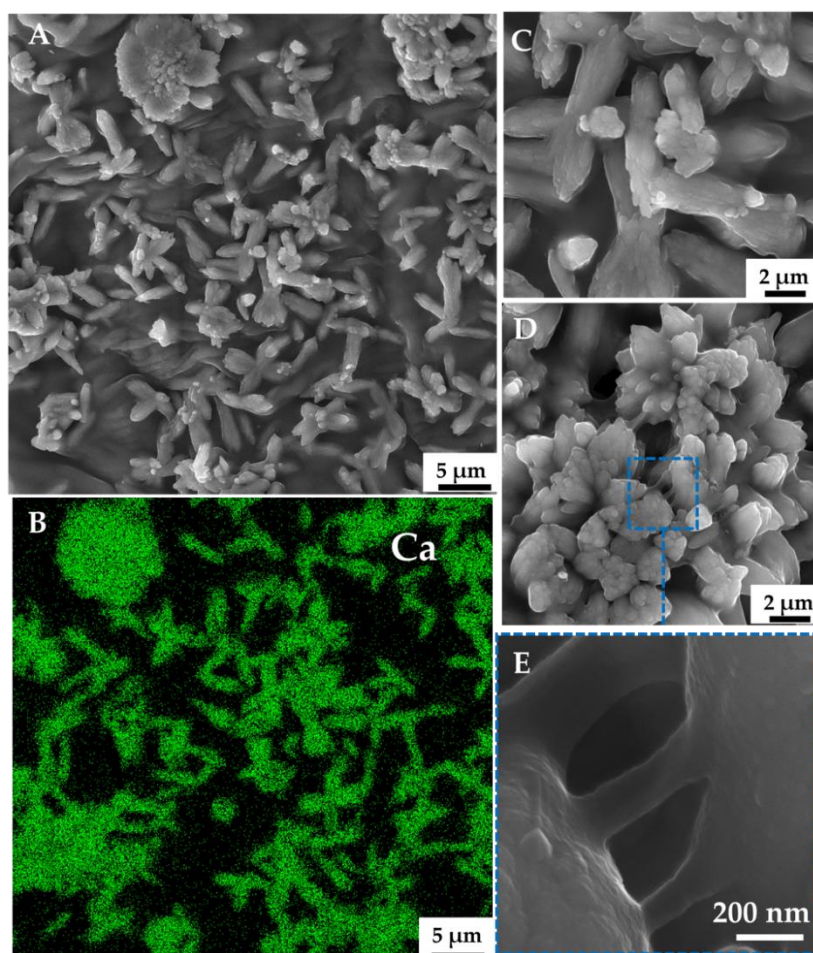
Figure 40. (A, C, D) SEM images of selected surface areas of the ex vivo biomineralized scaffolds at different magnifications. (B) EDS mapping for calcium (Ca) onto biomineralized scaffold surface. (E) Nano-connections between inorganic phases, based on [275].

This statement is in line with XRD analysis results. Nevertheless, possible glycoproteins origin should be analysed deeply in the future research using e.g. XPS analysis. The presence of calcium at the scaffold surface was confirmed by EDS maps (**Figure 40 B**) and spectra results (**Figure 41**). As showed in **Figure 41**, calcium content increased significantly from 0.1% (pure chitin) to 15.8% in biomineralized sample. Interestingly, increase in nitrogen contribution was

also observed in biomineralized scaffold surface up to 10.3% (even after sample washing).
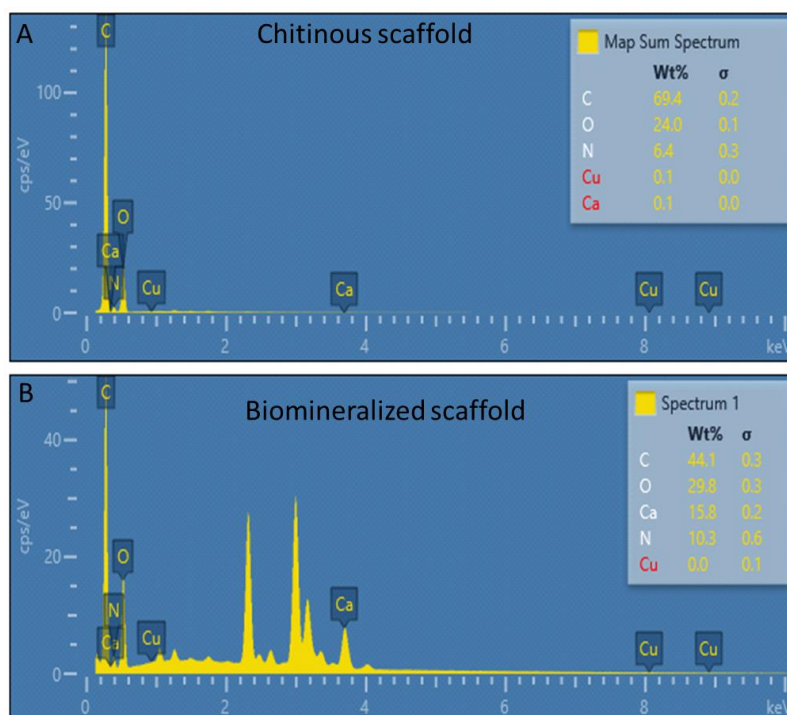
***Figure 41**. EDS analysis concerning distribution of chemical elements on the scaffold surface (A) before and (B) after ex vivo biomineralization performed using molluscan hemolymph.*

For a better understanding of the changes in surface roughness, a comparative AFM analysis was carried out (**Figure 42**). The measured kurtosis values represented in **Table 10,** reveal the presence (> 3) or the absence (< 3) of particles protruding from the surface of a scaffold [345]. The determined differences between the analysed specimens suggest that higher areas visible on the topographic maps for the biomineralized samples correspond with the inorganic agglomerates deposited on their surface (see **Figure 42**). Next, skewness parameter was determined. These value describes the main features of the surface: a positive value ($R_{sk} > 0$) correspond to the surface with a predominance of peaks, otherwise $R_{sk} < 0$ suggest that the surface is more smooth without any high peaks [346]. Moreover, surface of biomineralized samples were even four time rougher than pure chitin. Taking into consideration

obtained results, it can be concluded that proposed biofunctionalization method significantly affects the surface morphology and topography nature.
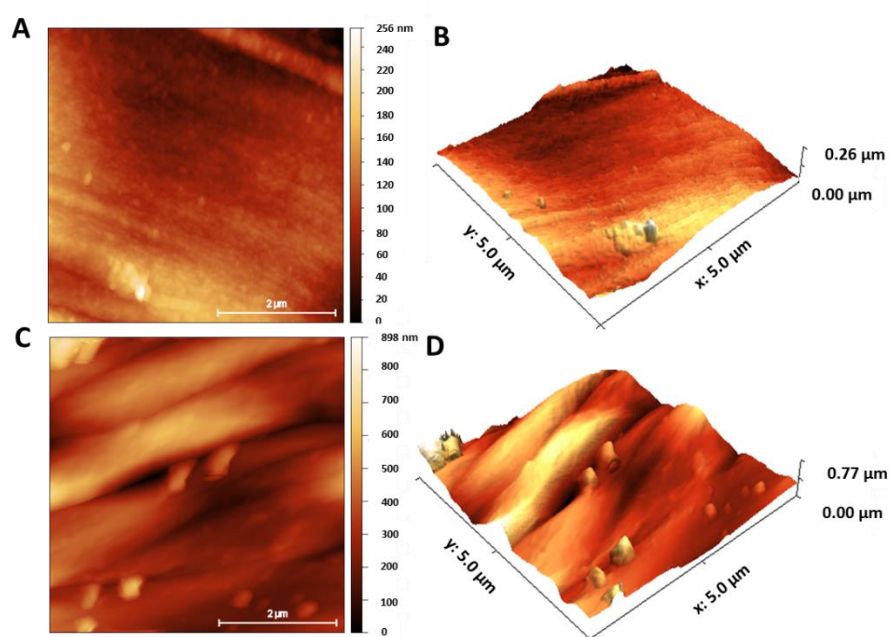
Figure 42. (A,B) 2D and 3D AFM maps of the surface of pure chitinous scaffold and (C,D) biomineralized chitinous scaffold, based on [275].

Table 10. Surface features and parameters quantified based on AFM topographical maps.

Parameter	Pure chitinous scaffold	Biomineralized chitinous scaffold
Roughness (R_q) (nm)	31.75 ± 2.7	120.7 ± 0.3
Roughness (R_a) (nm)	24.55 ± 2.81	91.8 ± 7.3
Skewness (R_{sk})	-0.59 ± 0.05	0.04 ± 0.15
Kurtosis (R_{ku})	0.09 ± 0.05	3.93 ± 0.77

7.3. Physicochemical and mechanical characterization of biomineralized scaffold

Spectroscopic methods, such as Raman or ATR−FTIR, were used previously as highly sensitive techniques for the identification of carbohydrates (especially polysaccharides) [347] and inorganic materials [348]. It is worth to

mention that vibrational spectroscopy gives a detailed insights into intermolecular interactions between sample components.
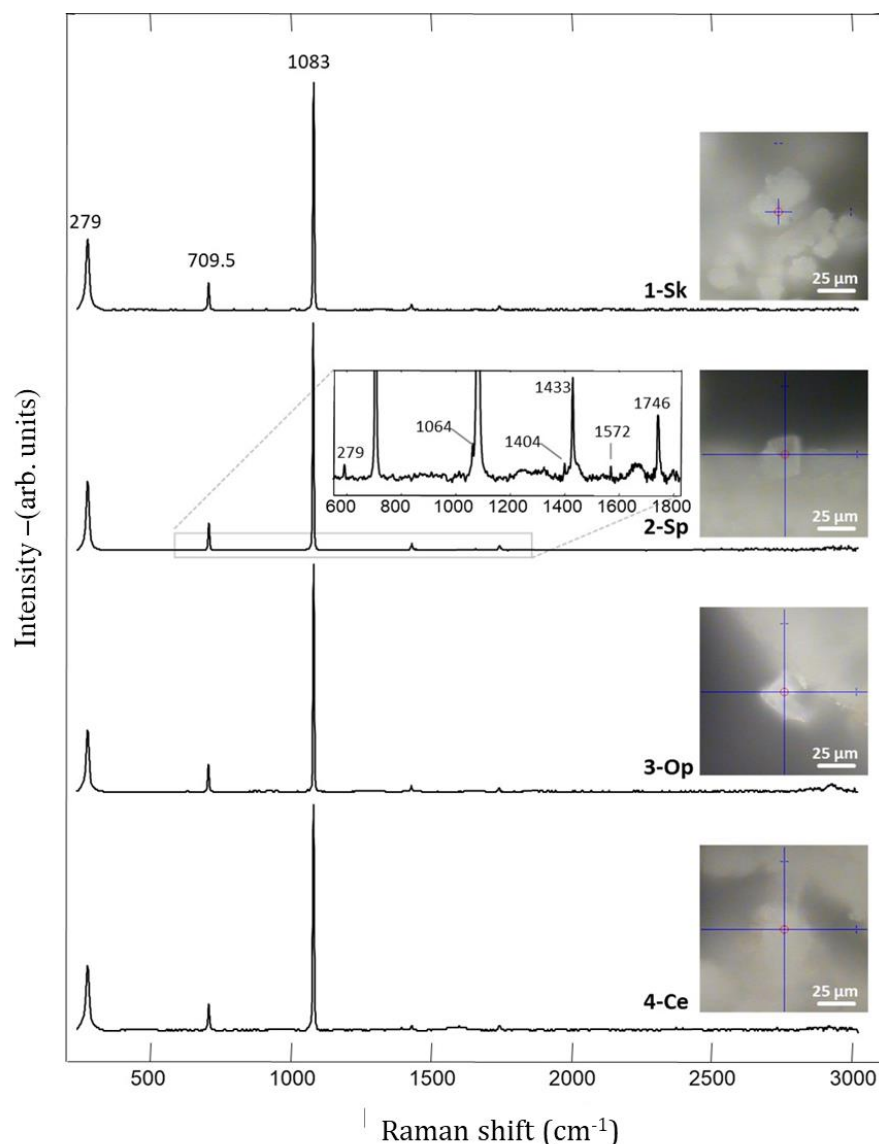
Figure 43. Raman spectra of the mineral phase attached on the surface of 3D chitin scaffold after ex-vivo biomineralization by snail hemolymph.

In these study, results of Raman spectroscopy analysis (**Figure 43**) clearly indicated, that inorganic phase obtained after biomineralization, corresponds to the spectrum acquired for the biogenic calcite [349,350]. The most intensive signal with maximum at about 1083 cm^{-1} is compatible with v_1 symmetric stretching vibrations of CO_3^{2-} of calcite [350]. Then, the band recorded at 1433 cm^{-1} corresponds to CO_3^{2-} v_2 asymmetric stretching vibrations [349]. Other evidences, confirming the presence of calcite polymorph, include peaks at

711 cm^{-1} and 279 cm^{-1}, attributed to plane $\nu 4$ bending vibrations of CO$_3^{2-}$ and vibrational modes of calcite, respectively [349]. Moreover, all of the recorded bands are consistent with calcite, as reported for the natural mineral in the online RRUFF database [351].

Further analysis was performed for pure and biomineralized chitinous scaffold as well as calcite standard (**Figure 44**) using ATR−FTIR spectroscopy.
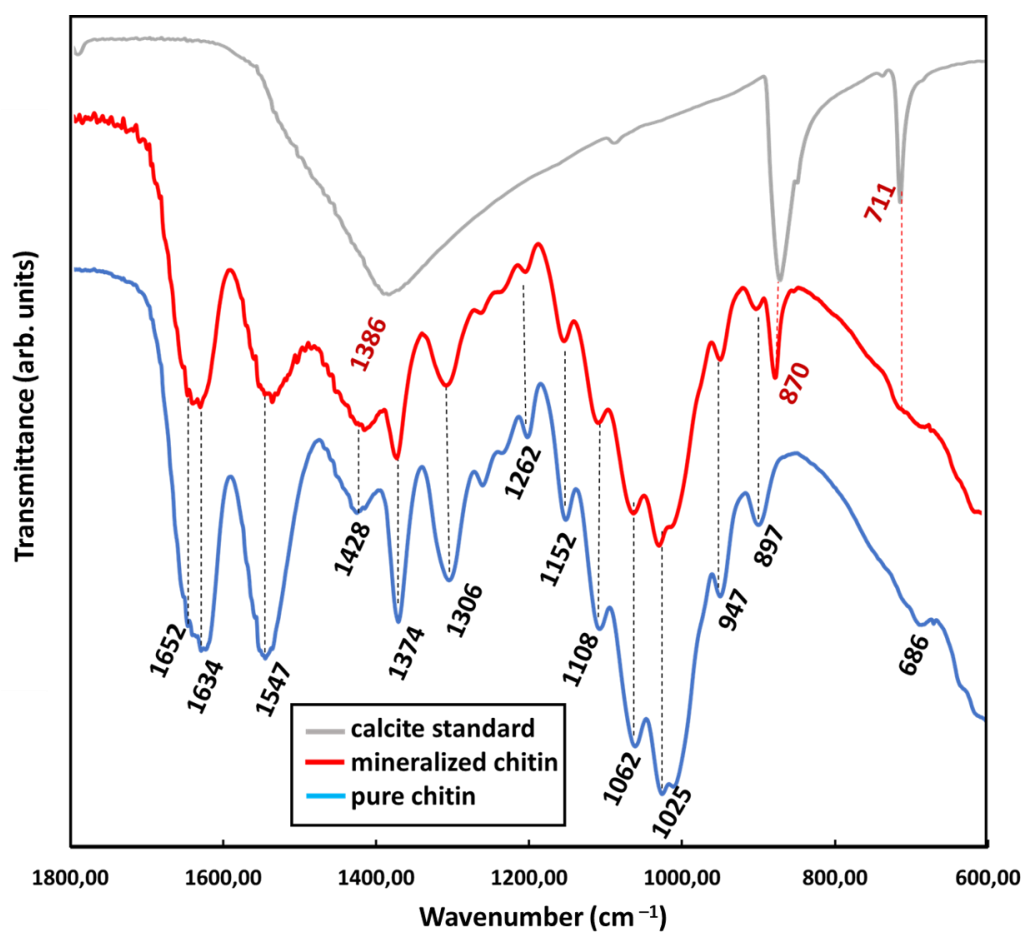
Figure 44. ATR−FTIR spectra of the pristine (blue line) and biomineralized chitin (red line) scaffold as well calcite standard (grey line).

Obtained spectra showed a characteristic split for α-chitin, such as amide I at 1652 cm^{-1} and 1634 cm^{-1} (see red and blue lines). This spectra region can be attributed to the stretching vibrations associated with intermolecular (C=O···HN) and intramolecular (C=O···HO(C6); C=O···HN) hydrogen bonds [202,253]. The bands for amide II (νN-H and νC-N) at 1547 cm^{-1}, amide III (νC–N and

δN–H) at 1306 cm^{-1} or very characteristic peak at 897 cm^{-1} (C-O-C bridge as well as β-glycosidic linkage) additionally confirmed the presence of *α*-chitin in *A. fistularis* marine sponge skeleton [227]. However, in case of inorganic phase identification, a sharp peak visible at 870 cm^{-1} is especially interesting. This signal clearly indicated the presence of calcium carbonate in calcite form [352,353]. Thus, *ex-vivo* biomineralization using hemolymph isolated from *C. aspersum* allowed to obtain chitin−CaCO$_3$ biocomposite.

The results obtained from thermogravimetric analysis allowed to answer two questions. First, how the thermal stability of biomineralized scaffold differ from pure chitin? Second, what is the inorganic phase content? The graphs showed three significant decreases at TGA curves (**Figure 45**).
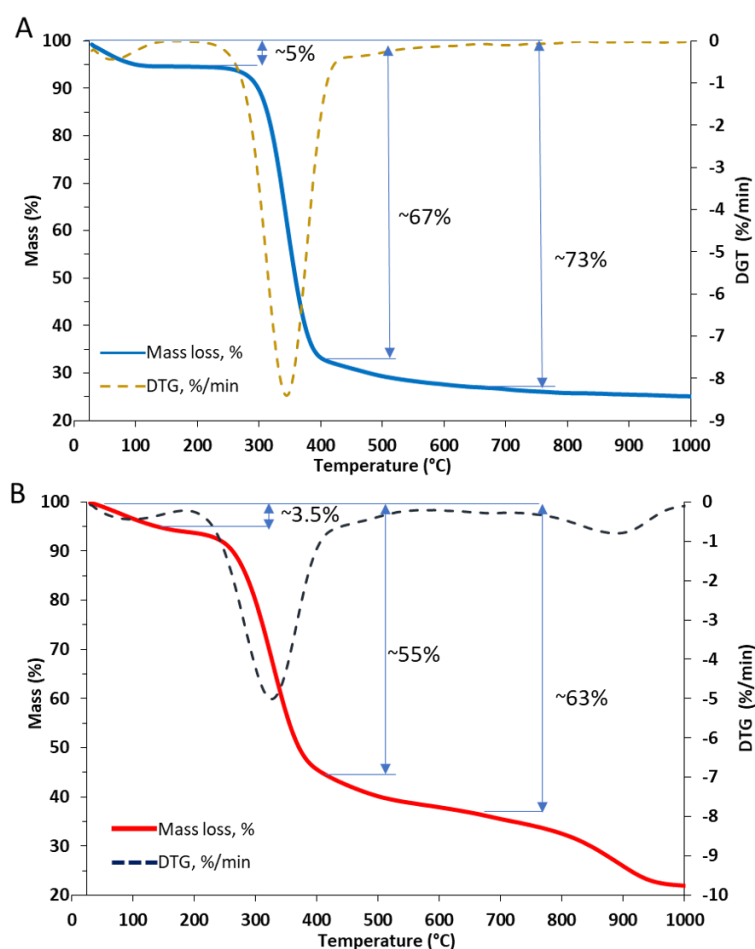
Figure 45. *TGA/DTG curves of (A) pure chitin scaffold isolated from marine sponge and (B) biomineralized scaffold.*

The first one lies at temperature of about 100 °C. This region corresponds to the loss of water molecules physically and chemically bound to the sample [311]. The quantity of water lost was estimated at 3.5% (pure chitin) and 5% (biomineralized chitin). The second important mass loss, related with the thermal and oxidative decomposition of the chitin was recorded in the temperature range of 200–400 °C [202]. As observed, pure chitin decomposed with a rate of 8%/min, for a biomineralized sample it was 5%/min at a temperature of about 330 °C. From the overall mass loss, it can be concluded that the presence of an inorganic phase increases the thermal stability of the sample. Then, after chitin decomposition, another mass loss in the temperature range 670–850 °C, was recorded for biomineralized scaffold. It is associated with the decomposition of $CaCO_3$ into CaO and CO_2 [354]. Experimentally, the calcium carbonate content in the biomineralized scaffold can be estimated at approximately 10%.

To determine the wettability changes of pure and biomineralized scaffold, contact angle was measured using Wilhelmy method. Due to the fact that chitin from marine sponge possess high fluids absorption rate and highly porous structure, the creation, and measurements of sensile drop was almost impossible. Thus, samples were alternately dipped and drawn, and the contact angle was measured (**Figure 46**). Finally, as a mean of 10 measurements contact angle was estimated as follow: for pure chitin − 29°, for biomineralized chitin − 40°.
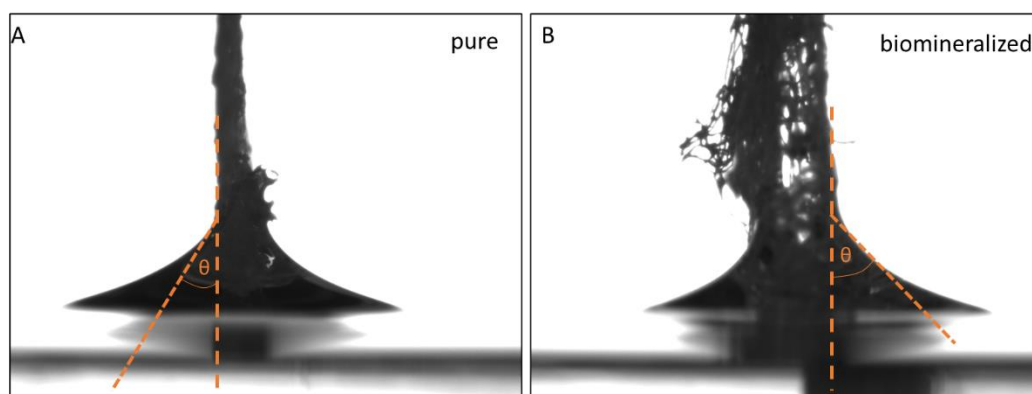
Figure 46. Exemplary measurements of contact angle using Wilhelmy method. (A) Pure chitinous scaffold and (B) ex-vivo biomineralized scaffold.

The macro-scale mechanical compression test was used to calculate Young's modulus (**Figure 47** and **Figure 48**). The α-chitinous scaffolds isolated from *A. fistularis* marine sponge, before and after biomineralization were characterized in water immersion. **Figure 47** showed that stress–strain curves exhibit a non-linear trend without exact yielding points. In the first stage of the test low stiffness may be observed, and then stiffness rapidly growth. However, the highest values were recorded for biomineralized scaffold. The overall macro-scale compressive modulus was calculated as ~0.6 kPa for pure chitin and ~1.4 kPa for biomineralized scaffold.
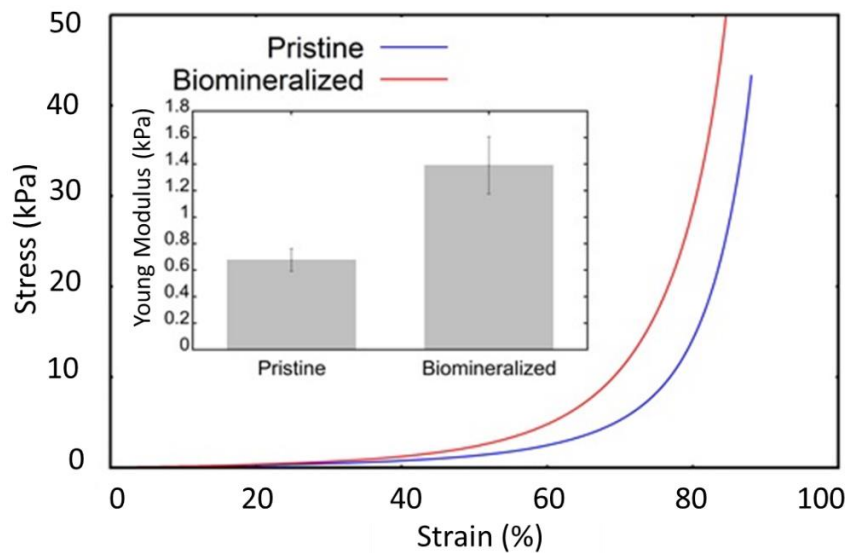
Figure 47. Representative strain-stress response and the compressive moduli for the investigated materials (in inset); (mean ± SD; n = 3), based on [275].

Further mechanical testing, using Dynamic Mechanical Analysis (DMA), of the investigated chitin–based scaffolds from *A. fistularis* marine sponge before and after biomineralization, was performed. **Figure 48** show the frequency dependence of the elastic modulus (E′) and viscous modulus (E″) for pure and biomineralized chitin samples. Biomineralization by snail hemolymph caused to a significant increase in elastic (storage) and viscous (loss) modulus (see **Figure 48 A, B**). This result suggesting that $CaCO_3$ layer reinforces the chitinous scaffold [355]. Both storage and loss modulus increased with rising frequency. For all of the studied samples, their E′ values are approx. 3 to 5 times greater than the

comparable E″ values in the measured frequencies (**Figure 48 C**). This fact may suggest that the bulk response of the examined specimens to an applied deformation reflect elastic character. Noteworthy is the fact that the values of both modulus are growing almost parallel to each other until increasing the frequency. Thus, their frequency-dependent relation, indicate typical for a solid-like materials viscoelastic performance [356,357]. As analysis of variance (ANOVA) showed, the statistically significant differences were observed after comparing the tan δ for pure and biomineralized samples (**Figure 48 C**).
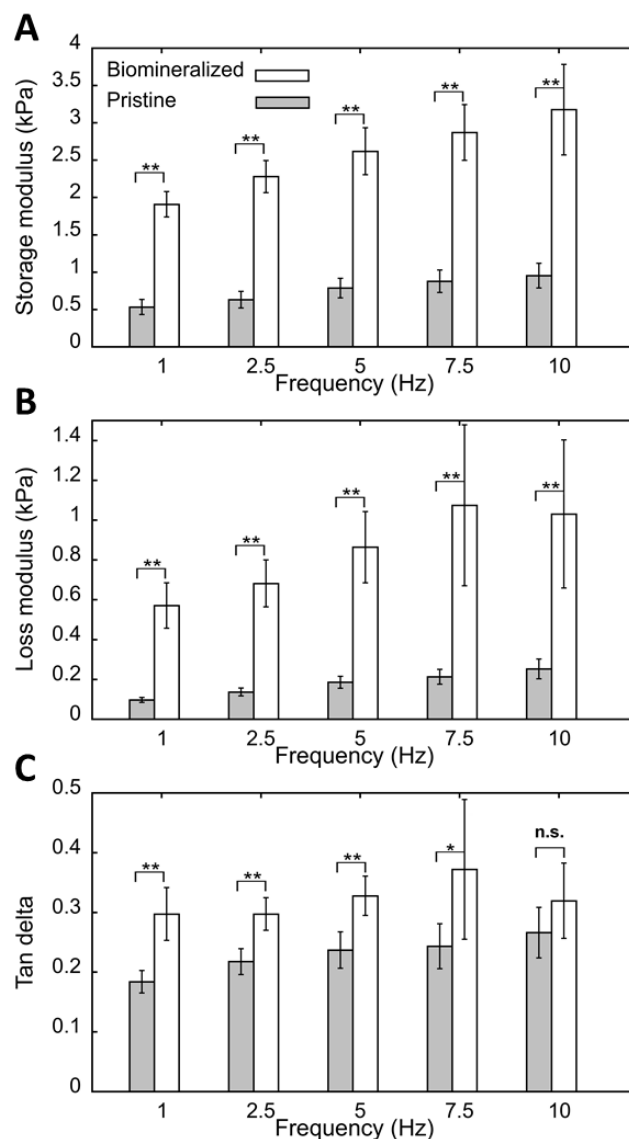
***Figure 48**. Dynamic mechanical analysis (DMA) results of pristine and biomineralized chitinous specimens as a function of frequency: (A) storage modulus, (B) loss modulus and (C) tangent of phase lag; (* p < 0.1, ** p < 0.05, n.s. – non-significant), based on [275].*

Results of the monotonic compression tests (see above) and data presented here, showed that the compressive modulus are comparable to the E' values obtained for low-frequency loading, what is in agreement with previously published data [358]. All of the analyzed samples achieved compressive moduli lower than 2 kPa, when tested in water immersion. These results make obtained material interesting from tissue engineering point of view. For example, it was developed [44] that porous scaffolds composed of collagen–hyaluronic acid, with a compressive modulus of 0.5 kPa and pores size of 90–300 μm can promote mesenchymal stem cells proliferation and cartilage-like matrix accumulation.

Atomic force microscopy, in force spectroscopy mode, was carried out to describe qualitative and quantitative variations of local (nanoscale) differences in the scaffolds surface stiffness (see **Figure 49**).
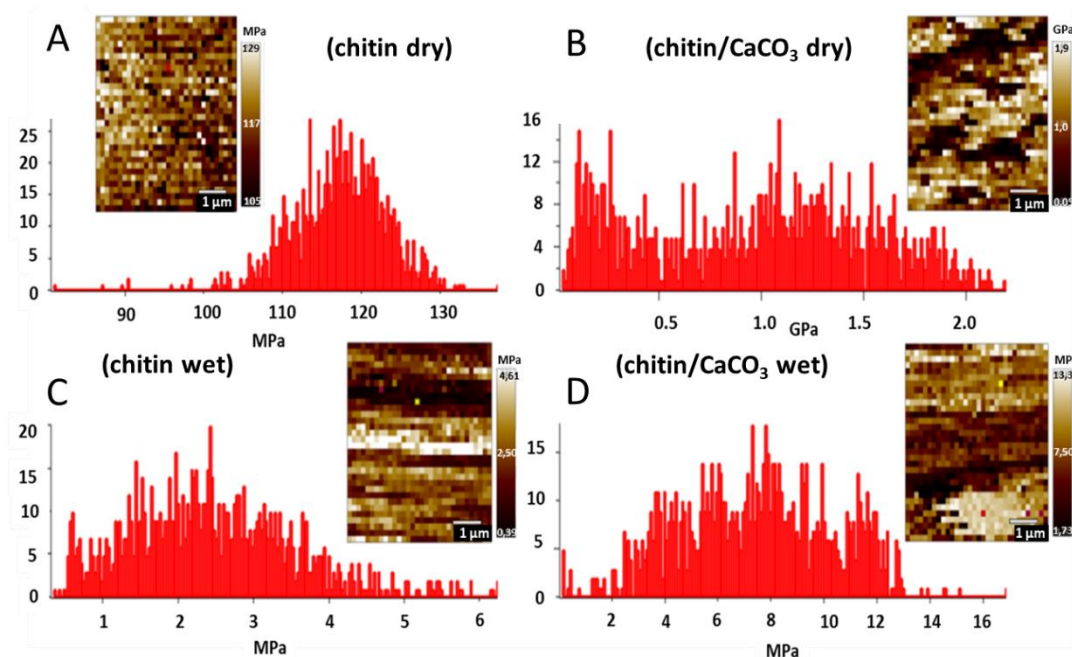
Figure 49. *AFM Force Spectroscopy results in nanomechanical range. (A) dry pure chitinous scaffold, (B) dry ex-vivo biomineralized chitinous scaffold, (C) water immersed pure chitinous scaffold, (D) water immersed ex-vivo biomineralized chitinous scaffold, based on* [275].

As observed, dehydrated specimens showed higher stiffness than immersed ones. The average elastic moduli of fiber were 117 ± 14 MPa (chitin dry), 875 ± 203 MPa (chitin/CaCO$_3$, dry). To compare with 2.1 ± 0.6 MPa (chitin wet)

and 7.5 ± 1.8 MPa (chitin/CaCO$_3$, wet). Taking into consideration obtained histograms combined with stiffness maps, it could be seen that dry pure chitin showed the most uniform mechanical properties within all tested specimens. It should be highlighted, that the histogram for dehydrated pure chitin scaffold was the narrowest, when all other specimens exhibited a wider distribution of stiffness values. Biomineralized scaffolds (CaCO$_3$ coated), in water immersion condition, had about 4 times higher stiffness values than those without biogenic calcite particles. The presence of stiffer inorganic phase is, therefore, reflected in the local distribution of surface mechanical properties (see **Figure 49**) [359].

The biomimetic coating of materials by calcium phosphates (Ca-P), produced by their soaking in the simulated body fluid (SBF), is an effective method of determination of biomaterials bioactivity. **Figure 50** showed calcium phosphates (Ca-P) produced on both, biomineralized and pure chitinous scaffold, by soaking in simulated body fluid (SBF). The presence of phosphates was confirmed by EDS analysis (**Figure 51**). Jaroszewicz and co-authors [61] noticed that evaluation of apatite formation in simulated body fluid is a valuable test for the *in vivo* bioactivity determination, which allow for reduction of animal sacrifices and savings in experimental time. As represented in **Figure 50**, biomineralized scaffold showed higher bioactivity: after 7 days scaffold fiber was almost completely covered by Ca-P layer. In next days, phosphates growth onto material. In case of pure chitin, after 7 days only pointwise inorganic dots were observed. However, in next days the Ca-P phase growth and created widest layer. The differences between both scaffold bioactivity may be related with the presence of calcium carbonate onto biomineralized fibers, which act like a nucleation center for phosphates. However, pure chitin also showed bioactivity but in less intensity.
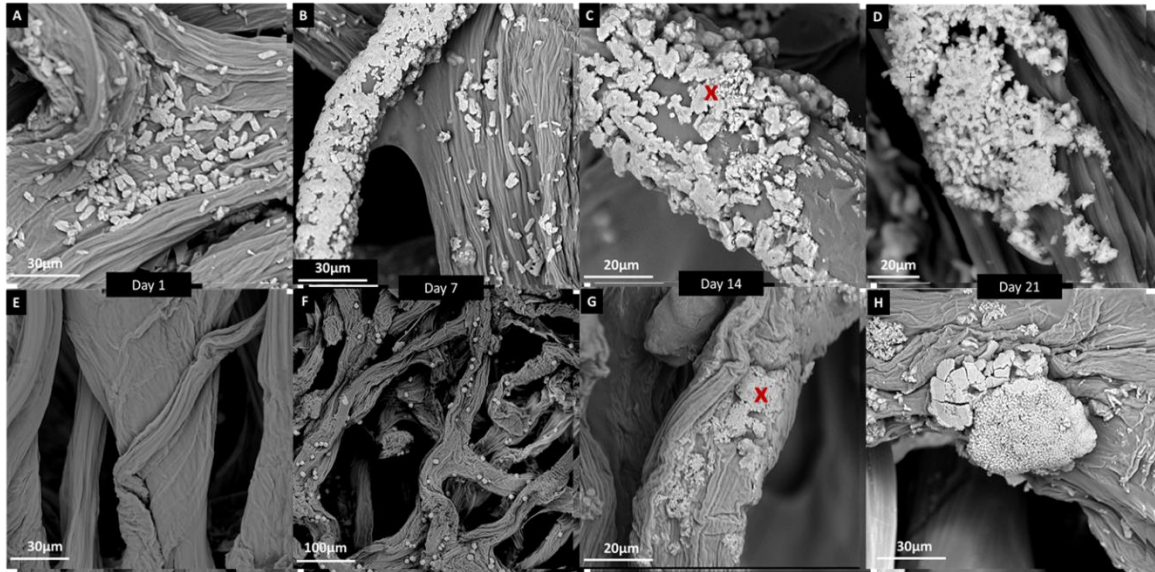
Figure 50. Bioactivity study of (A-D) biomineralized scaffold and (E-H) pure chitin immersed in the simulated body fluid. X – EDS measurements point.
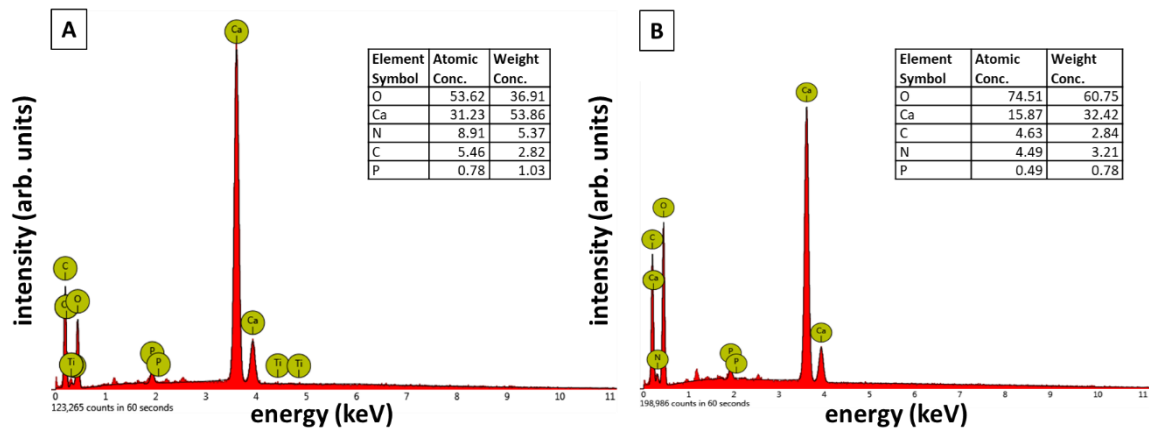
Figure 51. Distribution of chemical elements in point (see X above), obtained using EDS analysis of (A) biomineralized and (B) pure chitin scaffold surface after 14 days of soaking in SBF.

7.4. Preliminary research on application of biomineralized chitinous scaffold in tissue engineering

In these study proliferation and morphology of human fetal osteoblasts (hFOB) cells, seeded onto chitinous scaffolds of poriferan origin, were investigated. By specific staining and confocal microscopy observations several differences in cells behavior were recognized on pure and biomineralized scaffolds. As showed in **Figure 52 A**, after 24 h hFOB cells agglomerated into numerous spheroids/clusters about 200 μm in size (see **Figure 52**). After 7 days of culture on the pristine chitin scaffolds (**Figure 52 B**, **C**), cells showed a weak

F-actin filaments stain, which suggest their decomposition due to cell apoptosis [360]. Moreover, cells spreading was limited, what may indicate that cells did not find any attachment points or suitable scaffold substrate. Instead of spreading on a scaffold, cells preferred spheroids creation. As a consequence, such a morphology hinders the ingress of nutrients and oxygen and result in death of cells inside the spheroid (limited number of nucleus - blue **Figure 52 C**). Similar reduced cell spreading and rounded cell morphology were previously observed on pure chitin scaffolds after 12 h of *in vitro* culture [82].
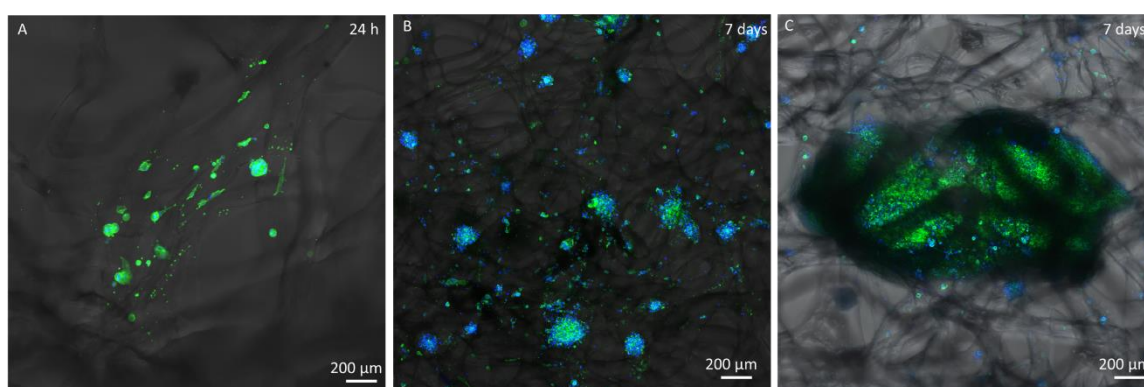
Figure 52. *(A) Morphology and bio-organization of F-actin cytoskeleton filaments of hFOB 1.19 seeded on pristine chitinous scaffold after 24 h and (B, C) 7 days, indicating the formation of aggregates and limited spreading. The cells were stained for F-actin (green) and cell nuclei (blue).*

As showed in **Figure 53**, treatment of the chitin scaffolds by *C. aspersum* snail hemolymph and creation of inorganic coating had a positive effect on the retention of cells by scaffolds. Based on the results showed above, it could be combined with their morphological and physicochemical properties improvements, as higher wettability, surface roughness and mechanical properties. These properties allowed for better cells attachment during inoculation and the culture period. It was due to the presence of both, $CaCO_3$ layer and proteins from the hemolymph [100]. Previously Jaroszewicz and co-authors [61] proved that inorganic coating of biopolymeric matrices improved cell attachment and spreading by raising the adsorption of proteins from culture medium. Oher study by Kumar and co-workers [82], proved that the inclusion of even 0.5% or 1% (w/w) of hydroxyapatite nanoparticles into chitin scaffolds

enhanced adsorption of serum proteins and positively affected at adhesion of various cell types. Herein, microscopic observation of hFOB stained against a cytoskeleton protein F-actin revealed that the cells spread correctly on the biomineralized scaffolds after 24 h and 7 days. The cross-section of scaffold fiber (**Figure 53 C**) clearly showed tightly attached osteoblasts cells onto chitin after 24 h.
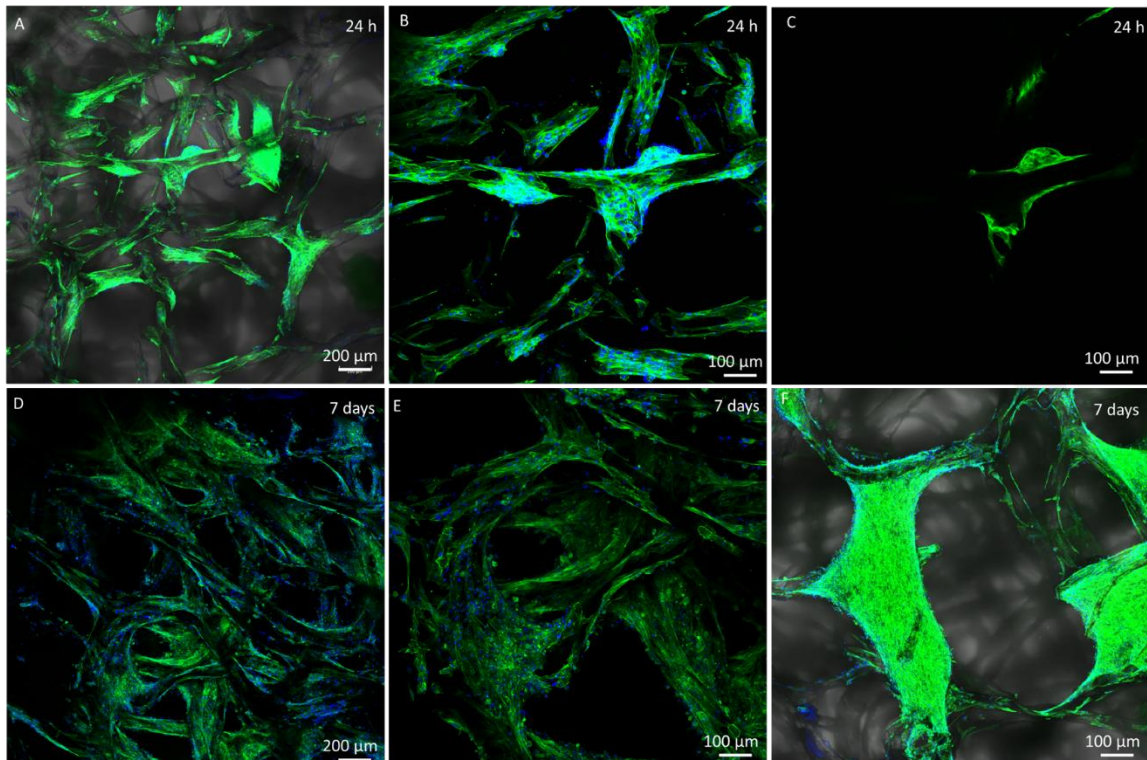
Figure 53. *(A, B) Morphology and organization of F-actin filaments of the human osteoblast's cells seeded on biomineralized chitinous scaffolds after 24 h and (D,E,F) 7 days reflect correct, wide spreading and cytoskeleton formation. (C) The slice of confocal microscopy image indicates a strong attachment of the cells to the single fiber surface. The cells were stained for F-actin (green) and cell nuclei (blue).*

Nevertheless, the fact that in case of biomineralized scaffold the metabolic activity of the osteoblasts after 7 days was on a similar level, suggests a limited cell proliferation. One possible reason is the insufficient stability of the created inorganic layer in the presence of cells. The stability of solidified hemolymph of *C. aspersum* should be investigated in future study. However, the positive is fact, that conversion of MTS tetrazolium compound into formazan did not show

significant changes on the biomineralized specimens (**Figure 54**). Thus, it may also be a result of high scaffold porosity and non-homogenous morphology or unexpected problem with cells culture conditions. In the case of pure chitin microscopic results supports the significant reduction of metabolic activity measured by means of the MTS assay (**Figure 54**). The significant reduction of formazan production may be related with cell detachment by the weak interactions of proteins adsorbed from the culture medium with the poriferan chitin scaffold. As a result, the tractional forces generated by the adhering cells upon reaching confluency, may exceeded the interactions between the proteins and chitin [38,361].
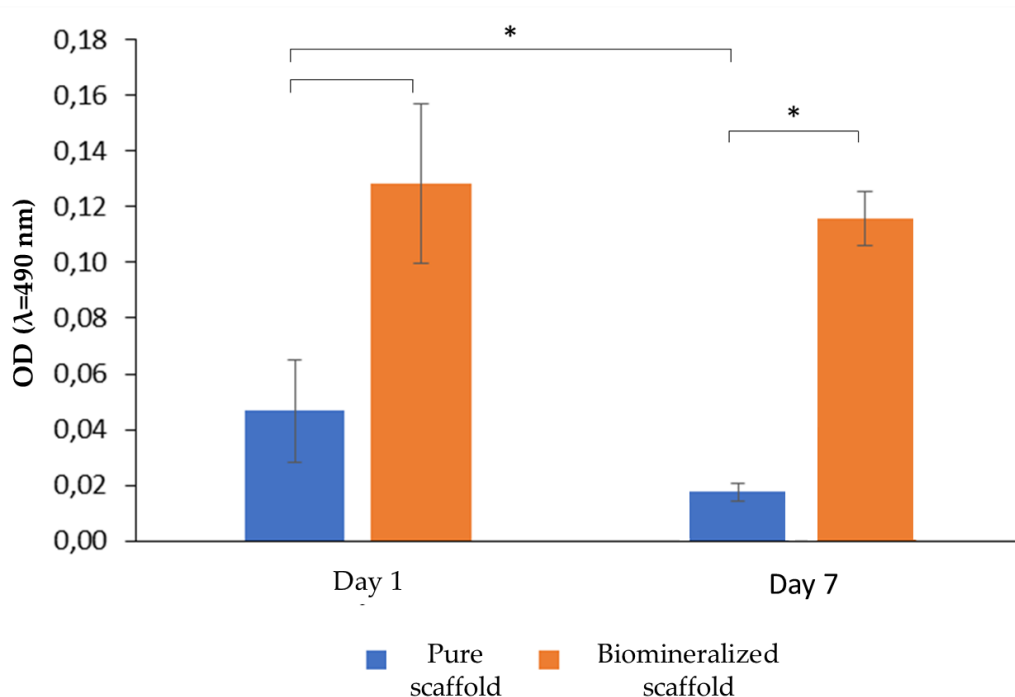
Figure 54. *Viability of hFOB cells seeded on the pristine chitinous and biomineralized chitinous scaffolds after 1 and 7 days of culture. Conversion of MTS to formazan salt by hFOB was significantly higher on the biofunctionalized scaffolds after 1 day of culture and decreased significantly on pristine scaffolds after 7 days of culture. * – $p \leq 0.05$, based on [275].*

7.5. Conclusions

In this study chitinous scaffold from *A. fistularis* marine sponge was biomineralized using *ex-vivo* biomineralization method. Novel way of inorganic coating deposition developed here, allowed to use natural medium, *C. aspersum*

snail hemolymph as biomineralization agent. As a result of this experiment the amorphous and crystalline (calcite) calcium carbonate layer was deposited onto chitin. This resulted in an improvement in the mechanical, textural (roughness) and bioactive properties of the final material. The overall macro-scale compressive modulus increased from ~0.6 kPa for pure chitin to ~1.4 kPa for biomineralized scaffold (static analysis). Similar relationship was confirmed by dynamic mechanical analysis. Surface topography parameters of the chitin scaffold, as roughness improved after biomineralization almost four times. Biofunctionalization allowed also to achieve changes in wettability. The mean contact angle increased from 29° (pure chitin) to 40° (biomineralized chitin). From biomedical point of view such parameters as surface wettability and surface topography are crucial for scaffold-cells interaction and obtained results confirm their significant improvement. Noteworthy is the fact, that even after biofunctionalization scaffolds maintain the natural high porosity.

Finally, biofunctionalized scaffolds were developed as support for human osteoblasts cells cultivation. The preliminary tests proved higher proliferation of cells seeded onto modified scaffold than pristine one. Furthermore, confocal microscopy observations showed the correct spreading of cells on the biomineralized specimens, which provides a strong motivation for future research. Without any doubt results described in this section confirm that assumed research hypothesis, that functionalization of chitinous scaffold surface improve its bio-integration with human cells, was correct. However, the fundamental question concerning the molecular mechanisms underlying the sensitivity of human cells to the surface of biopolymers, before and after biomineralization, remains open.

Chapter 8. Immobilization of laccase onto poriferan chitinous skeleton

Contents

Rising water pollution by pharmaceuticals and other endocrine-disrupting chemicals (EDCs) is today a serious risk to wildlife and ecology around the globe. It was proven that antibiotics, such as tetracycline (TTC), oxytetracycline (OTC), and chlortetracycline (CTC), promote the appearance of antibiotic-resistant bacteria's, what in consequence leads to higher treatment costs, prolonged hospital stays, and increased mortality [132]. Due to the constantly growing pharmaceutical, medical and veterinary markets the risk of environmental contamination by such compounds is a still recurring problem. Thus, effective, sustainable and "*green*" methods of pharmaceuticals removal are crucial to limit their entry into natural waters. Noteworthy is the fact, that some of them cannot be removed by traditional wastewater treatment methods (as e.g. oxidation with chlorine and ozone, membranes processes) because of their fat solubility and resistance to classic physico-chemical degradation [362].

Enzymatic degradation seems to be a very promising eco-friendly method for the elimination of various EDCs including pharmaceuticals from aqueous solutions [131]. Special attention should be paid to oxidoreductases, especially laccases, peroxidases, and tyrosinases, which can effectively oxidize phenolic compounds to usually less toxic products than initial substrate [363]. Laccase (EC 1.10.3.2) is as multicopper oxidoreductase biomolecule, that is naturally produced by higher plants, various bacteria, and several fungi [25]. Laccase is

able to catalyze the oxygen reduction reaction combined with the simultaneous oxidation of polyphenols, aminophenols and polyamines compounds. Thus, antibiotics like tetracycline consisting of phenolic structure, can be effectively degraded even by small amount of enzymes [362]. However, main limitation in using pure biocatalysts (enzymes) is the significant drop of their catalytic activity, low storage stability at varying process conditions and difficulties in recovery after the process. This fact prompts to look for effective and economically feasible methods to improve these defects. The great example of currently most widely used technique is immobilization, which allow to increase the stability and prolong the activity of enzymes. Such a solution opens industrial applicability of the enzyme-based materials [25] and allow to minimize costs, since both, enzyme and supports can be used in repeated reaction cycles, including also biodegradation processes [131].

Therefore, in this chapter utilization of biocatalytic system made of chitin−laccase is described. Its applicability was determined in case of tetracycline removal from model wastewater solutions. Chitinous skeleton of *A. archeri* marine demosponge was used as enzyme support. Immobilization of enzyme was performed by adsorption and several process parameters, such as effect of pH, temperature, or pollutant concentration, were determined.

8.1. Morphological analysis of biocatalytic systems

Figure 55 showed that the surface of chitinous skeleton isolated from *A. archeri* marine demosponge, before enzyme immobilization, is relatively smooth and has slightly folded surface, which is typical after drying. Moreover, any signals of microdamage or impurities were not detected in both, SEM and TEM images. However, after laccase immobilization, the number of aggregates with irregular shape and amount, were observed on the surface of the chitinous support. The support surface topography changed and became rougher than before immobilization (see **Figure 55 A**, **B**). These aggregates raise from the

agglomerates of the laccase molecules, and their existence indirectly proved effective enzyme immobilization.
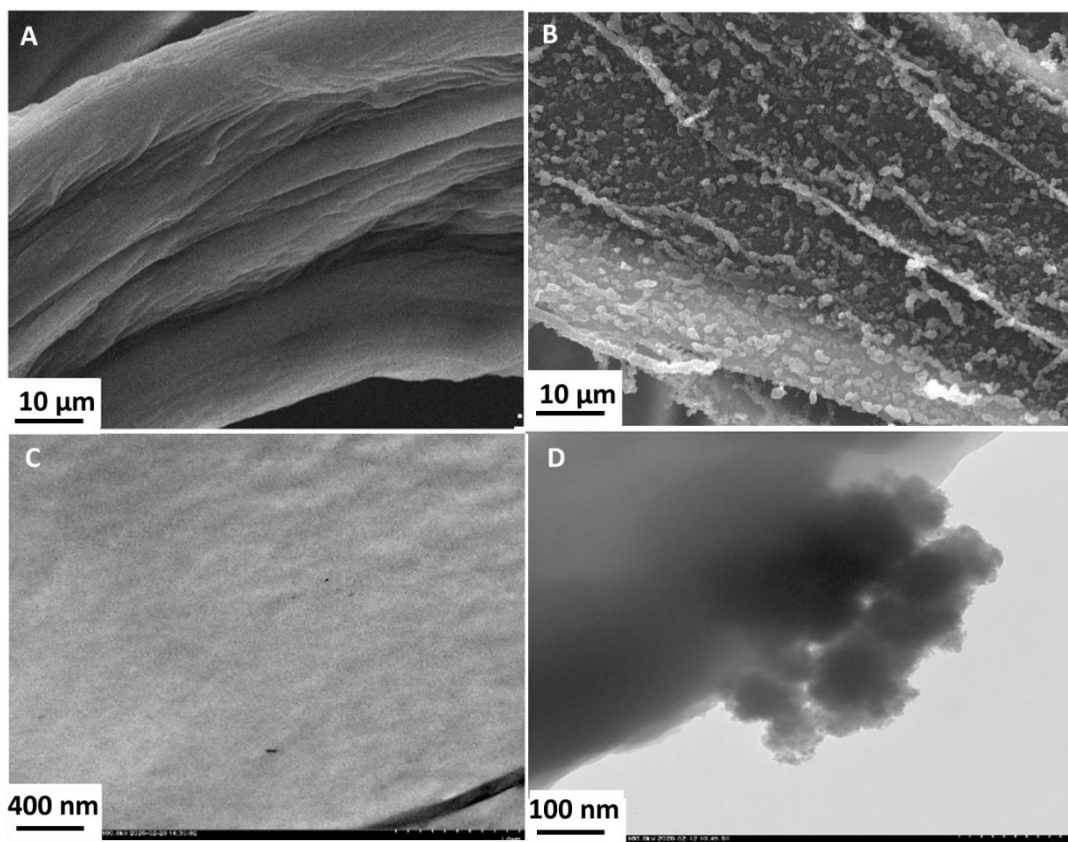
Figure 55. SEM and TEM images of the A. archeri sponge skeleton (A, C) before and (B, D) after laccase immobilization.

8.2. Storage and thermochemical stability of free and immobilized laccase

The results presented in **Table 11** showed that after 1 h of laccase immobilization, relatively high immobilization yield (91%) was obtained. As calculated, performed process allowed to immobilize around 1800 mg of the biomolecule per 1 g of the support. Achieved data indicated also that about 90% of initial activity was maintained by the immobilized enzyme - specific activity was determined as 52.5 U/mg, whereas free enzyme's activity equaled to 56 U/mg. Further analysis focused on determination of kinetic parameters of free and immobilized enzyme. A slight increase in the value of the Michaelis–Menten constant (K_M), from 0.093 to 0.113 mM, was noted after immobilization. These

135

data suggest a slightly lower substrate affinity, which is represented by the lower value of maximum reaction rate (0.048 mM/s) in case of immobilized laccase. As a consequence, a lower catalytic activity (0.516 1/s) was obtained for the immobilized enzyme. However, it should be noticed that the recorded changes did not exceed 20%. It may be related to the enzyme-support interactions or by limited access of reaction substances to enzyme active site, as compared to free enzyme. Nevertheless, the obtained biosystems can be considered as an effective biocatalyst for further applications.

Table 11. Parameters characterizing the immobilization process.

Parameter	Free Laccase	Immobilized Laccase
Immobilization yield (%)	-	91 ± 0.6
Amount of immobilized enzyme (mg/g)	-	1820 ± 90
Specific activity (U/mg)	56 ± 1.9	52.5 ± 1.5
Activity retention (%)	-	89 ± 3.2
K_M **(mM)**	0.093 ± 0.018	0.113 ± 0.022
V_{MAX} **(mM/s)**	0.048 ± 0.008	0.045 ± 0.011
V_{MAX}/K_M **(1/s)**	0.516	0.398

The next part of the study focused on the estimation of changes in the relative activity of free and immobilized enzyme versus time of storage and varying process conditions (pH 5, 25 °C). Obtained results allowed to establish their long-term and thermochemical stability. **Figure 56 A** showed that the activity of free laccase decreased over storage time and after 15 days achieved approximately 80% of its initial value. After that, more rapid decrease was observed; finally, after 30 day of storage, the relative activity of free laccase did not exceed 50%. Interestingly, the relative activity of the immobilized laccase stayed unchanged during the first 5 days of storage, and then began to decrease, showing around 93% after 15 days. Noteworthy is fact, that after 30 days of

storage at 4 °C, its final value was estimated as 85% of the initial catalytic activity, which is still over 50% higher than the value obtained for free enzyme. It can be concluded that laccase immobilized on *A. archeri* chitin scaffolds has higher storage stability than free enzyme. Similar observations were reported previously in case of other supports such as spongin scaffolds [24].

Other investigations showed the thermochemical stability of free and immobilized laccase under favored process conditions (pH 5, 25 °C). The analysis of obtained results (**Figure 56 B, C**) evidently indicates that, even though the initial activity of the immobilized enzyme was lower (see **Table 11**), the enzyme attached to the chitinous scaffold was able to exhibit a notably enhanced thermochemical stability in comparison to free laccase. As observed, after 120 min of incubation at pH 5, and at temperature 25 °C, immobilized enzyme maintained 77% of its relative activity. Hence, it was confirmed that the chitin–laccase biocatalytic systems were quite stable. Additionally, it was suggested that support can prevent against inactivation of the laccase. In case of free enzyme, the activity was significantly reduced after incubation at the same conditions (see **Figure 56 B**). After 120 min of incubation, free enzyme maintained less than 40% of its initial activity. Also, the inactivation constant (k_D) and half-life ($t_{1/2}$) of free and immobilized enzyme were analyzed and compared. In case of immobilized laccase, values equaled to 0.0038 1/min and 182.4 min, respectively, whereas the same parameters measured for free laccase were 0.0174 1/min and 39.8 min, respectively. As a result, the immobilized enzyme exhibited approx. 4 times lower inactivation constant (k_D) and 4.5 higher half-life as compared to its native form. The obtained results clearly indicate that chitin fibers support is an appropriate material for the immobilization of laccase, while creating a protective environment against thermal and chemical inactivation.
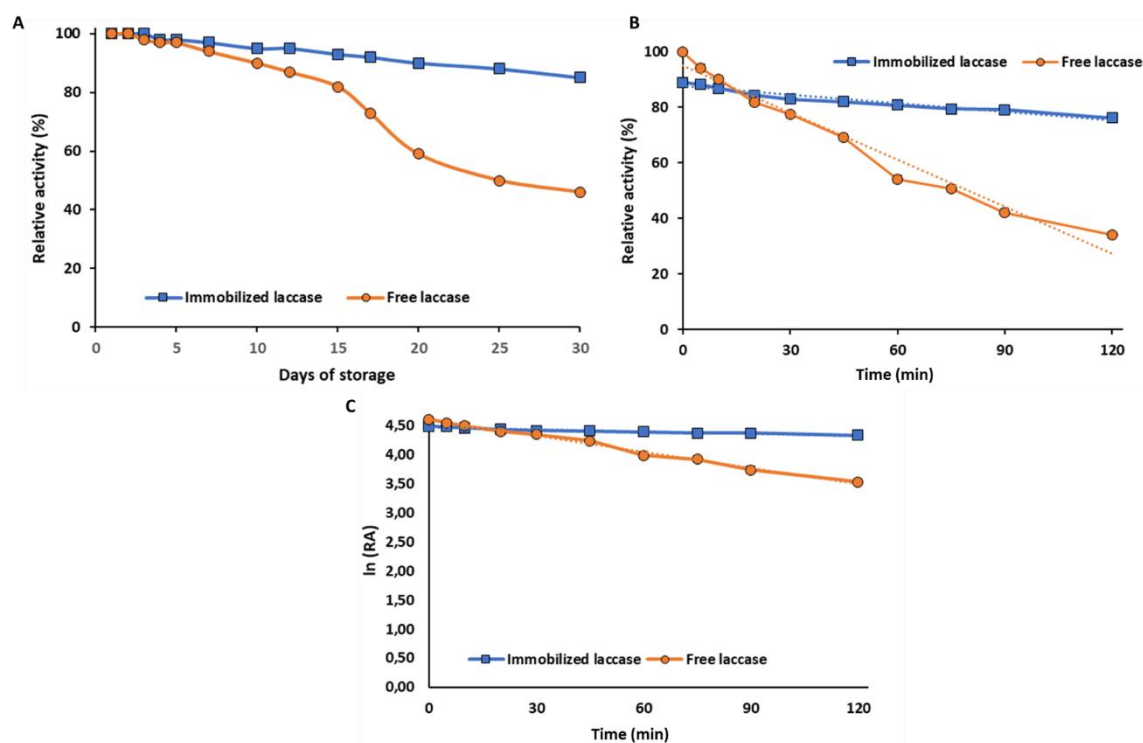
Figure 56. (A) Storage stability of the free and immobilized laccase (pH 5, temperature 4 °C) and (B, C) stability under optimal conditions (pH 5, temperature 25 ◦C). The error value, based on the mean and standard deviation from three experiments, did not exceed 3.5%, based on [25].

8.3. Application tests of the produced chitin−laccase biocatalytic systems: removal of tetracycline

In this study, chitin−laccase biosystem was applied in the removal of tetracycline, under various process parameters, including pH, temperature, and concentration of tetracycline solution. Moreover, detailed removal examination of tetracycline was carried out by simultaneous adsorption and biocatalytic conversion. Determination of adsorption obtained using pure *A. archeri* chitin skeleton and conversion performed using free laccase, resulted in tetracycline removal efficiencies equaled to 80% and 60% (at pH 5 and temperature 25 °C), respectively. Thus, as determined, total removal of the antibiotic by the separately applied components of biosystem was not possible to achieve.

The first stage of investigation concerned determination of pH influence on simultaneous adsorption and catalytic conversion of the antibiotic. The removal efficiency of tetracycline was determined over a wide pH range

3–9, at 25 °C, and using the antibiotic solution at a concentration of 1.0 mg/L (**Figure 57 A)**. The total removal efficiency of tetracycline increased from 5% (pH 3) up to 100% (pH 5), and then decreased to around 55% (pH 9). However, it should be stated that the total removal efficiency was above 90% at pH ranging 4-7. These results are significantly better than the efficiencies of adsorption obtained using pure *A. archeri* chitin skeleton and conversion performed using free laccase (80%, and 60%, respectively, at pH 5, with further decrease under even minor changes in environmental conditions). It should be stated once again that the removal of antibiotic was carried out by simultaneous adsorption and biocatalytic conversion. The adsorption process demonstrated similar efficiencies, at around 55%, at pH range 3–7, then, a decrease of around 15% was observed at basic pH (≥ 8). In the case of catalytic conversion, the total removal of tetracycline was significantly higher in an acidic environment, achieving a maximum of approx. 40% at pH 5 and pH 6. Additional increase in pH resulted in a decrease in the efficiency of enzymatic conversion to 30% at pH 7 and to around 15% at pH 9.

Afterward, analysis of the temperature influence on tetracycline removal was performed within a range of 5—65 °C (pH 5, tetracycline solution concentration 1.0 mg/L). Results presented in **Figure 57 B** suggest that tetracycline removal efficiency increased with increasing temperature, with a maximum value (100%) obtained at 25 °C and 35 °C. At higher temperatures, a decrease in removal efficiency was observed. Approx. 90% of tetracycline was removed at 55 °C. For temperatures 15 °C and 65 °C, removal efficiency of tetracycline was estimated as less than 80% (**Figure 57 B**). These results proved that the synthesized biocatalytic system can effectively eliminate tetracycline by simultaneous sorption and catalytic conversion over a much wider temperature range, than in the case of adsorption using pure support or conversion conducted using free enzyme separately. Noteworthy is fact that, the efficiencies

of both processes: adsorption and catalytic conversion, revealed similar profiles over the whole analyzed temperature range. However, the adsorption efficiency was about 20% higher than the results of catalytic conversion of the tetracycline. Decrease of removal efficiency at higher temperatures may be related to thermal deactivation of enzyme molecules.
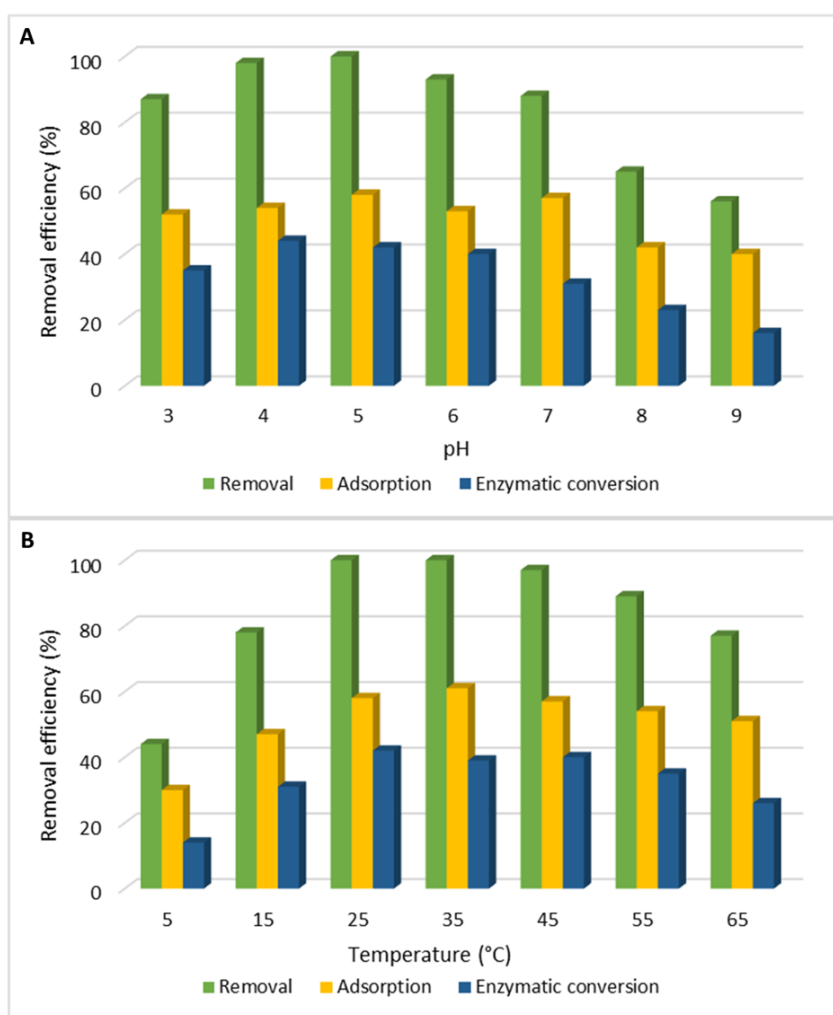
Figure 57. Effect of (A) pH and (B) temperature on the efficiency of tetracycline adsorption, enzymatic conversion, and total removal by chitin−laccase biocatalytic system. The error value in each of the experiments did not exceed 3.5%, based on [25].

In the next stage, the effect of concentration of antibiotic solution was determined. The study was performed using tetracycline solutions in concentration ranging from 0.1 to 3.0 mg/L (pH 5, temperature 25 °C). **Figure 58** clearly showed that proposed biosystem is capable to completely remove tetracycline from solutions at concentration of 0.1, 0.5, and 1.0 mg/L, after

60 min of the process. Increasing concentration of tetracycline solution (up to 3.0 mg/L) resulted in a decrease of its total removal efficiency of about 20%. Interestingly, an opposite relationship was observed for adsorption and enzymatic conversion. As the antibiotic concentration increased, the adsorption efficiency decreased, which was probably due to the blockage of pores and reduced interactions at the chitin scaffold surface. On the other hand, in the case of enzymatic conversion, increase of tetracycline solution concentration, in the range of 0.1–1.0 mg/L, resulted in an increase in the efficiency of the process. However, the highest concentration of the tested solution caused a slight decrease of removal efficiency, from about 40% (1.0 mg/L) to 30% (3.0 mg/L) – it was probably due to enzyme overloading with the substrate molecules.
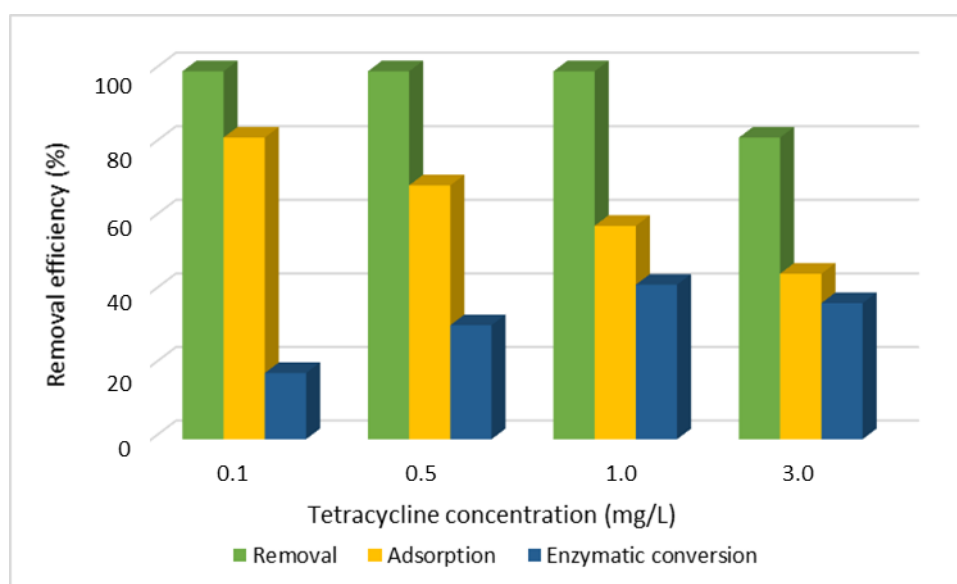
Figure 58. Effect of initial concentration of tetracycline solution on the efficiency of its removal by immobilized laccase-chitin biocatalytic system. The error value based on the mean and standard deviation from three experiments did not exceed 3.5%, based on [25].

Finally, reusability of prepared chitin−laccase biocatalytic system was determined. The recyclability of the immobilized laccase was carried out over 10 repetitions, by batch tests of tetracycline degradation under optimal process conditions (pH 5, temperature 25 °C, tetracycline concentration 1.0 mg/L). As showed in **Figure 59**, immobilization process allowed to achieve very good reusability. Antibiotic was removed with high efficiency within 10 removal

cycles. Although a slight drop-in removal rate was observed over repeated use, after 10 cycles removal efficiency of antibiotic was estimated at approx. 90%. Noteworthy is the fact that, over the first three catalytic cycles, the chitin−laccase biocatalytic system was capable to remove 100% of tetracycline from the solution.
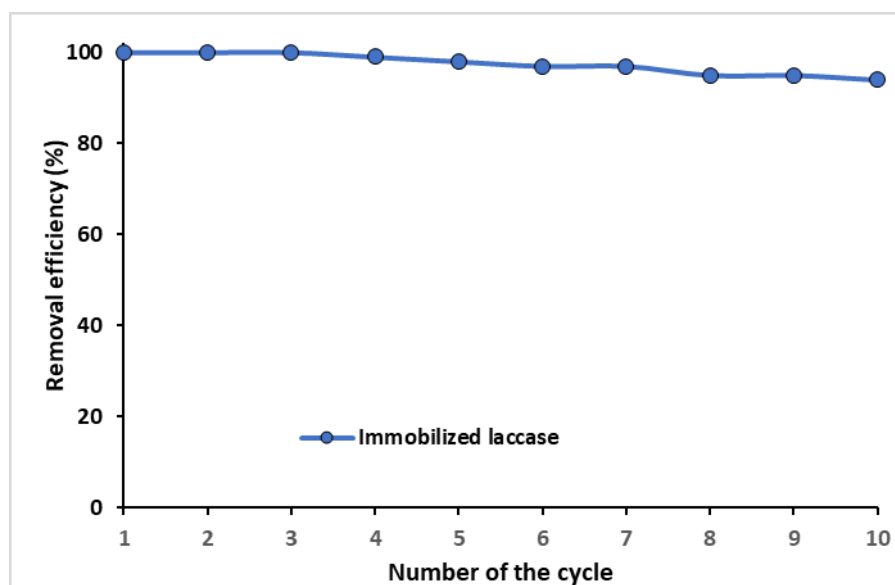
Figure 59. Reusability of the chitin−laccase biocatalytic system over repeated tetracycline removal cycles. The error value in each of the experiments (based on the mean and standard deviation from three experiments) did not exceed 5%, based on [25].

8.4. Conclusions

The unique 3D morphology of naturally formed chitinous scaffold from marine demosponges was used in various technological application. For instance, Wysokowski and co-authors, synthesized advanced functional materials, like chitin−ZrO_2 [263], chitin−GeO_2 [364] or chitin−$(Ti,Zr)O_2$ composites [27] in terms of their photoluminescent, catalytic and photocatalytic properties. Moreover, this natural biopolymer, in form of three-dimensional scaffold was used as a "*green*" adsorbent [142] or in biomedicine and tissue engineering [29–33]. In this study, chitinous scaffold isolated from *A. archeri* marine sponge was successfully used as a support for laccase immobilization and removal of tetracycline from aqueous solution [25]. As observed, the efficiency of antibiotic removal, by simultaneous adsorption and catalytic conversion, was

very high and achieved 100% at various pH (4-6) and temperature (25-35 °C), using tetracycline solutions at concentrations up to 1.0 mg/L. It is worth to highlight that pure support and free enzyme separately, enabled to obtain much lower removal efficiencies (around 80% and 60%, respectively). These data indicated that chitin−based biocatalytic systems might be considered as a highly effective alternative for the removal of pollutants from aqueous solutions. It can be concluded that immobilization is a very promising technique for enhancement of enzyme stability and opens a new application window for biocatalysis. From an industrial point of view, this technique may significantly reduce the cost and enhances the control of processes. However, the success of this technological solution is strictly related to the applied support. The utilization of chitin from marine sponges as a support for laccase immobilization revealed its broad range of versatility. Their natural fibers arrangement allows to obtain "ready to use" support directly after its isolation. Moreover, chitin owes its versatility to the presence of numerous of functional groups, mainly carbonyl and hydroxyl, typical for this aminopolysaccharide, which provide stable enzyme-matrix interactions without linking agents [202,253]. Other, valuable feature of chitin is its thermostability what was confirmed in previous chapter. As showed, the selection of the 3D chitin scaffold as a support improves enzyme stability in a wider range of temperature, pH and over storage time, as well as provides the ability of an immobilized molecule to be used repeatedly. It had a great impact on the removal of tetracycline from model wastewaters. These results are in agreement with research hypothesis which assumed that use of alternative sources of chitin such as marine demosponges' skeletons, allows to obtain functional three-dimensional scaffolds with a unique shape and properties, predisposing them for environmental protection applications.

Chapter 9. Determination of antibacterial properties of chitin–Ag/AgBr composite

Contents

The currently published data indicate a very disturbing fact that more than 1.2 billion people worldwide have no access to clean drinking water [143]. Moreover, the 1.8 billion people drink water from fecal contamination sources what may results in several diseases and even death [144]. One of the world's most serious health-water threats are bacterial contaminations (e.g. *E. coli* infection) [365]. Although we can manage to control its spread, the development of new materials that can rapidly inactivate dangerous pathogens present in water is an ongoing and crucial aspect nowadays [366].

Among various methods used to purify water, filtration is particularly attractive because of its simplicity, low cost and high efficiency [367,368]. Its potential application include synthetic polymers (e.g. polypropylene, polyurethane, polyethylene) [369–371], natural polysaccharides and proteins (e.g. chitin, keratin, cellulose, collagen) [372–374] and carbon-based materials [375,376], which can be coated with silver nanoparticles (AgNPs) by various methods. The use of silver to water disinfection and purification result by death of fungi, molds, bacteria and spores, and is known since ancient times, as described Atiyeh and others [377]. Recently, it is a well-known that direct contact with Ag kills microorganisms [378]. The basic mechanism assumes that silver involves the inhibition of microbial respiration through interaction of metal nanoparticles to the bacterial cell membranes [379]. As a consequence, it impairs the microbial respiratory system what result in their death. The most important features, involving the advanced antimicrobial properties of Ag-based filters, are

the size of silver particles and their specific surface area development. Nguyen and co-authors described that *"antimicrobial activity of the smaller Ag nanoparticles may be several orders of magnitude greater than that of the corresponding bulk solid"* [380].

Nowadays, the functionalization of naturally pre-fabricated 3D chitinous scaffolds draws particular attention [23]. Based on this state of knowledge 3D chitin–based scaffolds isolated from the *A. aerophoba* marine sponge were used as a basic structural component of antibacterial water filter. This bioscaffold was coated with silver and silver bromide nano- and microparticles, using chemical reduction of silver nitrate and glucose as reaction catalyst.

9.1. Structural and morphological characterization of chitin–Ag/AgBr composite

Three-dimensional skeleton scaffold obtained from *A. aerophoba* marine sponge represent very interesting structural similarity to synthetic polyurethane (PU) foam (see **Figure 60**). Due to the highly porous structure and well-developed spatial surface, natural skeleton seems to be interesting candidate for filtration. It is worth to highlight, that chitinous skeleton was not completely purified, what confirm its brownish color and higher rigidity than pure chitin. It is because of the presence of broad diversity of secondary metabolites (bromine-rich compounds) linked with chitinous fibers. Bromotyrosines have antimicrobial as well as antipredator activities. Their toxicity deters potential predators include bacteria's, what is crucial for organism leading a sedentary lifestyle. On the other hand, bromotyrosines isolated from marine sponges, like Isofistularin-3 or Aeroplysinin-1, are recognized as potential antibacterial, antiviral, antitumor bioactive marine drugs [33,295,381,382].
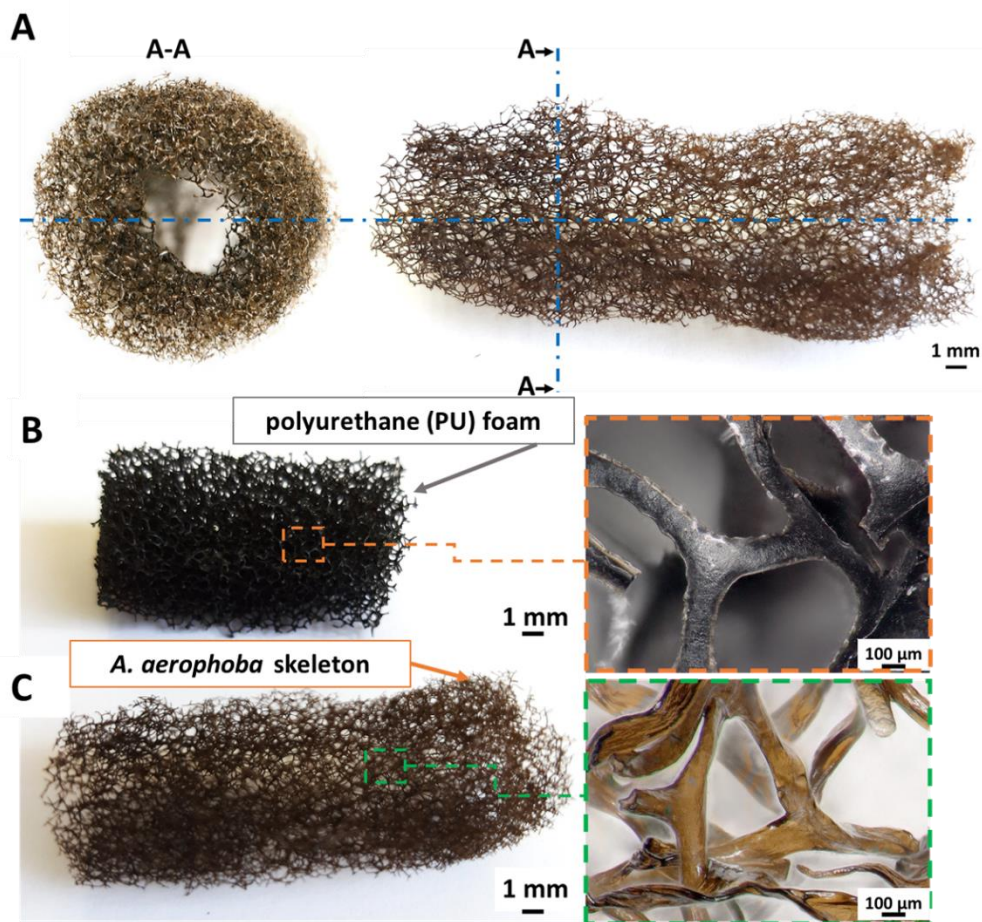
Figure 60. *(A,C) The images of a decellularized A. aerophoba marine sponge 3D chitinous skeleton scaffold; the cross-section (A-A). (B) Polyurethane (PU) foam filter. The brownish-like color is due to the presence of bromine-rich compounds naturally occurring in the skeleton fibers of the sponge, based on* [23].

The chemical reduction of AgNO₃ using glucose was performed in a reaction vessel in the presence of a submerged chitin matrix. The course of reaction required a highly alkaline environment, which favored the precipitation of metallic silver in nano- and microparticles (**Figure 61**). The reaction was manifested by the formation of a "*mirror effect*" on the walls of the vessel. However, what is very interesting, the high pH also caused surface releases of bromine-rich compounds from the *A. aerophoba* skeleton, and as a consequence the presence of silver bromide on the matrix surface was detected (see XRD analysis below).
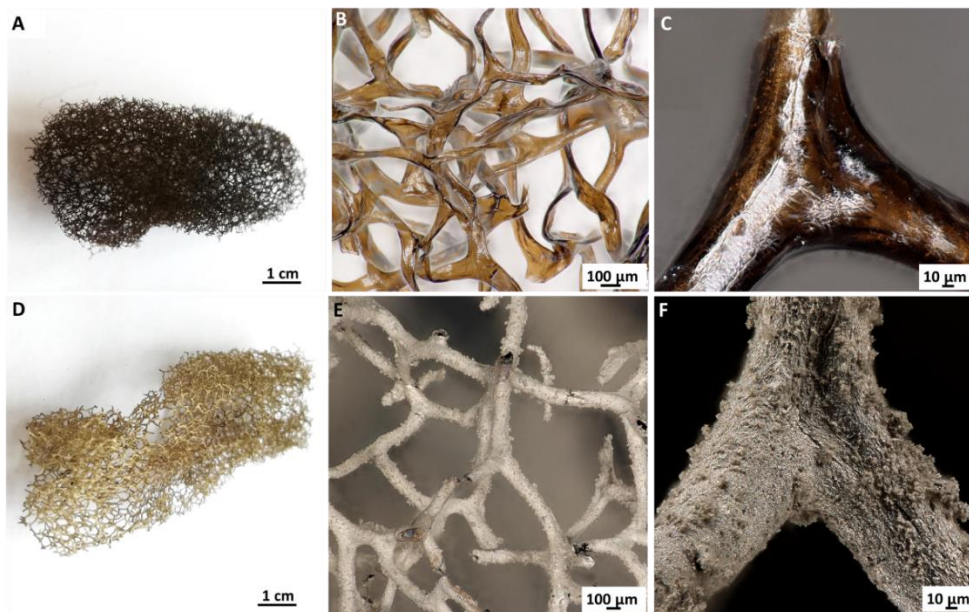
Figure 61. *(A-C) 3D chitinous skeleton of A. aerophoba marine sponge before and (D-F) after AgNO$_3$ reduction process. Occurrence of tightly bounded Ag/AgBr nano and microparticles was confirmed by their layer presence even after 20 min of ultrasonication, based on* [23].

Micro-CT analysis results showed high porosity of prepared biocomposite scaffold, estimated as 98,2% (**Figure 62**). However, it should be noted that analysis was carried out in a dry state. Thus, in the immersion, average fiber size parameters should slightly increase (**Table 12**).
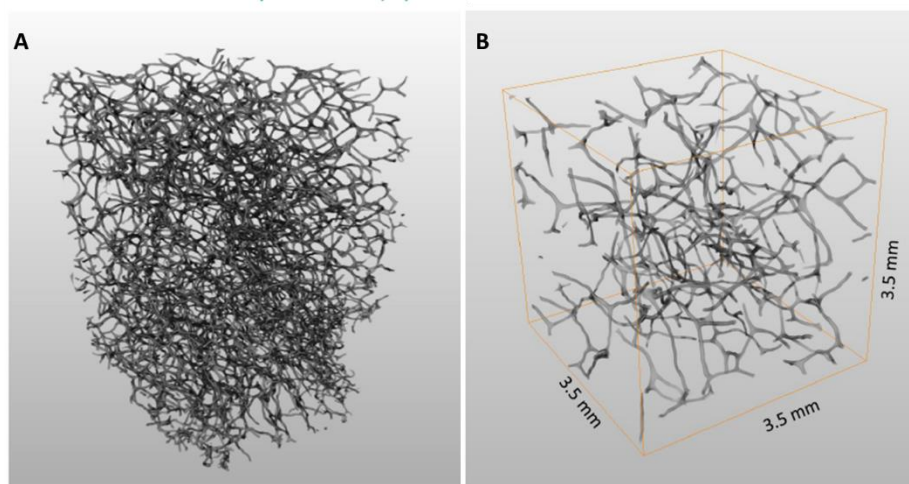
Figure 62. *The 3D model of the chitin–Ag/AgBr composite scaffold obtained by micro-CT analysis, based on* [23].

147

Table 12. Results of 3D µCT quantitative analysis of chitin−Ag/AgBr composite.

Parameter	Result
Porosity (%)	98.2
Average pore size (µm)	1300 µm (± 300)
Average fiber size (µm)	71 µm (± 18)

The formation of Ag/AgBr clusters can be characterized by the presence of tightly bounded aggregates of particles on the chitin surface with the use of the scanning electron microscopy (**Figure 63 C, D).** The surface of a single fiber of chitinous skeleton scaffold as a reference can be also observed using SEM (**Figure 63 A, B**) at lower and higher magnification, respectively.
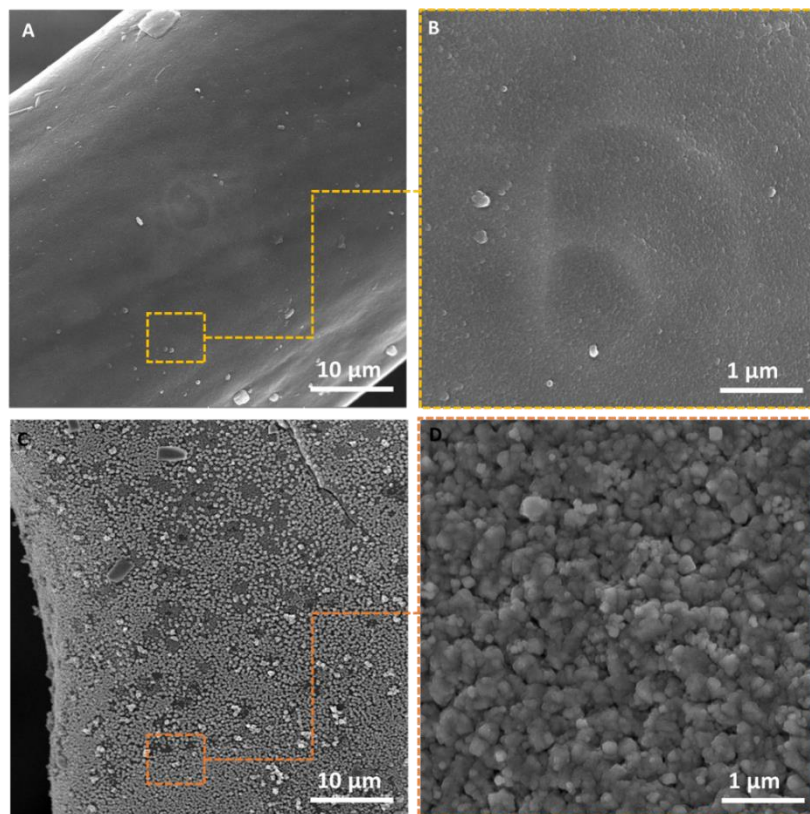
Figure 63. (A, B) SEM images of pure chitin skeleton from A. aerophoba marine sponge before metallization and (C, D) Ag/AgBr nano and micro particles distribution on the chitinous skeleton from marine sponge.

Presented in **Figure 64** particles sizes have been calculated from 200 measurements, using representative micrographs by the ImageJ software

(National Institutes of Health, Bethesda, MD, USA). Data indicate that 16% of particles is in the nanoparticle range (<100 nm), while the largest content consist of particle 200-300 nm in size (43%).
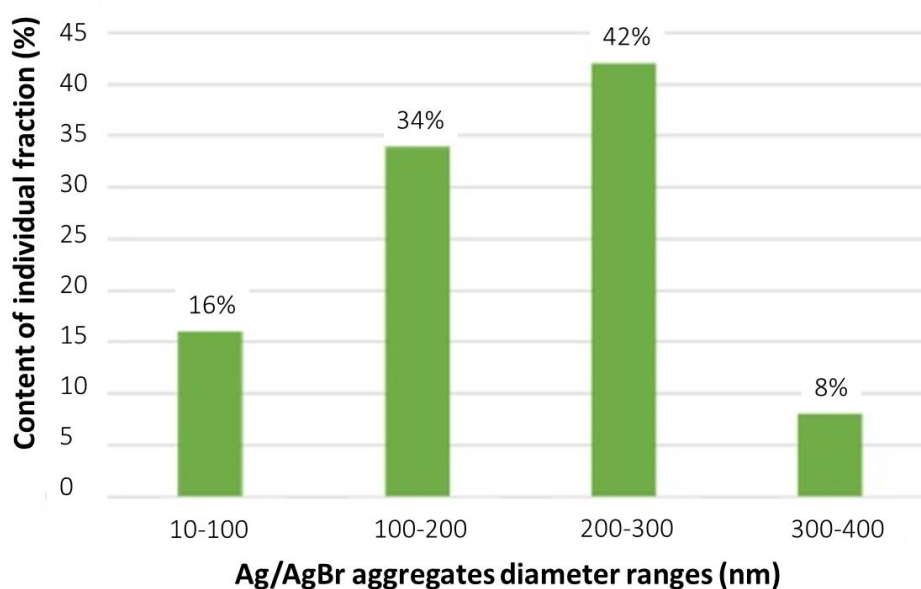
Figure 64. Percentage contribution of Ag/AgBr nanoaggregates in individual fractions as a function of diameter, obtained by SEM images analysis, based on [23].

The results of EDS and XRD analysis are showed in **Figure 65**. Interestingly, next to the silver, also bromine was detected using EDS analysis (**Figure 65 A**). Thus, more detailed analysis − X-ray diffraction was performed for both, pure chitinous skeleton specimens before and after $AgNO_3$ reduction (**Figure 65 B)**. Regardless of the sample, the chemical isolation pretreatment resulted in the reduction of the crystalline structure of chitin (see [245]). Nevertheless, some signals corresponding to chitin were detected, e.g. the diffraction maximum 021 at $2\theta \approx 12°$ as well as the signal beginning with the 110 reflection near $2\theta \approx 20°$. In addition, there are diffraction peaks which can be attributed to Ag (PDF# 04-004-6434) and AgBr (PDF# 00-006-0438). Subsequent Rietveld analysis indicated a nanocrystalline character of the synthesized particles, based on the crystallite size of $D_{iso} = (13 \pm 2)$ nm and metallic lattice parameter of a = (4.088 ± 0.001) Å, which is almost identical to the tabulated value of a = 4.089 Å. Moreover, AgBr crystals in space group $Fm\bar{3}m$ with a lattice parameter of

a = (5.555 ±0.002) Å, have been determined in the obtained XRD pattern. Further analysis of XRD patterns exclude presence of silver oxides, nitrides, and chlorides; positive match among the database entries were not found. Final amount of metallic Ag was estimated as approx. 75 vol.%, while the amount of AgBr at approx. 25 vol.%, as indicated by the quantitative XRD phase analysis.
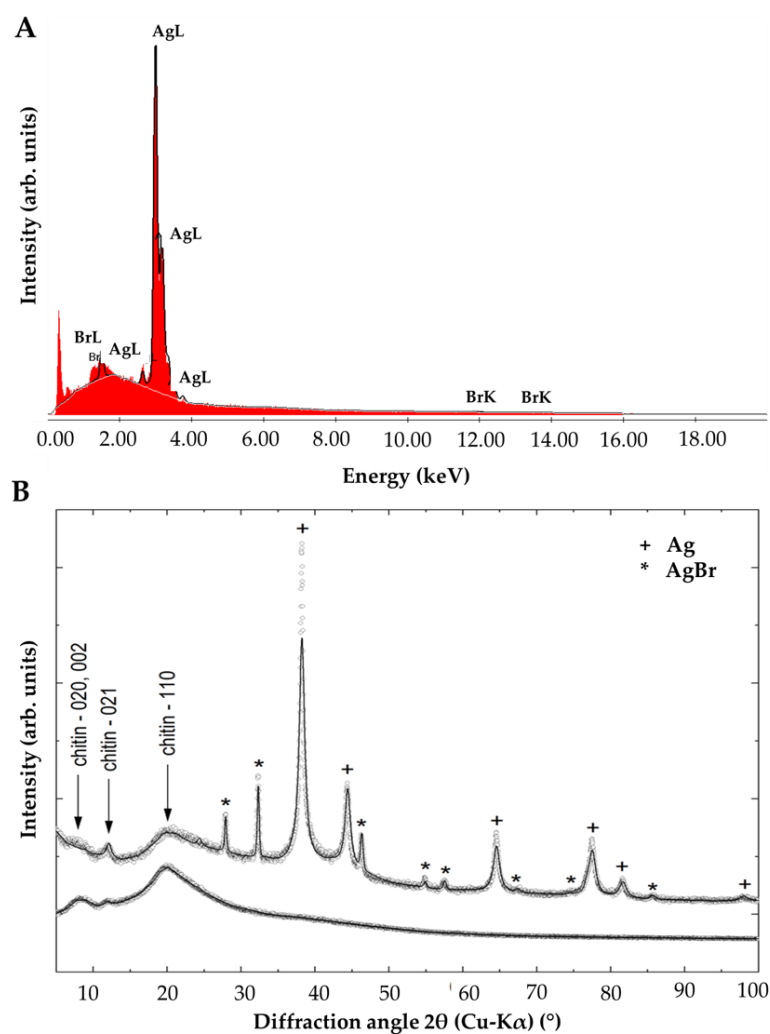
Figure 65. (A) EDS analysis confirms the presence of both Ag and Br within layer which cover chitin. (B) X-ray diffraction patterns (dopped line: measured intensities; lines: refinement) of the chitinous skeleton (lower signal intensity) and a chitin sample tightly covered with the Ag and AgBr nanoparticles (upper signal intensity), based on [23].

9.2. Determination of antibacterial properties of chitin–Ag/AgBr

The evaluation of the antibacterial activity of the prepared materials was carried out based on the agar diffusion method. **Table 13** presents overview results of the inhibition zone with respect to *E. coli* and *B. subtilis* bacteria strains. As could

be seen, prepared composites indicated the highest zones of inhibition, while the mean value was estimated as 23 mm and 24 mm for *E.coli* and *B. subtilis*, respectively. Without any doubt chitin−Ag/AgBr material reflect antibacterial properties. Relatively good results were also obtained for chitinous skeleton before metallization.

Table 13. Mean value of inhibition zone for both, strain (mm) and number of survived *E. coli* strains after 24 h of test tube test.

Material	Diameter of inhibition zone		Test tube test	
	E. coli (mm)	*B. subtilis* (mm)	*E. coli* (CFU/100 µl)	*% of reduction*
Chitin−Ag/AgBr scaffold	23	24	7	99.99
Chitin based scaffold	18	0	$>10^6$ (uncountable)	0
Suprasorb® A + Ag	0	0	$>10^6$ (uncountable)	0
Control probe	0	0	$>10^6$ (uncountable)	0

As showed in **Table 13**, mean zone of inhibition towards *E. coli* bacteria was estimated as 18 mm. However, with respect to Gram-positive *B. subtilis* any zone of inhibition was not observed. Recently, 3,5-dibromoquinolacetic acid, obtained from an aqueous extract of the dried demosponge *A. aerophoba,* was recognized as antimicrobial compound towards several bacteria's strains [283]. Thus, antibacterial effect of *A. aerophoba* skeleton results from the bromotyrosines presence. Interestingly, the commercial antibacterial dressing material with nanosilver "Suprasorb® A + Ag" used as a reference here, did not provide any zones of inhibition against both strains.
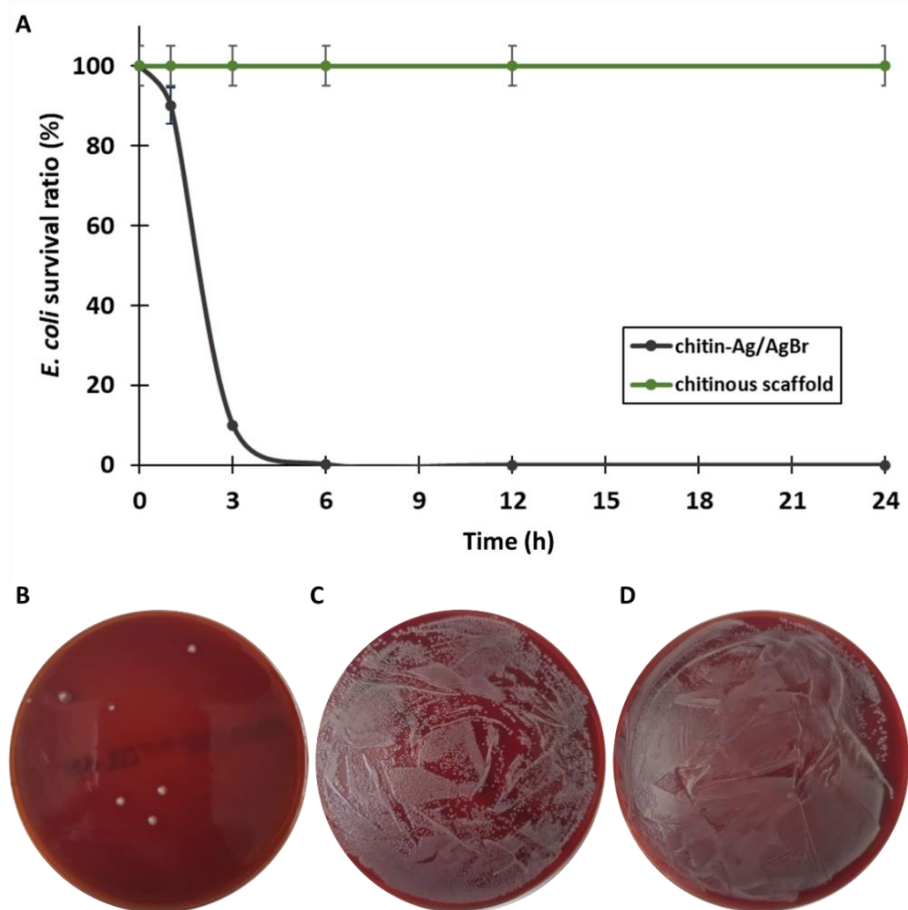
Figure 66. (A) The dynamics of the degradation of live E. coli bacteria colonies vs. time, by test tube assay (5% error bars). E. coli bacteria colonies survived after 24 h of testing using (B) chitin–Ag/AgBr scaffold, (C) chitin before silver coating and (D) commercially available material Suprasorb® A + Ag, based on [23].

Further analysis, focused on determination of utilization of prepared materials as antibacterial filter using test tube test [383]. As it could be seen in **Figure 66** after 3 h of direct contact, almost 90% of bacteria's have been deactivated by chitin−Ag/AgBr composite and almost 100% after 6 h. Experiment was carried out for 24 h and as showed in **Table 13**, only 7 bacteria colonies were observed. This results proved that almost 100% of the initial *E. coli* bacterial CFU was eliminated. In contrast to agar diffusion method, the bromotyrosines containing chitinous scaffold prior to silver coating did not exhibit any notable antibacterial potential against *E.coli* even after 24 h. Number of bacteria colonies was uncountable and because of that it was showed as constant in **Figure 66**. Similar

like in previous experiment, also here "Suprasorb® A + Ag" material did not provide any antibacterial properties.
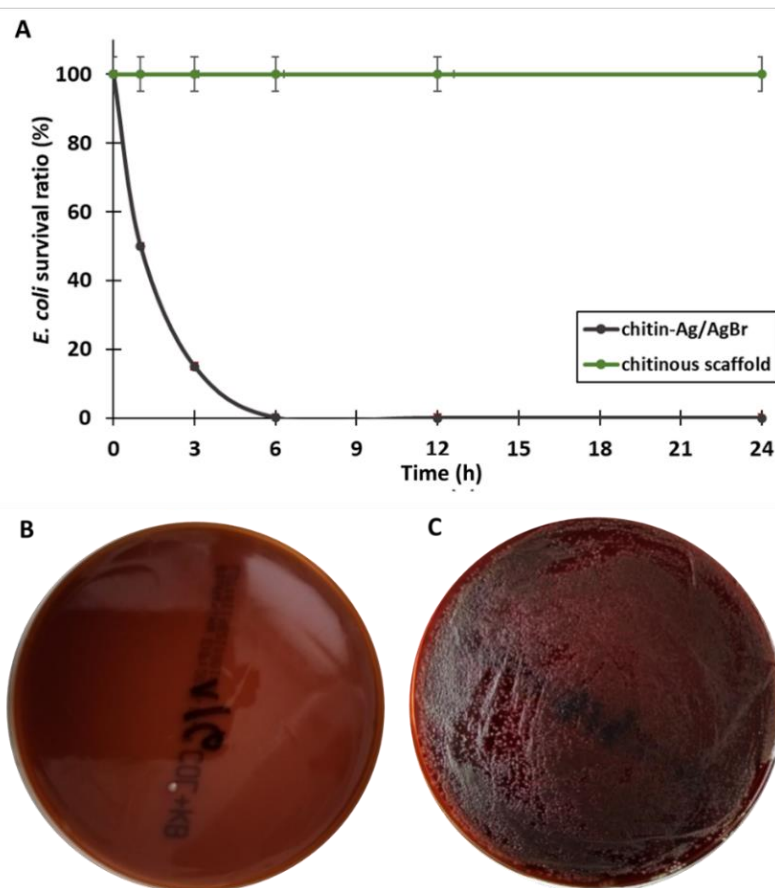
Figure 67. (A) Dynamics of bacteria's degradation vs. the time, during filtration process, with 5% error bars. (B) Filtration clearly indicate that chitin−Ag/AgBr scaffold possess antibacterial properties against E. coli (ATCC® 25922) strain (grey line), (C) chitinous scaffold before AgNO₃ reduction did not show any antibacterial effect. The number of survived bacteria's colony is uncountable, even after 24 h (green line), based on [23].

Finally, demosponge chitin skeleton and chitin−Ag/AgBr materials were used as filters. Results obtained after filtration (see **Figure 67**) clearly proved that 3D chitin−Ag/AgBr scaffold possess antibacterial properties against *E. coli* (ATCC® 25922) strains. In performed experiment, a great inhibitory effect was observed after 6 h of filtration. After 24 h of test, only one *E. coli* bacteria's colony survived. Similar like in experiment described above, also here chitinous skeleton before functionalization did not cause any visible changes in the number of survived bacteria (uncountable number). The stability of nanosilver

layer is crucial for commercial application. It should be highlighted, that after all experimental steps absorbance at 419 nm was measured. This wavenumber is characteristic for nanosilver presence in aqueous solution [383]. No signals at this particular wavenumber increased as compared to pure water, which indicate that the silver nanoparticles-based layer was stable on the developed 3D material and was not eluted with water flow even after 24 h of experiment.

9.3. Conclusions

Proposed method of silver nitrate reduction using glucose as reaction catalyst allows to create unique nanostructured Ag/AgBr layer, which remains strongly bound to the surface of the chitinous skeleton. XRD patterns exclude occurrence of silver oxides, nitrides, and chlorides. Final amount of metallic Ag was estimated at approx. 75 vol.%, while the amount of AgBr at approx. 25 vol.% of the layer, as indicated by the quantitative XRD phase analysis. Three experiments: agar diffusion test, test tube test and filtration test, without any doubt, indicated antibacterial properties of designed material against *E. coli* and *B. subtilis* bacteria strains. The results open the new path for functionalization of chitin−based skeleton matrices in the form of acellular scaffolds. Noteworthy is fact, that *A. aerophoba* demosponges possess outstanding regeneration possibilities of their skeletons. Thus, their cultivation under marine farming conditions at large scales may constitute interesting solution for future applications in bioinspired materials science and technology, what confirm first part of the research hypothesis. Future research should be focused on the optimization of functionalization process of such naturally derived matrices. The development of an effective method for the functionalization of chitin matrices using metallic silver allowed to achieve one of the main goals of this dissertation, and undoubtedly enhances the application potential of naturally formed chitinous scaffold.

Chapter 10. Aranean chitin and its practical utility

Contents

10.1. Structural and physicochemical characterization of spider's chitin

10.2. Preliminary investigation of tissue engineering application

10.3. Chitin/proteins-based spider cuticle for oil-spill remediation

10.4. Conclusions

Large scale chitin isolation is usually carried out by seafood processing wastes treatment, as shrimp, crab or lobster exoskeletons [4]. However, despite their relative abundance and easy availability, isolation of chitin requires chemical reagents and is time-consuming. Mostly, it is related with their high mineralization degree. Moreover, obtained in this way biopolymers are produced as powders, granules or flakes. Therefore, material requires further processing to make it usable. Thus, nowadays there is a need to look for alternative sources of chitin.

This part of PhD thesis focuses on the molting cuticles of Theraphosidae spiders as a unique source of naturally occurring chitin. To grow, spiders (like other arthropods) must form a new, larger exoskeletons and shed the old ones. These specific life process known as ecdysis or molting occurring several times per year [291]. The main scope of "*skin changing*" is the body growth (10-18%) and further development of the spider organism (as sexual maturation or lost limb regeneration) [286]. Results presented here showed relatively high chitin content in the spider molts and possibility of obtaining 3D constructs directly after MWI assisted isolation [245]. Especially attractive seems to be the part of walking leg/limb, which structurally mimic tubular scaffold. Material was carefully characterized by various analytical techniques such as, FTIR, Raman, NMR spectroscopies or XRD. Preliminary application tests presented below indicated that *C. versicolor* spider chitin, may be unique for tissue engineering, as a scaffold for human cardiomyocytes (iPSC-CM) cultivation. Moreover,

A. sp. "Peru purple" spiders' molts (before chitin isolation) in native form have been used in environmental study, as crude-oil sorbent.

10.1. Structural and physicochemical characterization of spider's chitin

As presented in **Figure 68,** chitin isolated from *C. versicolor* spider molt cuticle resemble the shape of spider molting cuticle. As calculated pure chitin content was determined as 19% of primary molt weight. Especially attractive are part of walking legs which looks like tubes with diameter of about 500 μm. These shapes of scaffolds are very interesting in context to biomedical application e.g. as scaffold for heart (cardiomyocytes) and vascular (endothelial) cells culture.
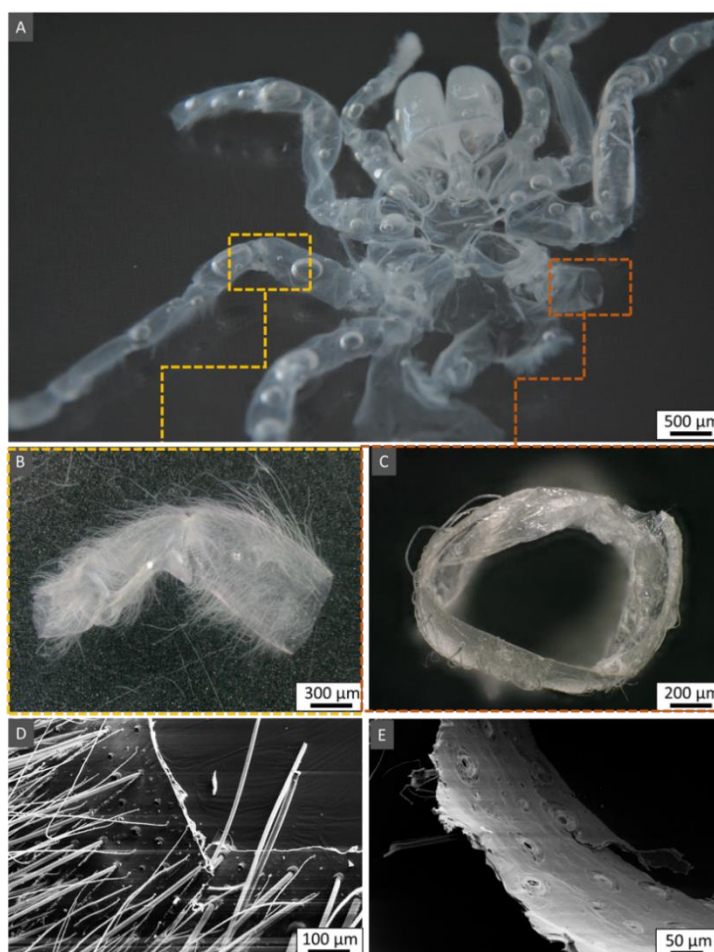
Figure. 68. (A) Translucent, pure chitinous skeleton obtained after microwave assisted isolation of C. versicolor molt, (B, C) the images of tubular scaffolds obtained from walking-legs fragments of spider molting cuticle, (D, E) SEM images of outer and inner side of scaffold showed their brush-like structure and porosity.

First, it could be seen that external surface is covered very tightly by microhairs. From inner side, well visible micropores may be observed. Cuticles of spiders are composed mostly of sclerotized chitin and present a wide diversity in appearance, similar like in insects because of evolutionary convergences. At their surface, several examples of cuticular setae, also known as cuticular mechanoreceptors or mechano-sensory hairs, can be observed [2]. These structures are involved in sensory detection within the environment by several arthropod species [2,384–386]. Nerve impulses transmitted by vibrations of microhairs enhance the sensory ability to detect environmental changes and spiders use this system for hunting, by sensing the vibration of approaching prey close to the web [236,387].

The biological material isolated from *C. versicolor* molt showed strong Calcofluor White (CFW) fluorescence, suggesting the presence of chitin (**Figure 69**). Moreover, two types of pores may be distinguished in the material structure. The bigger pores (about 20-50 µm) are residue locations where formerly mechanosensitive setae were anchored in the cuticle and smaller holes (about 5-10 µm) are places, where non-sensory hairs/setae were anchored in the cuticle before its experimental manipulation.
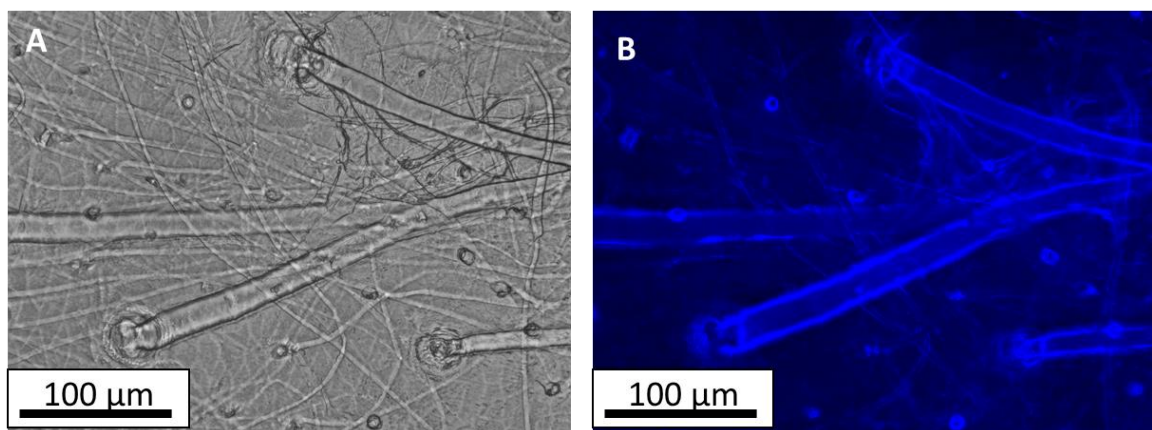
Figure 69. (A) Light microscopy and (B) fluorescence microscopy images principles of a selected fragment of the porous chitin isolated from C. versicolor and stained with CFW. Light exposure time in image: 1/4800 s.

Spiders cuticles have two fundamental chitin–based layers: the exo- and endocuticle [233] and non-chitinous epicuticle. The epicuticle is defined as the outermost proteins, waterproofing layer [388]. Lipids which are present at them, play a crucial role in saving of water loss and protecting the spider's body from dehydration. The endocuticle was recognized as a thick layer of chitin fibers tightly coated with proteins [388,389]. An external area of the endocuticle is laid down before the new cuticle formation after molting [388].
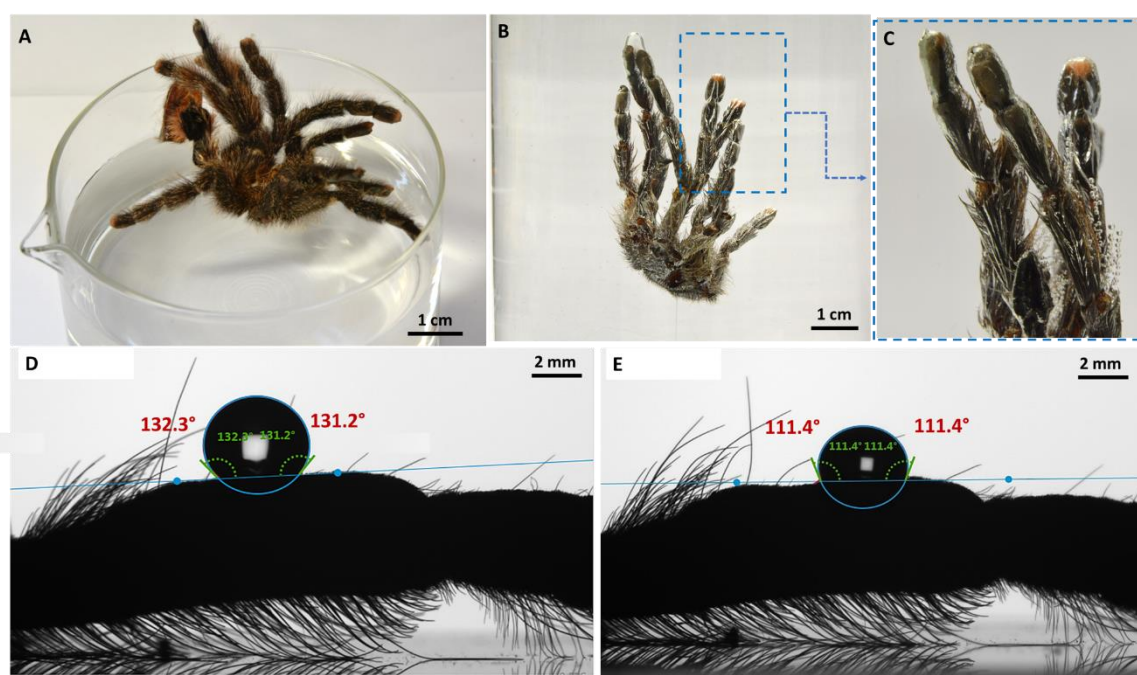
Figure 70. *(A-C) Images of the hydrophobic properties of A. sp. "Peru purple" molting cuticle. Hydrophobic molt immersed in water by an external force, and mirror-like effect on the surface (air bubbles). Average contact angle of (D) water and (E) diiodomethane on molting cuticle, based on Machałowski and co-authors [13].*

Noteworthy is the fact, that chitin with cross-linked protein constitute about 90% of the total organic content of the spider's exoskeleton [390]. Other components are pigments (e.g. ommochromes, bilins and others). The spider's cuticles have a non-homogeneous morphology what is strictly related with their functions [13]. Examination of the walking leg from molt of theraphosid spider *A. sp. "Peru purple"* [13], showed that this element combines two morphologically different elements: a structure of thick hair which imitates a brush and a porous

part of the cuticle which connects the setae (epicuticle). As presented **Figure 70**, *A. sp. "Peru purple"* spider molt floats freely on the water surface and when submerged creates a mirror effect. This proves its hydrophobicity, which is confirmed by the contact angle test.

Figure 71 presents the results of ATR–FTIR of the molt cuticle at various stages of isolation.
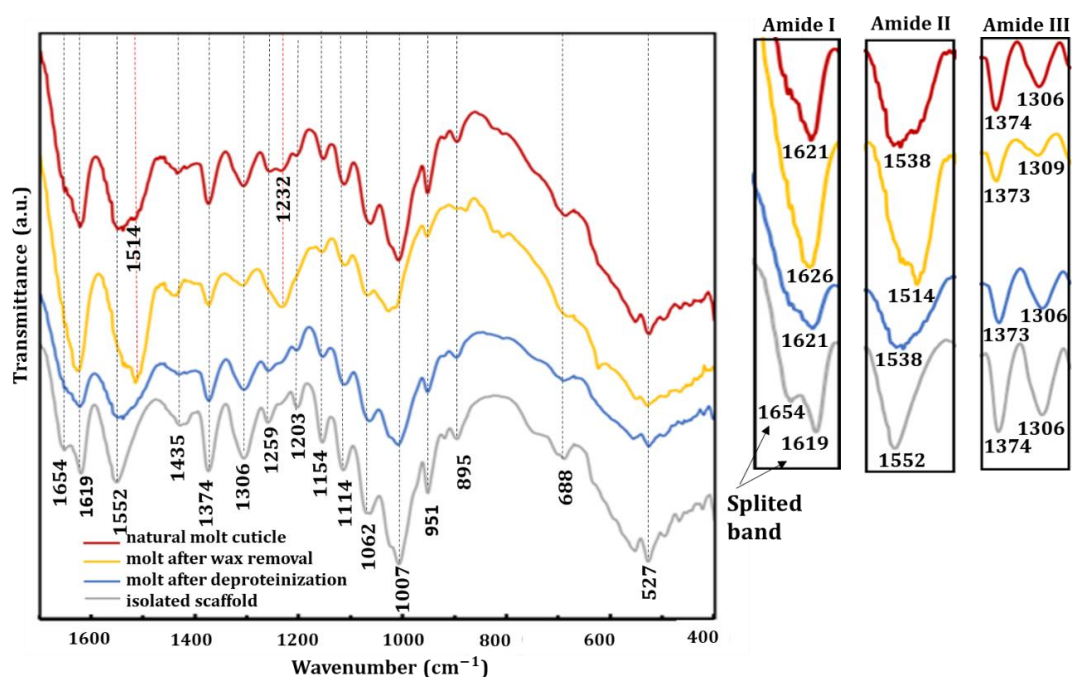
Figure 71. ATR–FTIR spectra of C. versicolor spider molt at different isolation steps. Natural spider molt cuticle (red line), molt after wax removal (yellow line), molt after deproteinization (blue line) and isolated chitin scaffold (gray line). Data clearly indicate the α–chitin presence (splitted band at amide I).

The spectrum obtained for the transparent, insoluble scaffold showed characteristic for α-chitin split of the amide I band (mainly associated with C=O stretching vibrations) with peaks at 1654 cm^{-1} and 1619 cm^{-1} (gray line). Splitting of the amide I band results from the stretching vibrations from intermolecular (C=O···HN) and intramolecular (C=O···HO(C6); C=O···HN) hydrogen bonds [2,3]. Additional features such as the presence of amide II (νN-H and νC-N), amide III (νC–N and δN–H), and specific bands at 951 cm^{-1} (ωCH$_x$) and 895 cm^{-1} (β-glycosidic bonds) in the final material confirmed data reported for α-chitin

[2–5]. What is more, acetylation degree was calculated as DA=98% and DD=2%. Such results confirms that the proposed isolation method, due to its very short duration, does not have a negative impact on the chitin structure.

Spectroscopic methods are currently considered as highly sensitive and useful techniques for the identification of carbohydrates (especially polysaccharides). It should be highlighted that vibrational spectroscopy also gives complete insights into intermolecular interactions between natural polysaccharides and proteins [391]. Raman spectroscopy resulted showed in **Figure 72,** proved that spectra for chitin isolated chitin from *C. versicolor* corresponds to the spectrum acquired for the α-chitin standard.
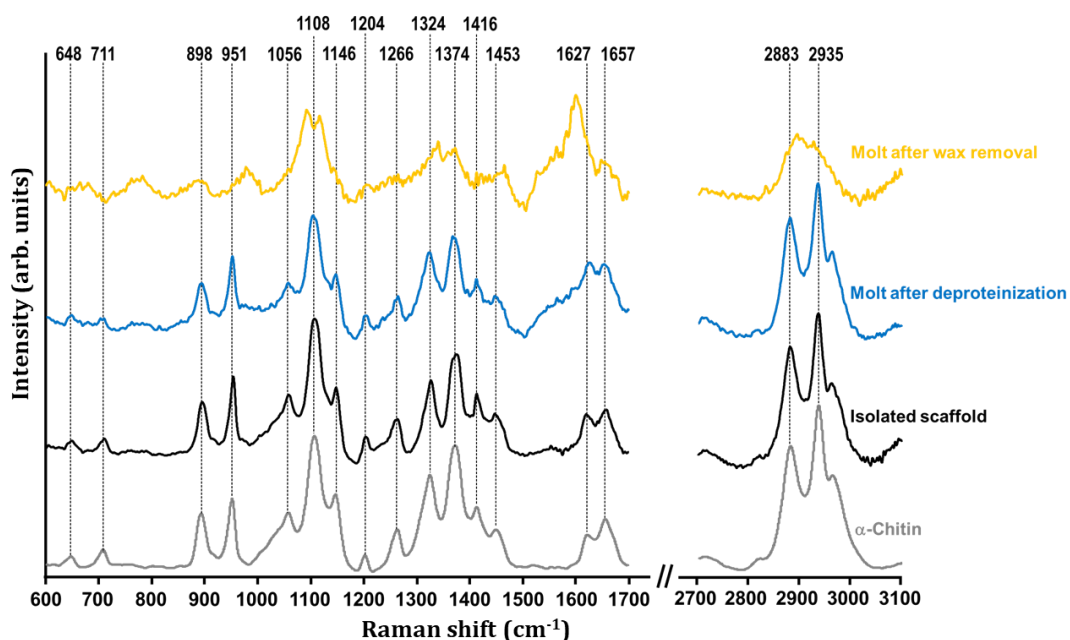
Figure 72. Raman spectra of spider cuticle obtained after ecdysis at different isolation step, compared to α-chitin standard, based on [245].

Aliphatic stretching features could be recorded at 2935 cm^{-1} and 2883 cm^{-1}, whereas the bending of these groups can be observed at 1453 cm^{-1} and 1374 cm^{-1} [392]. Furthermore, there are two peaks which can be attributed to the amide I band at v_{max} 1657 cm^{-1} and 1627 cm^{-1}, as well as a notable peak associated with the β-glycosidic bond at v_{max} 898 cm^{-1}. The obtained data indicates that the α isomorph is the major constituent of the isolated chitin. Subsequent analysis

reveals signals at 1324 cm⁻¹ and 1266 cm⁻¹ which can be attributed to the C–N stretching and N–H deformation of the amide III band. Finally, the peaks recorded in the range 950–1108 cm⁻¹ relates to C–O and C–C vibrations of the saccharide ring [202].

N₂ low-temperature sorption measurements (**Figure 73**) revealed that the natural molting cuticle (before chitin isolation) had a surface area greater than that of the pure spider chitin (17.0±1.5 m²/g and 9.00±0.78 m²/g, respectively).
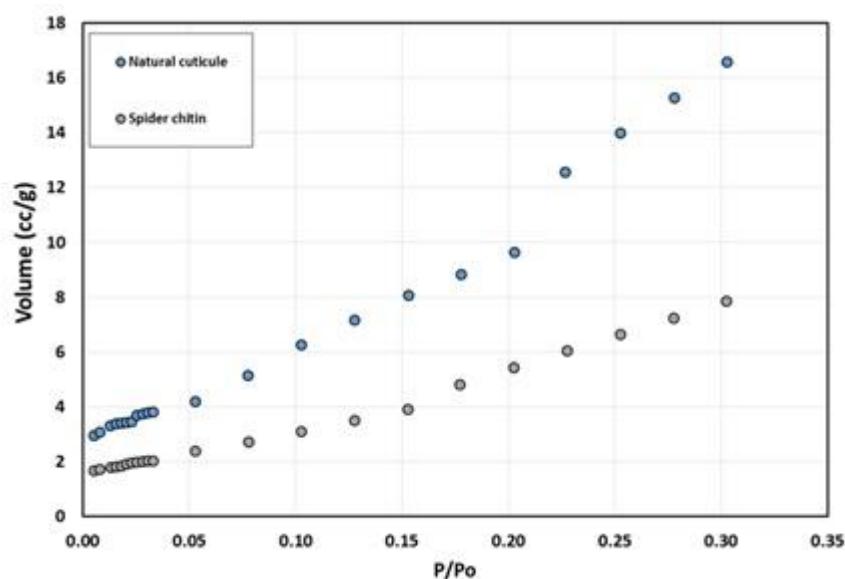
Figure 73. N₂ adsorption isotherms for natural spider cuticle obtained after ecdysis and isolated chitin, based on [245].

Based on the refinement involved, a preferred orientation of α-chitin was detected. Crystalline index (CrI; %) was calculated based on the intensity measurements at the following conditions: single peak fitting, dashed lines = individual peaks, solid line = sum profile, vertical bars = I_{am} and I_{110} determined at $2\theta \approx 16°$ and $2\theta \approx 19.5°$, respectively. In this case I_{am} represents the intensity of an amorphous phase visible in the diffraction pattern, approx. from the 020 to the 060 reflection (d $\approx$ 10,3 Å, for Cu-radiation: $2\theta \approx 8.30°$). The CrI values were calculated for the samples based on the values of intensity presented in **Figure 74 A** (right), at the positions indicated by the vertical bars: *C. versicolor* cuticle: 94%, spider chitin: 99%, respectively. Obtained results confirmed that the proposed

microwave irradiation-based isolation does not have a negative influence on the crystallinity of biopolymer.

The ^{13}C CP/MAS NMR spectrum of the chitin (**Figure 74 B**) indicates the presence of signals characteristic for α–chitin standard, which confirms the effective isolation of the pure material.
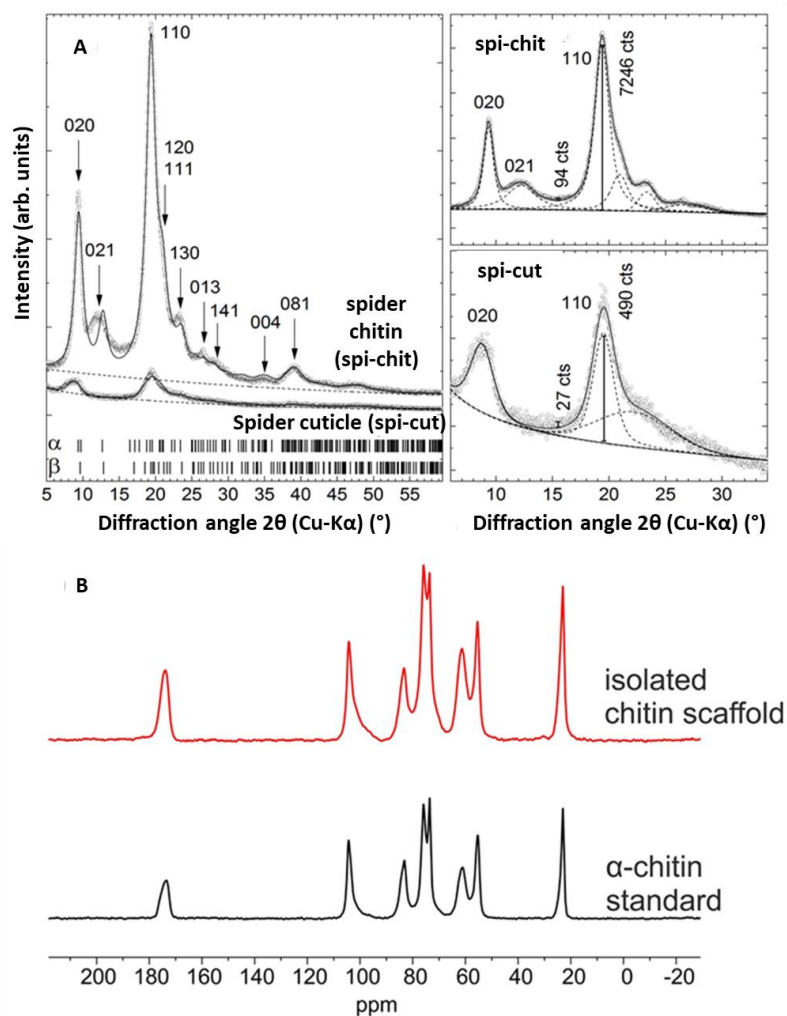
Figure 74*. (A) Diffraction patterns of natural spider molting cuticle (spi-cut) and isolated chitin scaffold (spi-chit). The well visible match between experimental (dots) and calculated data (line) proved the presence of α-chitin (left, Rietveld refinement, phase identification). For comparison, the theoretical line positions for α- and β-chitin were also showed, (B) ^{13}C CP/MAS NMR spectra of obtained chitin scaffold (red line) and α-chitin standard (black line), based on Machałowski and co-authors [245].*

Eight ^{13}C signals can be observed in the ^{13}C CP/MAS NMR spectrum of the investigated α-chitin (black line) within the range from 0 to 200 ppm, which can

be attributed to the chemical data shift reported for α-chitin [393]. The spectrum obtained for the material (red line) fully coincides with the reference sample. There are no signals confirming the presence of other structural elements in the material.

10.2. Preliminary investigation with respect to tissue engineering applications

This part of thesis assumes preliminary investigation of biocompatibility of spider chitin with human cardiomyocytes from pluripotent stem cells (iPSC-CMs). One month after differentiation of stem cells, beating of iPSC-CMs were separated from standard 2D culture and transferred to the pure tube-like chitin scaffolds surface, or onto chitin pre-coated with the collagenous matrix-Geltrex. The cardiomyocytes attachment was observed for uncoated and Geltrex-coated chitin scaffolds (**Figure 75 A, B**).
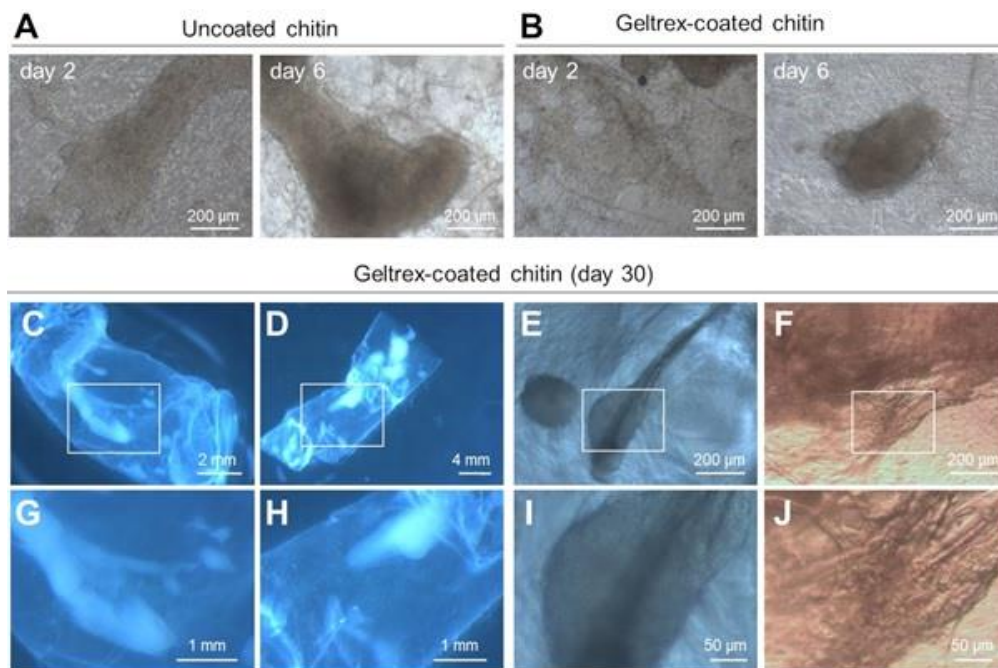
Figure 75. Microscopic images that visualize attachment and culture of iPSC-CM on isolated chitin scaffolds, (A, B) Attachment of iPSC-CM to uncoated and coated by collagenous matrix (Geltrex) chitin scaffolds, (C, D) Cardiomyocyte's muscle fibers formed inside the chitin segments of the spider leg after 30 days of culture, (E, F) Attachment and growing of cardiomyocytes on hair-like structures in the scaffold and on the edge of the chitin scaffold. (G-J) Higher magnification of areas indicated in C-F, adopted from Machalowski and co-authors [30].

As it was observed, the first cardiomyocytes (iPSC-CMs) started beating one day after seeding, what is comparable to its natural behavior under standard culture. Two days after seeding, cells spreading was observed. After 6–8 days, the cardiomyocytes formed groups of cells inside the chitin scaffold and attached to the setae forms. Intriguingly, long-term cells cultivation on the *C. versicolor* scaffold (about one month) allowed to form longer, muscle-like filaments by iPSC-CMs inside the chitin scaffolds (**Figure 75 C–F**). In this scaffolding utility determination, the quantitative proliferation of the cardiomyocytes is not a critical factor. As observed in this kind of cells, the proliferation capacity usually decrease over the time, and only 10% bromodeoxyuridine (BrdU) positive cells after four weeks were recorded [394]. However, the strong cells adhesion to the scaffolds indicates the good biocompatibility of chitinous support from *C. versicolor* spider.
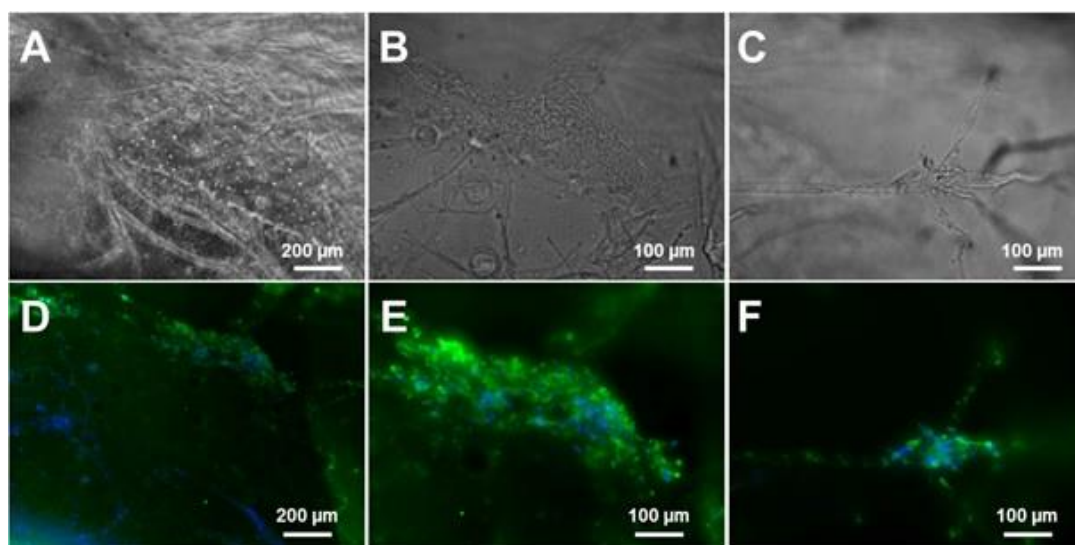
Figure 76. Results of immunofluorescent staining of iPSC-CM cells on isolated chitin scaffolds cultivated for 30 days in B27 medium. After fixation of the iPSC-CM with paraformaldehyde, specific staining showed targeting α-actinin cytoskeleton (green) and cell nuclei (blue) using Hoecht33342 dye, adopted from Machalowski and co-authors [30].

To characterize the cells attached to the *C. versicolor* chitin scaffold, immunofluorescent staining of the cytoskeleton protein α-actinin was carried out (**Figure 76**). The formation of groups of iPSC-CM cells inside the chitin tubes and at their surface (**Figure 76 A, B**) as well as their attachment was confirmed here

(**Figure 76 F**). As it is well visible, cells formed cytoskeletons made by *α*-actin. Cells nuclei was stained by blue color. Unfortunately, detection of individual sarcomeres was hampered by the 3D structure of the scaffold and hardware limitations. However, the scope of these preliminary study was experimental confirmation of biocompatibility of the chitin scaffolds from *C. versicolor* to culture cardiomyocytes and the goal was achieved. The further studies should focus on preliminary *in-vivo* tests.

10.3. Chitin/proteins-based spider cuticle for oil-spill remediation

Preliminary investigation of spider molting cuticle as crude oil sorbent was described in this subchapter. Research started by determination of wettability as a significant feature of sorbent materials in oil–water interactions. Mostly, it is controlled by the chemical composition and structural geometry of the sorbent surface. Therefore, evaluation of the contact angle in respect to polar and dispersive liquids — as e.g. water and diiodomethane, respectively, is crucial for surface free energy (SFE) determination. **Figure 70** (section 10.1) presents results of the contact angles (CA) calculations for water and diiodomethane (131.63 ± 0.54° and 114.52 ± 0.23° were obtained as mean values, respectively). These high values of CA indicate the particularly high hydrophobicity of the spider molt cuticle [395,396]. Further analysis allowed to determine the surface free energy (SFE) which equaled 4.47 ± 0.08 mN/m. Its very low value may suggest that the adhesive forces between oil molecules and sorbent surface are greater than those between material and water molecules. Thus, oil particles floating on the surface of water are simply trapped and retained. The minimal value of the polar component of SFE, determined as 0.12 mN/m, indicates neglected water pickup; what is a desirable parameter for oil clean up from the water surface by sorbent materials [397]. **Table 14** presents SFEs of the tested materials along with other natural sorbents. The results indicate quite unique nature of chitinous spiders' molts and its potential in

sorption processes. The morphology of a single spider microhair is similar to a bird's feather – a main core and micro-hairs protruding from it could be distinguished (see **Figures 77** and **78**). The hairs, which cover the cuticle, are between 0.5 to 1 mm in length. However, spider's cuticle surface also represents a complex system of pores and wax canals. During the contact with crude oil, spider cuticle absorbs these medium very quickly and retain it (see **Figures 79**).
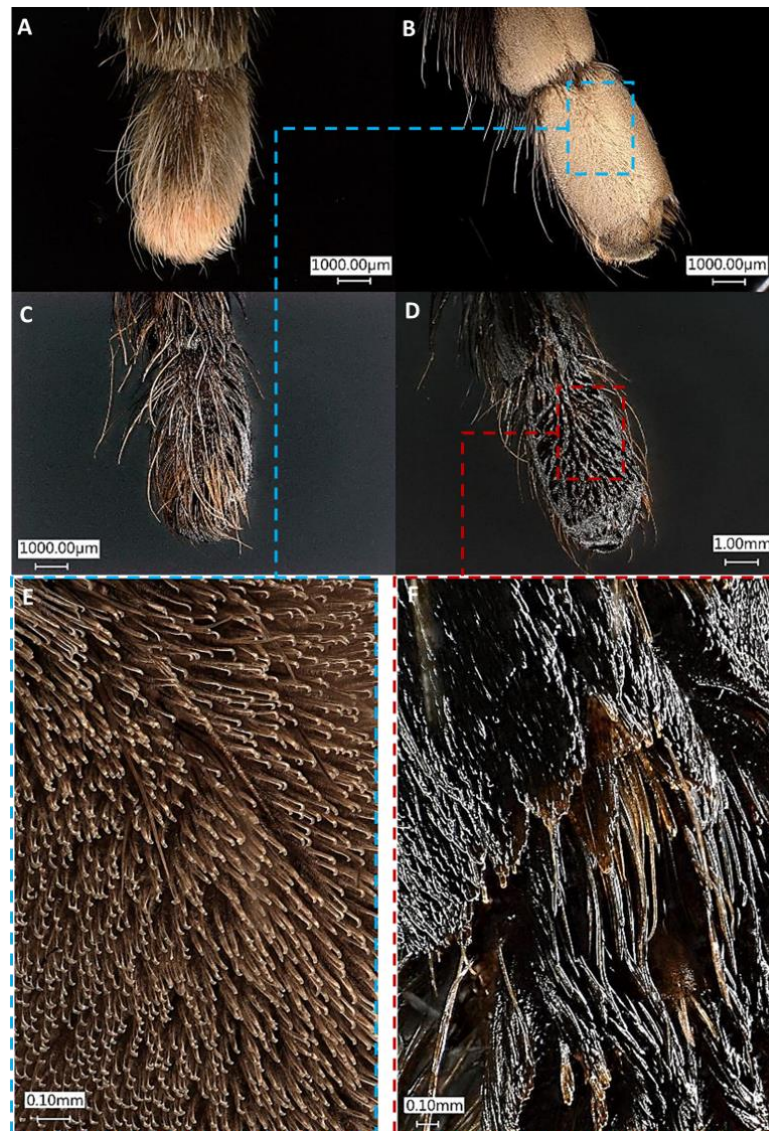
Figure 77. (A-D) Digital microscopy representation of contact between crude oil and spider cuticle walking leg, (E) High magnified images of the brush-like structure of walking leg before and (F) after crude oil contact, based on Machałowski and co-authors [13].

Table 14. Surface free energy (SFE) values, resolved into dispersive and polar parts.

Sorbent	SFE (mN/m)	SFE polar component (mN/m)	SFE dispersive component (mN/m)	Reference
Spider molting cuticle [a]	4.47±0.08	0.12±0.03	4.35±0.05	experimental data
Kapok fiber	40.64	7.60	33.04	[398]
Polyester fiber	59.15	7.14	52.01	[398]

[a] experimental results.

Figure 78. (A) Microscopic images of a selected fragment of A. sp. "Peru purple" molting cuticle – walking leg part, (B) Single hair isolated from a fragment described above, (C) Effect of maintenance of crude-oil by mutual bonding of five spider hairs, (D) Effect of trapping of crude oil on an individual hair, adopted from Machałowski and co-authors [13].

Based on digital and scanning electron microscopy the possible mechanism of crude-oil sorption was suggested (**Figure 79 A**).
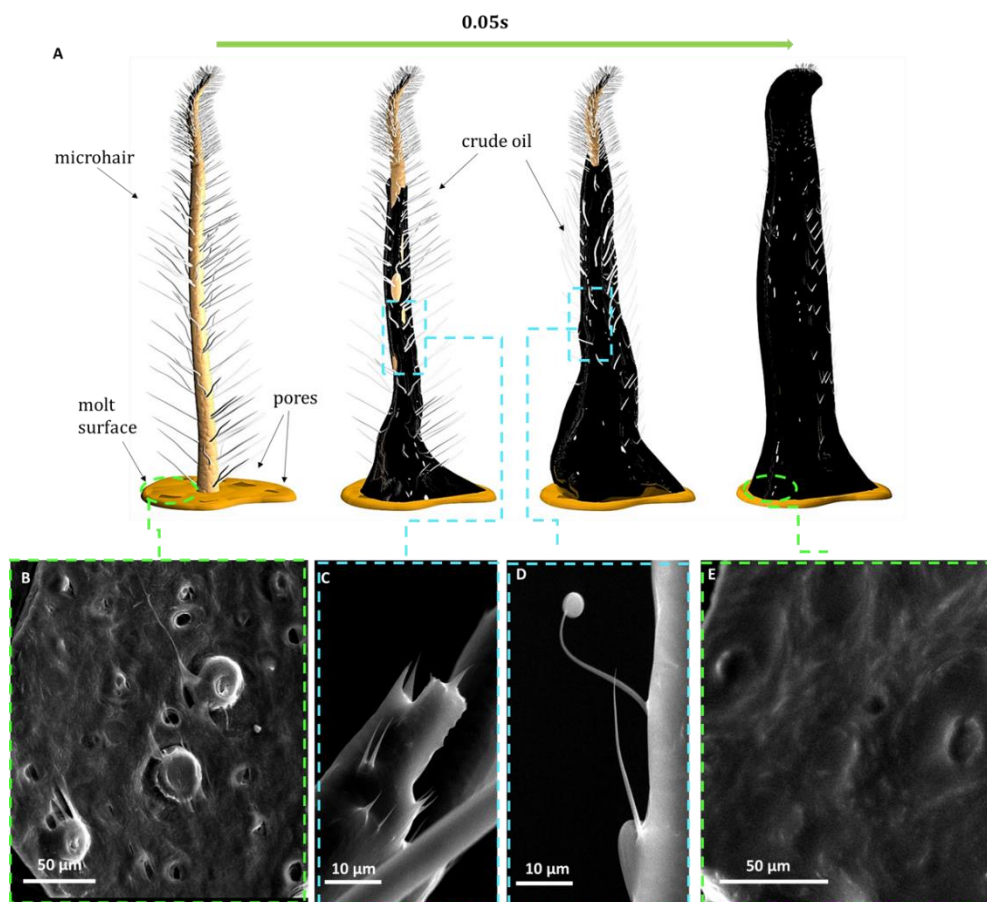
Figure 79. (A) Computer-design interaction model of the crude-oil-single hair of spider molting cuticle and pores located on its surface, (B) SEM representation of the spider molt surface before crude oil sorption, with well-visible open pores, (C-D) SEM images of crude oil surrounding a single spider hair, (E) Comparative SEM image of the molt surface after crude oil sorption, pores are filled with oil, based on Machałowski and co-authors [13].

Probably, the spider molting cuticle interact with crude oil drops by the physical trapping. The dry brush-like formation of the molting cuticle, composed by not regular branched hairs, forms an appropriate environment for physical trapping of crude oil and may be considered as a fiber surface. The irregular brushy units take oil sorption through the hair structure and retain oil particles by clumping them together as showed above. This behavior is controlled by weak interactions e.g. van der Waals forces, hydrophobicity or other physical and chemical interactions. As determined previously, parameters such as surface wax coverage, surface roughness and pores presence could significantly affect at efficiency of oil sorption [399,400]. Herein, based on chloroform/ethanol treatment, the total wax content was calculated as 1.9% of total material weight.

Pores present at cuticle allow the entry of crude-oil to the interior of the cuticle and reinforce the sorption process (see **Figure 79 E**), what were confirmed by SEM images.
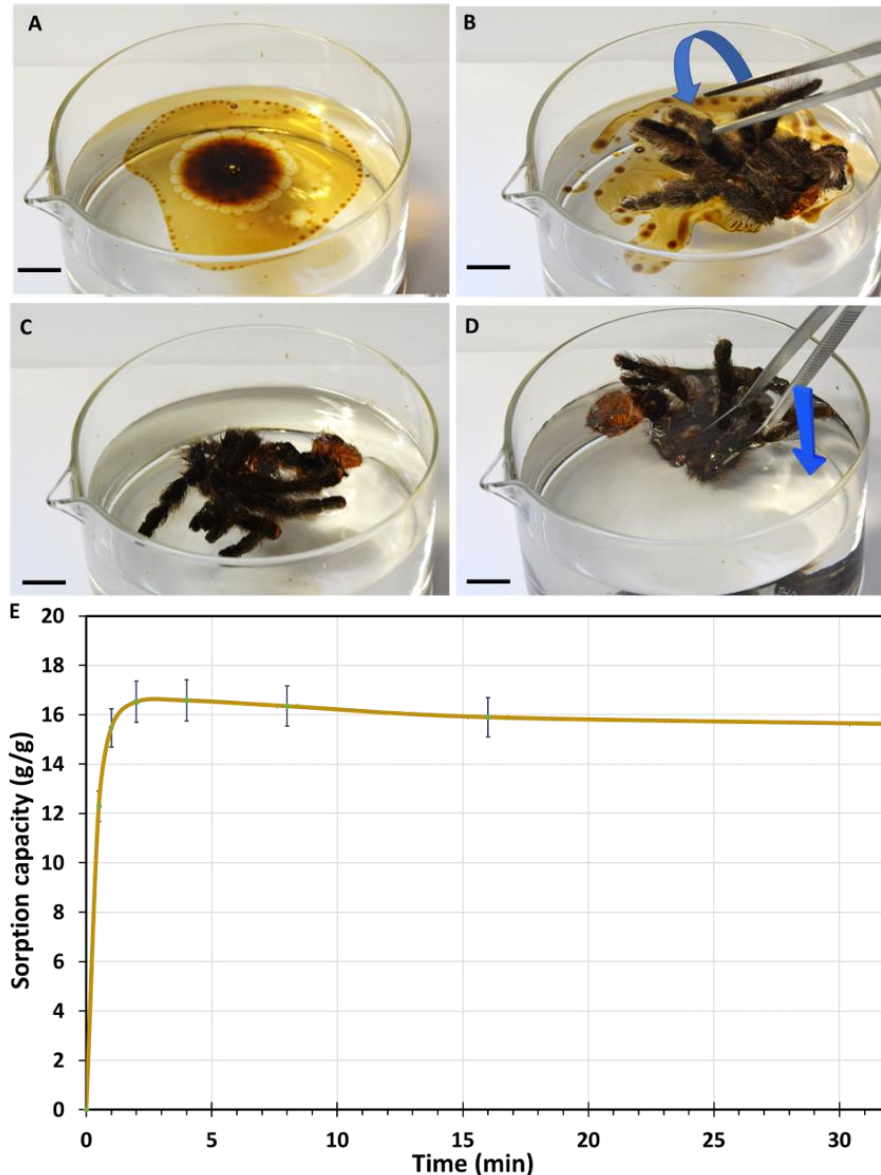
Figure 80. (A-D) Images representing various steps of crude oil sorption by A. sp. "Peru purple" molting cuticle at room temperature, (D) Visualization of retention of adsorbed crude oil by the natural sorbent by immersing in fresh tap water, (E) Crude oil adsorption capacity as a function of time, error did not exceed 5%, based on Machałowski and co-authors [13].

The results showed in **Figure 80** visualized that *A.* sp. *"Peru purple"* molt can be recognized as an efficient biosorbent. As estimated, material can remove up to 16.6 times more crude oil than its own mass (a sorption capacity of 16.6 g/g) after two minutes. Noteworthy is the fact, that after the first 30 s of interactions with

oil, the cuticle sorbed about 75% of its maximum capacity. As compared with other biosorbents, cuticle showed high retention of the sorbed crude oil, which confirmed strong sorption affinity (see **Figure 80 D**).

Table 15. Literature summary of the crude oil sorption capacity of natural plants and animals' sorbents, compared with experimental results.

Sorbent origin	Sorbent type	Sorption capacity (g/g)	Reference
Plants	Populus seed fibers	182.0–211.0	[401]
	Silk-floss fibers	85.0	[402]
	Kapok fibers	34.1–54.3	[398,400]
	Cotton grass	9.0–22.0	[403]
	Cattail fiber	13.4	[404]
	Rice husks ash	2.9-6.2	[405]
	Coir fiber	5.4	[402]
	Sponge gourd	4.6	[402]
Animals	Silkworm cocoon waste	37.0–52.0	[406]
	Natural wool	33.0 – 43.0	[298]
	Spider molting cuticle	16.6	experimental data
	Human hairs	5.2-7.4	[407]
	Chicken feathers	6.1	[399]
	Goat hair	3.0-4.5	[408]
	Chitosan from crab shell	0.28	[277]
	Pure chitin from crab shell	0.26	[276]

As showed in **Table 15,** these naturally ready-to-use biosorbent indicated higher sorption capacity than currently used sorbents such as human hairs, chicken feathers, goat hairs, or pure chitin or rice husks ash. Moreover, the proposed

sorbent exhibited outstanding ability to remain on the water surface for a long time. Water sorption is negligible and equal to about 0.1 g/g after 48 h of direct underwater immersion.

Analyzing the data presented in **Figure 81**, it could be seen that *A. sp. "Peru purple"* cuticle possesses the highest crude oil sorption efficiency from freshwater surface, in comparison to distilled and simulated sea water. Removal efficiency was determined as about 84 ± 5%. Then, 79 ± 4% and 63 ± 4% of removal efficiency was achieved for distilled and sea water, respectively. Thus, it could be concluded that sorption efficiency is not only matter of sorbent characteristic but also process parameters. Herein, 2 g of crude oil was added to a container with 60 mL of each water type, and 100 mg of cuticle was used as a sorbent.
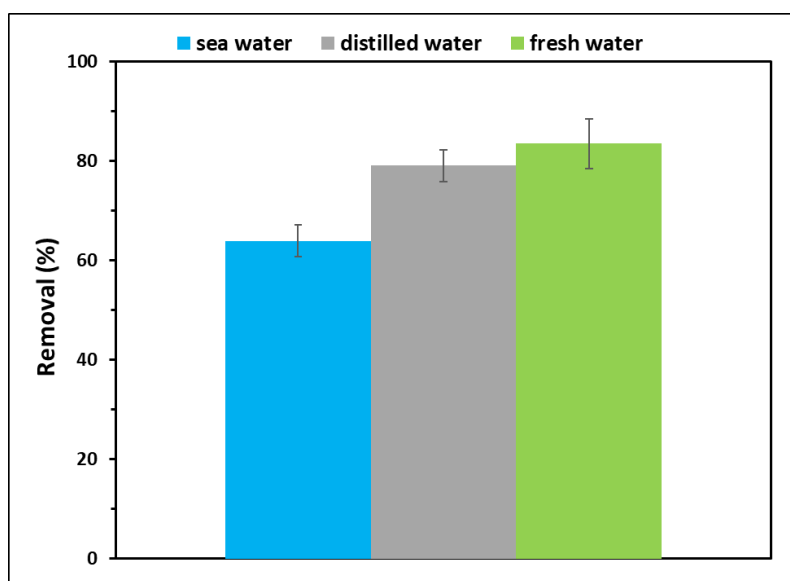
Figure 81. Crude oil removal efficiency by A. sp. "Peru purple" molting cuticle (walking leg part) from surfaces of various type of water (sea, distilled, and fresh water, respectively), based on Machałowski and co-authors [13].

Crude oil spill is a natural disaster that occurs most often in oceanic mines or during the transport of raw materials. In this context desorption assay was performed for simulated sea water. The results, presented in **Figure 82**, demonstrates a decreasing tendency in the sorption ability of *A. sp. "Peru purple"*

spider molting cuticle over next cycles. This fact may be related to two potential explanations. Firstly, the natural wax layer covering sorbent was removed with the crude oil after the first desorption using chloroform:ethanol medium. It was proved by the first significant decrease of removal efficiency between 1–2 cycle. Moreover, during next cycles (2–4) the sorption capacity remains at similar level 40–45%. The second possible explanation could be related with sorbent mass loss by the mechanical damage of the fragile sorbent during desorption. As calculated, the mass loss between the first and fourth cycle was estimated as 16%. However, observed decrease in removal efficiency may be a combination of few factors. Final removal capacity of the tested sorbent decreases successively from 12.6 g/g to 9 g/g.
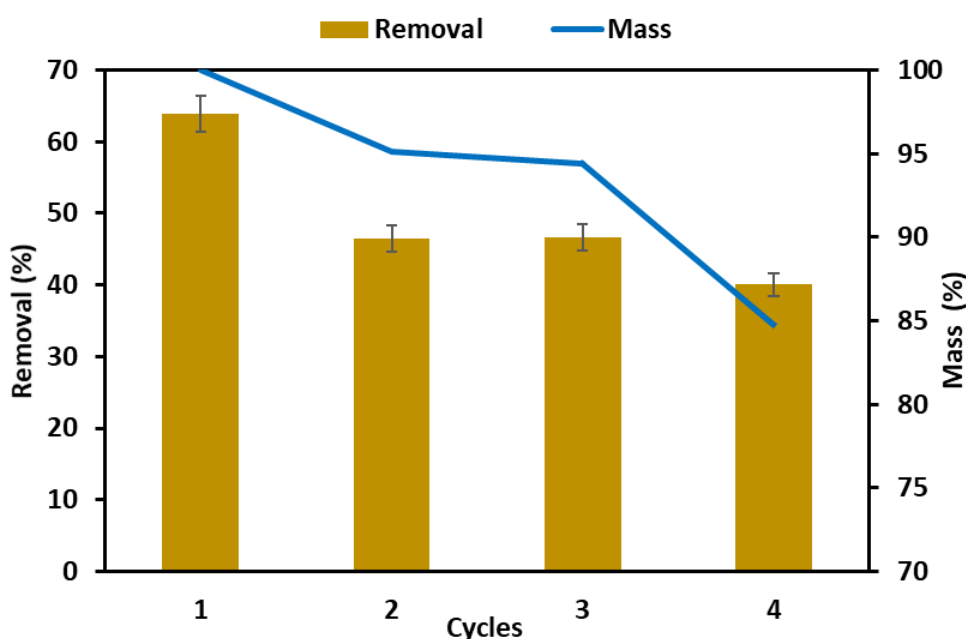
Figure 82. Efficiency of crude-oil removal during next sorption–desorption cycles, and related sorbent mass loss

10.4. Conclusions

The spiders were neglected among many years as potential and interesting source of chitin. However, their live cycle based on cyclic ecdysis process make them unique in this case. At the beginning, Theraphosidae *C. versicolor* spider's chitin was isolated using microwave assisted method. As determined, short-term

microwave treatment did not affect any structural changes of chitin structure. Spectroscopic methods as Raman, ATR–FTIR and ^{13}C CP/MAS NMR strongly confirmed that proposed method allowed to obtain highly pure α-chitin scaffold. Microscopic observations indicated the diverse 3D morphology of obtained material with porous and brushy-like regions.

Next goal of the following research was focused on determination of biomedical potential of spider's chitin. Thus, scaffolds were used as structural support for cultivation of human cardiomyocytes from pluripotent stem cells (iPSC-CMs). Further investigations showed that after 7 days, the cells formed groups inside the chitin scaffold and adhered to the setae. It should be noted that, during the prolonged culture (about one month) the iPSC-CMs form longer, contracting muscle filaments inside the chitin scaffolds and *"heart beating"* shrinks of cells are observed. Finally, *A. sp. Peru purple* spider molts were used as sorbent of crude oil spill. This experiment began with determination of wettability as a very significant feature of sorbent materials in oil–water interactions. As determined contact angles (CA) for water and diiodomethane were 131.63 ± 0.54° and 114.52 ± 0.23°, respectively. This high value of CA indicated the particularly high hydrophobicity of the spider molt cuticle. Moreover, surface free energy (SFE) was calculated as 4.47 ± 0.08 mN/m. Such a low value may suggest that the adhesive forces between oil molecules and sorbent surface are much higher than those between material and water molecules, what make spider molt especially attractive for oil-based impurities removal from water surface. Experimental data were confirmed by practical experiment, where crude oil sorption capacity was estimated as 16.6 g/g. Moreover, it was showed that material can work in several sorption-desorption cycles. Possible mechanism of sorbent-crude oil interactions was proposed and confirmed that it is based on physical trapping. Compared with other natural sorbents, spider chitinous molting cuticle possess extraordinary hydrophobicity

and minimal water retention. Moreover, it constitutes intriguing composition of chitin, proteins, and waxes and may be an inspiration for advanced sorbents synthesis. The results described in this section showed versatility of naturally formed chitinous scaffolds from spiders as candidates for both, biomedical and environmental protection applications. This confirms the assumptions of the research hypothesis as well as the stated goals of this dissertation.

General Summary

The biocompatibility, high porosity, renewability, and ecological safety of biological materials predispose them to become a real competition to synthetic ones. Chitin is one of the most fascinating examples among them. Its extraordinary biosynthesis causes that chitin can be found in more than 70% of all living organisms in the world. However, the difficulties in its processing, as non-solubility, makes its application very limited. The open window for chitin utility may results from the possibilities of its application in form of natural scaffolds.

Experience gained during experiments on the isolation of chitin from marine sponges allowed to develop of a new microwave-assisted chemical method for its extraction. The benefits of utilizing this method are extremely significant because reduces the isolation time from about 7 days (classical chemical isolation) to less than 1 h. Other advantages are the reduction of the volume of used reagents and their lower concentration. Finally, structural, and physicochemical studies proved no negative impact of microwaves on the chemical structure of chitin. The observations made during this part of research, allowed to predispose pure chitinous scaffold for further application, because of its unique 3-dimensional arrangement. As example, chitinous skeletons from *A. fistularis* marine sponge were used as scaffolds for skin cells cultivation. The cytotoxicity analysis confirmed that prepared material did not negatively affect cells morphology and ultrastructure. Specific staining allowed for a better understanding of the cell's attachment and proliferation onto a chitinous scaffold. Further studies focused on the functionalization of chitinous scaffold surface. Depending on the functionalization method, obtained materials were characterized by the unique properties that make them attractive for various sophisticated applications. For instance, deposition of calcium carbonate in form

of ACC and crystalline calcite, using *C. aspersum* snail hemolymph as a biomineralization agent, allowed for the improvement of desire properties, such as wettability, surface roughness, or mechanical resistance. These changes affected the beneficial behavior of human osteoblasts spreading and attachment during cells culture. Other experiments allowed laccase immobilization onto *A. archeri* 3D chitinous scaffolds. Created biosystem was able to remove of tetracycline from aqueous solution with almost 100% efficiency (depends on process conditions). This is an attractive aspect for the utilization of this biocatalytic system in future wastewater treatment and removal of harmful pollutants. Analysis of the application potential of chitin−Ag/AgBr materials revealed that these ternary composite can be used as an effective antibacterial filter. Performed tests proved that 100% of *E. coli* bacteria were deactivated after 6 h of the experiment.

The last chapter of the submitted doctoral dissertation describes the achievements on characterization and utilization of chitinous scaffolds from spiders molting cuticle origin. It should be highlighted, that besides diversity and abundance, the spiders were neglected in scientific reports as a source of chitin for many years. Thus, the several practical utilities proposed here, were described for the first time. The results of the physicochemical characterization made it possible the confirm presence of high purity α−chitin. Preliminary experiments on the utilization of tubular chitinous scaffolds as structural support for the cultivation of human cardiomyocytes from pluripotent stem cells showed very intriguing results. Long-term observations allowed to characterize the successive stages of the new tissue formation. From simple cells spreading, by higher groups formation, to the creation of contracting muscle filaments inside the chitin scaffolds and "heart beating" shrinks. Finally, the high hydrophobicity of spider molt was an inspiration for utilizing it as a sorbent of the crude oil spill. Experimental data determined crude oil sorption capacity as

16.6 g/g, which makes this chitinous material relatively unique, as compared with other animal-origin natural sorbents.

Results presented as a part of the submitted doctoral dissertation confirmed the achievement of the assumed research objectives and justify the research hypothesis. I fervently believe that the effort presented in these thesis, will be a spark for further scientific activities and in some way will expand the awareness of the properties and application possibilities of chitin in form of naturally prefabricated scaffolds.

References

1. Ehrlich, H. *Biological materials of marine origin invertabrates*; Gorb, S.N., Ed.; Springer International Publishing: Cham, Switzerland, 2016; ISBN 9783319463728.

2. Ehrlich, H. *Marine biological materials of invertebrate origin*; Gorb, S.N., Ed.; Springer International Publishing: Cham, Switzerland, 2019; ISBN 978-90-481-9129-1.

3. Pina, S.; Ribeiro, V.P.; Marques, C.F.; Maia, F.R.; Silva, T.H.; Reis, R.L.; Oliveira, J.M. Scaffolding strategies for tissue engineering and regenerative medicine applications. *Materials* **2019**, *12*, 1824.

4. Duan, B.; Huang, Y.; Lu, A.; Zhang, L. Recent advances in chitin based materials constructed via physical methods. *Prog. Polym. Sci.* **2018**, *82*, 1–33.

5. Addadi, L.; Joester, D.; Nudelman, F.; Weiner, S. Mollusk shell formation: a source of new concepts for understanding biomineralization processes. *Chem. - A Eur. J.* **2006**, *12*, 980–987.

6. Addadi, L.; Weiner, S. Biomineralization: mineral formation by organisms. *Phys. Scr.* **2014**, *89*, 098003.

7. Huang, J.; Li, S.; Liu, Y.; Liu, C.; Xie, L.; Zhang, R. Hemocytes in the extrapallial space of *Pinctada fucata* are involved in immunity and biomineralization. *Sci. Rep.* **2018**, *8*, 4657.

8. Hwang, J.; Jeong, Y.; Park, J.M.; Lee, K.H.; Hong, J.W.; Choi, J. Biomimetics: forecasting the future of science, engineering, and medicine. *Int. J. Nanomedicine* **2015**, *10*, 5701–5713.

9. Shimomura, M. The new trends in next generation biomimetics material technology: learning from biodiversity. *Sci. Technol. Trends* **2010**, *37*, 53–75.

10. Vincent, J.F.V.; Bogatyreva, O.A.; Bogatyrev, N.R.; Bowyer, A.; Pahl, A.K. Biomimetics: its practice and theory. *J. R. Soc. Interface* **2006**, *3*, 471–482.

11. Bobbio, A. The first endosseous alloplastic implant in the history of man. *Bull. Hist. Dent.* **1972**, *20*, 1–6.

12. Hargroves, K.; Smith, M. Innovation inspired by nature: biomimicry. *ECOS* **2006**, *129*, 27–29.

13. Machałowski, T.; Wysokowski, M.; Petrenko, I.; Fursov, A.; Fazilov, B.; Rahimi-Nasrabadi, M.; Amro, M.M.; Meissner, H.; Joseph, Y.; Ehrlich, H.; et al. Naturally pre-designed biomaterials: Spider molting cuticle as a functional crude oil sorbent. *J. Environ. Manage.* **2020**, *261*, 110218.

14. Ehrlich, H. *Extreme biomimetics*; Springer: Cham, Switzerland, 2016; ISBN

9783319453408.

15. Wysokowski, M.; Petrenko, I.; Stelling, A.L.; Stawski, D.; Jesionowski, T.; Ehrlich, H. Poriferan chitin as a versatile template for extreme biomimetics. *Polymers.* **2015**, *7*, 235–265.

16. Wysokowski, M.; Materna, K.; Walter, J.; Petrenko, I.; Stelling, A.L.; Bazhenov, V. V.; Klapiszewski, Ł.; Szatkowski, T.; Lewandowska, O.; Stawski, D.; et al. Solvothermal synthesis of hydrophobic chitin-polyhedral oligomeric silsesquioxane (POSS) nanocomposites. *Int. J. Biol. Macromol.* **2015**, *78*, 224–229.

17. Wysokowski, M.; Motylenko, M.; Walter, J.; Lota, G.; Wojciechowski, J.; Stöcker, H.; Galli, R.; Stelling, A.L.; Himcinschi, C.; Niederschlag, E.; et al. Synthesis of nanostructured chitin-hematite composites under extreme biomimetic conditions. *RSC Adv.* **2014**, *4*, 61743.

18. Szatkowski, T.; Kopczyński, K.; Motylenko, M.; Borrmann, H.; Mania, B.; Graś, M.; Lota, G.; Bazhenov, V. V.; Rafaja, D.; Roth, F.; et al. Extreme biomimetics: A carbonized 3D spongin scaffold as a novel support for nanostructured manganese oxide(IV) and its electrochemical applications. *Nano Res.* **2018**, *11*, 4199–4214.

19. Petrenko, I.; Summers, A.P.; Simon, P.; Żółtowska-Aksamitowska, S.; Motylenko, M.; Schimpf, C.; Rafaja, D.; Roth, F.; Kummer, K.; Brendler, E.; et al. Extreme biomimetics: Preservation of molecular detail in centimeter-scale samples of biological meshes laid down by sponges. *Sci. Adv.* **2019**, *5*, eaax2805.

20. Norman, M.; Żółtowska-Aksamitowska, S.; Zgoła-Grześkowiak, A.; Ehrlich, H.; Jesionowski, T. Iron(III) phthalocyanine supported on a spongin scaffold as an advanced photocatalyst in a highly efficient removal process of halophenols and bisphenol A. *J. Hazard. Mater.* **2018**, *347*, 78–88.

21. Norman, M.; Bartczak, P.; Zdarta, J.; Tomala, W.; Żurańska, B.; Dobrowolska, A.; Piasecki, A.; Czaczyk, K.; Ehrlich, H.; Jesionowski, T. Sodium copper chlorophyllin immobilization onto *Hippospongia communis* marine demosponge skeleton and its antibacterial activity. *Int. J. Mol. Sci.* **2016**, *17*, 1564.

22. Norman, M.; Zdarta, J.; Bartczak, P.; Piasecki, A.; Petrenko, I.; Ehrlich, H.; Jesionowski, T. Marine sponge skeleton photosensitized by copper phthalocyanine: A catalyst for Rhodamine B degradation. *Open Chem.* **2016**, *14*, 243–254.

23. Machałowski, T.; Czajka, M.; Petrenko, I.; Meissner, H.; Schimpf, C.; Rafaja, D.; Zietek, J.; Dziegiel, B.; Adaszek, Ł.; Voronkina, A.; et al.

Functionalization of 3D chitinous skeletal scaffolds of sponge origin using silver nanoparticles and their antibacterial properties. *Mar. Drugs* **2020**, *18*, 304.

24. Zdarta, J.; Antecka, K.; Frankowski, R.; Zgoła-Grześkowiak, A.; Ehrlich, H.; Jesionowski, T. The effect of operational parameters on the biodegradation of bisphenols by *Trametes versicolor* laccase immobilized on *Hippospongia communis* spongin scaffolds. *Sci. Total Environ.* **2018**, *615*, 784–795.

25. Zdarta, J.; Machałowski, T.; Degórska, O.; Bachosz, K.; Fursov, A.; Hermann Ehrlich, V.; Ivanenko, V.N.; Jesionowski, T. 3D chitin scaffolds from the marine demosponge *Aplysina archeri* as a support for laccase immobilization and its use in the removal of pharmaceuticals. *Biomolecules* **2020**, *10*, 646.

26. Stepniak, I.; Galinski, M.; Nowacki, K.; Wysokowski, M.; Jakubowska, P.; Bazhenov, V. V.; Leisegang, T.; Ehrlich, H.; Jesionowski, T. A novel chitosan/sponge chitin origin material as a membrane for supercapacitors-preparation and characterization. *RSC Adv.* **2016**, *6*, 4007–4013.

27. Wysokowski, M.; Motylenko, M.; Rafaja, D.; Koltsov, I.; Stocker, H.; Szalaty, T.J.; Bazhenov, V. V.; Stelling, A.L.; Beyer, J.; Heitmann, J.; et al. Extreme biomimetic approach for synthesis of nanocrystalline chitin-$(Ti,Zr)O_2$ multiphase composites. *Mater. Chem. Phys.* **2017**, *188*, 115–124.

28. Żółtowska, S.; Bielan, Z.; Zembrzuska, J.; Siwińska-Ciesielczyk, K.; Piasecki, A.; Zielińska-Jurek, A.; Jesionowski, T. Modification of structured bio-carbon derived from spongin-based scaffolds with nickel compounds to produce a functional catalyst for reduction and oxidation reactions: Potential for use in environmental protection. *Sci. Total Environ.* **2021**, *794*, 148692.

29. Machałowski, T.; Rusak, A.; Wiatrak, B.; Haczkiewicz-Leśniak, K.; Popie, A.; Jaroszewicz, J.; Żak, A.; Podhorska-Okołów, M.; Jesionowski, T. Naturally formed chitinous skeleton isolated from the marine demosponge *Aplysina fistularis* as a 3D scaffold for tissue engineering. *Materials.* **2021**, *14*, 2992.

30. Machałowski, T.; Wysokowski, M.; Żółtowska-Aksamitowska, S.; Bechmann, N.; Binnewerg, B.; Schubert, M.; Guan, K.; Bornstein, S.R.; Czaczyk, K.; Pokrovsky, O.; et al. Spider chitin. The biomimetic potential and applications of *Caribena versicolor* tubular chitin. *Carbohydr. Polym.* **2019**, *226*, 115301.

31. Mutsenko, V.; Gryshkov, O.; Rogulska, O.; Lode, A.; Petrenko, Alexander Yu. Gelinsky, M.; Glasmacher, B.; Ehrlich, H. Chitinous scaffolds from marine sponges for tissue engineering. In *Marine-Derived Biomaterials for*

Tissue Engineering Applications Chitinous; Choi, A., Ben-Nissan, B., Eds.; Springer Nature: Singapore, 2019; pp. 285–307.

32. Mutsenko, V. V.; Bazhenov, V. V.; Rogulska, O.; Tarusin, D.N.; Schütz, K.; Brüggemeier, S.; Gossla, E.; Akkineni, A.R.; Meißner, H.; Lode, A.; et al. 3D chitinous scaffolds derived from cultivated marine demosponge *Aplysina aerophoba* for tissue engineering approaches based on human mesenchymal stromal cells. *Int. J. Biol. Macromol.* **2017**, *104*, 1966–1974.

33. Binnewerg, B.; Schubert, M.; Voronkina, A.; Muzychka, L.; Wysokowski, M.; Petrenko, I.; Djurović, M.; Kovalchuk, V.; Tsurkan, M.; Martinovic, R.; et al. Marine biomaterials: Biomimetic and pharmacological potential of cultivated *Aplysina aerophoba* marine demosponge. *Mater. Sci. Eng. C* **2020**, *109*, 110566.

34. Ghosal, K.; Sarkar, P.; Saha, R.; Ghosh, S.; Sarkar, K. Advances in Tissue Engineering and Regeneration. In *Racing for the Surface: Antimicrobial and Interface Tissue Engineering*; Li, B., Moriarty, T., Webster, T., Xing, M., Eds.; Springer: Cham, 2020; pp. 577–640.

35. Litowczenko, J.; Woźniak-Budych, M.J.; Staszak, K.; Wieszczycka, K.; Jurga, S.; Tylkowski, B. Milestones and current achievements in development of multifunctional bioscaffolds for medical application. *Bioact. Mater.* **2021**, *6*, 2412–2438.

36. He, Y.; Hou, H.; Wang, S.; Lin, R.; Wang, L.; Yu, L.; Qiu, X. From waste of marine culture to natural patch in cardiac tissue engineering. *Bioact. Mater.* **2021**, *6*, 2000–2010.

37. Genova, T.; Roato, I.; Carossa, M.; Motta, C.; Cavagnetto, D.; Mussano, F. Advances on bone substitutes through 3D bioprinting. *Int. J. Mol. Sci.* **2020**, *21*, 7012.

38. Bacakova, L.; Filova, E.; Parizek, M.; Ruml, T.; Svorcik, V. Modulation of cell adhesion, proliferation and differentiation on materials designed for body implants. *Biotechnol. Adv.* **2011**, *29*, 739–767.

39. Peng, Z.; Tang, P.; Zhao, L.; Wu, L.; Xu, X.; Lei, H.; Zhou, M.; Zhou, C.; Li, Z. Advances in biomaterials for adipose tissue reconstruction in plastic surgery. *Nanotechnol. Rev.* **2020**, *9*, 385–395.

40. Liu, J.; Zheng, H.; Poh, P.S.P.; Machens, H.G.; Schilling, A.F. Hydrogels for engineering of perfusable vascular networks. *Int. J. Mol. Sci.* **2015**, *16*, 15997–16016.

41. Cox, T.R.; Erler, J.T. Remodeling and homeostasis of the extracellular matrix: Implications for fibrotic diseases and cancer. *Dis. Model. Mech.* **2011**, *4*, 165–178.

42. Newman, K.; Clark, K.; Gurumurthy, B.; Pal, P.; Janorkar, A. V. Elastin-collagen based hydrogels as model scaffolds to induce three-dimensional adipocyte culture from adipose derived stem cells. *Bioengineering* **2020**, *7*, 110.

43. Leipzig, N.D.; Shoichet, M.S. The effect of substrate stiffness on adult neural stem cell behavior. *Biomaterials* **2009**, *30*, 6867–6878.

44. Matsiko, A.; Gleeson, J.P.; O'Brien, F.J. Scaffold mean pore size influences mesenchymal stem cell chondrogenic differentiation and matrix deposition. *Tissue Eng. - Part A* **2015**, *21*, 486–497.

45. Chen, S.; Zhang, Q.; Nakamoto, T.; Kawazoe, N.; Chen, G. Gelatin scaffolds with controlled pore structure and mechanical property for cartilage tissue engineering. *Tissue Eng. Part C Methods* **2015**, *22*, 189–198.

46. Zhang, J.; Wehrle, E.; Adamek, P.; Paul, G.R.; Qin, X.H.; Rubert, M.; Müller, R. Optimization of mechanical stiffness and cell density of 3D bioprinted cell-laden scaffolds improves extracellular matrix mineralization and cellular organization for bone tissue engineering. *Acta Biomater.* **2020**, *114*, 307–322.

47. Pogoda, K. Rola sił mechanicznych generowanych przez macierz zewnątrzkomórkową w rozwoju raka prostaty, Polish Academy of Science, 2015, PhD thesis [access 08.04.2022].

48. Rufaihah, A.J.; Cheyyatraivendran, S.; Mazlan, M.D.M.; Lim, K.; Chong, M.S.K.; Mattar, C.N.Z.; Chan, J.K.Y.; Kofidis, T.; Seliktar, D. The effect of scaffold modulus on the morphology and remodeling of fetal mesenchymal stem cells. *Front. Physiol.* **2018**, *9*, 1555.

49. Pahlevanzadeh, F.; Emadi, R.; Valiani, A.; Kharaziha, M.; Poursamar, S.A.; Bakhsheshi-Rad, H.R.; Ismail, A.F.; RamaKrishna, S.; Berto, F. Three-dimensional printing constructs based on the chitosan for tissue regeneration: State of the art, developing directions and prospect trends. *Materials* **2020**, *13*, 2663.

50. https://pl.promega.com/resources/guides/cell-biology/3d-cell-culture-guide/. [access 19.06.2021]

51. Loh, Q.L.; Choong, C. Three-dimensional scaffolds for tissue engineering applications: role of porosity and pore size. *Tissue Eng. B* **2013**, *19*, 485–502.

52. Shimojo, A.A.M.; Rodrigues, I.C.P.; Perez, A.G.M.; Souto, E.M.B.; Gabriel, L.P.; Webster, T. Scaffolds for tissue engineering: A state-of-the-art review concerning types, properties, materials, processing, and characterization. In *Racing for the Surface: Antimicrobial and Interface Tissue Engineering*; Li, B., Moriarty, T., Webster, T., Xing, M., Eds.; Springer: Cham, 2020; pp. 647–677

53. Zhao, P.; Gu, H.; Mi, H.; Rao, C.; Fu, J.; Turng, L. sheng Fabrication of scaffolds in tissue engineering: A review. *Front. Mech. Eng.* **2018**, *13*, 107–119.

54. Szatkowski, T.; Kołodziejczak-Radzimska, A.; Zdarta, J.; Szwarc-Rzepka, K.; Paukszta, D.; Wysokowski, M.; Ehrlich, H.; Jesionowski, T. Synthesis and characterization of hydroxyapatite/chitosan composites. *Physicochem. Probl. Miner. Process.* **2015**, *51*, 575–585.

55. Baldino, L.; Cardea, S.; Scognamiglio, M.; Reverchon, E. A new tool to produce alginate-based aerogels for medical applications, by supercritical gel drying. *J. Supercrit. Fluids* **2019**, *146*, 152–158.

56. Chang, C.; Peng, N.; He, M.; Teramoto, Y.; Nishio, Y.; Zhang, L. Fabrication and properties of chitin/hydroxyapatite hybrid hydrogels as scaffold nano-materials. *Carbohydr. Polym.* **2013**, *91*, 7–13.

57. Park, K.E.; Kang, H.K.; Lee, S.J.; Min, B.-M.; Park, W.H. Biomimetic nanofibrous scaffolds: preparation and characterization of PGA/Chitin blend nanofibers. *Biomacromolecules* **2006**, *7*, 635–643.

58. Fernández-Cervantes, I.; Rodríguez-Fuentes, N.; León-Deniz, L. V.; Alcántara Quintana, L.E.; Cervantes-Uc, J.M.; Herrera Kao, W.A.; Cerón-Espinosa, J.D.; Cauich-Rodríguez, J. V.; Castaño-Meneses, V.M. Cell-free scaffold from jellyfish *Cassiopea andromeda* (Cnidaria; Scyphozoa) for skin tissue engineering. *Mater. Sci. Eng. C* **2020**, *111*, 110748.

59. Kosik-Kozioł, A.; Costantini, M.; Mróz, A.; Idaszek, J.; Heljak, M.; Jaroszewicz, J.; Kijeńska, E.; Szöke, K.; Frerker, N.; Barbetta, A.; et al. 3D bioprinted hydrogel model incorporating β-tricalcium phosphate for calcified cartilage tissue engineering. *Biofabrication* **2019**, *11*, 035016.

60. Idaszek, J.; Bruinink, A.; Swie, W. Ternary composite scaffolds with tailorable degradation rate and highly improved colonization by human bone marrow stromal cells. *J. Biomed. Mater. Res. A* **2015**, *103A*, 2394–2404.

61. Jaroszewicz, J.; Idaszek, J.; Choinska, E.; Szlazak, K.; Hyc, A.; Osiecka-iwan, A.; Swieszkowski, W.; Moskalewski, S. Formation of calcium phosphate coatings within polycaprolactone scaffolds by simple, alkaline phosphatase based method. *Mater. Sci. Eng. C* **2019**, *96*, 319–328.

62. Dušková-Smrčková, M.; Zavřel, J.; Bartoš, M.; Kaberova, Z.; Filová, E.; Zárubová, J.; Šlouf, M.; Michálek, J.; Vampola, T.; Kubies, D. Communicating macropores in PHEMA-based hydrogels for cell seeding: Probabilistic open pore simulation and direct micro-CT proof. *Mater. Des.* **2021**, *198*, 109312.

63. Janoušková, O.; Přádný, M.; Vetrík, M.; Chylíková Krumbholcová, E.;

Michálek, J.; Dušková Smrčková, M. Biomimetic modification of dual porosity poly(2-hydroxyethyl methacrylate) hydrogel scaffolds-porosity and stem cell growth evaluation. *Biomed. Mater.* **2019**, *14*, 055004.

64. Přádný, M.; Dušková-Smrčková, M.; Dušek, K.; Janoušková, O.; Sadakbayeva, Z.; Šlouf, M.; Michálek, J. Macroporous 2-hydroxyethyl methacrylate hydrogels of dual porosity for cell cultivation: morphology, swelling, permeability, and mechanical behavior. *J. Polym. Res.* **2014**, *21*, 579.

65. Park, K.E.; Jung, S.Y.; Lee, S.J.; Min, B.M.; Park, W.H. Biomimetic nanofibrous scaffolds: Preparation and characterization of chitin/silk fibroin blend nanofibers. *Int. J. Biol. Macromol.* **2006**, *38*, 165–173.

66. Yousefzade, O.; Katsarava, R.; Puiggalí, J. Biomimetic hybrid systems for tissue engineering. *Biomimetics* **2020**, *5*, 49.

67. Ji, Y.; Liang, K.; Shen, X.; Bowlin, G.L. Electrospinning and characterization of chitin nanofibril/polycaprolactone nanocomposite fiber mats. *Carbohydr. Polym.* **2014**, *101*, 68–74.

68. Khorshidi, S.; Solouk, A.; Mirzadeh, H.; Mazinani, S.; Lagaron, J.M.; Shari, S.; Ramakrishna, S. A review of key challenges of electrospun scaffolds for tissue-engineering applications. *J. Tissue Eng. Regen. Med.* **2016**, *10*, 715–738.

69. Costa, A.; Naranjo, J.D.; Londono, R.; Badylak, S.F. Biologic scaffolds. *Cold Spring Harb. Perspect. Med.* **2017**, *7*, a025676.

70. Gilbert, T.W.; Sellaro, T.L.; Badylak, S.F. Decellularization of tissues and organs. *Biomaterials* **2006**, *27*, 3675–3683.

71. Machałowski, T.; Amemiya, C.; Jesionowski, T. Chitin of Araneae origin: structural features and biomimetic applications: a review. *Appl. Phys. A* **2020**, *126*, 678.

72. Petrenko, I.; Khrunyk, Y.; Voronkina, A.; Kovalchuk, V.; Fursov, A.; Tsurkan, D.; Ivanenko, V. Poriferan chitin: 3D scaffolds from nano- to macroscale. A review. *Lett. Appl. NanoBioScience* **2020**, *9*, 1004–1014.

73. Tsurkan, M. V; Voronkina, A.; Khrunyk, Y.; Wysokowski, M.; Petrenko, I.; Ehrlich, H. Progress in chitin analytics. *Carbohydr. Polym.* **2021**, *252*, 117204.

74. Contessi Negrini, N.; Toffoletto, N.; Farè, S.; Altomare, L. Plant tissues as 3D natural scaffolds for adipose, bone and tendon tissue regeneration. *Front. Bioeng. Biotechnol.* **2020**, *8*, 723.

75. Klinger, C.; Żółtowska-Aksamitowska, S.; Wysokowski, M.; Tsurkan, M. V.; Galli, R.; Petrenko, I.; Machałowski, T.; Ereskovsky, A.; Martinović, R.; Muzychka, L.; et al. Express method for isolation of ready-to-use 3D chitin

scaffolds from *Aplysina archeri* (Aplysineidae: Verongiida) Demosponge. *Mar. Drugs* **2019**, *17*, 131.

76. Smith, C.A.; Board, T.N.; Rooney, P.; Eagle, M.J.; Richardson, M.; Hoyland, J.A. Human decellularized bone scaffolds from aged donors show improved osteoinductive capacity compared to young donor bone. *PLoS One* **2017**, *12*, e0177416.

77. Porzionato, A.; Stocco, E.; Barbon, S.; Grandi, F.; Macchi, V.; De Caro, R. Tissue-engineered grafts from human decellularized extracellular matrices: a systematic review and future perspectives. *Int. J. Mol. Sci.* **2018**, *19*, 4117.

78. Mutsenko, V. V.; Gryshkov, O.; Lauterboeck, L.; Rogulska, O.; Tarusin, D.N.; Bazhenov, V. V.; Schütz, K.; Brüggemeier, S.; Gossla, E.; Akkineni, A.R.; et al. Novel chitin scaffolds derived from marine sponge *Ianthella basta* for tissue engineering approaches based on human mesenchymal stromal cells: Biocompatibility and cryopreservation. *Int. J. Biol. Macromol.* **2017**, *104*, 1955–1965.

79. Stratton, S.; Shelke, N.B.; Hoshino, K.; Rudraiah, S.; Kumbar, S.G. Bioactive polymeric scaffolds for tissue engineering. *Bioact. Mater.* **2016**, *1*, 93–108.

80. Türk, S.; Altınsoy, I.; Çelebi Efe, G.; Ipek, M.; Özacar, M.; Bindal, C. 3D porous collagen/functionalized multiwalled carbon nanotube/chitosan/hydroxyapatite composite scaffolds for bone tissue engineering. *Mater. Sci. Eng. C* **2018**, *92*, 757–768.

81. Azami, M.; Samadikuchaksaraei, A.; Poursamar, S.A. Synthesis and characterization of a laminated hydroxyapatite/gelatin nanocomposite scaffold with controlled pore structure for bone tissue engineering. *Int. J. Artif. Organs* **2010**, *33*, 86–95.

82. Kumar, P.T.S.; Srinivasan, S.; Lakshmanan, V.K.; Tamura, H.; Nair, S. V.; Jayakumar, R. Synthesis, characterization and cytocompatibility studies of α-chitin hydrogel/nano hydroxyapatite composite scaffolds. *Int. J. Biol. Macromol.* **2011**, *49*, 20–31.

83. Pina, S.; Canadas, R.F.; Jiménez, G.; Perán, M.; Marchal, J.A.; Reis, R.L.; Oliveira, J.M. Biofunctional ionic-doped calcium phosphates: silk fibroin composites for bone tissue engineering scaffolding. *Cells Tissues Organs* **2017**, *204*, 150–163.

84. Jiang, L.B.; Su, D.H.; Liu, P.; Ma, Y.Q.; Shao, Z.Z.; Dong, J. Shape-memory collagen scaffold for enhanced cartilage regeneration: native collagen versus denatured collagen. *Osteoarthr. Cartil.* **2018**, *26*, 1389–1399.

85. Kolahreez, D.; Morshed, M. Fabrication of porous three-dimensional fibroin structures through a freezing process. *J. Appl. Polym. Sci.* **2018**, *135*,

46537.

86.   Fonseca, D.R.; Sobreiro-Almeida, R.; Sol, P.C.; Neves, N.M. Development of non-orthogonal 3D-printed scaffolds to enhance their osteogenic performance. *Biomater. Sci.* **2018**, *6*, 1569–1579.

87.   Wenz, A.; Borchers, K.; Tovar, G.E.M.; Kluger, P.J. Bone matrix production in hydroxyapatite-modified hydrogels suitable for bone bioprinting. *Biofabrication* **2017**, *9*, 044103.

88.   Kim, W.J.; Yun, H.S.; Kim, G.H. An innovative cell-laden α-TCP/collagen scaffold fabricated using a two-step printing process for potential application in regenerating hard tissues. *Sci. Rep.* **2017**, *7*, 3181.

89.   Shen, T.; Dai, Y.; Li, X.; Xu, S.; Gou, Z.; Gao, C. Regeneration of the Osteochondral defect by a wollastonite and macroporous fibrin biphasic scaffold. *ACS Biomater. Sci. Eng.* **2018**, *4*, 1942–1953.

90.   Pescosolido, L.; Schuurman, W.; Malda, J.; Matricardi, P.; Alhaique, F.; Coviello, T.; Van Weeren, P.R.; Dhert, W.J.A.; Hennink, W.E.; Vermonden, T. Hyaluronic acid and dextran-based semi-IPN hydrogels as biomaterials for bioprinting. *Biomacromolecules* **2011**, *12*, 1831–1838.

91.   Costantini, M.; Idaszek, J.; Szöke, K.; Jaroszewicz, J.; Dentini, M.; Barbetta, A.; Brinchmann, J.E.; Święszkowski, W. 3D bioprinting of BM-MSCs-loaded ECM biomimetic hydrogels for *in vitro* neocartilage formation. *Biofabrication* **2016**, *8*, 035002.

92.   Poldervaart, M.T.; Gremmels, H.; Van Deventer, K.; Fledderus, J.O.; Öner, F.C.; Verhaar, M.C.; Dhert, W.J.A.; Alblas, J. Prolonged presence of VEGF promotes vascularization in 3D bioprinted scaffolds with defined architecture. *J. Control. Release* **2014**, *184*, 58–66.

93.   Ostrovidov, S.; Salehi, S.; Costantini, M.; Suthiwanich, K.; Ebrahimi, M.; Sadeghian, R.B.; Fujie, T.; Shi, X.; Cannata, S.; Gargioli, C.; et al. 3D Bioprinting in Skeletal Muscle Tissue Engineering. *Small* **2019**, *15*, 1805530.

94.   Sharif, S.; Ai, J.; Azami, M.; Verdi, J.; Atlasi, M.A.; Shirian, S.; Samadikuchaksaraei, A. Collagen-coated nano-electrospun PCL seeded with human endometrial stem cells for skin tissue engineering applications. *J. Biomed. Mater. Res. - Part B Appl. Biomater.* **2018**, *106*, 1578–1586.

95.   Nazeer, M.A.; Yilgor, E.; Yilgor, I. Electrospun polycaprolactone/silk fibroin nanofibrous bioactive scaffolds for tissue engineering applications. *Polymer* **2019**, *168*, 86–94.

96.   Lee, J.B.; Jeong, S.I.; Bae, M.S.; Yang, D.H.; Heo, D.N.; Kim, C.H.; Alsberg,

E.; Kwon, I.K. Highly porous electrospun nanofibers enhanced by ultrasonication for improved cellular infiltration. *Tissue Eng. - Part A* **2011**, *17*, 2695–2702.

97. Kijeńska, E.; Prabhakaran, M.P.; Swieszkowski, W.; Kurzydlowski, K.J.; Ramakrishna, S. Electrospun bio-composite P(LLA-CL)/collagen I/collagen III scaffolds for nerve tissue engineering. *J. Biomed. Mater. Res. - Part B Appl. Biomater.* **2012**, *100 B*, 1093–1102.

98. Da, H.; Jia., S.-J.; Meng, G.-L.; Cheng, J.-H.; Zhou, W.; Xiong, Z.; Mu, Y.-J.; Liu, J. The impact of compact layer in biphasic scaffold on osteochondral tissue engineering. *PLoS One* **2013**, *8*, e54838.

99. Bao Ha, T. Le; Minh, T.; Nguyen, D.; Minh, D. Naturally derived biomaterials: preparation and application. In *Regenerative Medicine and Tissue Engineering*; 2013; pp. 248–274.

100. Machałowski, T.; Jesionowski, T. Hemolymph of molluscan origin: from biochemistry to modern biomaterials science. *Appl. Phys. A* **2021**, *127*, 3.

101. Hatchett, C. Experiments and observations on shell and bone. *Philos. Trans. R. Soc. London* **1799**, *89*, 315–334.

102. Frémy, M. e. Recherches chimiques sur les os. *Ann. Chim. Phys.* **1855**, *43*, 47–107.

103. Wu, Q.; Bao, J.; Zhou, Y.; Wang, Y.-J.; Du, Z.; Shi, Y.; Li, L.; Bu, H. Optimizing perfusion-decellularization methods of porcine livers for clinical-scale whole- organ bioengineering. *Biomed Res. Int.* **2015**, *2015*, 785474.

104. Schubert, M.; Binnewerg, B.; Voronkina, A.; Muzychka, L.; Wysokowski, M.; Petrenko, I.; Kovalchuk, V.; Tsurkan, M.; Martinovic, R.; Bechmann, N.; et al. Naturally prefabricated marine biomaterials: isolation and applications of flat chitinous 3D scaffolds from *Ianthella labyrinthus* (Demospongiae: Verongiida). *Int. J. Mol. Sci.* **2019**, *20*, 5105.

105. Rogulska, O.Y.; Mutsenko, V. V.; Revenko, E.. B.; Petrenko, Y.A.; Ehrlich, H.; Petrenko, A.Y. Culture and differentiation of human adipose tissue mesenchymal stromal cells within carriers based on sea sponge chitin skeletons. *Probl. Cryobiol. Cryomedicine* **2013**, *23*, 267–270.

106. Mol, A.; Kaya, M.; Mujtaba, M.; Akyuz, B. Extraction of high thermally stable and nanofibrous chitin from *Cicada* (Cicadoidea). *Entomol. Res.* **2018**, *48*, 480–489.

107. Yang, T.-L. Chitin-based materials in tissue engineering: Applications in soft tissue and epithelial organ. *Int. J. Mol. Sci.* **2011**, *12*, 1936–1963.

108. Khor, E.; Lim, L.Y. Implantable applications of chitin and chitosan. *Biomaterials* **2003**, *24*, 2339–2349.

109. Jayakumar, R.; Chennazhi, K.P.; Srinivasan, S. Chitin scaffolds in tissue engineering. *Int. J. Mol. Sci.* **2011**, *12*, 1876–1887.

110. Khrunyk, Y.; Lach, S.; Petrenko, I.; Ehrlich, H. Progress in modern marine biomaterials research. *Mar. Drugs* **2020**, *18*, 589.

111. Zhang, Z.; Zhang, L.; Li, C.; Xie, X.; Li, G.; Hu, Z.; Li, S. Research progress of chitosan-based biomimetic materials. *Mar. Drugs* **2021**, *19*, 372.

112. Intini, C.; Elviri, L.; Cabral, J.; Mros, S.; Bergonzi, C.; Bianchera, A.; Flammini, L.; Govoni, P.; Barocelli, E.; Bettini, R.; et al. 3D-printed chitosan-based scaffolds: An in vitro study of human skin cell growth and an *in-vivo* wound healing evaluation in experimental diabetes in rats. *Carbohydr. Polym.* **2018**, *199*, 593–602.

113. Kim, H.; Jung, G.; Yoon, J.; Han, J.; Park, Y.; Kim, D.; Zhang, M.; Kim, D. Preparation and characterization of nano-sized hydroxyapatite/alginate/chitosan composite scaffolds for bone tissue engineering. *Mater. Sci. Eng. C* **2015**, *54*, 20–25.

114. Collins, M.N.; Birkinshaw, C. Hyaluronic acid based scaffolds for tissue engineering — A review. *Carbohydr. Polym.* **2013**, *92*, 1262–1279.

115. Tang, S.; Chi, K.; Xu, H.; Yong, Q.; Yang, J.; Catchmark, J.M. A covalently cross-linked hyaluronic acid/bacterial cellulose composite hydrogel for potential biological applications. *Carbohydr. Polym.* **2021**, *252*, 117123.

116. Oliveira, J.T.; Reis, R.L. Polysaccharide-based materials for cartilage tissue engineering applications. *J. Tissue Eng. Regen. Med.* **2011**, *5*, 421–436.

117. Hickey, R.J.; Pelling, A.E. Cellulose biomaterials for tissue engineering. *Front. Bioeng. Biotechnol.* **2019**, *7*, 45.

118. Liu, J.; Willför, S.; Xu, C. A review of bioactive plant polysaccharides: Biological activities, functionalization, and biomedical applications. *Bioact. Carbohydrates Diet. Fibre* **2015**, *5*, 31–61.

119. Tsurkan, D.; Wysokowski, M.; Petrenko, I.; Voronkina, A.; Khrunyk, Y.; Fursov, A.; Ehrlich, H. Modern scaffolding strategies based on naturally pre-fabricated 3D biomaterials of poriferan origin. *Appl. Phys. A* **2020**, *126*, 382.

120. Ehrlich, H.; Wysokowski, M.; Żółtowska-Aksamitowska, S.; Petrenko, I.; Jesionowski, T. Collagens of poriferan origin. *Mar. Drugs* **2018**, *16*, 79.

121. Ashokkumar, M.; Cristian Chipara, A.; Tharangattu Narayanan, N.;

Anumary, A.; Sruthi, R.; Thanikaivelan, P.; Vajtai, R.; Mani, S.A.; Ajayan, P.M. Three-Dimensional porous sponges from collagen biowastes. *ACS Appl. Mater. Interfaces* **2016**, *8*, 14836–14844.

122. Silva, T.H.; Moreira-Silva, J.; Marques, A.L.P.; Domingues, A.; Bayon, Y.; Reis, R.L. Marine origin collagens and its potential applications. *Mar. Drugs* **2014**, *12*, 5881–5901.

123. Ehrlich, H.; Martinović, R.; Joksimović, D.; Petrenko, I.; Schiaparelli, S.; Wysokowski, M.; Tsurkan, D.; Stelling, A.L.; Springer, A.; Gelinsky, M.; et al. Conchixes : organic scaffolds which resemble the size and shapes of mollusks shells , their isolation and potential multifunctional applications. *Appl. Phys. A* **2020**, *126*, 562.

124. Oliveira, A.L.; Sampaio, S.C.; Sousa, R.A.; Reis, R.L. Controlled mineralization of nature-inspired silk fibroin/hydroxyapatite hybrid bioactive scaffolds for bone tissue engineering applications. In Proceedings of the 20th European Conference on Biomaterials; Nantes, France, 2006.

125. Cao, S.; Dong, T.; Xu, G.; Wang, F. Oil spill cleanup by hydrophobic natural fibers. *J. Nat. Fibers* **2017**, *14*, 1–9.

126. Varghese, A.G.; Paul, S.A.; Latha, M.S. Remediation of heavy metals and dyes from wastewater using cellulose-based adsorbents. *Environ. Chem. Lett.* **2019**, *17*, 867–877.

127. Norman, M.; Bartczak, P.; Zdarta, J.; Ehrlich, H.; Jesionowski, T. Anthocyanin dye conjugated with *Hippospongia communis* marine demosponge skeleton and its antiradical activity. *Dye. Pigment.* **2016**, *134*, 541–552.

128. Norman, M.; Bartczak, P.; Zdarta, J.; Tylus, W.; Szatkowski, T.; Stelling, A.L.; Ehrlich, H.; Jesionowski, T. Adsorption of C.I. Natural Red 4 onto spongin skeleton of marine demosponge. *Materials.* **2015**, *8*, 96–116.

129. Jankowska, K.; Zdarta, J.; Grzywaczyk, A.; Degórska, O.; Kijeńska-Gawrońska, E.; Pinelo, M.; Jesionowski, T. Horseradish peroxidase immobilised onto electrospun fibres and its application in decolourisation of dyes from model sea water. *Process Biochem.* **2021**, *102*, 10–21.

130. Jankowska, K.; Ciesielczyk, F.; Bachosz, K.; Zdarta, J.; Kaczorek, E.; Jesionowski, T. Laccase immobilized onto zirconia-silica hybrid doped with Cu^{2+} as an effective biocatalytic system for decolorization of dyes. *Materials.* **2019**, *12*, 1252.

131. Zdarta, J.; Jankowska, K.; Bachosz, K.; Degórska, O.; Kaźmierczak, K.; Nguyen, L.N.; Nghiem, L.D.; Jesionowski, T. Enhanced wastewater treatment by immobilized enzymes. *Curr. Pollut. Reports* **2021**, *7*, 167–179.

132. Lv, H.; Duan, Y.; Zhou, X.; Liu, G.; Wang, X.; Wang, Y.; Yuan, M.; Wang, C. Visible-light-driven Ag/AgCl@In_2O_3: a ternary photocatalyst for the degradation of tetracycline antibiotics. *Catal. Sci. Technol.* **2020**, *10*, 8230.

133. Azevedo, A.M.; Martins, V.C.; Prazeres, D.M.F.; Vojinović, V.; Cabral, J.M.S.; Fonseca, L.P. Horseradish peroxidase: a valuable tool in biotechnology. *Biotechnol. Annu. Rev.* **2003**, *9*, 199–247.

134. Auriol, M.; Filali-Meknassi, Y.; Tyagi, R.D.; Adams, C.D. Oxidation of natural and synthetic hormones by the horseradish peroxidase enzyme in wastewater. *Chemosphere* **2007**, *68*, 1830–1837.

135. Ai, J.; Zhang, W.; Liao, G.; Xia, H.; Wang, D. NH_2-Fe_3O_4@SiO_2 supported peroxidase catalyzed H_2O_2 for degradation of endocrine disrupter from aqueous solution: Roles of active radicals and NOMs. *Chemosphere* **2017**, *186*, 733–742.

136. Xiao, F.; Xiao, P.; Jiang, W.; Wang, D. Immobilization of horseradish peroxidase on Fe_3O_4 nanoparticles for enzymatic removal of endocrine disrupting chemicals. *Environ. Sci. Pollut. Res.* **2020**, *27*, 24357–24368.

137. Becker, D.; Rodriguez-Mozaz, S.; Insa, S.; Schoevaart, R.; Barceló, D.; De Cazes, M.; Belleville, M.P.; Sanchez-Marcano, J.; Misovic, A.; Oehlmann, J.; et al. Removal of endocrine disrupting chemicals in wastewater by enzymatic treatment with fungal laccases. *Org. Process Res. Dev.* **2017**, *21*, 480–491.

138. Gunatilake, S.R.; Clark, T.L.; Rodriguez, J.M.; Mlsna, T.E. Determination of five estrogens in wastewater using a comprehensive two-dimensional gas chromatograph. *Anal. Methods* **2014**, *6*, 5652–5658.

139. Cooper, C.M. Biological effects of agriculturally derived surface water pollutants on aquatic systems—a review. *J. Environ. Qual.* **1993**, *22*, 402–408.

140. Sdiri, A.; Higashi, T. Simultaneous removal of heavy metals from aqueous solution by natural limestones. *Appl. Water Sci.* **2013**, *3*, 29–39.

141. Klapiszewski, Ł.; Wysokowski, M.; Majchrzak, I.; Szatkowski, T.; Nowacka, M.; Siwińska-Stefańska, K.; Szwarc-Rzepka, K.; Bartczak, P.; Ehrlich, H.; Jesionowski, T. Preparation and characterization of multifunctional chitin/lignin materials. *J. Nanomater.* **2013**, *2013*, 1–13.

142. Schleuter, D.; Günther, A.; Paasch, S.; Ehrlich, H.; Kljajić, Z.; Hanke, T.; Bernhard, G.; Brunner, E. Chitin-based renewable materials from marine sponges for uranium adsorption. *Carbohydr. Polym.* **2013**, *92*, 712–718.

143. Batra, S.; Adhikari, P.; Ghai, A.; Sharma, A.; Sarma, R.; Suneetha, V. Study

and design of portable antimicrobial water filter. *Asian J. Pharm. Clin. Res.* **2017**, *10*, 268.

144. Khan, S.T.; Malik, A. Engineered nanomaterials for water decontamination and purification: from lab to products. *J. Hazard. Mater.* **2019**, *5*, 295–308.

145. Zdarta, J.; Jankowska, K.; Wyszowska, M.; Kijeńska-Gawrońska, E.; Zgoła-Grześkowiak, A.; Pinelo, M.; Meyer, A.S.; Moszyński, D.; Jesionowski, T. Robust biodegradation of naproxen and diclofenac by laccase immobilized using electrospun nanofibers with enhanced stability and reusability. *Mater. Sci. Eng. C* **2019**, *103*, 109789.

146. Ge, J.; Zhao, H.; Zhu, H.; Huang, J.; Shi, L.; Yu, S. Advanced sorbents for oil-spill cleanup: recent advances and future perspectives. *Adv. Mater.* **2016**, *21*, 10459–10490.

147. Hesas Hoseinzadeh, R.; Sharifzadeh Baeia, M.; Rostami, H.; Gardy, J. An investigation on the capability of magnetically separable Fe_3O_4/mordenite zeolite for refinery oily wastewater purification. *J. Environ. Manage.* **2018**, *241*, 525–534.

148. McMullan, G.; Meehan, C.; Conneely, A.; Kirby, N.; Robinson, T.; Nigam, P.; Banat, I.M.; Marchant, R.; Smyth, W.F. Microbial decolourisation and degradation of textile dyes. *Appl. Microbiol. Biotechnol.* **2001**, *56*, 81–87.

149. Barakat, M.A. New trends in removing heavy metals from industrial wastewater. *Arab. J. Chem.* **2011**, *4*, 361–377.

150. Siwińska-Stefańska, K.; Kubiak, A.; Piasecki, A.; Dobrowolska, A.; Czaczyk, K.; Motylenko, M.; Rafaja, D.; Ehrlich, H.; Jesionowski, T. Hydrothermal synthesis of multifunctional TiO_2-ZnO oxide systems with desired antibacterial and photocatalytic properties. *Appl. Surf. Sci.* **2019**, *463*, 791–801.

151. Ku, Y.; Jung, I.-L. Photocatalytic reduction of Cr(VI) in aqueous solutions by UV irradiation with the presence of titanium dioxide. *Sep. Purif. Technol.* **2001**, *35*, 135–142.

152. Sonune, A.; Ghate, R. Developments in wastewater treatment methods. *Desalination* **2004**, *167*, 55–63.

153. Maranon, E.; Suârez, F.; Alonso, F.; Fernândez, Y.; Sastre, H. Preliminary study of iron removal from hydrochloric pickling liquor by ion exchange. *Ind. Eng. Chem. Res.* **1999**, *38*, 2782–2786.

154. Varghese, A.G.; Sherely, A.P.; Latha, M.S. *Cellulose based green adsorbents for pollutant removal from wastewater*; Crini, G., Lichtfouse, E., Eds.; Springer: Cham, 2018; ISBN 9783540228608.

155. Stanisz, M.; Klapiszewski, Ł.; Jesionowski, T. Recent advances in the fabrication and application of biopolymer-based micro- and nanostructures: A comprehensive review. *Chem. Eng. J.* **2020**, *397*, 125409.

156. Sheibani, E.; Hosseini, A.; Sobhani Nasab, A.; Adib, K.; Ganjali, M.R.; Pourmortazavi, S.M.; Ahmadi, F.; Marzi Khosrowshahi, E.; Mirsadeghi, S.; Rahimi-Nasrabadi, M.; et al. Application of polysaccharide biopolymers as natural adsorbent in sample preparation. *Crit. Rev. Food Sci. Nutr.* **2021**, *1*, 1–28.

157. Gu, Y.; Ye, M.; Wang, Y.; Li, H.; Zhang, H.; Wang, G.; Zhang, Y.; Zhao, H. Lignosulfonate functionalized g-C_3N_4/carbonized wood sponge for highly efficient heavy metal ion scavenging. *J. Mater. Chem. A* **2020**, *8*, 12687–12698.

158. Markina, N.E.; Markin, A. V.; Zakharevich, A.M.; Goryacheva, I.Y. Calcium carbonate microparticles with embedded silver and magnetite nanoparticles as new SERS-active sorbent for solid phase extraction. *Microchim. Acta* **2017**, *184*, 3937–3944.

159. Nishimura, H.; Kamiya, A.; Nagata, T.; Katahira, M.; Watanabe, T. Direct evidence for α ether linkage between lignin and carbohydrates in wood cell walls. *Sci. Rep.* **2018**, *8*, 6538.

160. Kato, A.; Miyaji, H.; Ishizuka, R.; Tokunaga, K.; Inoue, K.; Kosen, Y.; Yokoyama, H.; Sugaya, T.; Tanaka, S.; Sakagami, R.; et al. Combination of root surface modification with BMP-2 and collagen hydrogel scaffold implantation for periodontal healing in beagle dogs. *Open Dent. J.* **2015**, *9*, 52–59.

161. Calvo-Flores, F.G.; Dobado, J.A. Lignin as renewable raw material. *ChemSusChem* **2010**, *3*, 1227–1235.

162. Szalaty, T.J.; Klapiszewski, Ł.; Jesionowski, T. Recent developments in modification of lignin using ionic liquids for the fabrication of advanced materials–a review. *J. Mol. Liq.* **2020**, *301*, 112417.

163. Abreu, H. dos S.; Nascimento, A.M. do; Maria, M.A. Lignin structure and wood properties. *Wood Fiber Sci.* **1999**, *31*, 426–433.

164. Jesionowski, T.; Jankowska, K.; Jędrzak, A.; Szalaty, T.J.; Żółtowska-Aksamitowska, S.; Klapiszewski, Ł.; Kołodziejczak-Radzimska, A.; Stasiewicz, M.; Wysokowski, M.; Zdarta, J. Advanced functional materials produced using substances of the natural origin. *Przem. Chem.* **2018**, *97*, 2026–2036.

165. Hubbe, M.A.; Hasan, S.H.; Ducoste, J.J. Cellulosic substrates for removal of pollutants from aqueous systems: A review. 1. Metals. *BioResources* **2011**, *6*,

2161–2287.

166. Dizhbite, T.; Zakis, G.; Kizima, A.; Lazareva, E.; Rossinskaya, G.; Jurkjane, V.; Telysheva, G.; Viesturs, U. Lignin — a useful bioresource for the production of sorption-active materials. *Bioresour. Technol.* **1999**, *67*, 221.

167. Klapiszewski, Ł.; Bartczak, P.; Wysokowski, M.; Jankowska, M.; Kabat, K.; Jesionowski, T. Silica conjugated with kraft lignin and its use as a novel "*green*" sorbent for hazardous metal ions removal. *Chem. Eng. J.* **2015**, *260*, 684–693.

168. Wysokowski, M.; Klapiszewski, Ł.; Moszyński, D.; Bartczak, P.; Szatkowski, T.; Majchrzak, I.; Siwińska-Stefańska, K.; Bazhenov, V. V.; Jesionowski, T. Modification of chitin with kraft lignin and development of new biosorbents for removal of cadmium(II) and nickel(II) ions. *Mar. Drugs* **2014**, *12*, 2245–2268.

169. Nongbe, M.C.; Bretel, G.; Ekou, T.; Ekou, L.; Yao, B.K.; Le Grognec, E.; Felpin, F.X. Cellulose paper grafted with polyamines as powerful adsorbent for heavy metals. *Cellulose* **2018**, *25*, 4043–4055.

170. Wei, W.; Kim, S.; Song, M.H.; Bediako, J.K.; Yun, Y.S. Carboxymethyl cellulose fiber as a fast binding and biodegradable adsorbent of heavy metals. *J. Taiwan Inst. Chem. Eng.* **2015**, *57*, 104–110.

171. Jamshaid, A.; Hamid, A.; Muhammad, N.; Naseer, A.; Ghauri, M.; Iqbal, J.; Rafiq, S.; Shah, N.S. Cellulose-based materials for the removal of heavy metals from wastewater – an overview. *ChemBioEng Rev.* **2017**, *4*, 240–256.

172. Garba, Z.N.; Lawan, I.; Zhou, W.; Zhang, M.; Wang, L.; Yuan, Z. Microcrystalline cellulose (MCC) based materials as emerging adsorbents for the removal of dyes and heavy metals – A review. *Sci. Total Environ.* **2020**, *717*, 135070.

173. Malik, D.S.; Jain, C.K.; Yadav, A.K. Removal of heavy metals from emerging cellulosic low-cost adsorbents: a review. *Appl. Water Sci.* **2017**, *7*, 2113–2136.

174. Nguyen, S.T.; Feng, J.; Le, N.T.; Le, A.T.T.; Hoang, N.; Tan, V.B.C.; Duong, H.M. Cellulose aerogel from paper waste for crude oil spill cleaning. *Ind. Eng. Chem. Res.* **2013**, *52*, 18386–18391.

175. Marandi, G.B.; Kermani, Z.P.; Kurdtabar, M. Fast and efficient removal of cationic dyes from aqueous solution by collagen-based hydrogel nanocomposites. *Polym. - Plast. Technol. Eng.* **2013**, *52*, 310–318.

176. Gu, Y.C.; Liao, X.P.; Huang, Y.J.; Shi, B. Adsorption of anionic dyes on Fe(III)-loaded collagen fibre from aqueous solution. *Int. J. Environ. Pollut.*

2008, *34*, 111–121.

177. Nakhjiri, M.T.; Bagheri Marandi, G.; Kurdtabar, M. Adsorption of Methylene Blue, Brilliant Green and Rhodamine B from aqueous solution using collagen-g-p(AA-co-NVP)/Fe_3O_4@SiO_2 nanocomposite hydrogel. *J. Polym. Environ.* **2019**, *27*, 581–599.

178. Szatkowski, T.; Kopczyński, K.; Motylenko, M.; Borrmann, H.; Mania, B.; Graś, M.; Lota, G.; Bazhenov, V. V.; Rafaja, D.; Roth, F.; et al. Extreme biomimetics: A carbonized 3D spongin scaffold as a novel support for nanostructured manganese oxide(IV) and its electrochemical applications. *Nano Res.* **2018**, *11*, 4199–4214.

179. Croockewit, J.H. Ueber die Zusammensetzung des Badeschwammes. *Justus Liebigs Ann. Chem.* **1843**, *48*, 43–56.

180. Jesionowski, T.; Norman, M.; Zółtowska-Aksamitowska, S.; Petrenko, I.; Joseph, Y.; Ehrlich, H. Marine spongin: Naturally prefabricated 3D scaffold-based biomaterial. *Mar. Drugs* **2018**, *16*, 88.

181. Ehrlich, H.; Maldonado, M.; Hanke, T.; Meissner, H.; Born, R. Spongins: nanostructural investigations and development of biomimetic material model,. *VDI Berichte* **2003**, *1843*, 287–292.

182. Szatkowski, T.; Siwińska-Stefańska, K.; Wysokowski, M.; Stelling, A.; Joseph, Y.; Ehrlich, H.; Jesionowski, T. Immobilization of titanium(IV) oxide onto 3D spongin scaffolds of marine sponge origin according to extreme biomimetics principles for removal of C.I. Basic Blue 9. *Biomimetics* **2017**, *2*, 4.

183. Chaitanya Reddy, C.; Khilji, I.A.; Gupta, A.; Bhuyar, P.; Mahmood, S.; Saeed AL-Japairai, K.A.; Chua, G.K. Valorization of keratin waste biomass and its potential applications. *J. Water Process Eng.* **2021**, *40*, 101707.

184. Ghosh, A.; Collie, S.R. Keratinous materials as novel absorbent systems for toxic pollutants. *Def. Sci. J.* **2014**, *64*, 209–221.

185. Khosa, M.A.; Ullah, A. In-situ modification, regeneration, and application of keratin biopolymer for arsenic removal. *J. Hazard. Mater.* **2014**, *278*, 360–371.

186. Song, K.; Qian, X.; Zhu, X.; Li, X.; Hong, X. Fabrication of mechanical robust keratin film by mesoscopic molecular network reconstruction and its performance for dye removal. *J. Colloid Interface Sci.* **2020**, *579*, 28–36.

187. Zhu, W.; Qian, X.; Yu, H.; Li, X.; Song, K. Fabrication of mechanical robust keratin adsorbent by induced molecular network transition and its dye adsorption performance. *Environ. Sci. Pollut. Res.* **2020**, *27*, 41577–41584.

188. Villanueva, M.E.; Puca, M.; Bravo, J.P.; Bafico, J.; Dall Orto, V.C.; Copello, G.J. Dual adsorbent-photocatalytic keratin–TiO$_2$ nanocomposite for trimethoprim removal from wastewater. *New J. Chem.* **2020**, *44*, 10964--10972.

189. Ramos, M.L.P.; Galaburri, G.; González, J.A.; Pérez, C.J.; Villanueva, M.E.; Copello, G.J. Influence of GO reinforcement on keratin based smart hydrogel and its application for emerging pollutants removal. *J. Environ. Chem. Eng.* **2018**, *6*, 7021–7028.

190. Benallou Benzekri, M.; Benderdouche, N.; Bestani, B.; Douara, N.; Duclaux, L. Valorization of olive stones into a granular activated carbon for the removal of Methylene Blue in batch and fixed bed modes. *J. Mater. Environ. Sci.* **2018**, *9*, 272–284.

191. Suhas; Gupta, V.K.; Carrott, P.J.M.; Singh, R.; Chaudhary, M.; Kushwaha, S. Cellulose: A review as natural, modified and activated carbon adsorbent. *Bioresour. Technol.* **2016**, *216*, 1066–1076.

192. Kadirvelu, K.; Namasivayam, C. Activated carbon from coconut coirpith as metal adsorbent: Adsorption of Cd(II) from aqueous solution. *Adv. Environ. Res.* **2003**, *7*, 471–478.

193. Kadirvelu, K.; Senthilkumar, P.; Thamaraiselvi, K.; Subburam, V. Activated carbon prepared from biomass as adsorbent: Elimination of Ni(II) from aqueous solution. *Bioresour. Technol.* **2002**, *81*, 87–90.

194. Zhang, S.; Shao, T.; Kose, H.S.; Tanju, K. Adsorption of aromatic compounds by carbonaceous adsorbents: A comparative study on granular activated carbon, activated carbon fiber, and carbon nanotubes. *Environ. Sci. Technol.* **2010**, *44*, 6377–6383.

195. Lin, P.Y.; Wu, H.M.; Hsieh, S.L.; Li, J.S.; Dong, C.; Chen, C.W.; Hsieh, S. Preparation of vaterite calcium carbonate granules from discarded oyster shells as an adsorbent for heavy metal ions removal. *Chemosphere* **2020**, *254*, 126903.

196. Checa, A.G.; Esteban-delgado, F.J.; Rodrı, A.B. Crystallographic structure of the foliated calcite of bivalves. **2007**, *157*, 393–402.

197. Falini, G.; Al, S.; Weiner, S.; Addadi, L. Control of aragonite or calcite polymorphism by mollusk shell macromolecules. *Science* **1996**, *271*, 67–69.

198. Yamanaka, S.; Oiso, T.; Kurahashi, Y.; Abe, H.; Hara, K.; Fujimoto, T.; Kuga, Y. Scalable and template-free production of mesoporous calcium carbonate and its potential to formaldehyde adsorbent. *J. Nanoparticle Res.* **2014**, *16*, 2266.

199. Qin, Q.; Li, M.; Lan, P.; Liao, Y.; Sun, S.; Liu, H. Novel CaCO₃/chitin aerogel: Synthesis and adsorption performance toward Congo Red in aqueous solutions. *Int. J. Biol. Macromol.* **2021**, *181*, 786–792.

200. Yadav, M.; Goswami, P.; Paritosh, K.; Kumar, M.; Pareek, N.; Vivekanand, V. Seafood waste: a source for preparation of commercially employable chitin/chitosan materials. *Bioresour. Bioprocess.* **2019**, *6*, 8.

201. Merzendorfer, H. The cellular basis of chitin synthesis in fungi and insects : Common principles and differences. *Eur. J. Cell Biol.* **2011**, *90*, 759–769.

202. Kaya, M.; Mujtaba, M.; Ehrlich, H.; Salaberria, A.M.; Baran, T.; Amemiya, C.T.; Galli, R.; Akyuz, L.; Sargin, I.; Labidi, J. On chemistry of γ-chitin. *Carbohydr. Polym.* **2017**, *176*, 177–186.

203. Pillai, C.K.S.; Paul, W.; Sharma, C.P. Chitin and chitosan polymers: chemistry, solubility and fiber formation. *Prog. Polym. Sci.* **2009**, *34*, 641–678.

204. Merzendorfer, H.; Zimoch, L. Chitin metabolism in insects: structure, function and regulation of chitin synthases and chitinases. *J. Exp. Biol.* **2003**, *206*, 4393–4412.

205. Ehrlich, H. Biomimetic potential of chitin-based composite biomaterials of poriferan origin. In *Biomimetic Biomaterials: Structure and Applications*; Ruys, A.J., Ed.; Woodhead Publishing Limited: Cambridge, UK, 2013; pp. 46–66

206. Bonneville, S.; Delpomdor, F.; Preat, A.; Chevalier, C.; Araki, T.; Kazemian, M.; Steele, A.; Schreiber, A.; Wirth, R.; Benning, L.G. Molecular identification of fungi microfossils in a Neoproterozoic shale rock. *Sci. Adv.* **2020**, *6*, eaax7599.

207. Ehrlich, H.; Rigby, J.K.; Botting, J.P.; Tsurkan, M. V.; Werner, C.; Schwille, P.; Petrášek, Z.; Pisera, A.; Simon, P.; Sivkov, V.N.; et al. Discovery of 505-million-year old chitin in the basal demosponge *Vauxia gracilenta. Sci. Rep.* **2013**, *3*, 3497.

208. Moussian, B. Chitin: Structure, Chemistry and Biology. In *Targeting chitin-containing organisms*; Yang, Q., Fukamizo, T., Eds.; Springer Singapore: Singapore, 2019; pp. 5–19 ISBN 9789811373176.

209. Crini, G. Historical review on chitin and chitosan biopolymers. *Environ. Chem. Lett.* **2019**, *17*, 1623–1643.

210. Braconnot, H. Des recherches analytiques sur la nature des champignons. In *Recueil de Mémoires con- cernant la chimie et les arts qui en dépendent et spécialement la pharmacie*; Klostermann, J., Ed.; 1811; Vol. Paris, pp. 272–292.

211. Braconnot, H. Sur la nature des champignons. In Recueil de Mémoires

concernant la chimie et les arts qui en dépendent et spécialement la pharmacie, vol Soixante-dix-neuf. Annales de Chimie. Librairie des Ecoles Impériales Polytech- nique et des Ponts et Chaussées; 1811; pp. 265–304.

212. Odier, A. Mémoire sur la composition chimique des parties cornées des insectes. Mémoires la Société d'Histoire Nat. Paris, vol Premier. Baudouin Frères Libr. **1823**, *Paris*, 29–42.

213. Fränkel, A.; Kelly, S. Beiträge zur constitution des chitins. Monatshefte für Chemie und verwandte Teile anderer Wissenschaften **1902**, *23*, 123–133.

214. Ehrlich, H.; Krautter, M.; Hanke, T.; Simon, P.; Knieb, C.; Heinemann, S.; Worch, H. First evidence of the presence of chitin in skeletons of marine sponges. Part II. Glass sponges (Hexactinellida: Porifera). *J. Exp. Zool.* **2007**, *308B*, 473–483.

215. Kertmen, A.; Ehrlich, H. Patentology of chitinous biomaterials. Part I: Chitin. *Carbohydr. Polym.* **2022**, *282*, 119102.

216. Chung, L.Y.; Schmidt, R.J.; Hamlyn, P.F.; Sagar, B.F.; Andrew, A.M.; Turner, T.D. Biocompatibility of potential wound management products: Fungal mycelia as a source of chitin/chitosan and their effect on the proliferation of human F1000 fibroblasts in culture. *J. Biomed. Mater. Res.* **1994**, *28*, 463–469.

217. Street, R.M.; Huseynova, T.; Xu, X.; Chandrasekaran, P.; Han, L.; Shih, W.Y.; Shiha, W.-H.; Schauer, C.L. Variable piezoelectricity of electrospun chitin. *Carbohydr. Polym.* **2018**, *195*, 218–224.

218. van Leeuwen, J.; Norton, G.A.; Ndlela, S.S.; Rudnick, D. Processes for isolating chitin and chitosan from fungal biomass. *Civil, Constr. Environ. Eng. Patents* 2016, 2–5.

219. Knidri, H.E.L.; Khalfaouy, R.E.L.; Laajeb, A.; Addaou, A.; Lahsini, A. Eco-friendly extraction and characterization of chitin and chitosan from the shrimp shell waste via microwave irradiation. *Process Saf. Environ. Prot.* **2016**, *104*, 395–405.

220. Das, S.; Gillin, F.D. Chitin synthase in encysting Entamoeba invadens. *Biochem. J.* **1991**, *280*, 641–647.

221. Campos-Góngora, E.; Ebert, F.; Willhoeft, U.; Said-Fernández, S.; Tannich, E. Characterization of chitin synthases from Entamoeba. *Protist* **2004**, *155*, 323–330.

222. Brunner, E.; Richthammer, P.; Ehrlich, H.; Paasch, S.; Simon, P.; Ueberlein, S.; Van Pée, K.H. Chitin-based organic networks: An integral part of cell wall biosilica in the diatom thalassiosira pseudonana. *Angew. Chemie - Int.*

Ed. **2009**, *48*, 9724–9727.

223. Spinde, K.; Kammer, M.; Freyer, K.; Ehrlich, H.; Vournakis, J.N.; Brunner, E. Biomimetic silicification of fibrous chitin from diatoms. *Chem. Mater.* **2011**, *23*, 2973–2978.

224. Wysokowski, M.; Jesionowski, T.; Ehrlich, H. Biosilica as a source for inspiration in biological materials science. *Am. Mineral.* **2018**, *103*, 665–691.

225. Ehrlich, H.; Motylenko, M.; Sundareshwar, P. V.; Ereskovsky, A.; Zgłobicka, I.; Noga, T.; Płociński, T.; Tsurkan, M. V.; Wyroba, E.; Suski, S.; et al. Multiphase biomineralization: enigmatic invasive siliceous diatoms produce crystalline calcite. *Adv. Funct. Mater.* **2016**, *26*, 2503–2510.

226. Talevski, T.; Talevska Leshoska, A.; Pejoski, E.; Pejin, B.; Machałowski, T.; Wysokowski, M.; Tsurkan, M. V.; Petrova, O.; Sivkov, V.; Martinovic, R.; et al. Identification and first insights into the structure of chitin from the endemic freshwater demosponge *Ochridaspongia rotunda* (Arndt, 1937). *Int. J. Biol. Macromol.* **2020**, *162*, 1187–1194.

227. Wysokowski, M.; Bazhenov, V. V.; Tsurkan, M. V.; Galli, R.; Stelling, A.L.; Stöcker, H.; Kaiser, S.; Niederschlag, E.; Gärtner, G.; Behm, T.; et al. Isolation and identification of chitin in three-dimensional skeleton of *Aplysina fistularis* marine sponge. *Int. J. Biol. Macromol.* **2013**, *62*, 94–100.

228. Ehrlich, H.; Ilan, M.; Maldonado, M.; Muricy, G.; Bavestrello, G.; Kljajic, Z.; Carballo, J.L.; Schiaparelli, S.; Ereskovsky, A.; Schupp, P.; et al. Three-dimensional chitin-based scaffolds from Verongida sponges (Demospongiae: Porifera). Part I. Isolation and identification of chitin. *Int. J. Biol. Macromol.* **2010**, *47*, 141–145.

229. Ehrlich, H.; Kaluzhnaya, O. V; Tsurkan, M. V; Ereskovsky, A.; Tabachnick, K.R.; Ilan, M.; Stelling, A.; Galli, R.; Petrova, O. V; Nekipelov, S. V; et al. First report on chitinous holdfast in sponges (Porifera). *Proc. R. Soc. B.* **2013**, *280*, 20130339.

230. Ehrlich, H.; Maldonado, M.; Spindler, K.D.; Eckert, C.; Hanke, T.; Born, R.; Goebel, C.; Simon, P.; Heinemann, S.; Worch, H. First evidence of chitin as a component of the skeletal fibers of marine sponges. Part I. Verongidae (demospongia: Porifera). *J. Exp. Zool.* **2007**, *308B*, 347–357.

231. Chandran, R.; Williams, L.; Hung, A.; Nowlin, K.; Lajeunesse, D. SEM characterization of anatomical variation in chitin organization in insect and arthropod cuticles. *Micron* **2016**, *82*, 74–85.

232. Vincent, J.F. V; Wegst, U.G.K. Design and mechanical properties of insect cuticle. *Arthropod Struct. Dev.* **2004**, *33*, 187–199.

233. Rudall, K.M. The chitin/protein complexes of insect cuticles. *Adv. In Insect Phys.* **1963**, *1*, 257–313.

234. Kaya, M.; Baublys, V.; Šatkauskienė, I.; Akyuz, B.; Bulut, E.; Tubelytė, V. First chitin extraction from *Plumatella repens* (Bryozoa) with comparison to chitins of insect and fungal origin. *Int. J. Biol. Macromol.* **2015**, *79*, 126–132.

235. Majtán, J.; Bíliková, K.; Markovič, O.; Gróf, J.; Kogan, G.; Šimúth, J. Isolation and characterization of chitin from bumblebee (Bombus terrestris). *Int. J. Biol. Macromol.* **2007**, *40*, 237–241.

236. Erko, M.; Younes-Metzler, O.; Rack, A.; Zaslansky, P.; Young, S.L.; Milliron, G.; Chyasnavichyus, M.; Barth, F.G.; Fratzl, P.; Tsukruk, V.; et al. Micro- and nano-structural details of a spider's filter for substrate vibrations: Relevance for low-frequency signal transmission. *J. R. Soc. Interface* **2015**, *12*, 20141111.

237. Zhang, J.; Feng, M.; Lu, X.; Shi, C.; Li, X.; Xin, J.; Yue, G.; Zhang, S. Base-free preparation of low molecular weight chitin from crab shell. *Carbohydr. Polym.* **2018**, *190*, 148–155.

238. Hamed, I.; Özogul, F.; Regenstein, J.M. Industrial applications of crustacean by-products (chitin, chitosan, and chitooligosaccharides): A review. *Trends Food Sci. Technol.* **2016**, *48*, 40–50.

239. Su, X.; Tan, M.; Duan, B.; Cai, J.; Jiang, W.; Zhang, L. Hierarchical microspheres with macropores fabricated from chitin as 3D cell culture. *J. Mater. Chem. B* **2019**, *7*, 5190–5198.

240. Du, X.; Fan, G.; Jiao, Y.; Zhang, H.; Guo, X.; Huang, R.; Zheng, Z.; Bian, C.; Deng, Y.; Wang, Q.; et al. The pearl oyster *Pinctada fucata* martensii genome and multi-omic analyses provide insights into biomineralization. *Gigascience* **2017**, *6*, 1–12.

241. Nakashima, K.; Kimura, S.; Ogawa, Y.; Watanabe, S.; Soma, S.; Kaneko, T.; Yamada, L.; Sawada, H.; Tung, C.H.; Lu, T.M.; et al. Chitin-based barrier immunity and its loss predated mucus-colonization by indigenous gut microbiota. *Nat. Commun.* **2018**, *9*, 3402.

242. Younes, I.; Rinaudo, M. Chitin and chitosan preparation from marine sources. Structure, properties and applications. *Mar. Drugs* **2015**, *13*, 1133–1174.

243. Kurita, K. Chitin and chitosan: Functional biopolymers from marine crustaceans. *Mar. Biotechnol.* **2006**, *8*, 203–226.

244. Ehrlich, H. Chitin and collagen as universal and alternative templates in biomineralization. *Int. Geol. Rev.* **2010**, *52*, 661–699.

245. Machałowski, T.; Wysokowski, M.; Tsurkan, M. V; Galli, R.; Żółtowska-Aksamitowska, S.; Petrenko, I.; Czaczyk, K.; Kraft, M.; Bertau, M.; Bechmann, N.; et al. Spider chitin: An ultrafast microwave-assisted method for chitin isolation from *Caribena versicolor* spider molt cuticle. *Molecules* **2019**, *24*, 3736.

246. Kaya, M.; Seyyar, O.; Baran, T.; Erdogan, S.; Kar, M. A physicochemical characterization of fully acetylated chitin structure isolated from two spider species: With new surface morphology. *Int. J. Biol. Macromol.* **2014**, *65*, 553–558.

247. Wysokowski, M.; Machałowski, T.; Petrenko, I.; Schimpf, C.; Rafaja, D.; Galli, R.; Zietek, J.; Pantovic, S.; Voronkina, A.; Ivanenko, V.K.V.N.; et al. 3D chitin scaffolds of marine Demosponge origin for biomimetic mollusk hemolymph-associated biomineralization *ex-vivo*. *Mar. Drugs* **2020**, *18*, 123.

248. Okafor, N. Isolation of chitin from the shell of the cuttlefish, *Sepia officinalis L. Acta, Biochim. Biophys. - Mucoproteins Mucopolysaccharides* **1965**, *101*, 193–200.

249. Kaur, S.; Dhillon, G.S. Recent trends in biological extraction of chitin from marine shell wastes: a review. *Crit. Rev. Biotechnol.* **2015**, *35*, 44–61.

250. Berton, P.; Shamshina, J.L.; Ostadjoo, S.; King, C.A.; Rogers, R.D. Enzymatic hydrolysis of ionic liquid-extracted chitin. *Carbohydr. Polym.* **2018**, *199*, 228–235.

251. Knidri, H.E.; Belaabed, R.; Addaou, A.; Laajeb, A.; Lahsini, A. Extraction, chemical modification and characterization of chitin and chitosan. *Int. J. Biol. Macromol.* **2018**, *120*, 1181–1189.

252. Nowacki, K.; Stępniak, I.; Machalowski, T.; Wysokowski, M.; Petrenko, I.; Schimpf, C.; Rafaja, D.; Ziętek, J.; Pantović, S.; Voronkina, A.; et al. Electrochemical method for isolation of chitinous 3D scaffolds from cultivated *Aplysina aerophoba* marine demosponge and its biomimetic application. *Appl. Phys. A* **2020**, *126*, 368.

253. Kumirska, J.; Czerwicka, M.; Kaczyński, Z.; Bychowska, A.; Brzozowski, K.; Thöming, J.; Stepnowski, P. Application of spectroscopic methods for structural analysis of chitin and chitosan. *Mar. Drugs* **2010**, *8*, 1567–1636.

254. Sikorski, P.; Hori, R.; Wada, M. Revisit of α-chitin crystal structure using high resolution X-ray diffraction data. *Biomacromolecules* **2009**, *10*, 1100–1105.

255. Minke, R.; Blackwell, J. The structure of α-chitin. *J. Mol. Biol.* **1978**, *120*, 167–181.

256. Ehrlich, H.; Simon, P.; Carrillo-Cabrera, W.; Bazhenov, V. V.; Botting, J.P.; Ilan, M.; Ereskovsky, A. V.; Muricy, G.; Worch, H.; Mensch, A.; et al. Insights into chemistry of biological materials: Newly discovered silica-aragonite-chitin biocomposites in demosponges. *Chem. Mater.* **2010**, *22*, 1462–1471.

257. Morin, L.G.; Smucker, R.A.; Herth, W. Effects of two chitin synthesis inhibitors on *Thalassiosira fluviatilis* and *Cyclotella cryptica*. *FEMS Microbiol. Lett.* **1986**, *37*, 263–268.

258. Lotmar, W.; Picken, L.E.R. A new crystallographic modification of chitin and its distribution. *Experientia* **1950**, *6*, 58–59.

259. Dweltz, N.E. The structure of β-chitin. *Biochem. Biophys. Acta* **1961**, *51*, 283–294.

260. Nishiyama, Y.; Noishiki, Y.; Wada, M. X-ray structure of anhydrous β -chitin at 1 A resolution. *Macromolecules* **2011**, *44*, 950–957.

261. Rudall, K.M.; Kenchington, W. The chitin system. *Biol. Rev.* **1973**, *48*, 597–636.

262. Wysokowski, M.; Motylenko, M.; Stöcker, H.; Bazhenov, V. V.; Langer, E.; Dobrowolska, A.; Czaczyk, K.; Galli, R.; Stelling, A.L.; Behm, T.; et al. An extreme biomimetic approach: Hydrothermal synthesis of β-chitin/ZnO nanostructured composites. *J. Mater. Chem. B* **2013**, *1*, 6469–6476.

263. Wysokowski, M.; Motylenko, M.; Bazhenov, V. V.; Stawski, D.; Petrenko, I.; Ehrlich, A.; Behm, T.; Kljajic, Z.; Stelling, A.L.; Jesionowski, T.; et al. Poriferan chitin as a template for hydrothermal zirconia deposition. *Front. Mater. Sci.* **2013**, *7*, 248–260.

264. Wysokowski, M.; Behm, T.; Born, R.; Bazhenov, V. V.; Meißner, H.; Richter, G.; Szwarc-Rzepka, K.; Makarova, A.; Vyalikh, D.; Schupp, P.; et al. Preparation of chitin-silica composites by *in vitro* silicification of two-dimensional *Ianthella basta* demosponge chitinous scaffolds under modified Stöber conditions. *Mater. Sci. Eng. C* **2013**, *33*, 3935–3941.

265. Nishiyama, A.; Shinohara, T.; Pantuso, T.; Tsuji, S.; Yamashita, M.; Shinohara, S.; Myrvik, Q.N.; Henriksen, R.A.; Shibata, Y. Depletion of cellular cholesterol enhances macrophage mapk activation by chitin microparticles but not by heat-killed mycobacterium bovis bcg. *Am. J. Physiol. Physiol.* **2008**, *295*, C341–C349.

266. Kogiso, M.; Nishiyama, A.; Shinohara, T.; Nakamura, M.; Mizoguchi, E.; Misawa, Y.; Guinet, E.; Nouri-Shirazi, M.; Dorey, C.K.; Henriksen, R.. Chitin particles induce size-dependent but carbohydrate-independent innate eosinophi. *J. Leukoc. Biol.* **2011**, *90*, 167–176.

267. Reese, T.A.; Liang, H.E.; Tager, A.M.; Luster, A.D.; van Rooijen, N. Voehringer, D.; Locksley, R.M. Chitin induces accumulation in tissue of innate immune cells associated with allergy. *Nature* **2007**, *447*, 92–96.

268. Vo, T.S.; Ngo, D.H.; Ta, Q.V.; Wijesekara, I.; Kong, C.S.; Kim, S.K. Protective effect of chitin oligosaccharides against lipopolysaccharide-induced inflammatory response in bv-2 microglia. *Cell. Immunol.* **2012**, *277*, 14–21.

269. Da Silva, C.A.; Chalouni, C.; Williams, A.; Hartl, D.; Lee, C.G.; Elias, J.A. Chitin is a size- dependent regulator of macrophage tnf and il-10 production. *J. Immunol.* **2009**, *182*, 3573–3582.

270. Alvarez, F.J. The effect of chitin size, shape, source and purification method on immune recognition. *Mol. Phylogenet. Evol.* **2014**, *19*, 4433–4451.

271. Sudheesh Kumar, P.T.; Srinivasan, S.; Lakshmanan, V.K.; Tamura, H.; Nair, S. V.; Jayakumar, R. β-Chitin hydrogel/nano hydroxyapatite composite scaffolds for tissue engineering applications. *Carbohydr. Polym.* **2011**, *85*, 584–591.

272. Anitha, A.; Sowmya, S.; Kumar, P.T.S.; Deepthi, S.; Chennazhi, K.P.; Ehrlich, H.; Tsurkan, M.; Jayakumar, R. Chitin and chitosan in selected biomedical applications. *Prog. Polym. Sci.* **2014**, *39*, 1644–1667.

273. Sharma, M.; Mukesh, C.; Mondal, D.; Prasad, K. Dissolution of α-chitin in deep eutectic solvents. *RSC Adv.* **2013**, *3*, 18149–18155.

274. Nikolova, M.P.; Chavali, M.S. Recent advances in biomaterials for 3D scaffolds: a review. *Bioact. Mater.* **2019**, *4*, 271–292.

275. Machałowski, T.; Idaszek, J.; Chlanda, A.; Heljak, M.; Piasecki, A.; Święszkowski, W.; Jesionowski, T. Naturally prefabricated 3D chitinous skeletal scaffold of marine demosponge origin, biomineralized *ex vivo* as a functional biomaterial. *Carbohydr. Polym.* **2022**, *275*, 118750.

276. Setti, L.; Mazzieri, S.; Pifferi, P.G. Enhanced degradation of heavy oil in an aqueous system by a *Pseudomonas* sp. In the presence of natural and synthetic sorbents. *Bioresour. Technol.* **1999**, *67*, 191–199.

277. Barros, F.C. de F.; Vasconcellos, L.C.G.; Carvalho, T.V.; do Nascimento, R.F. Removal of petroleum spill in water by chitin and chitosan. *Electron. J. Chem.* **2014**, *6*, 70–74.

278. Filipowska, U.; Rodziewicz, J. Effectiveness of dye RB5 adsorption onto chitin and chitosan under static and dynamic conditions. *Prog. Chem. Appl. Chitin its Deriv.* **2009**, *XIV*, 33–40.

279. Filipowska, U. Adsorption and desorption of reactive dyes onto chitin and

chitosan flakes and beads. *Adsorpt. Sci. Technol.* **2006**, *24*, 781–795.

280. Li, C.W.; Chen, J.Y.; Hua, T.E. Precambrian sponges with cellular structures. *Science* **1998**, *5352*, 879–882.

281. Turner, E.C. Possible poriferan body fossils in early Neoproterozoic microbial reefs. *Nature* **2021**, *596*, 87–91.

282. Ehrlich, H.; Demadis, K.D.; Pokrovsky, O.S.; Koutsoukos, P.G. Modern views on desilicification: Biosilica and abiotic silica dissolution in natural and artificial environments. *Chem. Rev.* **2010**, *110*, 4656–4689.

283. Muzychka, L.; Voronkina, A.; Kovalchuk, V.; Smolii, O.B.; Wysokowski, M.; Petrenko, I.; Youssef, D.T.A.; Ehrlich, I.; Ehrlich, H. Marine biomimetics: bromotyrosines loaded chitinous skeleton as source of antibacterial agents. *Appl. Phys. A* **2021**, *127*, 15.

284. Rohde, S.; Schupp, P.J. Growth and regeneration of the elephant ear sponge *Ianthella basta* (Porifera). In *Ancient Animals, New Challenges*; Springer: Amsterdam, 2011; pp. 219–226.

285. Benavides, L.R.; Hormiga, G. A morphological and combined phylogenetic analysis of pirate spiders (Araneae, Mimetidae): evolutionary relationships, taxonomy and character evolution. *Invertebr. Syst.* **2020**, *34*, 144–191.

286. Vette, R.S.; Rust, M.K. Periodicity of molting and resumption of post-molt feeding in the brown recluse spider *Loxosceles reclusa* (Araneae: Sicariidae). *J. Kansas Entomol. Soc.* **2010**, *83*, 306–312.

287. Platnick, N.I. World Spider Catalog (2019) Available online: http://wsc.nmbe.ch [access 01.09.2022].

288. Barth, F.G. A spider's tactile hairs. *Scholarpedia* **2015**, *10*, 7267.

289. Barth, F.G. Microfiber reinforcement of an arthropod cuticle. *Zeitschrift für Zellforsch. und Mikroskopische Anat.* **1973**, *144*, 409–433.

290. Nyffeler, M.; Birkhofer, K. An estimated 400 – 800 million tons of prey are annually killed by the global spider community. *Sci. Nat.* **2017**, *104*, 30.

291. Collatz, K.G.; Mommsen, T. Physiological conditions and variations of body constituents during the moulting cycle of the spider *Tegenaria atrica* C. L. Koch (Agelenidae). *Comp. Biochem. Physiol.* **1975**, *52A*, 465–476.

292. Abolins-Krogis, A. Ultrastructural study of the shell-repair membrane in the snail, *Helix pomatia* L. *. *Cell Tissue Res.* **1976**, *172*, 455–476.

293. Ziętek, J.; Guz, L.; Panasiuk, K.; Winiarczyk, S.; Adaszek, Ł. Nowa metoda przyżyciowego pobierania hemolimfy wraz z ustaleniem norm

fizjologicznych wybranych parametrów biochemicznych hemolimfy ślimaków *Cornu aspersum*. *Med. Weter.* **2017**, *73*, 366–369.

294. Bradford, M.M. A rapid and sensitive method for the quantitation microgram quantities of protein utilizing the principle of protein-dye binding. *Anal. Biochem.* **1976**, *72*, 248–254.

295. Kovalchuk, V.; Voronkina, A.; Binnewerg, B.; Schubert, M.; Muzychka, L.; Wysokowski, M.; Tsurkan, M. V.; Bechmann, N.; Petrenko, I.; Fursov, A.; et al. Naturally drug-loaded chitin: isolation and applications. *Mar. Drugs* **2019**, *17*, 574.

296. Nawrotek, K.; Marqueste, T.; Modrzejewska, Z.; Zarzycki, R.; Rusak, A.; Decherchi, P. Thermogelling chitosan lactate hydrogel improves functional recovery after a C_2 spinal cord hemisection in rat. *J. Biomed. Mater. Res. - Part A* **2017**, *105*, 2004–2019.

297. Tomanik, M.; Kobielarz, M.; Filipiak, J.; Szymonowicz, M.; Rusak, A.; Mroczkowska, K.; Antończak, A.; Pezowicz, C. Laser texturing as a way of influencing the micromechanical and biological properties of the poly(*L*-lactide) surface. *Materials.* **2020**, *13*, 3786.

298. Ifelebuegu, A.O.; Anh Nguyen, T.V.; Ukotije-Ikwut, P.; Momoh, Z. Liquid-phase sorption characteristics of human hair as a natural oil spill sorbent. *J. Environ. Chem. Eng.* **2015**, *3*, 938–943.

299. Bazargan, A.; Tan, J.; Mckay, G. Standardization of oil sorbent performance testing. *J. Test. Eval.* **2015**, *46*, 3–10.

300. da Costa Cunha, G.; Pinho, N.C.; Alves Silva, I.A.; Santana Costa, J.A.; da Silva, C.M.P.; Romão, L.P.C. Removal of heavy crude oil from water surfaces using a magnetic inorganic-organic hybrid powder and membrane system. *J. Environ. Manage.* **2019**, *247*, 9–18.

301. Gbenebor, O.P.; Adeosun, S.O.; Lawal, G.I.; Jun, S.; Olaleye, S.A. Acetylation, crystalline and morphological properties of structural polysaccharide from shrimp exoskeleton. *Eng. Sci. Technol. an Int. J.* **2017**, *20*, 1155–1165.

302. Hong, A.S.; Yang, Q.; Yuan, Y.; Chen, L.; Song, Y.; Lian, H. Sustainable co-solvent induced one step extraction of low molecular weight chitin with high purity from raw lobster shell. *Carbohydr. Polym.* **2019**, *205*, 236–243.

303. Pozzolini, M.; Tassara, E.; Dodero, A.; Castellano, M.; Vicini, S.; Ferrando, S.; Aicardi, S.; Cavallo, D.; Bertolino, M.; Petrenko, I.; et al. Potential biomedical applications of collagen filaments derived from the marine demosponges *Ircinia oros* (Schmidt, 1864) and *Sarcotragus foetidus* (schmidt, 1862). *Mar. Drugs* **2021**, *19*, 563.

304. Shavandi, A.; Bekhit, A.E.D.A.; Sun, Z.; Ali, A. A review of synthesis methods, properties and use of hydroxyapatite as a substitute of bone. *J. Biomimetics, Biomater. Biomed. Eng.* **2015**, *25*, 98–117.

305. Shaala, L.A.; Asfour, H.Z.; Youssef, D.T.A.; Zółtowska-Aksamitowska, S.; Wysokowski, M.; Tsurkan, M.; Galli, R.; Meissner, H.; Petrenko, I.; Tabachnick, K.; et al. New source of 3D chitin scaffolds: the Red Sea Demosponge *Pseudoceratina arabica* (Pseudoceratinidae, Verongiida). *Mar. Drugs* **2019**, *17*, 92.

306. Żółtowska-Aksamitowska, S.; Tsurkan, M. V.; Lim, S.C.; Meissner, H.; Tabachnick, K.; Shaala, L.A.; Youssef, D.T.A.; Ivanenko, V.N.; Petrenko, I.; Wysokowski, M.; et al. The demosponge *Pseudoceratina purpurea* as a new source of fibrous chitin. *Int. J. Biol. Macromol.* **2018**, *112*, 1021–1028.

307. Black, L.D.; Allen, P.G.; Morris, S.M.; Stone, P.J.; Suki, B. Mechanical and failure properties of extracellular matrix sheets as a function of structural protein composition. *Biophys. J.* **2008**, *94*, 1916–1929.

308. Fromont, J.; Żółtowska-Aksamitowska, S.; Galli, R.; Meissner, H.; Erpenbeck, D.; Vacelet, J.; Diaz, C.; Tsurkan, M. V.; Petrenko, I.; Youssef, D.T.A.; et al. New family and genus of a Dendrilla-like sponge with characters of Verongiida. Part II. Discovery of chitin in the skeleton of *Ernstilla lacunosa*. *Zool. Anz.* **2019**, *280*, 21–29.

309. Ehrlich, H.; Maldonado, M.; Parker, A.R.; Kulchin, Y.N.; Schilling, J.; Köhler, B.; Skrzypczak, U.; Simon, P.; Reiswig, H.M.; Tsurkan, M. V.; et al. Supercontinuum generation in naturally occurring glass sponges spicules. *Adv. Opt. Mater.* **2016**, *4*, 1608–1613.

310. Neinhuis, C.; Nickerl, J.; Tsurkan, M.; Werner, C.; Werner, C. The multi-layered protective cuticle of Collembola: a chemical analysis. *J. R. Soc. Interface* **2014**, *11*, 20140619.

311. Szatkowski, T.; Kołodziejczak-Radzimska, A.; Zdarta, J.; Szwarc-Rzepka, K.; Paukszta, D.; Wysokowski, M.; Ehrlich, H.; Jesionowski, T. Synthesis and characterization of hydroxyapatite/chitosan composites. *Physicochem. Probl. Miner. Process.* **2015**, *51*, 575–585.

312. Ehrlich, H.; Simon, P.; Motylenko, M.; Wysokowski, M.; Bazhenov, V. V.; Galli, R.; Stelling, A.L.; Stawski, D.; Ilan, M.; Stöcker, H.; et al. Extreme Biomimetics: Formation of zirconium dioxide nanophase using chitinous scaffolds under hydrothermal conditions. *J. Mater. Chem. B* **2013**, *1*, 5092–5099.

313. Focher, B.; Naggi, A.; Torri, G.; Cossani, A.; Terbojevich, M. Structural differences between chitin polymorphs and their precipitates from

solutions – evidence from CP-MAS ^{13}C NMR, FT-IR and FT-Raman spectroscopy. *Carbohydr. Polym.* **1992**, *17*, 97–102.

314. Green, D.W.; Lai, W.F.; Jung, H.S. Evolving marine biomimetics for regenerative dentistry. *Mar. Drugs* **2014**, *12*, 2877–2912.

315. Choi, A.H.; Ben-Nissan, B. *Marine-Derived Biomaterials for Tissue Engineering Applications*; 1st ed.; Springer: Singapore, 2019; ISBN 978-981-13-8857-6.

316. Barzic, I.A.; Albu, R.M. Optical properties and biointerface interactions of chitin. *Polym. Bull.* **2020**, *78*, 6535–6548.

317. Walejewska, E.; Idaszek, J.; Heljak, M.; Chlanda, A.; Choinska, E.; Hasirci, V.; Swieszkowski, W. The effect of introduction of filament shift on degradation behaviour of PLGA- and PLCL-based scaffolds fabricated via additive manufacturing. *Polym. Degrad. Stab.* **2020**, *171*, 109030.

318. Idaszek, J.; Kijeńska, E.; Łojkowski, M.; Swieszkowski, W. How important are scaffolds and their surface properties in regenerative medicine. *Appl. Surf. Sci.* **2016**, *388*, 762–774.

319. Steck, E.; Burkhardt, M.; Ehrlich, H.; Richter, W. Discrimination between cells of murine and human origin in xenotransplants by species specific genomic in situ hybridization. *Xenotransplantation* **2010**, *17*, 153–159.

320. Ulivieri, C. Cell death: Insights into the ultrastructure of mitochondria. *Tissue Cell* **2010**, *42*, 339–347.

321. Tinari, A.; Giammarioli, A.M.; Manganelli, V.; Ciarlo, L.; Malorni, W. Analyzing morphological and ultrastructural features in cell death. In *Methods in Enzymology*; Khosravi-Far, R., Zakeri, Z., Lockshin, R.A., Piacentini, M., Eds.; 2008; Vol. 442, pp. 1–26.

322. Piipponen, M.; Li, D.; Landén, N.X. The immune functions of keratinocytes in skin wound healing. *Int. J. Mol. Sci.* **2020**, *21*, 8790.

323. Breuls, R.G.M.; Jiya, T.U.; Smit, T.H. Scaffold stiffness influences cell behavior: opportunities for skeletal tissue engineering. *Open Orthop. J.* **2008**, *2*, 103–109.

324. Mei, N.; Chen, G.; Zhou, P.; Chen, X.; Shao, Z.-Z.; Luan-Feng Pan, C.; Wu, H.-G. Biocompatibility of poly(e-caprolactone) scaffold modified by chitosan— The fibroblasts proliferation *in vitro. J. Biomater. Appl.* **2005**, *19*, 323–339.

325. Nakielski, P.; Rinoldi, C.; Pruchniewski, M.; Pawłowska, S.; Gazińska, M.; Strojny, B.; Rybak, D.; Jezierska-Woźniak, K.; Urbanek, O.; Denis, P.; et al. Laser-Assisted Fabrication of Injectable Nanofibrous Cell Carriers. *Small* **2021**, *2104971*, 2104971.

326. Mount, A.S.; Gohad, N. V.; Hansen, D.C.; Hansen, K.M.; Beth, M.; Johnstone, M.B. Deposition of nanocrystalline calcite on surfaces by a tissue and cellular bomineralization, US Patent no. US 9,371,451 B2, 2016, *2*, 1–16.

327. Johnstone, M.B.; Gohad, N. V; Falwell, E.P.; Hansen, D.C.; Hansen, K.M.; Mount, A.S. Cellular orchestrated biomineralization of crystalline composites on implant surfaces by the eastern oyster, *Crassostrea virginica* (Gmelin, 1791). *J. Exp. Mar. Bio. Ecol.* **2015**, *463*, 8–16.

328. Fernandez Robledo, J.A.; Yadavalli, R.; Bassem, A.; Pales-Espinosa, E.; Gerdol, M.; Greco, S.; Stevick, R.J.; Gómez-Chiarr, M.; Zhang, Y.; Heil, C.A.; et al. From the raw bar to the bench: Bivalves as models for human health. *Dev. Comp. Immunol.* **2019**, *92*, 260–282.

329. https://www.polityka.pl/tygodnikpolityka/ludzieistyle/1708362,1,polska-staje-sie-potega-w-hodowli-winniczkow.read [access 01.06.2022].

330. Li, S.; Liu, Y.; Liu, C.; Huang, J.; Zheng, G.; Xie, L.; Zhang, R. Hemocytes participate in calcium carbonate crystal formation, transportation and shell regeneration in the pearl oyster *Pinctada fucata*. *Fish Shellfish Immunol.* **2016**, *51*, 263–270.

331. Kapur, S.P.; Sen Gupta, A. The role of amoebocytes in the regeneration of shell in the land pulmonate, *Euplecta indica* (Pfieffer). *Biol. Bull.* **1970**, *139*, 502–509.

332. Mount, A.S.; Wheeler, A.P.; Paradkar, R.P.; Snider, D. Hemocyte-mediated shell mineralization in the eastern oyster. *Science* **2004**, *304*, 297–300.

333. Wagge, L.E. The activity of amoebocytes and of alkaline phosphatases during the regeneration of the shell in the snail , Helix aspersa. *J. Cell Sci.* **1951**, *92*, 307–320.

334. Auzoux-Bordenave, S.; Fouchereau-Peron, M.; Helleouet, M.-N.; Doumenc, D. CGRP regulates the activity of mantle cells and hemocytes in abalone primary cell cultures (*Haliotis tuberculata*). *J. ofShellfish Res.* **2007**, *26*, 887–894.

335. De Waele, A. Le sang d'Anodonta cygnea et la formation de la coquille. *Bull. l'Académie R. des Sci. Belgique Cl. des Sci.* **1930**, *10*, 1–52.

336. Lopez, C.; Carballal, M.J.; Azevedo, C.; Villalba, A. Morphological characterization of the hemocytes of the clam , *Ruditapes decussatus* (Mollusca: Bivalvia). *J. Invertabrates Pathol.* **1997**, *69*, 51–57.

337. Izzetoglu, S. A new approach for classification of major larval hemocytes (prohemocytes, plasmatocytes and granulocytes) in the greater wax moth,

Galleria mellonella L. (Lepidoptera: Pyralidae) by acridine orange staining. *Turkish J. Entomol.* **2012**, *36*, 163–168.

338. Noda, S.; Loker, S. Effects of infection with Echinostoma paraensei on the circulating haemocyte population of the host snail *Biomphalaria glabrata*. *Parasitology* **1989**, *98*, 35–41.

339. Machałowski, T.; Wysokowski, M.; Petrenko, I.; Langer, E.; Tsurkan, D.; Jesionowski, T.; Ehrlich, H. *In vivo* biomimetic calcification of selected organic scaffolds using snail shell regeneration: a new methodological approach. *Appl. Phys. A* **2020**, *126*, 469.

340. Chen, J.H.; Yang, H.Y.; Peng, S.W.; Chen, Y.J.; Tsai, K.Y. Characterization of Abalone (*Haliotis diversicolor*) hemocytes *in vitro*. *Biol. Bull.* **1996**, *31*, 31–38.

341. Xie, J.; Liang, J.; Sun, J.; Gao, J.; Zhang, S.; Liu, Y.; Xie, L.; Zhang, R. Influence of the extrapallial fluid of *Pinctada fucata* on the crystallization of calcium carbonate and shell biomineralization. *Cryst. Growth Des.* **2016**, *16*, 672–680.

342. Modreski, P.J.; Aumente-Modreski, R. Fluorescent Minerals. *Rocks Miner.* **1996**, *71*, 14–22.

343. Jin, W.; Jiang, S.; Pan, H. Amorphous phase mediated crystallization: fundamentals of biomineralization. *Crystals* **2018**, *8*, 48.

344. Azizur, M.; Shinjo, R. Control of CaCO₃ Crystal Growth by the Acidic Proteinaceous Fraction of Calcifying Marine Organisms: An <i>In Vitro</I> Study of Biomineralization. In *Advanced Topics in Biomineralization*; Seto, J., Ed.; InTech: Rijeka, Croatia, 2012; pp. 50–62.

345. Duboust, N.; Ghadbeigi, H.; Pinna, C.; Ayvar-Soberanis, S.; Collis, A.; Scaife, R.; Kerrigan, K. An optical method for measuring surface roughness of machined carbon fibre-reinforced plastic composites. *J. Compos. Mater.* **2017**, *51*, 289–302.

346. Sedlaček, M.; Podgornik, B.; Vižintin, J. Correlation between standard roughness parameters skewness and kurtosis and tribological behaviour of contact surfaces. *Tribol. Int.* **2012**, *48*, 102–112.

347. Gómez-Ordóñez, E.; Rupérez, P. FTIR-ATR spectroscopy as a tool for polysaccharide identification in edible brown and red seaweeds. *Food Hydrocoll.* **2011**, *25*, 1514–1520.

348. Fernández, M.S.; Valenzuela, F.; Arias, J.I.; Arias, J.L. Is the snail shell repair process really influenced by eggshell membrane as a template of foreign scaffold? *J. Struct. Biol. J.* **2016**, *196*, 187–196.

349. Bischoff, W.D.; Sharma, S.K.; MacKenzie, F.T. Carbonate ion disorder in synthetic and biogenic magnesian calcites: a Raman spectral study. *Am. Mineral.* **1985**, *70*, 581–589.

350. Wehrmeister, U.; Jacob, D.E.; Soldati, A.L.; Häger, T.; Hofmeister, W. Vaterite in freshwater cultured pearls from China and Japan. *J. Gemmol.* **2007**, *30*, 399–412.

351. http://www.rruff.info/ [access 01.05.2022]

352. Prinsloo, L.C. Rock hyraces: a cause of San rock art deterioration? *J. Raman Spectrosc.* **2007**, *38*, 496–503.

353. Bosch Reig, F.; Adelantado Gimeno, J. V.; Moreno Moya, M.C.M. FTIR quantitative analysis of calcium carbonate (calcite) and silica (Quartz) mixtures using the constant ratio method. Application to geological samples. *Talanta* **2002**, *58*, 811–821.

354. Arma, L.H.; Saitoh, A.; Ishibashi, Y.; Asahi, T.; Sueoka, Y.; Sakakibara, M.; Takebe, H. Red fluorescence lamellae in calcitic prismatic layer of *Pinctada vulgaris* shell (Mollusc, bivalvia). *Opt. Mater. Express* **2014**, *4*, 1813.

355. Čadež, V.; Šegota, S.; Sondi, I.; Lyons, D.M.; Saha, P.; Saha, N.; Sikirić Dutour, M. Calcium phosphate and calcium carbonate mineralization of bioinspired hydrogels based on β-chitin isolated from biomineral of the common cuttlefish (*Sepia officinalis* , L). *J. Polym. Res.* **2018**, *25*, 226.

356. Mendes, A.C.; Shekarforoush, E.; Engwer, C.; Beeren, S.R.; Gorzelanny, C.; Goycoolea, F.M.; Chronakis, I.S. Co-assembly of chitosan and phospholipids into hybrid hydrogels. *Pure Appl. Chem.* **2016**, *88*, 905–916.

357. Singh, Y.P.; Bhardwaj, N.; Mandal, B.B. Potential of Agarose/Silk Fibroin Blended Hydrogel for *in vitro* cartilage tissue engineering. *ACS Appl. Mater. Interfaces* **2016**, *8*, 21236–21249.

358. Menard, K.P. Dynamic Testing and instrumentation. In *Dynamic mechanical analysis a practical introduction*; CRC Press: Boca Raton, 2008; pp. 71–93 [access 05.05.2022].

359. Chlanda, A.; Oberbek, P.; Heljak, M.; Górecka, Ż.; Czarnecka, K.; Chen, K.-S.; Woźniak, M.J. Nanohydroxyapatite adhesion to low temperature plasma modified surface of 3D-printed bone tissue engineering scaffolds - qualitative and quantitative study. *Surf. Coatings Technol.* **2019**, *375*, 637–644.

360. Coleman, M.L.; Olson, M.F. Rho GTPase signalling pathways in the morphological changes associated with apoptosis. *Cell Death Differ.* **2002**, *9*, 493–504.

361. Tamada, Y.; Ikada, Y. Fibroblast growth on polymer surfaces and biosynthesis of collagen. *J. Biomed. Mater. Res.* **1994**, *28*, 783–789.

362. Xu, R.; Yuan, J.; Si, Y.; Li, F.; Zhang, B. Estrone removal by horseradish peroxidase immobilized on a nanofibrous support with Fe_3O_4 nanoparticles. *RSC Adv.* **2016**, *6*, 3927–3933.

363. Naghdi, M.; Taheran, M.; Brar, S.K.; Kermanshahi-pour, A.; Verma, M.; Surampalli, R.Y. Removal of pharmaceutical compounds in water and wastewater using fungal oxidoreductase enzymes. *Environ. Pollut.* **2018**, *234*, 190–213.

364. Wysokowski, M.; Motylenko, M.; Beyer, J.; Makarova, A.; Stöcker, H.; Walter, J.; Galli, R.; Kaiser, S.; Vyalikh, D.; Bazhenov, V. V.; et al. Extreme biomimetic approach for developing novel chitin-GeO_2 nanocomposites with photoluminescent properties. *Nano Res.* **2015**, *8*, 2288–2301.

365. Fewtrell, L. Silver: water disinfection and toxicity. In Proceedings of the Geneva: Centre for Research into Environment and Health, World Health Organization; 2014; pp. 1–50.

366. Wang, L.; Hu, C.; Shao, L. The antimicrobial activity of nanoparticles: present situation and prospects for the future. *Int. J. Nanomedicine* **2017**, *12*, 1227–1249.

367. Pronk, W.; Ding, A.; Morgenroth, E.; Derlon, N.; Desmond, P.; Burkhardt, M.; Wu, B.; Fane, A.G. Gravity-driven membrane filtration for water and wastewater treatment: a review. *Water Res.* **2019**, *149*, 553–565.

368. Karumuri, A.K.; Oswal, D.P.; Hostetler, H.A.; Mukhopadhyay, S.M. Silver nanoparticles attached to porous carbon substrates: robust materials for chemical-free water disinfection. *Mater. Lett.* **2013**, *109*, 83–87.

369. Phong, N.T.P.; Thanh, N.V.K.; Phuong, P.H. Fabrication of antibacterial water filter by coating silver nanoparticles on flexible polyurethane foams. *J. Phys. Conf. Ser.* **2009**, *187*, 012079.

370. Picca, R.A.; Paladini, F.; Sportelli, M.C.; Pollini, M.; Giannossa, L.C.; Di Franco, C.; Panico, A.; Mangone, A.; Valentini, A.; Cioffi, N. Combined approach for the development of efficient and safe nanoantimicrobials: The case of nanosilver-modified polyurethane foams. *ASC Biomater. Sci.* **2017**, *3*, 1417–1425.

371. Shi, Y.; Li, Y.; Zhang, J.; Yu, Z.; Yang, D. Electrospun polyacrylonitrile nanofibers loaded with silver nanoparticles by silver mirror reaction. *Mater. Sci. Eng. C* **2015**, *51*, 346–355.

372. Heinemann, S.; Heinemann, C.; Ehrlich, H.; Meyer, M.; Baltzer, H.; Worch,

H.; Hanke, T. A novel biomimetic hybrid material made of silicified collagen: Perspectives for bone replacement. *Adv. Eng. Mater.* **2007**, *9*, 1061–1068.

373. Cooper, A.; Oldinski, R.; Ma, H.; Bryers, J.D.; Zhang, M. Chitosan-based nanofibrous membranes for antibacterial filter applications. *Carbohydr. Polym.* **2013**, *30*, 254–259.

374. Jain, S.; Bhanjana, G.; Heydarifard, S.; Dilbaghi, N.; Nazhad, M.M.; Kumar, V.; Kim, K.; Kumar, S. Enhanced antibacterial profile of nanoparticle impregnated cellulose foam filter paper for drinking water filtration. *Carbohydr. Polym.* **2018**, *202*, 219–226.

375. Karwowska, E. Antibacterial potential of nanocomposite-based materials – a short review. *Nanotechnol. Rev.* **2017**, *6*, 243–254.

376. Zeng, X.; Mccarthy, D.T.; Deletic, A.; Zhang, X. Silver/reduced graphene oxide hydrogel as novel bactericidal filter for point-of-use water disinfection. *Adv. Funct. Mater.* **2015**, *25*, 4344–4351.

377. Atiyeh, B.S.; Costagliola, M.; Hayek, S.N.; Dibo, S.A. Effect of silver on burn wound infection control and healing: Review of the literature. *Burns* **2007**, *33*, 139–148.

378. Cho, K.-H.; Park, J.-E.; Osaka, T.; Park, S.-G. The study of antimicrobial activity and preservative effects of nanosilver ingredient. *Electrochim. Acta* **2005**, *51*, 956–960.

379. Imani, R.; Talaiepour, M.; Dutta, J.; Ghobadinezhad, M.R.; Hemmasi, A.H.; Nazhad, M.M. Production of antibacterial filter paper from wood cellulose. *BioResources* **2011**, *6*, 891–900.

380. Nguyen, V.Q.; Ishihara, M.; Nakamura, S.; Hattori, H.; Ono, T.; Miyahira, Y.; Matsui, T. Interaction of silver nanoparticles and chitin powder with different sizes and surface structures: the correlation with antimicrobial activities. *J. Nanomater.* **2013**, *2013*, 467534.

381. García-Vilas, J.A.; Martínez-Poveda, B.; Quesada, A.R.; Medina, M.Á. Aeroplysinin-1, a sponge-serived multi-targeted bioactive marine drug. *Mar. Drugs* **2016**, *14*, 1.

382. Bechmann, N.; Ehrlich, H.; Eisenhofer, G.; Ehrlich, A.; Meschke, S.; Ziegler, C.G.; Bornstein, S.R. Anti-tumorigenic and anti-metastatic activity of the sponge-derived marine drugs aeroplysinin-1 and isofistularin-3 against pheochromocytoma *in vitro*. *Mar. Drugs* **2018**, *16*, 172.

383. Jain, P.; Pradeep, T. Potential of silver nanoparticle-coated polyurethane foam as an antibacterial water filter. *Biotechnol. Bioeng.* **2005**, *90*, 59–63.

384. Howse, P.E. The fine structure and functional organization of chordotonal organs. *Syrup Zoolological Soc. London* **1968**, *23*, 167–198.

385. Sminia, T.; Barendsen, L. A comparative morphological and enzyme histochemical study on blood cells of the freshwater snails *Lymnaea stagnalis*, *Biomphalaria glabrata*, and *Bulinus truncatus*. *J. Morphol.* **1980**, *165*, 31–39.

386. Kouyama, N.; Shimozawa, T.; Hisada, M. Transducing element of crustacean mechano-sensory hairs. *Experientia* **1981**, *37*, 379–380.

387. Speck-Hergenroder, J.; Barth, F.G. Vibration sensitive hairs on the spider leg. *Experientia* **1988**, *44*, 13–14.

388. Sewell, M.T. The histology and histochemistry of the cuticle of a spider, Tegenaria domestica. *Ann. Entomol. Soc. Am.* **1955**, *48*, 107–117.

389. Erko, M.; Hartmann, M.A.; Zlotnikov, I.; Valverde Serrano, C.; Fratzl, P.; Politi, Y. Structural and mechanical properties of the arthropod cuticle: comparison between the fang of the spider *Cupiennius salei* and the carapace of American lobster Homarus americanus. *J. Struct. Biol.* **2013**, *183*, 172–179.

390. Nentwig, W. *Ecophysiology of spiders*; Springer-Verlag: Berlin, 1987;

391. Shang, S.; Zhu, L.; Fan, J. Intermolecular interactions between natural polysaccharides and silk fibroin protein. *Carbohydr. Polym.* **2013**, *93*, 561–573.

392. Machovic, V.; Lapcak, L.; Havelcova, M.; Borecka, L.; Novotna, M.; Novotna, M.; Javurkova, I.; Langrova, I.; Hajkova, S.; Brozova, A.; et al. Analysis of European honeybee (*Apis mellifera*) wings using ATR-FTIR and Raman spectroscopy: a pilot study. *Sci. Agric. Bohem.* **2017**, *48*, 22–29.

393. Andrade, C.T.; Silva, K.M.P.; Tavares, M.I.; Simao, R.A.; Achete, C.; Perez, C.A. Comparative study on structural features of α chitin from *Xiphopenaeus kroyeri* and its precipitated product from phosporic acid solution. *J. Appl. Polym. Sci.* **2001**, *83*, 151–159.

394. McDevitt, T.C.; Laflamme, M.A.; Murry, C.E. Proliferation of cardiomyocytes derived from human embryonic stem cells is mediated via the IGF/PI 3-kinase/Akt signaling. *J. Mol. Cell. Cardiol.* **2005**, *39*, 865–873.

395. Cunha, A.G.; Gandini, A. Turning polysaccharides into hydrophobic materials : a critical review. Part 1. Cellulose. *Cellulose* **2010**, *17*, 875–889.

396. Wu, D.; Fang, L.; Qin, Y.; Wu, W.; Mao, C.; Zhu, H. Oil sorbents with high sorption capacity , oil/water selectivity and reusability for oil spill cleanup. *Mar. Pollut. Bull.* **2014**, *84*, 263–267.

397. Aboul-Gheit, A.K.; Khalil, F.H.; Abdel-Moghny, T. Adsorption of spilled oil from seawater by waste plastic. *Oil Gas Sci. Technol. –Rev* **2006**, *61*, 259–268.

398. Dong, T.; Xu, G.; Wang, F. Adsorption and adhesiveness of kapok fiber to different oils. *J. Hazard. Mater.* **2015**, *296*, 101–111.

399. Ifelebuegu, A.O.; Johnson, A. Nonconventional low-cost cellulose- and keratin-based biopolymeric sorbents for oil/water separation and spill cleanup: A review. *Crit. Rev. Environ. Sci. Technol.* **2017**, *47*, 964–1001.

400. Sabir, S. Approach of cost-effective adsorbents for oil removal from oily water. *Crit. Rev. Environ. Sci. Technol.* **2015**, *45*, 1916–1945.

401. Likon, M.; Rem, M.; Ducman, V.; Svegl, F. Populus seed fibers as a natural source for production of oil super absorbents. *J. Environ. Manage.* **2013**, *114*, 158–167.

402. Annunciado, T.R.; Sydenstricker, T.H.D.; Amico, S.C. Experimental investigation of various vegetable fibers as sorbent materials for oil spills. *Mar. Pollut. Bull.* **2005**, *50*, 1340–1346.

403. Suni, S.; Kosunen, A..; Hautala, M.; Pasila, A.; Ramantschuk, M. Use of a by-product of peat excavation, cotton grass fibre, as a sorbent for oil-spills. *Mar. Pollut. Bull.* **2004**, *49*, 916–921.

404. Cui, Y.; Xu, G.; Liu, Y. Oil sorption mechanism and capability of cattail fiber assembly. *Hournal Ind. Text.* **2014**, *43*, 330–337.

405. Vlaev, L.; Petkov, P.; Dimitrov, A.; Genieva, S. Cleanup of water polluted with crude oil or diesel fuel using rice husks ash. *J. Taiwan Inst. Chem. Eng.* **2011**, *42*, 957–964.

406. Moriwaki, H.; Kitajima, S.; Kurashima, M.; Hagiwara, A.; Haraguchi, K.; Shirai, K.; Kanekatsu, R.; Kiguchi, K. Utilization of silkworm cocoon waste as a sorbent for the removal of oil from water. *J. Hazard. Mater.* **2009**, *165*, 266–270.

407. Ukotije-Ikwut, P.R.; Idogun, A.K.; Iriakuma, C.T.; Aseminaso, A.; Obomanu, T. A novel method for adsorption using human hair as a natural oil spill sorbent. *Int. J. Sci. Eng. Res.* **2016**, *7*, 1754–1765.

408. Nduka, J.K.; Ezenweke, L.O.; Ezenwa, T.E. Comparison of the mopping ability of chemically modified and unmodified biological wastes on crude oil and its lower fractions. *Bioresour. Technol.* **2008**, *99*, 7902–7905.

Abstract

Presented PhD thesis is oriented towards the preparation and practical application of naturally formed chitin matrices as a final product or intermediates for further functionalization. The research has an interdisciplinary character as its combine not only the approaches of chemical technology, materials engineering or biochemistry, but also are close to the assumptions of bioinspired materials science and biomimetics. The uniqueness of the work can be confirmed by the fact that during the research three-dimensional chitinous skeletons of marine sponges of the order Verongiida and spiders molting cuticles from the family Theraphosidae, were used for selected application fields for the first time. This approach and utility of naturally formed matrices allows to significantly accelerate the synthesis of the final product and eliminates the undesirable effects arising during the biopolymers processing because of their natural character. Special attention was paid to the description of the novel method of chitin isolation assisted by microwaves. The innovative approach, used so far for the isolation of other biopolymers (e.g. cellulose), allowed here to significantly reduce the isolation time and the necessary reagents, while keeping intact the chemical structure of chitin. The obtained biopolymer was thoroughly characterized including morphological and physicochemical aspects. Due to its biocompatibility, high porosity, and unique three-dimensional structure, it was proposed to use be used in tissue engineering, as a scaffold for cultivation of human skin and heart cells. The biomedical "weaknesses" of chitin observed during the study, such as low roughness or mechanical strength, were improved by using, for the first time, a natural medium - the hemolymph of the snail *C. aspersum*. By the *ex-vivo* shell regeneration process mimicking, the chitin matrix was coated with natural calcium carbonate to improve the aforementioned parameters. The described biofunctionalization positively influenced the culture quality of human bone cells - osteoblasts. In subsequent studies, the well-developed chemical structure of

chitin was used as a support to immobilize enzyme of the oxidoreductase class - laccase. It was demonstrated, for the first time, that the synthesized biosystems, can efficiently remove selected pharmacological impurities from aqueous solutions. Moreover, an effective method of coating the skeleton of the marine demosponge *A. aerophoba* with nano- and microparticles of silver and silver bromide, was proposed. The composite obtained by chemical reduction of silver nitrate, showed high antibacterial properties against both Gram-positive and Gram-negative strains. Using the obtained material, a simple filtration system was proposed and its application potential as an antibacterial filter was investigated. Finally, the sorption properties of natural spider skin *A. sp. "peru purple"* as a sorbent of crude oil from water surface, were also investigated. As observed, this material being a natural chitin/protein biocomposite has superhydrophobic properties, which positively affected the sorption potential of crude oil. The thesis is divided into 10 chapters:

Chapter 1 "Introduction".

Provides a general introduction to the topic and problems of the dissertation.

Chapter 2 "Literature Review".

The literature review of a submitted doctoral dissertation show issues concerning state-of-the-art of biomimetics, tissue engineering, and chitin chemistry. The first section focuses on the importance of the biomimetic concept, which assumes the creation of technology and materials synthesis. Then, special attention was paid to the 3D scaffold as support for diverse cell cultures. Several methods of scaffold creation and modification have been described carefully. Additionally, a separate chapter was devoted to bioscaffolds as a crucial research area of modern tissue engineering. Finally, the importance of chitin was pointed out from several points of view. Chitin was analyzed in case of its natural sources, isolation methods, structural properties, and potential utility.

Chapter 3 "Aim of work and research hypothesis".

This chapter deals with the presentation of the research hypothesis and the research objectives of this dissertation.

Chapter 4 "Materials and methods".

It contains a description of raw materials used during the study and the methods of synthesis. In addition, the analytical techniques used during the characterization of the obtained materials are described.

Chapter 5 "Structural and physicochemical properties of chitin scaffolds of poriferan origin".

The information presented in this chapter focuses on the physicochemical properties of selected chitin scaffolds isolated from Verongida marine sponges. Many of the analyses presented were performed for the first time, such as μCT and compression testing. These analyses were carried out in immersion, allowing the characterization of the scaffold in its natural form. Moreover, the results of several analyses are presented, proving that the microwave method has no negative effect on the chemical structure of chitin.

Chapter 6 "Evaluation of the biomedical utility of pure chitinous scaffold frm selected marine demosponge".

This chapter is a collection of results showing the application potential of pure chitin matrix isolated from the marine sponge *A. fistularis* as a scaffold for culturing dermal/skin cells of keratinocytes and fibroblasts. Among other things, the cytotoxicity of the material and cell proliferation and growth were investigated by qualitative methods.

Chapter 7 "Naturally pre-designed chitinous scaffold biomineralized *ex-vivo*, characterization and application".

The chapter describes a novel *ex-vivo* biomineralization approach which involves transferring the regeneration process of *C. aspersum* snail shell to an external chitinous matrix. The obtained material was thoroughly characterized. Its application potential as a support for the proliferation of human osteoblast bone cells was also tested for the first time.

Chapter 8 "Immobilization of laccase on chitinous skeleton".

The chapter discusses the results of the synthesis of biosystem constructed with a 3D chitin support from a marine sponge and the enzyme - laccase. This part describes the chitin-immobilized laccase system for the removal of tetracycline from aqueous solutions. The preferred process conditions and potential reusability are described here.

Chapter 9 "Determination of antibacterial properties of chitin–Ag/AgBr composite".

The chapter presents the results of applying silver and silver bromide nanoparticles and microparticles to the surface of chitin fibers. The first part of the chapter is devoted to the characterization of the obtained material. Then its antibacterial properties against *E. coli* and *B. subtilis* strains were presented. The investigated material was also tested as an antibacterial filter for purification of water from bacterial contaminants.

Chapter 10 "Aranean chitin and its practical applications".

The last chapter is devoted to chitin obtained from the spiders formed during the molting cuticles. After a brief theoretical introduction, there is a description of morphological and physicochemical properties of the material discussed. Then, it is focused on presenting the results of preliminary application tests in tissue engineering as a scaffold for culturing human cardiomyocytes. The last part of this chapter describes the sorption properties of pure spider epidermis against crude oil.

Streszczenie

Niniejsza rozprawa doktorska zorientowana jest na otrzymanie i wykorzystanie naturalnie uformowanych matryc chitynowych jako gotowego produktu aplikacyjnego lub półproduktu do dalszej funkcjonalizacji. Praca posiada interdyscyplinarny charakter, gdyż łączy nie tylko technologię chemiczną, inżynierię materiałową, biologię czy biochemię, lecz również jest bliska założeniom biomimetyki. O unikatowości pracy może świadczyć fakt, że w trakcie badań wykorzystano po raz pierwszy trójwymiarowe chitynowe szkielety gąbek morskich rzędu Verongida oraz powstałe w procesie linienia naskórki pająków z rodziny Theraphosidae w wybranych obszarach aplikacyjnych. Takie podejście, pozwala znacznie przyspieszyć syntezę końcowego produktu jak i eliminuje niepożądane efekty powstające w trakcie przetwórstwa biopolimeru. Na szczególną uwagę zasługuje opis metody izolacji chityny z wykorzystaniem techniki mikrofalowej. Nowatorskie podejście wykorzystywane do tej pory do izolacji innych biopolimerów, jak celuloza, pozwoliło na znaczne zaoszczędzenie czasu izolacji oraz niezbędnych reagentów, przy jednoczesnym zachowaniu nienaruszonej struktury chemicznej chityny. Otrzymany biopolimer został wnikliwie scharakteryzowany pod kątem morfologicznym oraz fizykochemicznym. Ze względu na biokompatybilność, wysoką porowatość oraz unikatową trójwymiarową strukturę zaproponowano jego zastosowanie w inżynierii tkankowej, jako *scaffold* do hodowli ludzkich komórek skórnych i sercowych. Zaobserwowane w trakcie badań „słabe strony" chityny w ujęciu biomedycznym, takie jak niska chropowatość czy wytrzymałość mechaniczna, skorygowano wykorzystując po raz pierwszy naturalne medium – hemolimfę ślimaka *C. aspersum*. Naśladując proces regeneracji muszli tego bezkręgowca *ex-vivo*, pokryto matrycę chitynową naturalnym węglanem wapnia, co pozwoliło na poprawę wyżej wymienionych parametrów. Opisana biofunkcjonalizacja pozytywnie wpłynęła na jakość hodowli ludzkich

komórek kostnych. W kolejnych badaniach wykorzystano dobrze rozwiniętą strukturę chemiczną chityny jako nośnik do immobilizacji enzymu z klasy oksydoreduktaz - lakazy. Udowodniono, że zsyntezowany system biokatalityczny, jest w stanie efektywnie usunąć wybrane zanieczyszczenia farmakologiczne z roztworów wodnych. Ponadto, zaproponowano efektywną metodę pokrywania szkieletu gąbki morskiej *A. aerophoba* nano- i mikrocząstkami srebra i bromku srebra. Otrzymany poprzez chemiczną redukcję azotanu srebra kompozyt, wykazywał istotne właściwości antybakteryjne wobec szczepów zarówno Gram-dodatnich jak i Gram-ujemnych. Wykorzystując otrzymany materiał zaproponowano prosty układ filtracyjny badając jego potencjał aplikacyjny jako filtr antybakteryjny. Finalnie, zbadano także właściwości sorpcyjne, naturalnych oskórków pająka *A. sp. „peru purple"* jako sorbentu ropy naftowej z powierzchni wody. Jak zaobserwowano, materiał ten będąc naturalnym biokompozytem chitynowo/białkowym posiada właściwości superhydrofobowe, co pozytywnie wpłynęło na potencjał sorpcyjny ropy naftowej. Pracę podzielono na 10 rozdziałów:

Rozdział 1 „Wprowadzenie".

Stanowi ogólny wstęp do tematyki i problematyki pracy doktorskiej.

Rozdział 2 „Przegląd literaturowy".

Przegląd literatury przedłożonej pracy doktorskiej ukazuje zagadnienia dotyczące stanu wiedzy z zakresu biomimetyki, inżynierii tkankowej oraz charakterystyki chityny. W pierwszej części skupiono się na znaczeniu koncepcji biomimetyki, która zakłada tworzenie technologii i syntezy materiałów w oparciu o naturę. Następnie szczególną uwagę zwrócono na scaffoldy 3D jako podłoże do hodowli zróżnicowanych komórek. Dokładnie opisano kilka metod tworzenia i modyfikacji scaffoldów. Dodatkowy podrozdział poświęcono tematyce bioscaffoldów, jako istotnemu obszarowi badawczemu współczesnej

inżynierii tkankowej. Na koniec zwrócono uwagę na znaczenie chityny z wielu punktów widzenia. Przeanalizowano chitynę pod kątem jej naturalnych źródeł, metod izolacji, właściwości strukturalnych oraz potencjalnej użyteczności.

Rozdział 3 „Cel i zakres pracy".

Rozdział ten dotyczy przedstawienia hipotezy badawczej oraz cząstkowych celów badawczych niniejszej dysertacji.

Rozdział 4 „Materiały i metody".

Zawiera opis wszystkich surowców wykorzystanych w trakcie badań oraz metod syntezy. Ponadto opisano techniki analityczne stosowane w trakcie charakterystyki otrzymanych materiałów.

Rozdział 5 „Strukturalne i fizykochemiczne właściwości scaffoldów chitynowych otrzymywanych z gąbek morskich".

Informacje przedstawione w tym rozdziale skupiają się wokół właściwości fizykochemicznych wybranych szkieletów chitynowych izolowanych z gąbek morskich rzędu Verongida. Wiele z przedstawionych analiz zostało wykonane po raz pierwszy, warto wymienić chociażby analizę mikrotomografii komputerowej (μCT) czy analizę właściwości wytrzymałościowych (test ściskania). Analizy te prowadzono w zanurzeniu, co pozwoliło na charakterystykę scaffoldu w jego naturalnym kształcie. Ponadto, przedstawiono wyniki szeregu analiz udowadniając, że metoda mikrofalowa nie ma negatywnego wpływu na strukturę chemiczną chityny.

Rozdział 6 „Określenie właściwości aplikacyjnych czystej matrycy chitynowej z gąbki morskiej w ujęciu biomedycznym".

Rozdział ten jest zbiorem wyników pokazujących potencjał aplikacyjny czystej matrycy chitynowej, wyizolowanej z gąbki morskiej *A. fistularis* jako scaffoldu do hodowli komórek skórnych keratynocytów i fibroblastów. Zbadano m.in.

cytotoksyczność materiału oraz proliferację i wzrost komórek metodami jakościowymi.

Rozdział 7 „Naturalnie uformowane scaffold chitynowy zbiomineralizowany *ex-vivo*, charakterystyka i zastosowanie".

Rozdział opisuje nową metodę biomineralizacji *ex-vivo,* która zakłada przeniesienie procesu regeneracji muszli ślimaka *C. aspersum* na zewnętrzną matrycę chitynową. Otrzymany materiał wnikliwie scharakteryzowano pod kątem morfologicznym i fizykochemicznym. Przetestowano również jego potencjał aplikacyjny jako scaffold do proliferacji ludzkich komórek kostnych osteoblastów.

Rozdział 8 „Immobilizacja lakazy na chitynowym szkielecie".

W rozdziale omówione są wyniki badań nad syntezą biosystemu katalitycznego zbudowanych z 3D nośnika chitynowego z gąbki morskiej oraz enzymu - lakazy. W części tej opisano układ chityna–immobilizowana lakaza do usuwania tetracykliny z roztworów wodnych. Ponadto, przedstawiono preferencyjne warunki prowadzenia procesu oraz potencjał ponownego wykorzystania zsyntezowanego układu biokatalitycznego.

Rozdział 9 „Określenie właściwości antybakteryjnych kompozytu chityna-Ag/AgBr".

Rozdział przedstawia rezultaty naniesienia nano- i mikrocząstek srebra i bromku srebra na powierzchnię włókiem chitynowych. Pierwszą część rozdziału poświęcono charakterystyce otrzymanego materiału. Następnie przedstawiono jego właściwości antybakteryjne wobec szczepów *E. coli* i *B. subtilis.* Badany materiał został także przetestowany jako antybakteryjny filtr do oczyszczania wody z zanieczyszczeń bakteryjnych.

Rozdział 10 „Chityna pajęcza i jej praktyczne zastosowanie".

Ostatni rozdział poświęcony jest chitynie otrzymanej z naskórków pająków powstałych w trakcie procesu linienia. Po krótkim wprowadzeniu teoretycznym, znaleźć tam można opis właściwości morfologicznych oraz fizykochemicznych omawianego materiału. Następnie skupiono się na przedstawieniu wyników wstępnych testów aplikacyjnych w inżynierii tkankowej jako scaffold do hodowli kardiomiocytów ludzkich. Ostatnia część tego rozdziału opisuje właściwości sorpcyjne czystych naskórków pajęczych wobec ropy naftowej.

Scientific activity

PUBLICATIONS

CUMULATIVE IMPACT FACTOR: 94.499

1. Christine Klinger, Sonia Żółtowska-Aksamitowska, Marcin Wysokowski, Mikhail V. Tsurkan, Roberta Galli, Iaroslav Petrenko, <u>Tomasz Machałowski</u>, Alexander Ereskovsky, Rajko Martinović, Lyubov Muzychka, Oleg B. Smolii, Nicole Bechmann, Viatcheslav Ivanenko, Peter J. Schupp, Teofil Jesionowski, Marco Giovine, Yvonne Joseph, Stefan R. Bornstein, Alona Voronkina, Hermann Ehrlich, *Express method for isolation of ready-to-use 3D chitin scaffolds from Aplysina archeri (Aplysineidae: Verongiida) Demosponge*, Marine Drugs (2019), 17,131-155, **IF: 6.085, MES: 100**

2. <u>Tomasz Machałowski</u>, Marcin Wysokowski, Sonia Żółtowska-Aksamitowska, Nicole Bechmann, Björn Binnewerg, Mario Schubert, Kaomei Guan, Stefan R. Bornstein, Katarzyna Czaczyk, Oleg Pokrovsky, Michael Kraft, Martin Bertau, Christian Schimpf, David Rafaja, Mikhail Tsurkan, Roberta Galli, Heike Meissner, Iaroslav Petrenko, Andriy Fursov, Alona Voronkina, Marek Figlerowicz, Yvonne Joseph, Teofil Jesionowski, Hermann Ehrlich, *Spider Chitin. The biomimetic potential and applications of Caribena versicolor tubular chitin*, Carbohydrate Polymers (2019), 226, 115301, **IF: 10.723, MES: 140**

3. <u>Tomasz Machałowski</u>, Marcin Wysokowski, Mikhail V. Tsurkan, Roberta Galli, Christian Schimpf, David Rafaja, Erica Brendler, Christine Viehweger, Sonia Żółtowska-Aksamitowska, Iaroslav Petrenko, Katarzyna Czaczyk, Michael Kraft, Martin Bertau, Nicole Bechmann, Kaomei Guan, Stefan R. Bornstein, Alona Voronkina, Andriy Fursov, Magdalena Bejger, Katarzyna Biniek-Antosiak, Wojciech Rypniewski, Marek Figlerowicz, Oleg Pokrovsky, Teofil Jesionowski, Hermann Ehrlich, *Spider Chitin: An ultrafast microwave-assisted method for chitin isolation from Caribena versicolor spider molt cuticle*, Molecules (2019), 24, 3736, **IF: 4.927, MES: 100**

4. <u>Tomasz Machałowski</u>, Marcin Wysokowski, Iaroslav Petrenko, Andriy Fursov, Mehdi Rahimi Nasrabadi, Moh'd M. Amro, Heike Meissner, Yvonne Joseph, Bakhtiyor Fazilov, Hermann Ehrlich, Teofil Jesionowski, *Naturally pre-designed biomaterials: spider molting cuticle as a functional crude oil sorbent*, Journal of Environmental Management (2020), 261, 110218, **IF: 8.910, MES: 100**

5. Marcin Wysokowski, <u>Tomasz Machałowski</u>, Iaroslav Petrenko, Christian Schimpf, David Rafaja, Roberta Galli, Jerzy Ziętek, Snežana Pantović, Alona Voronkina, Valentine Kovalchuk, Viatcheslav N. Ivanenko, Bert W. Hoeksema, Cristina Diaz, Yuliya Khrunyk, Allison L. Stelling, Marco Giovine, Teofil Jesionowski, Hermann Ehrlich, *3D chitin scaffolds of marine demosponge origin for biomimetic mollusk hemolymph-associated biomineralization ex-vivo*, Marine Drugs (2020), 18, 123, **IF: 6.085, MES: 100**

6. Krzysztof Nowacki, Izabela Stępniak, <u>Tomasz Machalowski</u>, Marcin Wysokowski, Iaroslav Petrenko, Christoph Schimpf, David Rafaja, Jerzy Ziętek, Snežana Pantović, Alona Voronkina, Valentine Kovalchuk, Viatcheslav Ivanenko, Yuliya Khrunyk, Roberta Galli, Yvonne Joseph, Michael Gelinsky, Teofil Jesionowski, Hermann Ehrlich, *Electrochemical method for isolation of chitinous 3D scaffolds from cultivated Aplysina aerophoba marine demosponge and its biomimetic application*, Applied Physics A (2020), 126, 368, **IF: 2.938, MES: 70**

7. Jakub Zdarta, <u>Tomasz Machałowski</u>, Oliwia Degórska, Karolina Bachosz, Andriy Fursov, Hermann Ehrlich, Viatcheslav N. Ivanenko, Teofil Jesionowski, *3D chitin scaffolds from the marine demosponge Aplysina archeri as a support for laccase immobilization and its use in the removal of pharmaceuticals*, Biomolecules (2020), 10, 646, **IF: 6.064, MES: 100**

8. <u>Tomasz Machałowski</u>, Hermann Ehrlich, Marcin Wysokowski, Iaroslav Petrenko, Enrico Langer, Dmitri Tsurkan, Teofil Jesionowski, *In-vivo biomimetic calcification of selected organic scaffolds using regeneration of snail's shell: methodological approach*, Applied Physics A (2020),126, 469, **IF: 2.938, MES: 70**

9. <u>Tomasz Machałowski</u>, Maria Czajka, Iaroslav Petrenko, Heike Meissner, Christian Schimpf, David Rafaja, Jerzy Ziętek, Beata Dzięgiel, Łukasz Adaszek, Alona Voronkina, Valentin Kovalchuk, Jakub Jaroszewicz, Andriy Fursov, Mehdi Rahimi-Nasrabadi, Dawid Stawski, Nicole Bechmann, Teofil Jesionowski , Hermann Ehrlich, *Functionalization of 3D chitinous scaffolds of sponge origin using silver nanoparticles and their antibacterial properties*, Marine Drugs (2020)**,** 18, 304, **IF: 6.085, MES: 100**

10. Jens Götze, Beda Hofmann, Berthold Ottens, <u>Tomasz Machałowski</u>, Mikhail V. Tsurkan, Teofil Jesionowski, Hermann Ehrlich, *Biosignatures in subsurface filamentous fabrics (SFF) from the Deccan Volcanic Province, India*, Minerals (2020), 10, 540**, IF: 2.818, MES: 100**

11. Trajce Talevski, Aleksandra Talevska Leshoska, Elena Pejoski , Boris Pejin, <u>Tomasz Machałowski</u>, Marcin Wysokowski, Mikhail V. Tsurkan, Olga Petrova, Viktor Sivkov, Rajko Martinovic, Snezana Pantovich, Yulia Khrunyk, Volodymyr Trylis, Andrij Fursov, Mirko Djurovic, Teofil Jesionowski, Hermann Ehrlich, *Identification and first insights into the structure of chitin from the endemic freshwater demosponge Ochridaspongia rotunda (Arndt, 1937)*, International Journal of Biological Macromolecules (2020), 162, 1187–1194, **IF: 8.025, MES: 100**

12. <u>Tomasz Machalowski</u>, Chris Amemiya, Teofil Jesionowski, *Chitin of Araneae origin: structural features and biomimetic applications-review*, Applied Physics A (2020), 126, 678, **IF: 2.938, MES: 70**

13. <u>Tomasz Machalowski</u>, Teofil Jesionowski, *Hemolymph of molluscan origin: from biochemistry to modern biomaterials science – review article,* Applied Physics A (2021), 127, 3, **IF: 2.938, MES: 70**

14. Katarzyna Solarska-Ściuk , Kinga Adach, Sylwia Cyboran-Mikołajczyk, Dorota Bonarska-Kujawa, Agnieszka Rusak, Łucja Cwynar-Zając, <u>Tomasz Machałowski</u>, Teofil Jesionowski, Katarzyna Grzywacz, Mateusz Fijałkowski, *Are biogenic and pyrogenic mesoporous SiO_2 nanoparticles safe for normal cells?* Molecules (2021), 26, 1427, **IF: 4.927, MES: 100**

15. <u>Tomasz Machałowski</u>, Agnieszka Rusak, Benita Wiatrak, Katarzyna Haczkiewicz-Leśniak, Aneta Popie, Jakub Jaroszewicz, Andrzej Żak, Merzenna Podhorska-Okołów, Teofil Jesionowski, *Naturally formed chitinous skeleton isolated from the marine demosponge Aplysina fistularis as a 3D scaffold for tissue engineering*, Materials (2021), 14, 2992, **IF: 3.748, MES: 140**

16. <u>Tomasz Machałowski,</u> Joanna Idaszek, Adrian Chlanda, Marcin Heljak, Adam Piasecki, Wojciech Święszkowski, Teofil Jesionowski, *Naturally prefabricated 3D chitinous skeletal scaffold of marine demosponge origin, biomineralized ex vivo as a functional biomaterial*, Carbohydrate Polymers (2022), 275, 118750, **IF: 10.073, MES: 140**

17. <u>Tomasz Machałowski</u>, Katarzyna Jankowska, Karolina Bachosz , Wojciech Smułek, Hermann Ehrlich, Ewa Kaczorek, Jakub Zdarta, Teofil Jesionowski, *Biocatalytic system made of 3D chitin, silica nanopowder and horseradish peroxidase for the removal of 17α-ethinylestradiol: Determination of process efficiency and degradation mechanism,* Molecules (2022), 27, 1354, **IF: 4.927, MES: 100**

18. <u>Tomasz Machałowski</u>, Mikołaj Kozłowski, Agnieszka Kołodziejczak-Radzimska, Jarosław Jakubowicz, Teofil Jesionowski, *Chitin nanofibers as reinforcement for hydroxyapatite-based composites preparation,* Progress on Chemistry and Application of Chitin and its Derivatives (2022), 27, (accepted 21.06.2022), **IF: –, MES: 70**

CONFERENCES

- Posters

19-21.09.2018 XXIV Conference of Polish Chitin Society, „New Aspects on Chemistry and Application of Chitin and its Derivatives" *Sponges (Porifera) as source of morphologically defined chitin*, Tyniec, Poland

9-13.09.2019 30th Annual Conference of the European Society for Biomaterials, *Tubular chitin of spider molt origin as new scaffold for tissue engineering*, Dresden, Germany

03.11.2020 3rd National Scientific Conference "Polymers in Medicine", Łukasiewicz Research Network - Institute of Biopolymers and Chemical Fibers,

Naturalnie ustrukturyzowana matryca chitynowa z gąbki morskiej Aplysina fistularis jako funkcjonalny biomateriał, Lodz, Poland

23-24.09.2021 XXVI Conference of Polish Chitin Society, „New Aspects on Chemistry and Application of Chitin and its Derivatives" *Biosystem made of 3D chitin, silica nanopowder and horseradish peroxidase for the removal of estrogens*, online

- Oral presentation

25-27.09.2019 XXV Conference of Polish Chitin Society „New aspects on chemistry and application of chitin and its derivatives", *Ready to use chitin-based scaffold from spider molt cuticle - isolation, characterization and biomedical application*, Torun, Poland

03.11.2020 3rd National Scientific Conference "Polymers in Medicine", Łukasiewicz Research Network - Institute of Biopolymers and Chemical Fibers, *Trójwymiarowe matryce chitynowe biomineralizowane ex vivo jako potencjalne rusztowania na potrzeby inżynierii tkankowej*, Lodz, Poland

23-24.09.2021 XXVI Conference of Polish Chitin Society, „New Aspects on Chemistry and Application of Chitin and its Derivatives", *Chitin-based skeleton of porifera origin as a functional 3D scaffold for tissue engineering*, online

22-23.09.2022 XXVII Conference of Polish Chitin Society, „New Aspects on Chemistry and Application of Chitin and its Derivatives", *Diverse views in naturally formed 3d chitinous scaffolds and their practical utility*, Poznan, Poland

SCIENTIFIC INTERNSHIPS AND SCHOLARSHIPS

15.01-17.03.2019, Erasmus+ Traineeships Program at TU Bergakademie Freiberg in

01.07-31.09.2019 Biomineralogy and Extreme Biomimetics Laboratory

01.10.2019-31.07.2020 One-Year Research Grant 2019/20 for Doctoral Candidates from Deutscher Akademischer Austauschdienst (DAAD) realized at TU Bergakademie Freiberg in Biomineralogy and Extreme Biomimetics Laboratory

01.09-31.11.2021 Internship at Warsaw University of Technology, Department of Materials Engineering, Biomaterials Scientific Group

AWARDS

09.2019 3rd prize for the best oral presentation at XXV Conference of Polish Chitin Society „New aspects on chemistry and application of chitin and its derivatives", Torun, Poland

11.2020	1st prize for the best poster National Scientific Conference "Polymers in Medicine", Łukasiewicz Research Network - Institute of Biopolymers and Chemical Fibers, Lodz, Poland, Lodz, Poland
09.2021	1st prize for the best poster at XXVI Conference of Polish Chitin Society „New aspects on chemistry and application of chitin and its derivatives", online
	Scientific scholarship awarded by the Rector of the Poznan University of Technology for the PhD students, 2018/2019, 2019/2020, 2020/2021, 2021/2022